



Monitoring Coastal Morphology: Exploring the use of a Multi-Camera Platform for 3D Reconstruction

Thesis submitted in accordance with the requirements of the University of
Liverpool for the degree of Doctor in Philosophy

By

Samantha Godfrey

School of Environmental Science

Department of Geography and Planning

September 2020

Declaration

This thesis is the result of my own work and includes nothing which is the outcome of work done in collaboration except where specifically indicated in the text. It has not been previously submitted, in part or whole, to any university or institution for any degree, diploma, or other qualification. In accordance with The University of Liverpool guidelines, this thesis does not exceed 100,000 words.

Signed: *Samantha Godfrey*

Date: 19.09.20

Contributions by authors to manuscripts:

Chapter 4: Godfrey, S., Cooper, J., Bezombes, F., & Plater, A. (2020). Monitoring coastal morphology: the potential of low-cost fixed array action cameras for 3D reconstruction. *Earth Surface Processes and Landforms*, esp.4892. <https://doi.org/10.1002/esp.4892>

- S. Godfrey: Principal investigator and author, research design and development, data acquisition, processing, analysis, display and manuscript creation.
- J. Cooper: Advice and manuscript development.
- F. Bezombes: Advice and manuscript development
- A. J. Plater: Advice and manuscript development.

Signed: *Samantha Godfrey*

Date: 19.09.20

Acknowledgements

I would like to acknowledge the support and feedback provided from my supervisors, Professor Andrew Plater and Dr James Cooper. This research was made possible through the support of the European Regional Development Fund (22R15P00045), Low Carbon Eco-innovatory and industrial partner Marlan Maritime Technologies. I would also like to thanks my friends, colleagues and family for their support and encouragement throughout this research.

Abstract

Coastal environments are becoming increasingly vulnerable to the effects of climate change. Increased storm severity and rising sea-levels have the potential to cause devastating flood and erosion events placing a significant financial burden on governments in response and recovery. Areas of coastal recession are a particular concern for coastal managers and researchers as these already vulnerable locations are at higher risk of further erosion. Monitoring of coastal recession aids the prevention of significant land loss by promoting pre-emptive management and resilience measures. However, acquisition of 3D data, essential for tracking and determining morphological change, is not always easily obtained.

Consequently, coastal managers and researchers look to 3D monitoring techniques, such as Terrestrial Laser Scanners (TLS), to provide high resolution site-specific surveys. However, many surveying methods come with several limitations such as cost, long surveying times and requirement for specialist personnel which, as a consequence, leads to less regular monitoring and decreased temporal resolution. However, the advent of Structure-from-Motion combined with Multi-View Stereo (SfM-MVS), an image-based 3D reconstruction technique, has democratised access to 3D topographic data and has become an increasingly popular method for monitoring coastal change.

The infusion of SfM-MVS into the geoscience community is still in its infancy and, consequently, current image acquisition schemes and guidance are broad. Therefore, this research offers an assessment of image acquisition and processing of SfM-MVS for sites of coastal recession using multiple cameras. The research is split into three sequential projects that develop the findings and rationale of the previous. The overall aim is to provide a streamlined and holistic approach to monitoring coastal recession using SfM-MVS.

The first project addresses the fundamental impact of camera pose and orientation using an action camera and systematic camera grid as a robust method of image acquisition. This approach examines the effect of camera placement on scene reconstruction to aid the design of a multi-camera array. SfM-MVS dense point clouds displayed millimetre accuracy when compared to equivalent TLS scans and internal precision estimates of < 3 mm (x , y & z).

The second project used the results from the first to develop a multi-camera rig which was validated against a TLS at three sites of coastal recession. The research simultaneously examined the impact of processing parameters on overall point cloud reconstruction. Surveys conducted with the multi-camera rig produced consistent results across all three sites with millimetre accuracy compared to TLS point clouds. Software processing was found to have a significant influence on overall point cloud reconstruction and deformation with the most effective parameter resulting in 18 times less reprojection error.

Validation of the multi-camera rig in these previous two projects provided the basis for the third - monitoring morphological change over a 4-month period at a saltmarsh margin. Erosional and depositional changes were identified through volumetric analysis, undercutting and area loss then related to prevailing wave hydrodynamics. Monthly volumetric erosion rate was estimated at 0.97 m^3 with an overall area of loss of 3.27 m^2 . Comparison with wave hydrodynamics showed a strong correlation with significant wave height. Furthermore, the site displayed persistent levels of undercutting leading to saltmarsh cliff slumping and collapse.

The results reported in these three projects demonstrate the considerable potential for multi-camera setups to monitor coastal recession and improve temporal resolution. Furthermore, this research fundamentally develops concepts and techniques in the field of SfM-MVS and speaks directly to researchers and coastal managers. This work offers both the ability for alternative low-cost image acquisition procedures and practical guidance for users to produce an evidence base for coastal resilience measures.

Abbreviations

AOV	Angle of View
CAA	Civil Aviation Authority
C2C	Cloud-to-Cloud
DEM	Digital Elevation Model
dGPS	Differential Global Positioning System
DoD	DEM of Difference
DSLR	Digital Single-Lens Reflex
EWL	Extreme Water Level
FOV	Field of View
GCP	Ground Control Point
GNSS	Global Navigation Satellite Systems
HAT	Highest Astronomical Tide
IPCC	International Panel on Climate Change
ICP	Iterative Closest Point
LiDAR	Light Detection and Ranging
MP	Megapixel
MVS	Multi-View Stereo
RMSE	Root Mean Square Error
RTK-GPS	Real-Time Kinematic Global Positioning System
SfM	Structure-from-Motion
SfM-MVS	Structure-from-Motion and Multi-View Stereo
SIFT	Scale Invariant Feature Transform
TLS	Terrestrial Laser Scanner
UAV	Unmanned Aerial Vehicle

Contents

1. Introduction	12
1.1 Rationale.....	12
1.2 Structure-from-Motion & Multi-View Stereo	15
1.3 Research Aim & Objectives	16
1.4 Thesis Structure	17
2. Literature Review	20
2.1 Current Monitoring Methods	20
2.1.1 Large-scale Monitoring Techniques.....	21
2.1.2 Small-Scale Monitoring Techniques.....	23
2.1.3 SfM-MVS for Monitoring	24
2.2 Structure-from-Motion Photogrammetry Fundamentals.....	28
2.2.1 Georeferencing & Precision.....	31
2.2.2 Image network.....	33
2.2.3 Optical Sensors	39
3. Research Methodology.....	42
3.1 Overall Methodology.....	42
3.2 Study Sites.....	43
3.2.1 Crosby	44
3.2.2 Thurstaston.....	45
3.2.3 Silverdale.....	46
3.3 Methodology for Stage 1 of Research - Camera Grid.....	47
3.3.1 Camera Grid Design.....	48
3.3.2 Initial Site Representation	52
3.3.3 Concurrent Data Acquisition	54
3.3.4 Comparative testing with TLS.....	55

3.3.5	Standalone Precision Assessment.....	58
3.4	Methodology for Stage 2 of Research - Camera Rig.....	59
3.4.1	Camera Rig Design.....	60
3.4.2	Concurrent Data Acquisition.....	62
3.4.3	Point Cloud Generation.....	62
3.4.4	Comparative Testing with TLS.....	64
3.5	Methodology for Stage 3 of Research – Temporal Change using the Camera Rig	64
3.5.1	Data Acquisition.....	64
3.5.2	Point Cloud Generation.....	65
3.5.3	Geomorphological Change Assessment.....	65
4.	Monitoring coastal morphology: The potential of low-cost fixed array action	
	cameras for 3D reconstruction.....	67
4.1	Introduction.....	68
4.2	Study Site.....	71
4.3	Methods.....	72
4.3.1	Camera Grid Design.....	73
4.3.2	Initial Site Representation.....	74
4.3.3	Data Acquisition.....	75
4.3.4	SfM-MVS Point Cloud Generation.....	76
4.3.5	Performance Assessment.....	78
4.4	Results.....	81
4.4.1	Stage One: Positional Camera Parameters.....	81
4.4.2	Stage Two: Minimal Image Capture.....	86
4.5	Discussion.....	92
4.6	Conclusions.....	95

5. Monitoring Coastal Morphology: Using a Multi-Camera Array with Structure-from-Motion	96
5.1 Introduction	97
5.2 Study Sites.....	100
5.2.1 Crosby	100
5.2.2 Thurstaston.....	102
5.2.3 Silverdale.....	102
5.3 Methods.....	102
5.3.1 Camera Rig Design	102
5.3.2 Data Acquisition.....	105
5.3.3 SfM-MVS Point Cloud Generation	107
5.3.4 Performance Assessment	109
5.4 Results.....	113
5.4.1 Stage One: Initial Processing Results	113
5.4.2 Stage Two: Densification Testing	114
5.5 Discussion	123
5.5.1 Reconstruction Comparison	123
5.5.2 Influence of Processing and GCPs.....	125
5.5.3 Future Avenues for Research	128
5.6 Conclusions	129
6. Tracking Coastal Morphology using a Multi-Camera Array: A Novel Approach to Saltmarsh Monitoring.....	131
6.1 Introduction	132
6.2 Study Site.....	134
6.3 Methods.....	135
6.3.1 Data Acquisition.....	136
6.3.2 Point Cloud Processing.....	136

6.3.3	Geomorphological Change Assessment.....	137
6.4	Results.....	140
6.4.1	Topographic Differencing for Volumetric Assessment.....	140
6.4.2	Alongshore Profile Extraction & Area Loss Analysis	146
6.4.3	Identification of Undercutting Extent.....	148
6.4.4	Meteorology & Hydrodynamics.....	154
6.5	Discussion	163
6.5.1	Implications	166
6.6	Conclusions	167
7.	Discussion	169
7.1	Technique Comparison.....	169
7.2	Wider Implications	171
7.2.1	Fostering Innovation	171
7.2.2	Flood and Erosion Management	172
7.2.3	SfM-MVS & Photogrammetry Research SfM-MVS	173
7.3	Future Development and Research	174
8.	Conclusions.....	176
8.1	Concluding Remarks	178
9.	References.....	179
	Appendix A – Python Script.....	199
	Appendix B – Risk Assessments	200

List of Tables

Table 2.1. Summary of platforms used with SfM-MVS for coastal monitoring	26
Table 5.1: Data acquisition information for TLS and camera rig SfM-MVS surveys at Thurstaston, Silverdale and Crosby.....	106
Table 5.2: Reprojection Errors (m) for point clouds constructed under different Image Alignment parameters for Thurstaston, Silverdale and Crosby.	113
Table 5.3: Calculation of dimensionless indicator based on standard deviation.	124
Table 6.1: Silverdale Saltmarsh area (ha) after Gray, 1972; Pringle, 1995	135

List of Figures

Figure 2.1: General SfM-MVS workflow	30
Figure 2.2: Example of SfM surface model distortions as a result systematic error. (Source: Carbonneau & Dietrich, 2017).	32
Figure 2.3: a) The effect of camera obliqueness on image acquisition. Source: Wolf & DeWitt (2000) b) Aerial view of camera orientation for convergent imagery.....	36
Figure 2.4: Image acquisition using three fixed cameras to monitor soil erosion after rainfall events. Source: Eltner et al. (2017).	38
Figure 3.1: Depiction of the workflow of research	43
Figure 3.2: Technical drawing of the Camera Grid. The internal dimensions of the grid frame were 0.99 m in height and 1.65 m in length. The frame was constructed with fifteen, 0.11 m horizontal grid squares (columns) and nine 0.11 m vertical grid squares (rows). The grid size of 0.11 x 0.11 m was chosen to accommodate the camera's dimensions.....	49
Figure 3.3: Technical drawing of the 'traveller' used for camera movement across the grid.....	50
Figure 3.4: Technical drawing of full camera grid setup ('Height 2') including timber base platform needed for uneven terrain and timber prop attachments to maintain the z-axis of the grid. The base platform would not be necessary at a site of even terrain.	51
Figure 3.5: GoPro Hero 4 Black FOV representation modelled in SketchUp. Calculation incorporated a 3 m distance FOV.....	52
Figure 3.6: SketchUp representation for FOV estimations. a) FOV estimate for camera in position at 'Height 2' Row D (40°) b) Zoomed in image of FOV estimate at position 'Height 2' Row D (40°) showing the FOV not encroaching onto the equipment c) Zoomed in image of FOV estimate at position 'Height 2' Row E (40°) showing FOV estimate encroaching onto the equipment suggesting a change in angle from 40° to 30° declination around Row E (Height 2) may be required in the field.	53
Figure 3.7: Sketch-up modelled representation of three degrees of camera obliqueness from the z-axis. a) No declination or 0° ('Height 1' – Rows A-I); b) 30° declination ('Height 2' – Rows E-I); c) 40° declination ('Height 2' – Rows A-D).....	54

Figure 3.8: Segmented TLS point cloud for Completeness test. a) 2D cliff image with artificial background colouring used for filtering in Python OpenCV programming. b) 2D floor image with artificial background colour.....56

Figure 3.9: Technical drawing of Camera Rig. Height displayed is that used at Silverdale and Thurstaston with cliff heights of approximately 1 m.....61

Figure 3.10: Workflow depicting the process of point cloud generation and assessment. Cross-hatching reflect the parameters used in processing.63

Figure 4.1: Study site location. a) Location map with marker indicating test location. b) General site photograph showing landward retreat with cliffs at a height of ~1.5 m taken January 2018.....72

Figure 4.2: a) Camera Grid for image acquisition. Annotations display the labelled rows (A-I) and columns (1-15). The internal dimensions of the grid were set so each grid square was of equal size. b) Traveller used to move the camera seamlessly to each grid square.....74

Figure 4.3: Camera grid at 'Height 1' on the levelled base - 2 m distance from frontage.76

Figure 4.4: Representation of the position of images used along each row of the camera grid for Stage One Analysis. Camera symbol indicates the position of image that was used in the eight image set. Images taken from these positions had 98% overlap...77

Figure 4.5: The position of images used in Stage Two analysis. Image combinations were taken from the successful row established in Stage One analysis. Camera symbol indicates the position of the image that was used in the creation of the point cloud. Image overlap moves from ~99% to ~94% as images are reduced.81

Figure 4.6: Mean C2C distance for point clouds created from each row of the camera grid when compared to the equivalent TLS point cloud.82

Figure 4.7: C2C scalar field for a) 'Height 1', Row A (highest mean C2C value - 9.69 mm) dense point cloud. b) 'Height 1', Row D (lowest mean C2C value - 4.12 mm) dense point cloud.83

Figure 4.8: Perspective view of point clouds for the best and worst completeness results with a source image from the image set. a) Point cloud from Height 2 Row D had a value of 1.046 - above that of the TLS. b) Point cloud from Height 1 Row I which had the worst value for completeness at 0.795.84

Figure 4.9: The results from the three comparative metrics (Deviation, Completeness, GCP) compared to the TLS reconstruction benchmark for a.) Height 1 b.) Height 2.

c.) The overall SfM-MVS point cloud performance for each row of the camera grid at 'Height 1 and 'Height 2' compared to the equivalent TLS point cloud. Row D from Height 2 provided the best overall balance for camera positional parameters at a height of 2.13 m and an angle of declination of 40°.....85

Figure 4.10: Mean C2C distance for point clouds created from image combination when compared to the equivalent TLS point cloud.87

Figure 4.11: C2C scalar field for a) three images (highest deviation value – 89.08 mm) dense point cloud b) six images (lowest deviation value – 4.43 mm) dense point cloud.....87

Figure 4.12: a.) The results of the three comparative metrics (Deviation, Completeness, GCP) compared to the TLS reconstruction benchmark for the impact of imagery redundancy b.) The overall SfM-MVS point cloud performance for different image combinations along Row D ('Height 2') compared to the equivalent TLS point cloud.89

Figure 4.13: Precision error maps separated into x, y & z components for the six-image point cloud. a) displays overall survey precision including georeferencing error. b) displays internal precision (surface shape error) excluding any georeferencing error and reflects the relative precision of point cloud. Mean precision (mm) is displayed on the bottom left of each map.....90

Figure 5.1: Locations and aerial images of Crosby (a), Thurstaston (b) and Silverdale (c) study sites..... 101

Figure 5.2: Camera Grid representation in SketchUp 2018. a) Camera grid dimensions showing height, width and spacing of camera. b) Camera declination from the z-axis. c) Estimated camera FOVs for the camera rig. d) Representation of camera rig movement in relation to the scene of reconstruction – the cross marks the location of the camera rig for image capture. 104

Figure 5.3: Example images used in the point cloud generation showing the estimated central placement of markers onto GCPs in Agisoft Photoscan a) Thurstaston b) Silverdale c) Crosby..... 108

Figure 5.4: Crosby dense point cloud deformation under differing image alignment parameters. a) 'Medium' image alignment plus 'Ultra-High' densification. b) 'Highest' image alignment plus 'Ultra-High' densification. 114

Figure 5.5: Scalar fields displaying the highest C2C values for each site a) Thurstaston, ‘Ultra High’ densification (highest mean C2C value – 9.01 mm) dense point cloud. b) Silverdale, ‘Low’ densification (highest mean C2C value – 10.4 mm) dense point cloud. c) Crosby, ‘Ultra High’ densification (highest mean C2C value 9.23 mm) dense point cloud. 116

Figure 5.6: Surface density for each site and densification parameter compared to the equivalent TLS result. 117

Figure 5.7: Results of the three comparative tests (Deviation, Surface Density, GCP) compared to the TLS reconstruction benchmark for a.) Thurstaston b.) Silverdale c.) Crosby. Reconstruction accuracies of SfM-MVS and the TLS for each site and densification parameter. A result of 1 would imply that SfM-MVS and the TLS were equivalently accurate in surveying the GCPs. 118

Figure 5.8: The overall SfM-MVS point cloud performance for each site and densification parameter compared to the TLS point cloud. The timescale for computer processing is included as a label on each column. ‘Ultra High’ provided the best overall score but poorest processing times. 119

Figure 5.9: Precision error maps separated into x, y & z components for Thurstaston. Overall survey precision including georeferencing error and internal precision (surface shape error) excluding any georeferencing error are displayed in two columns. Mean precision (mm) is displayed on the bottom left of each map. 120

Figure 5.10: Precision error maps separated into x, y & z dimensions for Silverdale. Overall survey precision including georeferencing error and internal precision (surface shape error) excluding any georeferencing error are displayed in two columns. Mean precision (mm) is displayed on the bottom left of each map. 121

Figure 5.11: Precision error maps separated into x, y & z dimensions for Crosby. Overall survey precision including georeferencing error and internal precision (surface shape error) excluding any georeferencing error are displayed in two rows. Mean precision (mm) is displayed on the bottom left of each map. 122

Figure 6.1: Study site location a) Aerial image showing location of Silverdale test site b) Photograph of Silverdale site with ebb tide (Photograph: Author’s Own). 134

Figure 6.2: Depiction of how the choice of DEM enables undercutting to be identified. 139

Figure 6.3: Negative (erosion) and positive (deposition) volume extracted from DoDs for the survey domain. Higher values for both erosion and deposition recorded between January and March represent 2-months of erosion and deposition. Numbers above bars represent the daily average volume change for that month. 141

Figure 6.4: November to December 2018 elevation differencing map (DoD). Highlighted area shows notable erosion or deposition (>0.1 m) referenced to photographs from the site (aerial view). 143

Figure 6.5: December 2018 to January 2019 elevation differencing map (DoD). Any notable erosion or deposition is highlighted (>0.1 m) referenced to photographs from the site (aerial view). 144

Figure 6.6: January to March 2019 elevation differencing map (DoD). Highlighted area shows notable (>0.1 m) erosion and deposition referenced to photographs from the site (aerial view). January to March represents two months' worth of change. 145

Figure 6.7: The area lost from the saltmarsh cliff between November 2018 and March 2019 plus the monthly area loss rate. Erosion rate based on the digitisation of shoreline profiles and polygonal area. January to March represents two months' worth of change. Numbers above bars represent the daily average area lost for that month. 146

Figure 6.8: Spatial and temporal comparison of saltmarsh cliff profiles. Along shore profile of the cliff, digitised from the SfM-MVS generated DEMs (aerial view). 147

Figure 6.9: Total undercut area (m²) over the 4-month period (November 2018 – March 2019). 148

Figure 6.10: Undercutting extent in November 2018 based on the digitisation of maximum and minimum height DEM shoreline profiles. Notable undercutting is highlighted in maps inserts a, b and c (aerial view). 149

Figure 6.11: Undercutting extent in December 2018 based on the digitisation of maximum and minimum height DEM shoreline profiles. Notable undercutting is highlighted in maps inserts a, b and c (aerial view). Cliff collapse since November noted in insert map c. 150

Figure 6.12: Undercutting extent in January 2019 based on the digitisation of maximum and minimum height DEM shoreline profiles. Notable undercutting is highlighted in maps inserts a, b and c (aerial view). Only minor changes to the area of undercutting were recorded from December 2018. 151

Figure 6.13: Undercutting extent in March 2019 based on the digitisation of maximum and minimum height DEM shoreline profiles. Notable undercutting is highlighted in maps inserts a, b and c (aerial view). Significant erosion since January 2019 (Insert a)..... 152

Figure 6.14: Average wind speed and gust speeds for Silverdale over the period from 17th November 2018 to 17th March 2019. Source: Ehideaway, 2020. 156

Figure 6.15: Wave buoy, tide gauge, wind and storm data for the Morecambe Bay Estuary from Nov 2018 to March 2019. Highlighted are survey dates and period of significantly higher wave heights. Source: Channel Coastal Observatory, Ehideaway (2020) & PolTips™ tidal prediction software (2020). 162

Figure 6.16: Relationship between monthly erosion and monthly significant wave height..... 164

Figure 6.17: Location of Silverdale saltmarsh survey at HAT of ~10.3 m (Photograph: Author's own)..... 165

1. Introduction

1.1 Rationale

Coastal areas have been a location for human settlement and activity throughout history. Globally, greater than 600 million people reside within coastal zones, a figure which is expected to rise by up to 71% by 2050, increasing population estimates to over 1 billion in these regions (Merkens et al., 2016; Barnard et al., 2019). In England, the 31,368 km long coastline is occupied by approximately 5.5 million people – roughly 10% of the total population (Office of National Statistics, 2014). These highly populated areas continue to develop due to the wealth of resources present around coastal zones and the resultant pull of improved economic prospects. Consequently, coastal settlements and estuaries are home to valuable infrastructure and ecosystems, making the protection of these areas a priority. The Environment Agency (2019a) estimates that over 60% of properties in England are serviced by networks and critical infrastructure situated in flood risk areas.

Coastal zones are incredibly dynamic regions that offer a natural barrier of protection from the hydrodynamic power of tides, waves and currents. Natural habitats such as saltmarsh (Wamsley et al., 2010; Temmerman et al., 2013) and beach (van Slobbe et al., 2013) environments can be used as alternative management approaches for protecting coastal settlements (Arkema et al., 2013; Powell et al., 2019). However, the dissipation of energy from hydrodynamic processes results in morphological evolution, in some cases driving erosion and causing a landward retreat of the shoreline. Damage caused by flooding and erosion costs, on average, £260 million per year in the UK alone (Committee on Climate Change, 2018). The future threat of coastal flooding and erosion has resulted in the Environment Agency investing £2.6 billion in future management and monitoring projects between 2015 and 2021 (Environment Agency, 2019a).

The impacts of coastal hydrodynamics, such as erosion, are the outcome of a complex global climatic system. These impacts occur over a variety of spatial and temporal scales which determine the morphological changes along coastlines. Fluctuations in this complex system and the long-term threat of climate change affect the current and future use of coastal areas and increases the prospect of damage to coastal infrastructure (HM

Government, 2016; Environment Agency, 2019a). The long-term threat of climate change will exacerbate the rate of recession as sea level rise and increased storm severity expose already vulnerable sites to the drivers of morphological change (Nicholls et al., 2011; Mentaschi et al., 2018). The inundation of coastal areas in the UK for example, has resulted in 17.3% of the coastline suffering from erosion and 28% of England and Wales experiencing erosion of 0.1 m.yr^{-1} or greater (Masselink and Russell, 2013). In the future, this erosion rate may rise by 100% to 400% due to the effects of climate change (Defra, 2012).

There are two significant impacts of a changing climate; the first is an increase in mean sea level which is expected to exceed previous projections with a rise of 0.61 – 1.10 m by 2100 (RCP 8.5) (International Panel on Climate Change (IPCC), 2019). The second is an increase in the severity of weather conditions affecting global and local wave climates (Earlie et al., 2015). The IPCC (2019) calculated an increase in extreme wave heights of approximately 8 mm.yr^{-1} between 1985-2018 (medium confidence). The time scales on which these impacts operate are vastly different but are fundamentally related, as increases in mean sea-level shortens Extreme Water Level (EWL) return periods, enabling storm conditions to reach higher elevations and increase the impact of storms on coastal areas (Pittock, Walsh and McInnes, 1996; Lowe, Gregory and Flather, 2001; Prime, Brown and Plater, 2015). Changes to the frequency, duration and severity of coastal storms will have a greater and more immediate impact than the slow inundation of mean sea level (Lowe, Gregory and Flather, 2001). The combined effect of increased mean sea level and increased storm severity has the potential to exacerbate storm surge conditions causing erosion and flooding (Zhang and Li, 2019). The uncertainty of coastal storm events is a concern to coastal managers and authorities with a large proportion of morphological changes occurring due to the impact of extreme storms (Lowe, Gregory and Flather, 2001).

The projected impacts of a changing climate are likely to make current coastal management approaches unsustainable (Committee on Climate Change, 2018). As a result, adaptation plans in a variety of sectors are required such as community engagement, legislative changes and restoration of natural coastal resilience measures combined with improved monitoring and understanding of coastal change. Full understanding of morphological change is essential to flood management,

environmental impact assessment and erosion protection (Huang, Wang and Chen, 2010). However, a key obstacle for coastal managers is regular monitoring of these sites.

Monitoring the morphology and retreat of coastal land regularly provides an evidence base from which coastal managers can choose the most suitable time to intervene or adapt resilience plans to successfully protect from flooding and erosion events. Regular monitoring also aids flood and erosion risk modelling as it provides current topographic datasets on which to model projections and validate predictions. Simply pin-pointing and monitoring 'hotspots' of erosion along vulnerable coasts can also provide valuable information for coastal engineering assessments (Ružić et al., 2014).

To provide accurate information on coastal recession, regular repeat surveys are highly beneficial (Harley et al., 2011; Westoby et al., 2018). For example, Pikelj et al. (2018) used regular beach monitoring over 1.5 years to reveal continuous sediment loss even while beach nourishment schemes were in place. There has been enhanced academic and practitioner interest in technological advancements to help improve the process of both onshore and offshore coastal monitoring networks (Environment Agency, 2009). The last decade has seen considerable advancement in digital technologies.

Consequently, there are a range of surveying methods available for monitoring landward retreat each with varying degrees of spatial resolution and coverage. However, many of these surveying methods can be expensive, requiring specialist operators or may not be efficient enough to provide regular repeat surveys in dynamic coastal environments. There is, therefore, a case for alternative methods of monitoring coastal change that can be deployed more regularly.

Increased digital technologies and subsequent global connectivity is producing a shift towards the research and development of innovative techniques in a range of disciplines. The development of this research is funded by the Low Carbon Eco-Innovatory which establishes partnerships between research and industrial firms such as Marlan Maritime Technologies. These connections help to shape the initial direction of the research by the identification of current market needs and, as a result, situates the research within the wider movement towards risk reduction through digital innovations.

1.2 Structure-from-Motion & Multi-View Stereo

Structure-from-Motion and Multi-View Stereo (SfM-MVS), also referred to as simply SfM, is a 3D reconstruction method based on traditional photogrammetric principles. SfM-MVS offers a flexible and cost-effective method of acquiring 3D data. The details of both SfM and MVS are described fully in Chapter 2. In fundamental terms, the technique uses multiple overlapping images that can be acquired from digital cameras, to establish internal and external camera parameters from which 3D points can be projected onto an arbitrary coordinate system. The advancement in computer vision (Bemis et al., 2014) has allowed the underlying photogrammetric calculations to be developed into a systematic workflow and branded as SfM-MVS. The incorporation of this process into automated commercial software packages, and other open-source alternatives, has made it accessible to both professional and less experienced users (Snavely, Seitz and Szeliski, 2008).

The popularity of the technique has increased in recent years with a multitude of disciplines using SfM-MVS due to its flexibility of scale, resolution, availability and its potential to be used in a wide range of environmental conditions. Previously, a TLS was considered the preferred method for 3D data acquisition over image-based techniques. However, comparative results between TLS and SfM-MVS outputs have shown SfM-MVS compares well to TLS, with centimetre accuracy (Wilkinson et al., 2016; Westoby et al., 2018). Brunier et al. (2016) described SfM-MVS as having the reproducibility of Global Navigation Satellite Systems (GNSS) survey techniques but with the high accuracy of laser-based methods.

The quality of SfM-MVS output is often considered to be positively associated with the number of images used: the more images the better (Westoby et al., 2012). This link has prompted initial experimentation with multiple cameras (Eltner et al., 2017) for more rapid image acquisition. However, Eltner et al. (2017) referred to the need for improved camera positions in their research to provide a higher coverage point cloud. In much SfM-MVS research there is little reference to the specific impacts camera position and orientation has on overall reconstruction. There is, therefore, a need for greater examination of the significance of camera position and the impact of image redundancy on 3D reconstruction. The ability to capture multiple images from a fixed array of cameras would be beneficial for speed of data acquisition, particularly for areas

dependent upon tidal cycles. However, to make simultaneous multiple image acquisition possible it is first necessary to understand the significance of camera placement in relation to the scene. Optimal camera placement would result in a simplification of image capture geometry and would entail fuller scrutiny of the combined effect of some positional parameters (beyond simply number of images) that effect image suitability: overlap, obliqueness and convergence (Eltner et al., 2016).

Once these fundamental image acquisition parameters are established for sites of coastal recession, the development of a multi-camera array would provide an effective and efficient data collection procedure. Optimised image processing settings for this form of SfM-MVS image acquisition would provide a streamlined reconstruction workflow. This potential, however, is currently underexplored. The relatively low-cost and ease of use of this type of coastal monitoring technique would mean that regular coastal monitoring is possible for users of SfM-MVS. The potential for more frequent monitoring would provide a valuable resource for coastal managers and policy makers when addressing issues of coastal erosion, climate change and coastal resilience.

1.3 Research Aim & Objectives

The aim of this research is to produce an effective multi-camera array that can be efficiently used with SfM-MVS to monitor coastal recession. To achieve this, it is necessary to experiment with image acquisition and processing parameters to generate a high-quality reconstruction with a minimal number of images. An analysis of multiple camera positions will be performed, the results of which will be used to inform the construction of a multi-camera rig prototype. A processing workflow will be constructed to guide efficient and accurate 3D reconstruction. The prototype developed will be used for tracking temporal morphological change at sites of coastal recession.

Objectives:

1. Conduct an experimental SfM-MVS survey at a small-scale site of typical coastal recession using a novel method of image acquisition which controls the optical camera axes.
 - a. Design and build suitable equipment for the control of camera movement in x , y & z axes.

- b. Devise a set of comparative tests that account for all aspects of overall point cloud quality.
 - c. Critically compare, using the tests established in (b), the impact of camera height, overlap and obliqueness on dense point cloud reconstruction against the results of an industry standard technique.
 - d. Identify optimal camera positions that would be suitable for a multi-camera array.
 2. Explore the potential of a multi-camera array with SfM-MVS for image acquisition at different sites of coastal recession.
 - a. Design and build field equipment based on the optimal camera positions established in Objective One.
 - b. Systematically compare results obtained using the multi-camera setup at different sites against results acquired by an industry standard monitoring system.
 3. Identify the impact of software processing on point cloud reconstruction
 - a. Explore relationships between computational processing and the potential for deformation.
 - b. Review and compare the impact of processing parameter on computational times and overall point cloud reconstruction.
 - c. Identify optimal processing parameters that would be suitable for a multi-camera array and less experienced users of SfM-MVS.
 4. Investigate the capacity of techniques identified above for the monitoring of temporal changes in coastal morphology.
 - a. Conduct repeat surveys at a site of coastal retreat using the multi-camera setup.
 - b. Assess the capacity of the setup to detect geomorphic changes.
 - c. Examine the relationship between hydrodynamics and erosion at the chosen site.

1.4 Thesis Structure

This research is presented in a thesis format containing three sequential, empirical chapters written in the form of journal papers – the first of which (Chapter 4) is published. An outline of the thesis structure is provided below:

Chapter One outlines the content and rationale for the research, examining the greater need for regular coastal erosion monitoring. The chapter highlights the need to further examine SfM-MVS image acquisition procedure and the development of a multi-camera setup. A streamlined image capture and processing workflow is proposed for practical use with SfM-MVS.

Chapter Two provides an overview of relevant literature. The chapter outlines the importance of coastal monitoring and current monitoring techniques. The use of SfM-MVS and its fundamentals are discussed in relation to image network and optical sensors. Current research gaps that have led to the development of this research are identified and discussed.

Chapter Three presents the overarching approach to the research methodology and discusses research procedure in order to achieve the aim of the thesis. This is followed by detailed methodologies for the three empirical chapters.

Chapter Four is the first empirical journal paper in the thesis: *Godfrey, S., Cooper, J., Bezombes, F., & Plater, A. (2020). 'Monitoring coastal morphology: the potential of low-cost fixed array action cameras for 3D reconstruction'. Earth Surface Processes and Landforms, esp.4892. <https://doi.org/10.1002/esp.4892>*. The paper describes the potential of a multi-camera rig and the importance of a suitable image network geometry. The research uses a purpose-built camera grid to control the optical axis and movement of an action camera tested at a site of landward retreat. The impact of positional camera changes on 3D reconstruction are quantified through a comparison with an equivalent TLS survey.

Chapter Five builds on the findings presented in Chapter Four and is the second journal style chapter in this thesis intended for submission to *Earth Surface Processes and Landforms*: *'Monitoring Coastal Morphology: Using a Multi-Camera Array with Structure-from-Motion.'* The paper details the design and deployment of a prototype multi-camera rig which is based on the optimal camera positions from chapter four. The prototype is tested over greater alongshore distances at three locations of landward retreat against the TLS as a comparator benchmark. The efficacy of software parameters is addressed, and a standardised workflow created.

Chapter Six is the final empirical chapter in the thesis intended for submission to *Geomorphology: 'Tracking Coastal Morphology using a Multi-Camera Array: A Novel Approach to Saltmarsh Monitoring'*. This paper compounds the research undertaken in Chapters Four and Five using the multi-camera rig prototype for tracking morphological change. The repeat surveys were undertaken between 2018 – 2019 over a 4-month period. The prevalent wave hydrodynamics and meteorological conditions are evaluated in relation to erosion at the site.

Chapter Seven provides a synthesis of all research results and the suitability of this technique for coastal monitoring. The technique is compared to other coastal monitoring methods and wider implications of the research discussed. The chapter finishes with avenues for further research.

2. Literature Review

Over the last decade advances in remote sensing and 3D image reconstruction techniques have made it easier to monitor dynamic and rugged coastal environments (Maiti and Bhattacharya, 2009; Earlie et al., 2013, 2015; Mancini et al., 2013; Conlin, Cohn and Ruggiero, 2018; Westoby et al., 2018). These advancements in technology have allowed a variety of surveying methods to be used to provide information on geomorphological change, in turn aiding the understanding of coastal processes and responses to hydrodynamic forces (Smith and Pain, 2009). The highly dynamic and hazardous nature of coastal environments means that gathering topographic data can be difficult. Within hours coastal landforms can migrate or erode and understanding these movements requires rugged surveying equipment and techniques (Morang and Gorman, 2005). Shoreline retreat can be a particular concern for coastal managers and, without modification or adaption, will result in the loss of habitats, infrastructure and communities. Advances in digital technology have spurred huge developments in the quality and speed at which topographic information can be gathered (Westoby et al., 2012). These data play a vital role in the detection of shoreline change, rate of loss and future predictions. Topographic data is commonly used in the form of Digital Elevation Models (DEMs). DEMs are used in a variety of ways to track morphological change, such as DEMs of Difference (DoD), and are frequently used in flood and erosion model projections and validation. Consequently, the accuracy and, therefore, the reliability of the DEMs directly influences the quality of model outputs (Fisher and Tate, 2006; Darnell, Tate and Brunson, 2008). However, obtaining reliable topographic data for coastal recession can still be a challenge and not all remote sensing equipment is suitable for every monitoring project.

2.1 Current Monitoring Methods

The majority of modern surveying and coastal monitoring techniques take advantage of 'non-contact' or remote measuring methodologies. These techniques ensure little disruption to the environment and permit natural processes to be monitored without physical contact by a surveyor. However, there are several factors that need to be taken into account when establishing a suitable monitoring plan.

Remote sensing can monitor large areas at different spatial and temporal resolutions (Klemas, 2015). The remote sensors used can be either ground-based or mounted on aerial platforms or satellites. Consequently, the spatial range and resolution of a technique is generally a function of this variation in altitude or distance. A sensor's spatial resolution is determined by its pixel size. The pixel size equates to the smallest possible feature that can be detected by the sensor. Temporal resolution is dependent upon the frequency with which a site is surveyed. In general, regular low-resolution surveys are achieved with satellite imagery compared with more irregular commissioned ground or aerial based methodologies. However, for all techniques this may be contingent upon the equipment, weather conditions and the availability of skilled labour, which as a result, can mean that vulnerable coastal environments are not frequently surveyed or assessed. Remote sensing over the last two decades has been used to highlight morphodynamic complexities present within the coastal zone (Brooks, Spencer and Christie, 2017). The choice of remote sensing technique is contingent upon the accuracy, coverage and spatial and temporal resolution required from the deployment. However, beyond these parameters there are practical limitations too, such as cost and availability of resources, which may lead to one remote sensing technique being more suitable than another. Furthermore, coastal environments are notoriously difficult to monitor with periods of extreme hydrodynamic activity. As a result, coastal managers and researchers must strike a balance between surveying resolution and quality, budget and the logistical suitability of equipment for coastal recession.

2.1.1 Large-scale Monitoring Techniques

It is possible to achieve large scale (kilometres) coastal coverage with satellite imagery, airborne LiDAR (Light Detection and Ranging), Argus monitoring and CoastSnap.

Satellite imagery has become an effective tool for coastal monitoring such as the extraction of shoreline features (Loos and Niemann, 2002), tracking shoreline change (White and El Asmar, 1999), monitoring coastal ecosystems (Long et al., 2014), inlet migration (Chaumillon et al., 2014) and shoreline recovery (Maiti and Bhattacharya, 2009). However, the large monitoring spatial extent provided by satellites can result in poor image resolution for sub-metre geomorphological change and an uncontrollable survey frequency, making it less useful when trying to monitor directly after a storm

event. In addition, satellite imagery can frequently suffer from the impact of cloud cover meaning data coverage cannot be guaranteed (Long et al., 2016).

Airborne LiDAR has been frequently used in coastal environments for examining the magnitude and spatial distribution of change. The technique is considered to be accurate to decimetre vertical resolution and can cover extensive areas in a single flight (>10 km). For example, Dudzińska-Nowak and Wężyk (2014) used aerial laser scanning to monitor a 2 km section of coastal cliff at Wolin Island, Baltic Sea from 2008-2012. Erosion was calculated at 49,080 m³ over the timeframe and large changes were witnessed due to slope instability. Coastal recession has also been tracked with the technique. Earlie et al. (2013) used airborne LiDAR to monitor the retreat of coastal cliffs and calculate the linear rate of retreat showing the potential for the technique to aid coastal management plans. Pye and Blott (2016) used airborne LiDAR to monitor the impact of storms and storm clusters on coastal dune recession and further recommended an increase in the frequency of airborne LiDAR to aid coastal management plans. Although changes to temporal resolution are more achievable with airborne LiDAR than satellite imagery, the aerial nature of the platform means they are vulnerable to adverse weather conditions and flights can be costly - consequently reducing temporal resolution (Kolzenburg et al., 2016). Furthermore, the nature of aerial data acquisition means that monitoring sites of shoreline retreat or recession only covers horizontal topography and does not provide adequate detail on vertical topography, such as cliff-faces. Consequently, surveys provide long-term topographical changes based on more sporadic survey times rather than continuous data sets which display frequent morphological adaptations.

Video or image monitoring techniques have had less of an input into general surveying deployment than techniques such as LiDAR and satellite imagery. Argus systems and CoastSnap are image-based methods that provide 2D representation of changes at the coast. Argus is a coastal video monitoring system developed by Holman and Stanley (2007) and CoastSnap uses citizen acquired images to track coastal change. Argus uses fixed surveillance cameras mounted on the land to capture images of the beach and near-shore environment. The technique is used for beach monitoring, and recording the movement and processes of waves, tides and currents (Hattori, Sato and Yamanaka, 2019). Argus and CoastSnap both use fixed cameras to estimate the movement of the

sediment across the surf or intertidal zone. These types of systems are advantageous in that they require little surveying input. However, the fixed nature of the cameras means that only pre-determined viewpoints are possible. Therefore, monitoring is only applicable to pre-set points of interest making it difficult to assess coastal change other than in a general sense of beach movement. For this reason, it has been argued that video monitoring does not acquire sufficiently high-precision data to accurately record changes in beach morphology (Abualhin, 2016).

2.1.2 Small-Scale Monitoring Techniques

Coastal researchers and managers also have the option of smaller scale (kilometre to sub-kilometre) topographic coverage. Techniques such as TLS or roving GNSS provide high spatial accuracy (centimetre) (Young, 2015) with a more flexible deployment strategy, making them useful for more frequent surveying than previously mentioned techniques.

Differential Global Positioning Systems (dGPS) and Real-Time Kinematic Global Positioning Systems (RTK-GPS) are generally best suited to small-scale surveying for geomorphology. The techniques have been used to monitor dune topography (Mitasova, Overton and Harmon, 2005) and can be useful for the monitoring of cliff top and base settings (Baptista et al., 2008; Westoby et al., 2018). GNSS systems use satellite configurations to provide geospatial locations through base receivers and roving units. These systems are frequently used for control points when using other surveying methods such as TLS, photogrammetry or aerial LiDAR. The benefits GNSS offer coastal managers are in terms of accuracy, accessibility and versatility. However, this technique is not suitable for continuous monitoring nor able to provide DEMs of sufficient resolution for retreat monitoring. There are also several practical limitations to the use of this equipment. These include surveys being highly labour intensive, particularly for higher density outputs, and the GNSS equipment requires multiple points of physical contact with the surface making it potentially dangerous for surveyors.

TLS, in comparison, has become one of the more favourable techniques for the small-scale monitoring of coastal settings. Over recent years, the TLS has been used for

monitoring of beach-dune sand budgets (Anthony, Vanhee and Ruz, 2006), sand dune topography (Nagihara, Mulligan and Xiong, 2004) and coastal cliff monitoring (Rosser et al., 2013; Letortu et al., 2018; Westoby et al., 2018). The fine resolution and spatially continuous topographic data generated from the TLS means that erosional processes can be successfully analysed. It is particularly useful for detailed monitoring of 'hot-spots' or areas of concern. However, the ground coverage provided by TLS can be restrictive and the equipment complex to operate. Slight impracticalities of TLS equipment, such as internal temperature failure, portability and long surveying periods (James and Robson, 2012), during short tidal windows make it not ideally suited to the dynamic environment of the coast. Access to the foreshore can be limited due to tides therefore restricting the numbers of scans and so impacting survey coverage (Jaud et al., 2017). As with the majority of surveying techniques, weather impacts surveying expeditions. The presence of water in the scanning area can impair surveys due to the backscattering of emitted light (Jaud et al., 2016). Moreover, the technique can also incur very high costs for both the equipment and processing (Westoby et al., 2018) and can be difficult to implement without adequate training. TLS has been considered an industry standard for surveying and monitoring with other surveying results regularly compared to TLS outputs (James and Robson, 2012; Mancini et al., 2013; Nouwakpo, Weltz and McGwire, 2016; Westoby et al., 2018).

The increased variety of remote sensing techniques provides coastal researchers and managers with a range of tools for monitoring coastal change. However, each has specific shortcomings, be it cost, expertise or resolution, that do not make them wholly suitable for monitoring of coastal recession. There is, therefore, a case for alternative methods of monitoring coastal change that are rugged, have good spatial and temporal resolution, are cost effective and can be used routinely by users. However, it would be essential that any such methods were of comparable accuracy to those that have become established as the 'industry standard' (Westoby et al., 2018). The advent of SfM-MVS could achieve some of these criteria.

2.1.3 SfM-MVS for Monitoring

SfM-MVS photogrammetry has become increasingly popular as a method for acquiring topographic information. The technique uses 2D overlapping images to recreate 3D

scene geometry (described in greater detail in Section 2.2). The flexibility of scale and accessible software workflow have resulted in the uptake of the technique in a broad range of disciplines from archaeology (Willis et al., 2016), fluvial geomorphology (Jaud et al., 2016) to glaciology (Vargo et al., 2017).

SfM-MVS can be employed at scales from millimetres to kilometres which results in a variety of platforms and image acquisition procedures. SfM-MVS displays a scale dependent practicality (Smith and Vericat, 2015; Eltner et al., 2016) whereby error can be significantly reduced at smaller scale sites and more pronounced at larger sites. As with other remote sensing techniques, the spatial resolution and associated error, is a function of distance between optical sensor and the surface of the scene; an increase in distance decreases image resolution and so increases the potential for error.

Photogrammetry was traditionally undertaken with aircraft but advances in digital technology, particularly camera size, has allowed a whole range of platforms to be used for SfM-MVS image acquisition. The improved quality and reduction in size and cost of sensors has improved the uptake of the technique. The versatility of SfM-MVS has allowed more traditional platforms, such as kites, to be taken advantage of, as well as more modern developments such as Unmanned Aerial Vehicles (UAVs). In addition, ground-based imagery is used regularly for 3D reconstruction. Image acquisition for SfM-MVS reconstruction requires 'line of sight' and consequently is strongly influenced by the position of deployment which, if located in a poor vantage point, can create occlusions and poor reconstructions (Kolzenburg et al., 2016) which can be particularly problematic for monitoring cliff erosion with vertical planes.

In general, each platform has several advantages and limitations, as described in the following sections, which impacts image resolution, spatial coverage and cost. Table 2.1 displays a variety of platforms plus the advantages and disadvantages of each.

Table 2.1. Summary of platforms used with SfM-MVS for coastal monitoring

Platform	Advantages	Limitations	Examples
Blimps or Balloons	<ul style="list-style-type: none"> - Used at lower altitudes (>500 m) than aircraft & satellites but >UAVs. - Not restricted by regulations. - Allows a variety of cameras. - Low fuel consumption. - Low-cost. 	<ul style="list-style-type: none"> - Intervalometer & gimbal required - Dependent upon weather conditions. Susceptible to high winds common in coastal environments. - Less controllable than other platforms. - Correct overlap and position of camera is difficult to guarantee. - Covers only the specific area they hover over. - Small payload. 	<ul style="list-style-type: none"> - Fonstad et al. (2013) used a 10MP DSLR camera attached to a helium filled blimp to survey approximately 3.6ha of a river channel using a 100m control line in Pedernales Falls State Park in Texas, USA. Comparison with LiDAR showed average deviations of 0.6 m in the z-elevation. - A helium blimp was used with a 16MP DSLR by Johnson et al. (2014) for mapping fault zone topography and generated results 0.41 m similar (90%) to an equivalent LiDAR reconstruction.
Kites	<ul style="list-style-type: none"> - Higher payload than blimps/balloons - Long flight times - Large spatial coverage - Low-cost - No fuel required 	<ul style="list-style-type: none"> - Intervalometer & gimbal required - Impacted by wind and weather conditions – max. wind speed of 8 ms⁻¹ (Conlin, Cohn and Ruggiero, 2018). - Less controllable than other platforms. - Lack of stability can produce blurred images and unstable image acquisition patterns. - Poor temporal resolution due to dynamic weather conditions at the coast. 	<ul style="list-style-type: none"> - Gimenez et al. (2009) used a kite and DSLR to capture vertical and oblique images across a 0.04 km² with the aim of tracking gully morphology. The overall (x, y & z) Root Mean Square Error (RMSE) for the GCPs was 5-16 mm. - Duffy et al. (2018) used a kite and 12.1 MP DSLR to track coastal dune changes over a 12-month period to sub-decimetre accuracy.
UAVs	<ul style="list-style-type: none"> - Autonomous flights & predetermined flights plans maintain forward and lateral overlap. - Reduced risk to user. - Flexible spatial & temporal resolution. - Adjustable sensor settings during flight. - Built-in GNSS - Flight planning software available. 	<ul style="list-style-type: none"> - Expensive. - Short flight endurance (~30 mins). - Requires specialist training to be flown commercially also requires a ‘spotter’ (Westoby et al., 2018). - Altitude restrictions. - Built-in GNSS can be of poor accuracy. - Severely impacts by wind and weather conditions. - Image blur created by UAV vibrations (Dunford et al., 2009; Smith, Carrivick and Quincey, 2016). - Strong legislative restrictions. - Sudden changes in elevation impacts reconstruction quality (Mancini et al., 2013). 	<ul style="list-style-type: none"> - Long et al. (2016) used a fixed wing UAV and 16 MP DSLR to monitor spit formation in a Lagoon-inlet, France and achieved RMSE discrepancies of 100-170 mm. - Jaud et al. (2016) reconstructed mudflats in the Seine Estuary, France using a hexacopter and 12 MP DSLR and achieved ≤100 mm accuracy. - Harwin and Lucieer (2012) surveyed a 70 m coastline in Tasmania using a 12 MP DSLR camera and multi-rotor micro-UAV to achieve sub-decimetre accuracy.

All the platforms in Table 2.1 have a number of advantages and disadvantages. However, the popularity of UAVs with SfM-MVS in geoscience research has increased dramatically in recent years. This is due to the accessibility and improvements in UAV capabilities and a reduction in the size and cost of sensors. There is no doubt that the advancement in UAV technology has advantages. However, as popularity and use has increased, so too have the number of restrictions placed on flights. A major drawback to regular UAV deployments is the restrictive legislation placed upon their use (JNCC, 2019). There has been growing concern over the application of UAVs and their safety. All commercially flown UAVs are now subject to regulations by the Civil Aviation Authority (CAA) in the UK. UAV flight distance, height and proximity to people and buildings are just some of the restrictions placed on their commercial operation. The rules and regulations of flying can seriously impede regular flight plans and, therefore, reduce temporal resolution of monitoring of coastal settings.

However, the least expensive and most flexible option for SfM-MVS image acquisition has been terrestrial or close-range image acquisition. The proximity to the scene provides excellent pixel resolution and image quality. The main disadvantage to this approach is the reduction in spatial extent. However, the addition of non-permanent, moveable masts, poles and booms can improve the cameras vantage point or viewshed and overall perspective.

Terrestrial SfM-MVS has gained increased attention because the flexibility of image acquisition is useful for the different environments seen at the coast. For example, Ružić et al. (2014) used ground-based SfM-MVS to reconstruct 500 m of coastal cliffs and rock undercuts on the Island of Krk, Croatia. A single DSLR camera captured 800 images from various camera heights and angles. The resulting reconstruction provided a 0.7 m deviation from an equivalent RTK-GPS survey. Coastal cliff monitoring was also undertaken by James, Ilic and Ružić (2013) with the reconstruction of 50 m stretch with a hand-held DSLR camera. The point cloud was then compared with a TLS and showed deviations of < 20 mm for much of the cliff face.

The flexibility of terrestrial SfM-MVS can encourage increased temporal resolution as there are fewer restrictions on its deployment. However, the control over camera movement and image overlap is currently less defined. In particular, for a less

experienced user, the broad guidelines on image acquisition and image interaction may be difficult to employ when using a handheld or pole mounted setup. As the restrictions increase for the use of UAVs, particularly in coastal settings, there is an opportunity to provide improved guidance and control over terrestrial image acquisition with SfM-MVS, and in-so-doing, provide a cost effective and high-resolution option.

2.2 Structure-from-Motion Photogrammetry Fundamentals

The SfM method uses a set of algorithms to identify and track features (image observations) across a series of overlapping images captured from different perspectives (Ferreira et al., 2017). The foundations for this methodology were initiated by Marr and Poggio (1976) with the recovery of a 3D scene structure from stereo-pairs through the identification of corresponding features via an iterative cooperative algorithm. Similar to the current SfM process, the algorithm searched for matching points between two images and created a form of 3D depth (Jebara, Azarbajani and Pentland, 1999). Further developments led to feature matching algorithms, such as Scale Invariant Feature Transform (SIFT), that are used to identify and track features across different scales and image resolutions, previously unsuitable in traditional photogrammetry (Fonstad et al., 2013). The inclusion of SIFT in modern SfM allows greater flexibility during image acquisition; in traditional photogrammetry continuous straight lines of overlapping images were essential.

Furthermore, essential calculations to determine internal (e.g. focal length, pixel size) and external (e.g. position and orientation) camera parameters can be conducted without the necessary inclusion of pre-recorded GCPs (Westoby et al., 2012; Micheletti, Chandler and Lane, 2015b). These parameters are now solved through repeated bundle adjustments which aim to minimise error on the image observations and adjust the established tie points and camera parameters accordingly (James, Robson and Smith, 2017). The output from SfM is a set of tie points (sparse point cloud) and estimated camera parameters in an arbitrary coordinate system which reflect prominent features across the observed surface (James and Robson, 2012). However, alone this sparse point cloud provides insufficient detail. Consequently, SfM is used in combination with MVS to increase the density of the point cloud. MVS uses the camera orientations and point positions established by SfM and multiplies the reconstructed tie points by two or three orders of magnitude whilst filtering out noise (James and Robson, 2012).

The incorporation of SfM and MVS into a single workflow has facilitated the development of semi-automated software packages. The availability of commercial (e.g. Agisoft Photoscan; Pix4D) and open-source software (e.g. Bundler with PMVS2; VisualSfM; APERO with MicMAC) has made the technique accessible to both professional and non-expert users. Minor variations in the workflow of these software packages exist due to differences in the underlying code. James and Robson, (2012), Westoby et al. (2012), Fonstad et al. (2013), Micheletti, Chandler and Lane, (2015a), Eltner et al. (2016) have outlined various SfM-MVS workflows but a general workflow is detailed below and in Figure 2.1:

1. *Image alignment is established.* This process identifies, matches and tracks common features across the set of images. The algorithm used for this stage is based on SIFT, which is an ‘image-to-image registration method’, allowing the identification of thousands of common points which are matched and used to create tie points to represent the surveyed surface (Brunier et al., 2016).
2. *Calculation of intrinsic (e.g. principle point, radial distortion, focal length) and extrinsic (position, orientation) camera parameters through a Least Squares Bundle Adjustment.* The geometric image acquisition configuration, parameters of relative motion and the 3D coordinates of a sparse point cloud are reconstructed (Westoby et al., 2012; Eltner et al., 2016).
3. *Densification of the sparse point cloud.* MVS is used to generate high resolution point clouds by multiplying the numbers of points in the cloud. The algorithms simultaneously isolate and remove extreme errors (Micheletti, Chandler and Lane, 2015b).
4. *Generation of a 3D polygonal mesh (geometry) based on the dense point cloud.* The constructed mesh is coloured with the image colours and represents the calculated surface of the surveyed area or object.

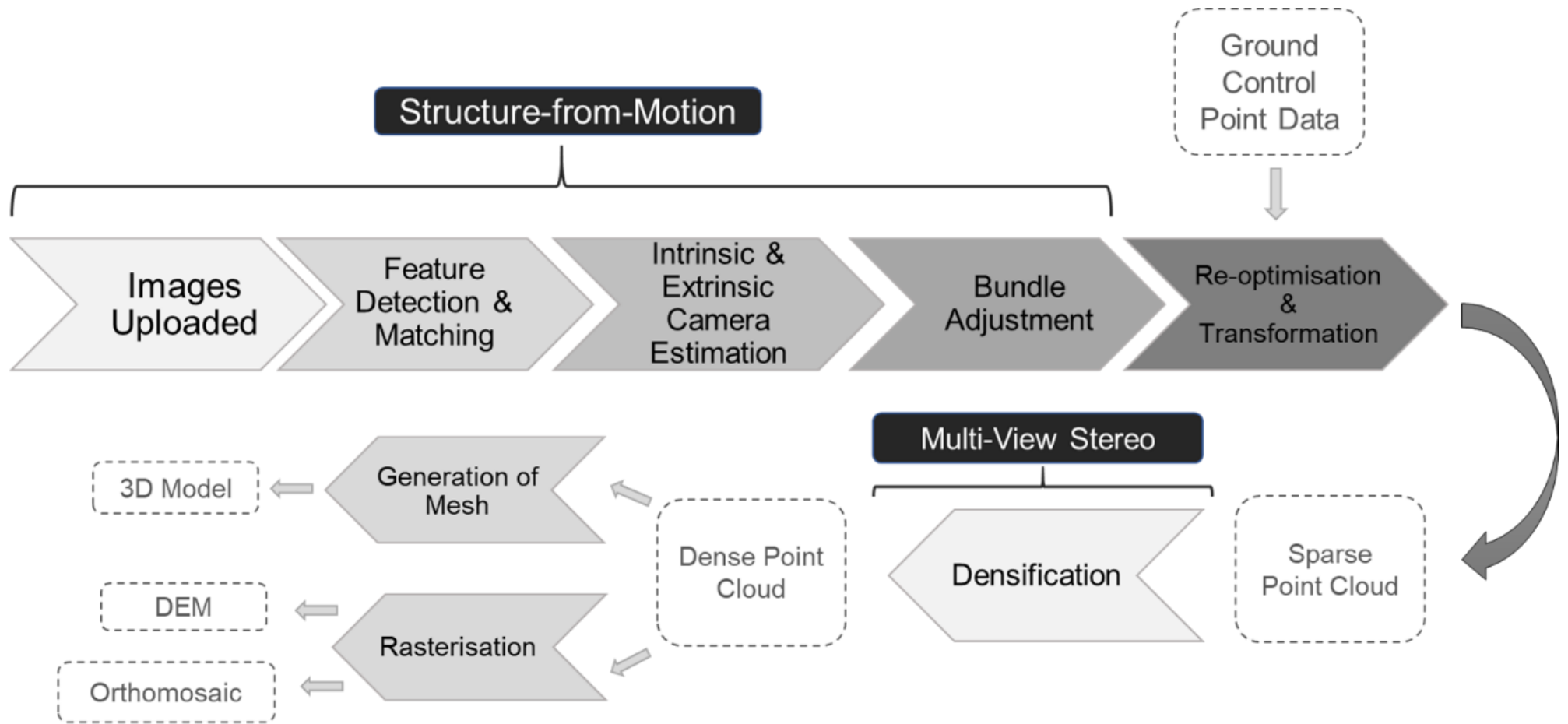


Figure 2.1: General SfM-MVS workflow

2.2.1 Georeferencing & Precision

Georeferencing information (such as GNSS measurements of GCPs) can be included into the reconstruction during the second stage of processing (after the calculation of internal and external camera parameters) or at the end of the workflow. The addition of GCPs provides the point cloud with an external reference source and an absolute coordinate system. Nevertheless, the timing of GCP inclusion is significant to the overall processing. Including precise GCP measurements at an earlier stage can reduce deformation and improve overall reconstruction through the correct estimation of camera position and tie points in the sparse point cloud (Liu and Mason, 2016).

Further research using GCPs in SfM-MVS software has led to the creation of standalone precision estimates which describe the repeatability of measurements within the point cloud (James, Robson and Smith, 2017). The use of GCPs in this way has established two different estimations of precision of the point cloud: internal (the relative distances between points) and external precision (the measured distance e.g. mm between points). External precision includes internal precision estimates and precision of GNSS equipment used for measuring GCPs. If there is a high error from the GNSS this propagates through the workflow and causes the overall precision of the point cloud to be poor when in fact the internal precision created by an appropriate image network could be strong.

Research into the effect of GCP field placement on point cloud reconstruction is beginning to increase in SfM-MVS research. Westoby et al. (2018) varied the number and distribution of GCPs during SfM-MVS surveys of a coastal cliff to define the optimal arrangement when compared to a TLS survey. Their work found that the reconstruction generally improved with an increase in the number of GCPs distributed in the survey. However, the improvement was not linear as the reconstruction did not continue to improve with a higher number of GCPs. Instead, the reconstruction improved when GCPs were distributed at the base of the cliff and on the top (where possible) at a spacing approximately equal to the cliff's height. James and Robson (2012) and James, Robson and Smith (2017) also advocate the importance of a well distributed and precise GCP network. The inclusion of GCPs has the potential to reduce systematic error, to which SfM-MVS can be prone, and improve overall survey precision and accuracy. Systematic error is a product of persistent inaccuracies in camera calibration that cause

camera estimation to 'drift', as a result, DEM doming and deformation are a common outcome. Figure 2.2 displays the appearance of systematic deformation or doming in a SfM surface reconstruction. These forms of systematic error can be caused by the nature of the environment captured, e.g. linear cliff faces, incorrect image capture or incorrect camera calibration.

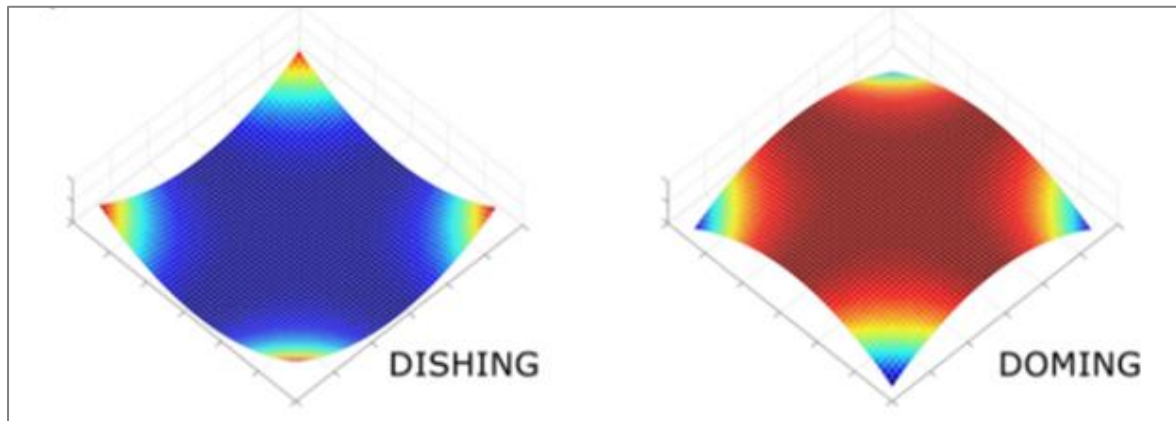


Figure 2.2: Example of SfM surface model distortions as a result systematic error. (Source: Carbonneau & Dietrich, 2017).

The extent to which the placement of GCPs in the processing stage of SfM-MVS affects reconstruction quality is currently under-explored. Furthermore, the extent to which the choice of processing parameters impact reconstruction quality and systematic deformation has gained less academic attention. The optimisation of processing parameters may have the potential to reduce processing times but also aid accurate reconstructions and effectively reduce error.

However, the influence of GCPs and optimised processing parameters is reduced if images are acquired from a poor image network geometry. The influence of image network geometry has the potential to diminish precision despite a strong GCP network. James, Robson and Smith (2017) found the presence of a strong GCP network did not eradicate the presence of deformation caused through poor image network geometry. Therefore, to capture a reliable 3D reconstruction, of suitable completeness and appropriate metric integrity it is essential to capture images in a deliberate and conscientious way (Wessling, Maurer and Krenn-Leeb, 2014) that ensures good internal precision.

2.2.2 Image network

Image network geometry plays a vital role in the creation of an accurate and precise 3D reconstruction. Yet little more than broad outlines for image acquisition are available. The ability to test the accuracy of a point cloud against standardised forms of 3D reconstruction is an important step in verifying the accuracy and overall quality of a point cloud (James and Robson, 2012; Mancini et al., 2013; Nouwakpo, Weltz and McGwire, 2016; Westoby et al., 2018). Moreover, the use of these comparative tests in conjunction with standalone precision estimates allows the influence of image network geometry to be independently assessed.

Traditional photogrammetry required images to be taken near parallel to the scene with approximately ~60% overlap and a series of systematically placed GCPs (James and Robson, 2012). Many of the fundamental aspects of photogrammetry remain the same for SfM-MVS, such as the requirement for overlapping images. However, the degree of overlap between photographs, though still crucial, does not need to be of a parallel nature and the resolution of images can vary (Micheletti, Chandler and Lane, 2015a). Image overlap and redundancy are intrinsically linked, in that, generally, increasing the number of images equates to an increase in the degree of overlap. As a consequence of SfM-MVS flexibility, there are now extra positional camera parameters that can impact 3D reconstruction, beyond simply image overlap and redundancy. All these parameters, such as overlap, height, convergence, obliqueness and number of images (Eltner et al., 2016), impact the strength of the image network geometry and therefore the quality of the reconstruction.

2.2.2.1 Image redundancy

Addressing one of these parameters, Westoby et al. (2012) suggests that a higher volume of images overall allows the technique to produce a more effective reconstruction. Their work implied that the quality of SfM-MVS output is positively associated with the number of images used: more images allow greater optimisation of the number of keypoints or common features identified across the image set. However, the impact of image redundancy is underdeveloped. It has been suggested by Micheletti, Chandler and Lane (2015a) that an increase in images does not linearly increase accuracy. On the contrary, there is the potential that a greater number of poorly

captured images may increase processing and surveying times whilst not effectively improving the quality of the output. Although image acquisition procedure is a site-specific task, understanding the effects of image redundancy on reconstruction may guide users to acquire more appropriately placed images.

Furthermore, capturing a large number of images will require time in the field, which is not always possible, particularly in areas controlled by tidal cycles. Processing of large image sets will also come at a computational cost and, as discussed by Pierrot-Deseilligny and Clery (2012), could potentially overcomplicate processing of the reconstruction.

2.2.2.2 Image Overlap

Similar to image redundancy, image overlap is fundamental to SfM-MVS. The greater the degree of overlap the higher the likelihood of capturing common points across the image set (Stumpf et al., 2015). The degree of image overlap has previously been suggested at approximately 60% (James and Robson, 2012). Moreover, Westoby et al. (2018) advocate high degrees of image overlap for an appropriate image acquisition. However, as image redundancy and overlap generally correlate, an increase in image overlap would necessitate an increase in the number of images. However, the impact of wider-angle lens cameras on optimal image overlap is under-explored. As a result, the idea of wider-angle lens cameras is an intriguing one, potentially having the capability to acquire fewer images of the scene but still provide an effective overlap between images.

2.2.2.3 Image Obliqueness and Convergence

Obliqueness and convergence are important considerations for improving the image network geometry and reducing the potential for error within the point clouds. Obliqueness is defined as the declination of the camera from the z-axis (Figure 2.3a). Convergence is the angle at which the camera is positioned around the scene or object (Figure 2.3b). An increase in both obliqueness and camera convergence has the potential to improve 3D reconstruction. Warrick et al. (2017) described how oblique imagery is also beneficial for mapping cliff environments as it gains data on vertical sections of the scene which are generally poorly resolved with airborne platforms. James and Robson (2014) have discussed the improvements to reconstruction with

inclusion of convergent or oblique imagery for both aerial and terrestrial image acquisitions. The study documented a one to two order of magnitude reduction in DEM deformation when using oblique imagery during UAV flights. Micheletti, Chandler and Lane (2015b) and Nouwakpo, Weltz and McGwire (2016) also highlighted the impact of improved oblique imagery on reconstructions.

However, there is also the potential for 'over-complicating' the image network and providing the software with apparently contradictory information (Pierrot-Deseilligny and Clery, 2012; Eltner et al., 2016) which could lead to long processing times for poorly constructed point clouds. The angle of obliqueness is generally site-specific but understanding its potential impact is valuable for all image acquisition schemes. Stumpf et al. (2015) suggested an 'angle of incidence' from the object of interest of $< 30^\circ$ to provide a suitability oblique view. However, in practice this would be difficult to guarantee, replicate and maintain with a camera and a large-scale image acquisition.

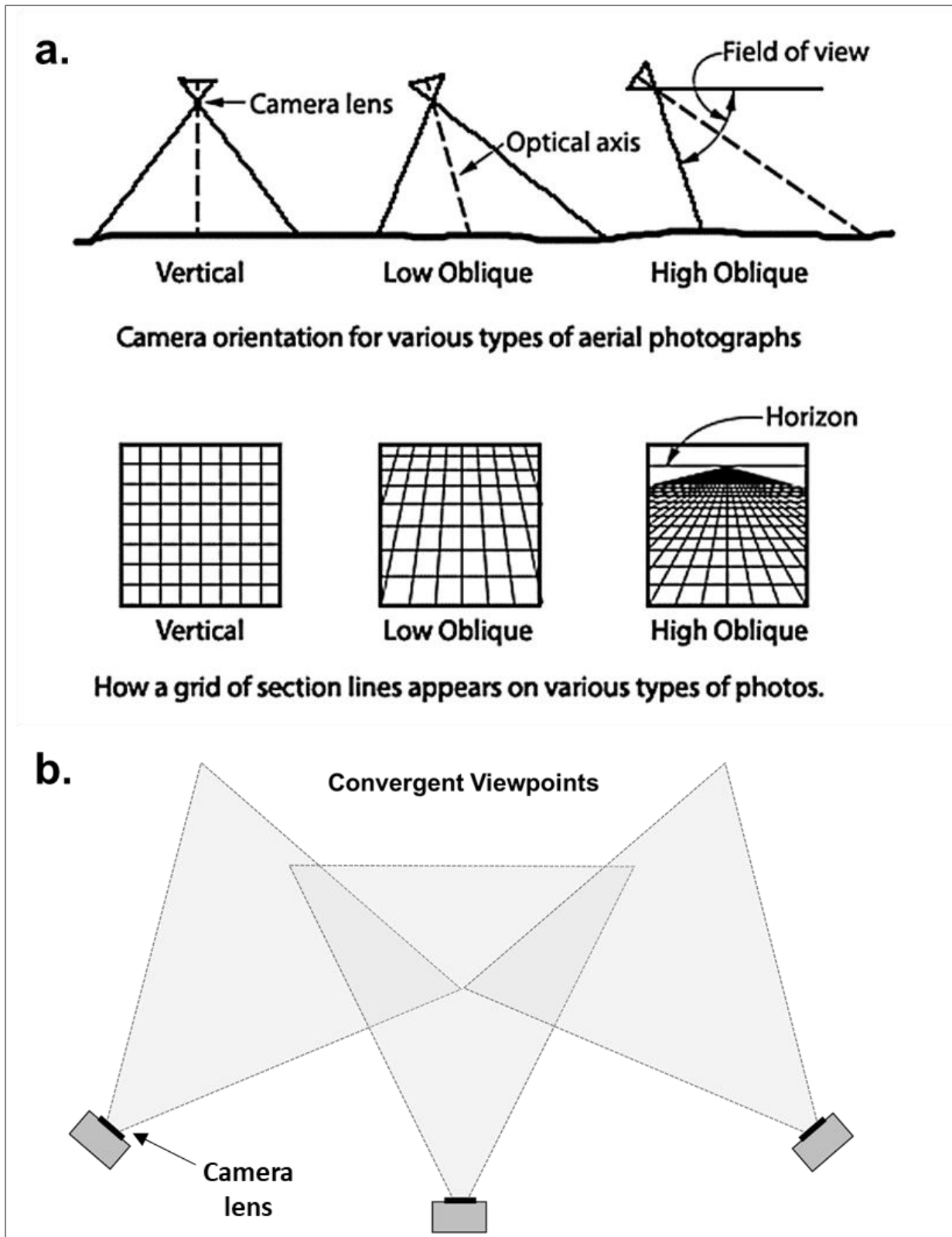


Figure 2.3: a) The effect of camera obliqueness on image acquisition. Source: Wolf & DeWitt (2000) b) Aerial view of camera orientation for convergent imagery.

2.2.2.4 Image Acquisition Schemes

Currently, research within the field provides broad rules for the acquisition of images suitable for SfM-MVS. These current SfM-MVS guidelines are more easily achieved with a UAV system due to flight planning software but using a handheld terrestrial image acquisition it can be difficult to guarantee appropriate scene coverage.

Consequently, several important questions about terrestrial image acquisition cannot be fully answered. How can it be guaranteed that images are interacting suitably to produce a quality point cloud, particularly when the advice is to capture as many images as possible? How can their interaction be understood and guaranteed in terms of overlap and obliqueness? How can the image network geometry be strengthened and maintained by changes to the camera position?

Pre-determination of the image network, based on multiple cameras, would not only determine the overlap, height, obliqueness and, therefore, image interaction beforehand but also potentially speed up image acquisition. This form of image acquisition could provide users with specific guidelines to follow effectively and streamline computational processing.

The ability to acquire multiple images simultaneously with known interaction would be advantageous. However, the degree to which optimised camera positions may reduce the number of images required for a multi-camera setup is currently under-researched. James and Robson (2014) successfully used stereo pairs with DSLR cameras to reconstruct advancing lava flows with intervalometers. Experimentation with multiple cameras, three in total, has been undertaken by Eltner et al. (2017) for the purposes of monitoring soil erosion after rainfall events with a time-lapse camera setup (Figure 2.4). Although, this work has produced many encouraging findings, the paper also identified the necessity for further research on the significance of camera position and setup.



Figure 2.4: Image acquisition using three fixed cameras to monitor soil erosion after rainfall events. Source: Eltner et al. (2017).

Eltner et al. (2017) found the quality of the point cloud across the plot diminished as distance from the sensor increased. The standard deviation of distance when compared to an SfM-MVS UAV point cloud ranged from 6-10 mm accuracy over a spatial area of 4 x 5 m. However, the research did not address the coverage of points or completeness across the reconstruction. Occlusions have a large impact on point cloud completeness; the completeness is the number of holes present within the point cloud. The authors noted that completeness and accuracy decreased with increasing distance from the cameras but did not take into account completeness in the overall assessment of point cloud reconstruction.

With more diligent and precise camera positioning and specific understanding of the significant effect image redundancy can have on point cloud quality, this result could potentially have been improved. The ability to simultaneously acquire images from a fixed array of multiple cameras would be advantageous – ideally with cameras set in positions to maximise efficacy.

The use of a multiple fixed camera array contrasts with other SfM-MVS research (Table 2.1) where single cameras are commonly used for image acquisition. Current best

practice for SfM-MVS is to acquire many images at multiple angles around the subject (Micheletti, Chandler and Lane, 2015b). However, how significantly would reducing the number of images affect the quality of the model output - particularly if camera position and orientation were optimised? Could the number of images acquired be reduced significantly? These overlooked questions are of significant consideration for the use of terrestrial SfM-MVS.

A reduced number of higher quality images over a larger quantity of less ideal images could not only reduce fieldwork but also allow fixed cameras to be used in monitoring. However, to truly make this approach a possibility, it is first necessary to understand the significance of camera placement in relation to the scene. Optimal camera placement would result in a simplification of image capture geometry and would entail fuller scrutiny of the combined effect of the previously mentioned positional parameters (beyond simply number of images) that effect image suitability: overlap, obliqueness and convergence (Eltner et al., 2016).

The above review has highlighted some fundamental gaps in current SfM-MVS image acquisition practicalities, as well as revealing the potential benefits of streamlining both image acquisition and processing to provide more effective reconstructions with less images. Multiple cameras with predetermined camera movements could provide fast terrestrial image acquisition. Furthermore, the impact of image interaction on point cloud quality could also be investigated to improve 3D reconstruction quality. Streamlining image acquisition and processing parameters could provide a more rapid, but still metrically sound, 3D reconstruction which may help to increase the likelihood and frequency of surveys by coastal managers and researchers.

2.2.3 Optical Sensors

The choice of camera for a multi-camera system is critically important. DSLR cameras have a number of qualities that make them useful for SfM-MVS research. Generally, they produce high resolution images due to large sensors containing large photosites (pixels on the sensor) and so an improved measurement of photons. Pixel number alone does not provide information on the sensor size. A combination of large sensor and high pixel density is considered to provide better quality images (Eltner et al., 2016) which is advantageous for the identification of features and creation of tie points in SfM-MVS.

Furthermore, a fixed focal length is required (Shortis et al., 2006; Micheletti, Chandler and Lane, 2015b) to ensure effective tracking of these features across the image set. The focal length is determined by the physical distance between the optical centre of the lens and the camera sensor. In DSLR cameras this is variable meaning it must be fixed before SfM-MVS image acquisition.

However, for a wider Field of View (FOV) than a standard DSLR camera, it is necessary to use a lens that shortens this focal length significantly. Wider angle lenses, such as a fisheye lens, have an Angle of View (AOV) up to 180°. The value of the AOV describes the angular extent of the camera's view and is a function of the sensor size and the lens type. A camera's AOV is provided in vertical, horizontal and diagonal planes by the manufacturer. Knowledge of a camera's AOV is also essential for the predetermination of image interaction and estimation of the camera's FOV or 'footprint'. However, as AOV increases up to 180°, radial distortion impacts the images. Straight lines appear to be curved, as light is bent onto the surface of the sensor by the lens. The further away from the optical centre or principle point of the camera, the greater the impact of distortion. Although wide angle lenses deviate from the standard rectilinear projection for SfM-MVS this may be recompensed by the increased scene coverage provided by the wider AOV.

Fisheye lens cameras were previously considered unsuitable for creating 3D models with accurate metric integrity (Perfetti, Polari and Fassi, 2017) due to the radial distortion created by the wide AOV. However, advancements in image processing has meant that distortion can be reduced or completely removed through the rectification of images. The increased use of action cameras with platforms such as UAVs means that many photogrammetric software packages now offer lens distortion correction or remapping. The availability of these rectification processes in software is a clear indication of the increased use of wider AOV cameras with photogrammetric applications (Perfetti, Polari and Fassi, 2017). Research outside geomorphology, such as in Ballarin, Balletti and Guerra (2015) and Hastedt, Ekkel and Luhmann (2016) in the fields of archaeology and remote sensing have successfully used fisheye lenses with SfM-MVS.

However, the extent of correction required to point clouds is under-explored. How can software parameters be used in order to aid or minimise the distortion present? What

guidelines could be suggested specifically for sites of landward retreat with a very parallel image acquisition? These are essential considerations when using cameras with inherent distortion.

In terms of a multi-camera setup with fixed camera positions, there are several physical advantages action cameras hold over the conventional DSLR. Action cameras offer an accessible, easily operable, manoeuvrable, and rugged alternative. In addition, GoPro action cameras offer the option for wireless multi-camera synchronisation – a significant advantage for a camera array. DSLR cameras, in contrast would not provide as practical a setup due to weight, power, lack of robustness and sensitivity to environmental conditions such as windblown debris. The synchronisation of DSLR cameras is more difficult owing to the use of intervalometers instead of wifi synchronisation.

As the popularity of action cameras with photogrammetry increases, the capability of these cameras in SfM-MVS needs to be established for coastal monitoring. It is, therefore, essential to understand how the impact of distortion can be minimised in software in order to take full advantage of these cameras and what level of reconstruction quality could be achieved if these images were gathered using an optimal image network with streamlined processing adapted to the camera type. These questions highlight some of the potential advances and improvements that could be made to SfM-MVS image acquisition and processing to aid users.

This chapter has highlighted some of the current limitations within coastal monitoring and SfM-MVS research and indicated the potential benefit of multi-camera arrays for monitoring coastal recession. However, this application of SfM-MVS has raised several research questions on which there is little current literature. First, little is known on the impact of camera position on reconstruction and how this may diminish with the number of images required. Second, further research is required on the positioning of cameras to guarantee image interaction during terrestrial image acquisition. Third, there are limited examples of the ability to directly control camera movement. Fourth, the literature has revealed little testing of SfM-MVS with action cameras and whether there is potential for them to provide reconstructions with accurate metric integrity. Finally, further research is needed on the level of influence software parameter choice has on overall reconstruction and deformation.

3. Research Methodology

The limitations in current surveying outlined in the previous chapter highlighted the need for an alternative method of monitoring coastal change that is rugged, has the potential for good temporal and spatial resolution, is cost-effective and can be routinely deployed. Such an advance could potentially be achieved through the use of SfM-MVS and multiple cameras for simultaneously acquiring images - ideally with cameras set in fixed positions to maximise efficacy.

This chapter contains an overview of the methods used in the three subsequent journal style chapters (4, 5 and 6). The published article (Chapter 4) required much of the methodological description to be included in an appendix. To aid clarity, information in this appendix has been modified and included in this methods chapter (Chapter 3). Furthermore, an overview of the methodology from the two subsequent journal style chapters (5 and 6) has also been included. Reference has been made to the relevant chapter so there is not excessive repetition between this chapter and the methodology sections contained in Chapters 5 and 6.

3.1 Overall Methodology

The overall aim of this research was to design and implement a multi-camera rig with GoPro action cameras for coastal monitoring. The purpose of which was to provide a streamlined workflow for users to systematically monitor small-scale sites of landward retreat with SfM-MVS. The first stage of this workflow was to establish optimal camera positions, in terms of height, obliqueness and overlap. The optimal positions were then used to create a multi-camera rig which was tested and used to monitor coastal recession. Therefore, the research followed the three main steps depicted in Figure 3.1:

1. An essential step was to control and vary camera parameters (height, obliqueness and overlap) during image acquisition. Based on the images gathered, the impact of these parameters was assessed against an industry standard measure (TLS) and an independent assessment of precision. The first requirement was the development of a camera grid that could control camera movement. From there, the impact of a changing camera position was tested in relation to the quality of the subsequent reconstruction.

The camera grid was deployed at a site of landward retreat. After which, a systematic process of assessment was used to evaluate the performance of each created point cloud, and from there the most suitable camera positions for a multi-camera array.

2. Once the optimal camera positions were established, a roving multi-camera rig was designed and constructed for the purposes of acquiring images at small-scale areas of landward retreat. The rig was tested at three sites of landward retreat. The images were processed using varying software parameters and the reconstruction quality tested against the TLS and an independent measure of precision. Subsequent point clouds were assessed in terms of output quality and processing duration.

3. Once the reconstruction quality of the camera rig was established, the rig was used to monitor morphological changes over a 4-month winter period at a site of coastal recession. The morphological changes were tracked and evaluated against wave hydrodynamics and meteorological conditions at the site during a dynamic winter season. Estimates were made of volumetric and area loss, and a novel method developed to quantify undercutting, to provide information on the rates of erosion at the site.

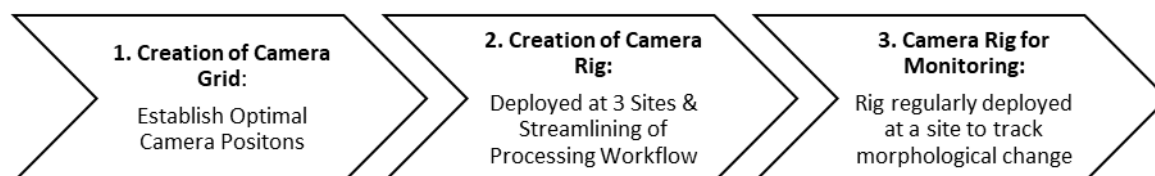


Figure 3.1: Depiction of the workflow of research

3.2 Study Sites

The three stages of research required deployment locations of actively eroding coastal cliff forms. Consequently, Crosby, Thurstaston, Silverdale – NW England were used for deployment, testing and research development due to the presence of active erosion.

The three sites were used in different stages of the research project. Crosby was used in Stages 1 and 2, Thurstaston in Stage 2 and Silverdale in Stages 2 and 3 (Figure 3.1). Each of the deployment locations are described in the following sub-sections.

3.2.1 Crosby

Crosby is located on the Sefton Coast in North-West England, UK. Situated north of the Mersey Estuary and south of the Ribble Estuary in Liverpool Bay. The Sefton coastline extends for approximately 36 km and is influenced by the processes occurring in the Irish Sea and the adjacent estuaries (Dissanayake et al., 2014). The coastline is susceptible to some of the highest surge conditions in the UK owing to the shallow nature of the north-eastern Irish Sea. The surveyed site is within a macro-tidal environment with a mean spring tidal range of 8 m (Gladstone Dock tide gauge). Local waves are generated by dominant west and north-westerly winds (Plater and Grenville, 2010). The tidal regime of the Irish Sea and the natural orientation of the coast in relation to the prevailing winds has resulted in complex coastal processes that influence the Sefton coastline.

The Mersey estuary was a natural geological fault that was deepened by the progress of the Irish sea ice sheet and flooded during the last ice age. The underlying stratigraphy is glacial till variably overlain by peat and dune sand up to 2.5 m thick (Plater et al., 2010). Anthropogenic interventions have subsequently affected the dynamics and capacity of the estuary. From 19th century onwards significant modifications have been made to the channel and bay area such as dredging and dumping of material, land reclamation, developments of Liverpool Docks and training wall construction to prevent channel migration (Halcrow, 2013). As a result of consistent modifications, the Sefton coastline has been vastly altered to accommodate human activities and has consequently suffered from large-scale morphological change.

The study site surveyed has previously suffered dramatic lateral recession during the 20th century due to sand shifting southwards from Formby Point and causing the mouth of the River Alt to migrate South-East. The fixed dune environment, consisting of well-sorted fine to medium quartz sand (Plater and Grenville, 2010) and mature dune grasses and shrubs, was eroded due to the river channel migration allowing waves to encroach on the terrestrial land behind. Consequently, rubble was dumped from Liverpool bombing raids in 1946 to bolster defences against coastal recession. The rubble, consisting mostly of brick, has since been smoothed and sorted due to continued wave action. However, whilst the rubble previously provided a level of protection,

deprived of sediment deposition the wave and storm action has continued the landward retreat causing a cliff formation of approximately 1.5 m.

The Crosby site is used in Stages 1 and 2 of the research (Figure 3.1). Stage one uses a ~7 m long stretch of coastal cliff (~1.5 m in height) for the application of the camera grid. A longer stretch (~27 m) of cliff is used in Stage two of the research (Figure 3.1) for the application of the camera rig.

3.2.2 Thurstaston

Thurstaston is located on the west-side of the Wirral Peninsula, North West England in the Dee Estuary. The Dee is a high energy, shallow, macro-tidal environment with strong currents and a tidal range of 7.7 m (Gladstone Dock Tide Gauge) (Halcrow, 2013). The estuary was previously a valley formation cut by the presence of the Dee river which was flooded during the last ice age. The estuary is approximately 30 km in length (a reduction from 35-40 km) due to drastic human canalisation and land reclamation during the 18th century. The alterations to the estuary caused the channel to migrate to the Welsh shore increasing saltmarsh development along the English shore (Moore et al., 2009). The position of the Dee channel continues to be dynamic and the prediction of its potential movement is difficult. The channel continues to migrate across the estuary heavily impacting the shoreline through deposition and erosion of sediment.

The Thurstaston cliffs range from ~10 to 1 m and are bordered by saltmarshes to the south-east and 'Caldy Blacks' sandflats to the north-west. The underlying superficial sediments consist of alluvial deposits of sand, silt and clay underlain by a sedimentary sandstone bedrock (BGS, 2020). The cliff faces are unvegetated, but the lower levels are sparsely covered by pioneer grass species. The majority of the Wirral coastline is defended by varying forms of coastal engineering such as rock revetments. However, the Thurstaston cliffs remain undefended and erode in response to tidal currents and constructive waves breaking against the sandstone and boulder clay cliff base during storms (Halcrow, 2017). Furthermore, drainage pipes located within the cliffs saturate the sediment leading to a weakening of the cliff face and increased risk of collapse. The Thurstaston cliffs are expected to erode further as the current Shoreline Management

Plan for the area is 'No Active Intervention' with an expected 10 m retreat distance at the 95th percentile (medium term – 20 years) (Environment Agency, 2019b).

The study site is a lower cliff platform (~1 m) with a less steep cliff front. The site has had heavy vehicle use by the local sailing club and has experienced progressive retreat over recent decades. The area is very lightly vegetated along the cliff top with coastal grasses.

3.2.3 Silverdale

Silverdale is located on the North West coast of England, near the border between the counties of Cumbria and Lancashire. Situated in Morecambe Bay, Silverdale saltmarsh is influenced by sedimentary processes occurring in the Morecambe Bay estuary and those from the River Kent (north of the site) and River Keer (south) which drain into Morecambe Bay. The estuary is a very shallow, macro-tidal environment with a spring tidal range of 9 m (JNCC, 2020). The geology of the area is Carboniferous limestone deposited approximately 300 million years ago which shows evidence of glacial and post-glacial processes and forms the basis of the ecosystems present at Silverdale (Askew and Skelcher, 2014). The coastal edges are dominated by intertidal foreshores which contain mudflats and saltmarshes surrounded by low limestone cliffs (Natural England, 2015). The main sediment supply is from Morecambe Bay and the Irish sea which have a high load of suspended sediment. However, there is smaller sediment supply from the erosion and redistribution of saltmarsh sediment. The redistribution of sediment is triggered by the strong tidal cycles causing meandering channels that encroach onto saltmarsh margins (Halcrow, 2013).

The Silverdale saltmarsh is situated on the north-east shore of the River Kent estuary. Silverdale and the adjoining Arnside were classified as an 'Area of Outstanding Natural Beauty' in 1972. The surveyed site is an upper-marsh environment and therefore is occupied by grassland vegetation which would previously have been grazed. The site has suffered from cycles of sediment erosion and accretion, cutting away at the saltmarsh edge and causing 'coastal narrowing' (Pringle, 1995). These processes are caused by an intricate system of sediment circulation and deposition based upon the tidal regime of the Irish Sea interacting with estuarine sediment pathways (Arnside & Silverdale AONB Partnership, 2015). Erosion has been driven by the position of the

River Kent main channel. The closer position of the Kent channel to the Silverdale saltmarsh facilitates erosion as larger waves encroach on the land. Significant lateral erosion was experienced at the saltmarsh historically but sediment deposition in Morecambe Bay developed a sandbank protecting the saltmarsh from the worst tidal waves. In 1967 the Silverdale saltmarsh covered an area of 244 ha but a phase of rapid erosion in the 1970s left only 40 ha by the 1990s (Pringle, 1995). Unless a drastic movement in the River Kent channel occurs, the saltmarsh will continue to be exposed to erosion (Arnside & Silverdale AONB Partnership, 2015).

The management plan for this area is conservation with the restoration of saltmarsh encouraged (Cumbria County Council, 2011). The current shoreline management plan for the area directly behind the saltmarsh is 'No Active Intervention' and the coastline is considered 'Erodible' with 'Natural' defences (Environment Agency, 2019b). The natural defence would be the saltmarsh but with the progressive erosion of the site it will make the current coastline increasingly susceptible to erosion.

The study site is ~30 m section of Silverdale saltmarsh cliff margin at ~ 1 m in height. The site is an upper-marsh profile containing mature saltmarsh grasses which has and continues to suffer from significant erosion.

3.3 Methodology for Stage 1 of Research - Camera Grid

This section provides an overview of the methodological approach applied to establish optimal camera locations (height, obliqueness and overlap) for a multi-camera setup. Further details can be found in Chapter Four (Godfrey et al., 2020).

The streamlining of image acquisition requires optimised camera positions. Consequently, it was essential to examine the impact of a changing image network on 3D reconstruction, and from there establish idealised camera locations. To determine the combined effect of camera height, obliqueness and overlap on reconstruction, a systematic and controlled approach to image acquisition was necessary. A systematic image acquisition necessitated a camera setup that could be adjusted to change and control camera movement. The point clouds generated from these changing camera positions were compared against a TLS to confirm optimal locations.

Therefore, this section describes the methods used to determine and construct a camera grid that allowed controlled camera movement without the impact of human error or

environmental conditions. The camera grid was designed and built for an initial test at Crosby, NW England.

3.3.1 Camera Grid Design

The grid allowed the camera to be moved across a set of referenced grid squares and an image captured in each. This approach meant images could be effectively catalogued and the number of images systematically reduced to test image redundancy (Figure 3.2). The positional variables used in the setup were: camera height, obliqueness and overlap. Therefore, it was essential these parameters could be adjusted in relation to the scene. The camera position was easily adjusted in all three parameters (height, obliqueness and overlap) whilst maintaining no rotational movement of the camera in relation to the grid itself.

The height parameter was examined using two elevations of the camera grid and a series of rows at each of these elevations (Figure 3.2). The size of the GoPro camera meant the baseline between images could be very small (~ 0.11 m) resulting in a maximum of $\sim 99\%$ image overlap. Obliqueness angle (declination from the z-axis) was estimated prior to deployment and was based on a modelled scenario which provided the most appropriate view of the scene (Section 3.3.2). The camera mounts held the cameras oblique position at a specified angle, either 0° , 30° or 40° declination (details provided in Section 3.3.2).

The grid had fifteen rows and nine columns. The size of the grid was chosen to represent an array of cameras that could be a practical camera setup when developing a camera rig. In other words, the camera grid had to be a practical size so when optimal camera positions were established, they were already within the manoeuvrable dimensions for a camera rig. A traveller was used to move the camera across the grid face whilst maintaining the x , y & z optical camera axes (Figure 3.3). Levelling the platform was essential to guarantee the impact of the tested parameters, therefore, a base was created. Two tripods were used to increase the height of the camera grid accordingly and props used to maintain its z -axis (Figure 3.4). The grid had a 2 m stand-off distance from the cliff which was held constant throughout image acquisition.

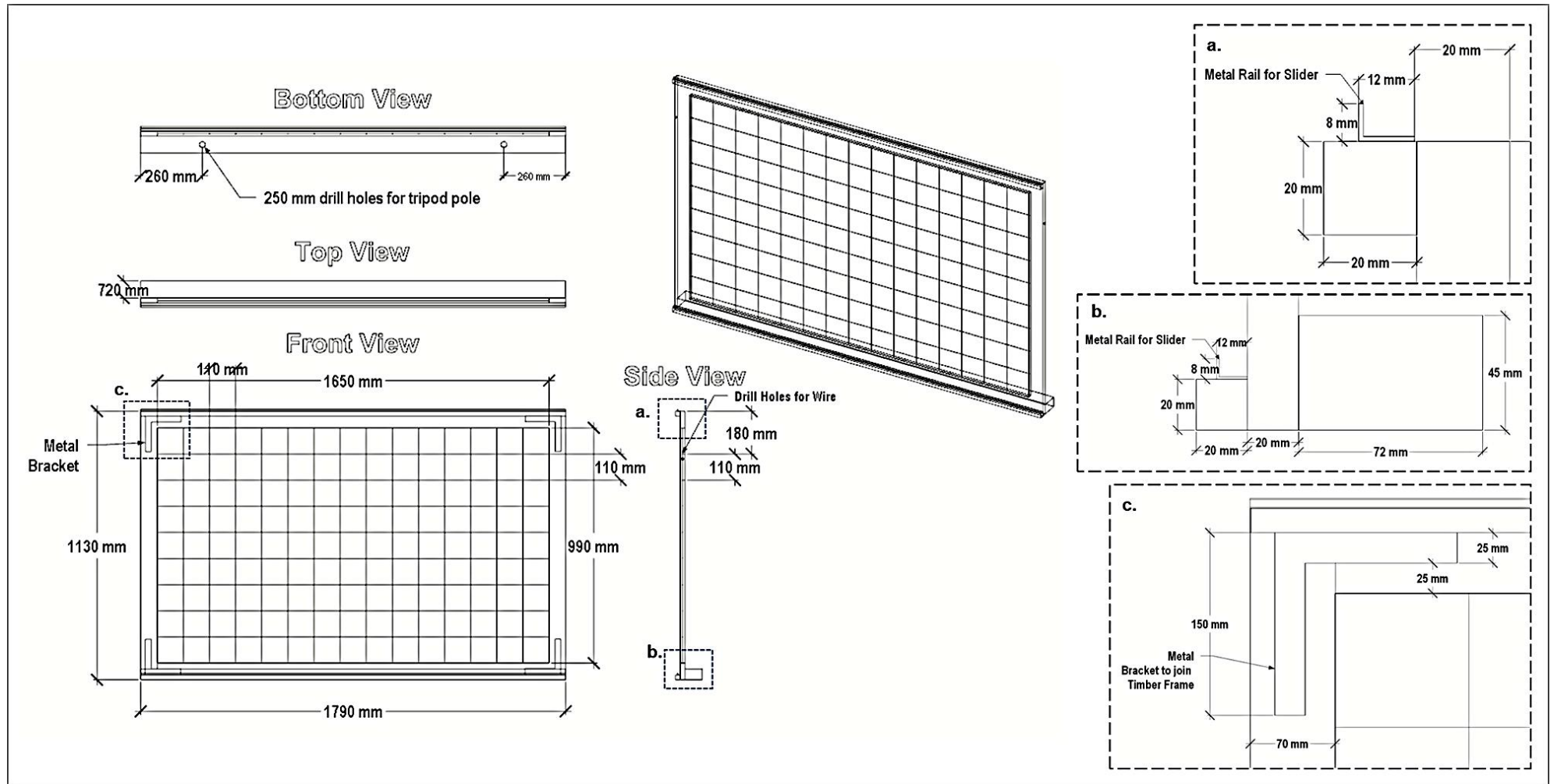


Figure 3.2: Technical drawing of the Camera Grid. The internal dimensions of the grid frame were 0.99 m in height and 1.65 m in length. The frame was constructed with fifteen, 0.11 m horizontal grid squares (columns) and nine 0.11 m vertical grid squares (rows). The grid size of 0.11 x 0.11 m was chosen to accommodate the camera's dimensions.

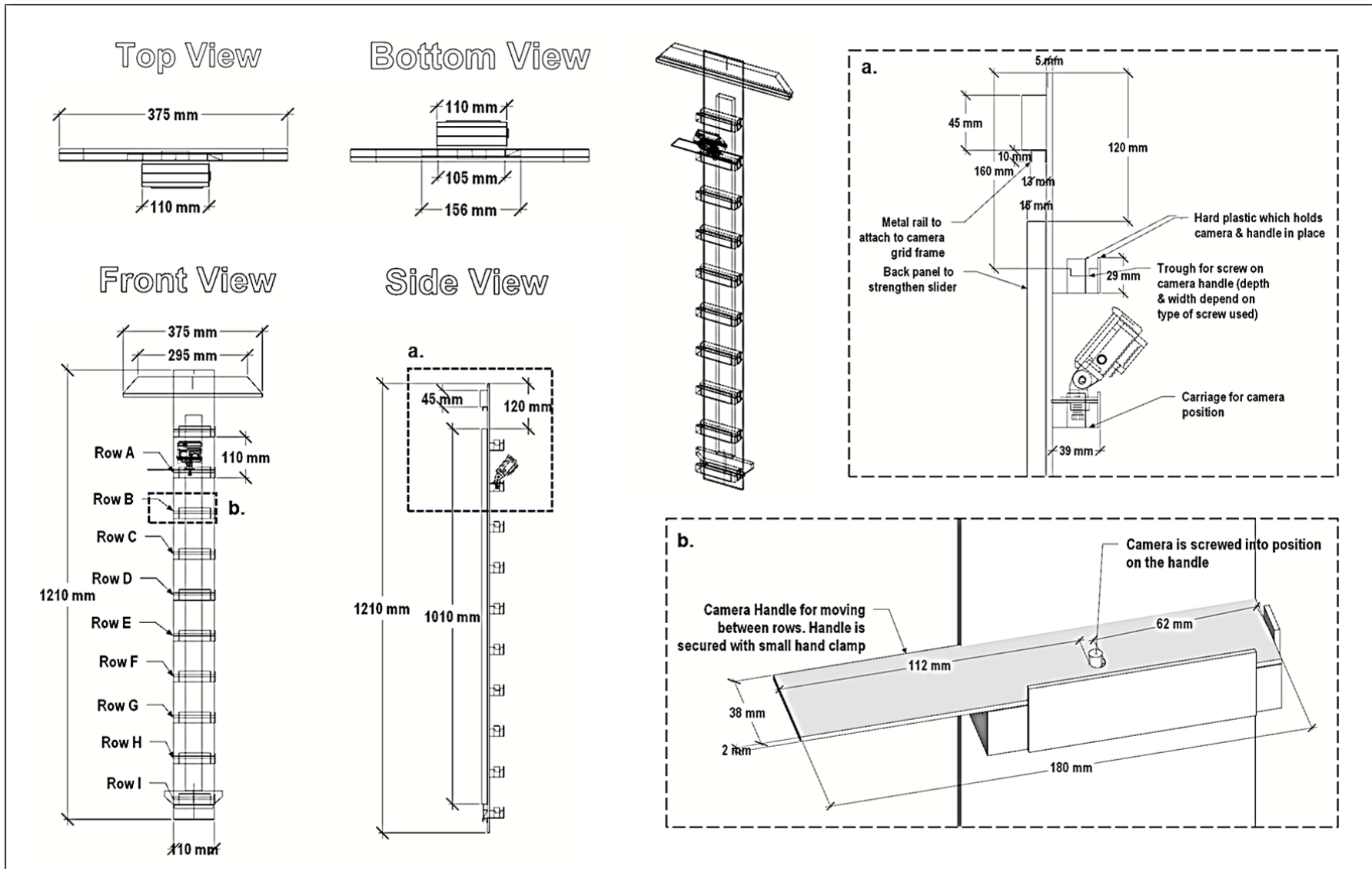


Figure 3.3: Technical drawing of the 'traveller' used for camera movement across the grid.

Exploring the use of a Multi-Camera Platform for 3D Reconstruction

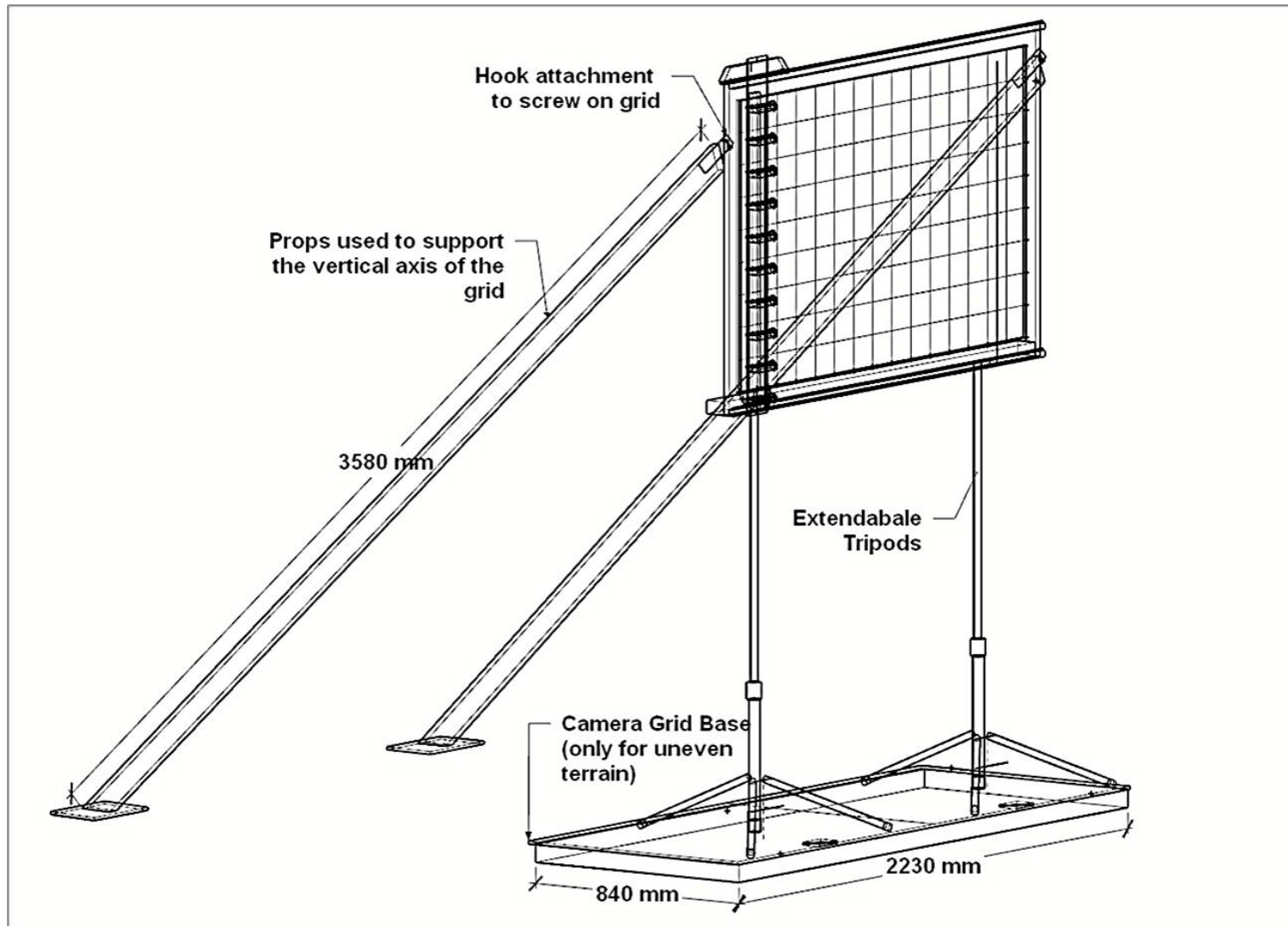


Figure 3.4: Technical drawing of full camera grid setup ('Height 2') including timber base platform needed for uneven terrain and timber prop attachments to maintain the z-axis of the grid. The base platform would not be necessary at a site of even terrain.

3.3.2 Initial Site Representation

Prior to deployment, it was essential the camera's FOV provided appropriate coverage of the scene. Therefore, the angle of obliqueness was estimated beforehand based on a 3D model representation of the site (Figures 3.5 & 3.6). The GoPro's FOV was modelled in SketchUp Pro 2018 (v. 18.0.16975) software using a hypothetical estimate of the camera's potential footprint (Equation 1). Hypothetical vertical (H_v) and horizontal (H_h) FOVs were estimated based on the GoPro AOV specifications: 122.6° horizontal (AOV_h) and 94.4° vertical (AOV_v). These values were used in Equation 1 to estimate potential FOV or 'footprint' of the camera, where D is the desired FOV distance (m):

$$(1) \quad H_v = 2DTan\left(\frac{AOV_v}{2}\right)$$

These estimations of camera FOV were then modelled in SketchUp to provide a visual representation of the camera's view (Figure 3.5). The modelled FOV was then used in conjunction with the modelled camera grid to simulate potential scene coverage (Figure 3.6). The model was used to estimate potential angle changes at each height variation of the grid i.e., movement of the camera from one row to the next.

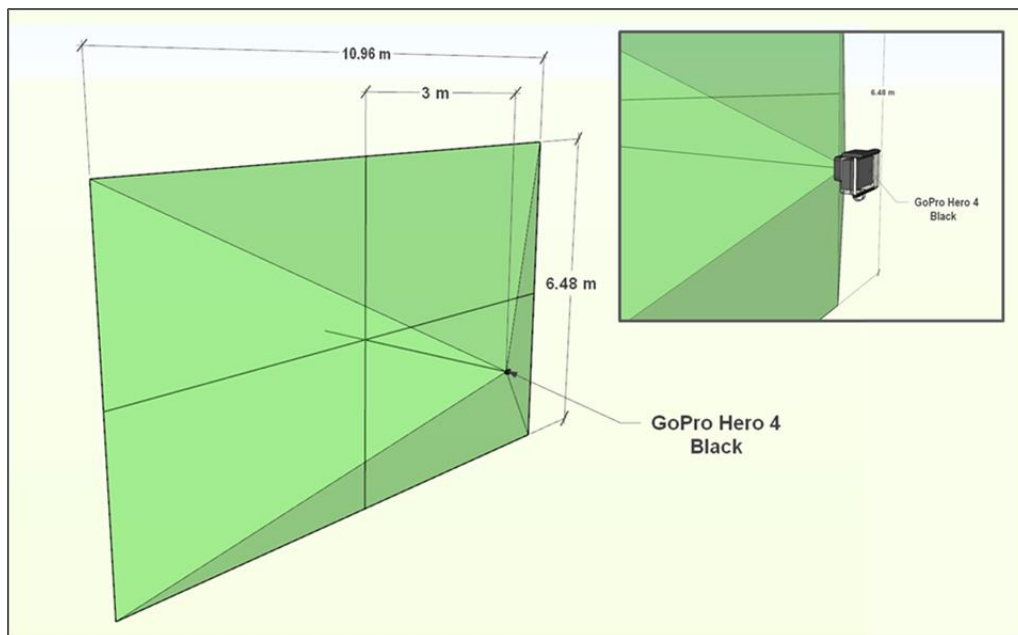


Figure 3.5: GoPro Hero 4 Black FOV representation modelled in SketchUp. Calculation incorporated a 3 m distance FOV.

The simulated model displayed where the FOV could potentially interact with the cliff front and the equipment (Figure 3.6). This estimation is of particular importance for fixed multi-camera arrays as the cameras are stationary making it essential that any equipment (e.g., cameras or grid) would not encroach on the images whilst still offering effective scene coverage.

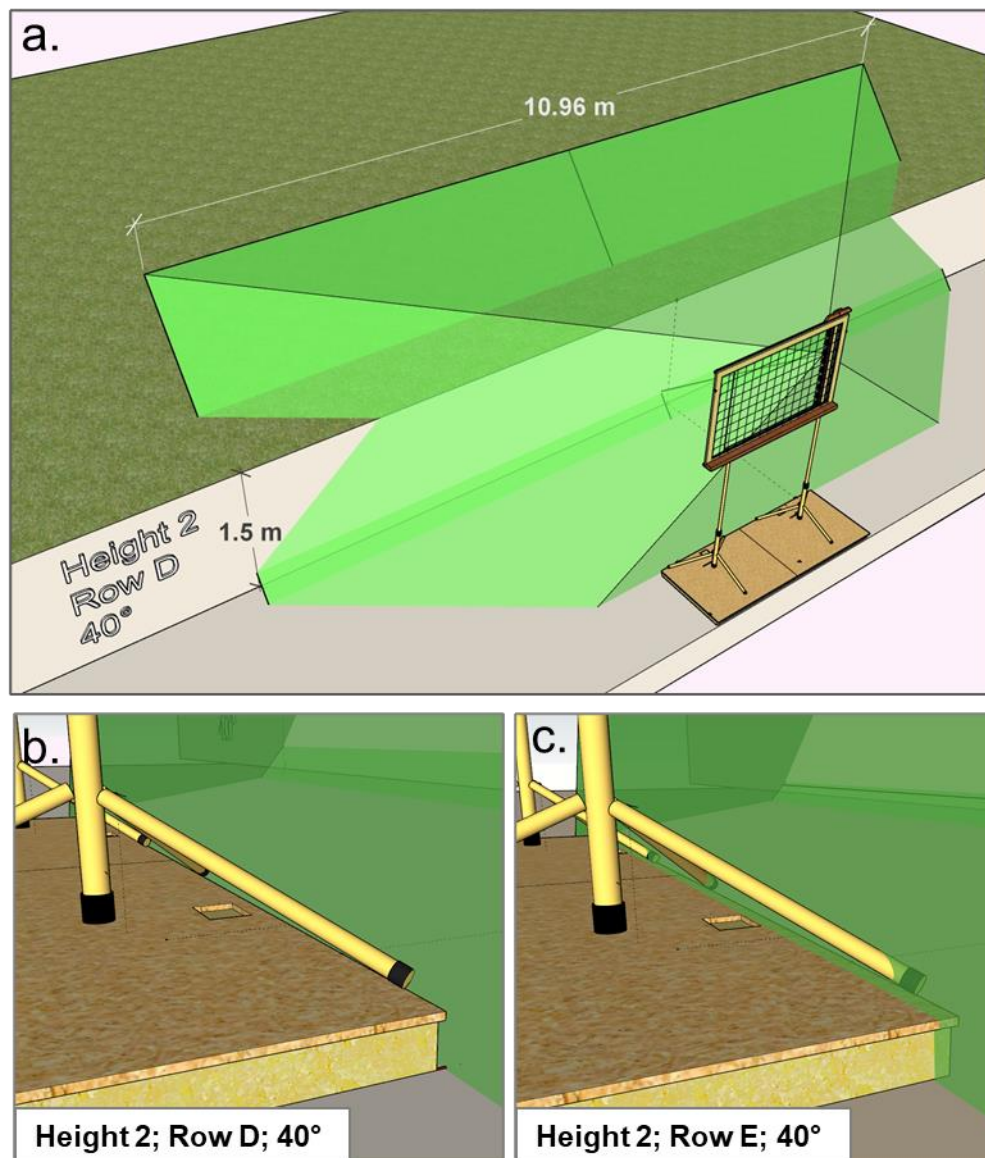


Figure 3.6: SketchUp representation for FOV estimations. **a)** FOV estimate for camera in position at 'Height 2' Row D (40°) **b)** Zoomed in image of FOV estimate at position 'Height 2' Row D (40°) showing the FOV not encroaching onto the equipment **c)** Zoomed in image of FOV estimate at position 'Height 2' Row E (40°) showing FOV estimate encroaching onto the equipment suggesting a change in angle from 40° to 30° declination around Row E (Height 2) may be required in the field.

Based on the model simulation, the camera obliqueness angle had to be varied to maintain an appropriate coverage of the target and prevent encroachment of equipment. This analysis revealed the potential change of camera obliqueness from 40° declination from the z-axis to 30° (Figures 3.6-3.7) and from 30° declination to 0° (Figure 3.7), the details of which are provided in Chapter 4 (Godfrey et al., 2020).

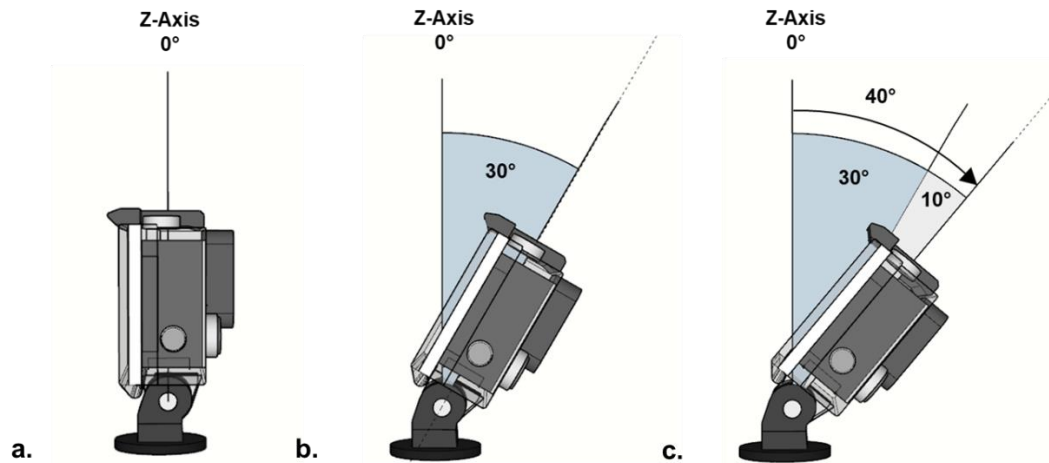


Figure 3.7: Sketch-up modelled representation of three degrees of camera obliqueness from the z-axis. a) No declination or 0° ('Height 1' – Rows A-I); b) 30° declination ('Height 2' – Rows E-I); c) 40° declination ('Height 2' – Rows A-D).

3.3.3 Concurrent Data Acquisition

A TLS was used as a benchmark for point cloud reconstruction quality. Three TLS scans were acquired to guarantee a high level of coverage and accuracy. The TLS has an integrated digital camera which automatically captures images of the scene. These images were used to colourise the dense point clouds and 3D models (Thoeni et al., 2014). Scan resolution was set at 1/5 point spacing and 4x quality which represented a standard outdoor 20 m scan profile. The three scans were processed in Faro SCENE 3D (v. 7.1) and edited to remove noise, errors, duplicated points and crop areas not relevant to the survey. The three scans were co-registered using GCPs as markers to provide correct orientation and scale.

GCP measurements were also taken for the purposes of providing the point cloud with a reference coordinate system. Checkerboards (0.15 m²) were chosen as they are

recognised in both the Faro Scene and Agisoft Photoscan software. One of the GCPs was a cube at 0.15 m³. The cube was levelled and could be used as an axes reference for model orientation, if necessary. These three checkerboards were georeferenced using a Trimble RTK-GPS R6 which optimised orientation and alignment for the dense point cloud (horizontal accuracy of 0.01 m and vertical accuracy of 0.02 m). The horizontal coordinates for the reference points were set to the British National Grid (OSTN02) while the vertical coordinates were referenced to the mean sea level using the geoid model OSGM02.

3.3.4 Comparative testing with TLS

The assessment of reconstruction quality, in comparison to the TLS, was undertaken using a two-stage process that aimed to assess some of the most influential parameters that effect overall point cloud quality. The first stage established optimal camera positions based on combined height and camera obliqueness within the camera grid. The second used that result to establish a minimal image capture network for a fixed multi-camera array and an estimate of precision for the final output. In this chapter an overview of the tests and equations designed for this assessment is provided but a greater degree of detail and context is contained in Chapter 4 (Godfrey et al., 2020), section 4.3.5.1.

Deviation metric (B): Prior to calculation, the reference point cloud (TLS) and the SfM-MVS point cloud were aligned using GCPs as point locations in CloudCompare software (V. 2.9). An Iterative Closest Point (ICP) (Nouwakpo et al., 2014; Westoby et al., 2018) was used for a finer registration, then the point clouds were cleaned and cropped to equivalent sizes. The final product was a mean Cloud-to-Cloud (C2C) distance, standard deviation in distance and scalar field that was coloured to represent areas with greater deviation. The result of this test was used in Equation (2), where the C2C mean value (j) is measured relative to a 100 mm scale.

$$(2) \quad B = \lim_{j \rightarrow 100} 1 - \left(\frac{j}{100} \right)$$

Completeness metric (C): The point clouds were equally segmented along the base of the cliff and separate nadir images produced for testing. The background of the image was

changed to an artificial colour which would allow for the identification of ‘holes’. This process was repeated for the TLS point cloud and the TLS images used as a benchmark for comparison with equivalent SfM-MVS images (Figure 3.8).

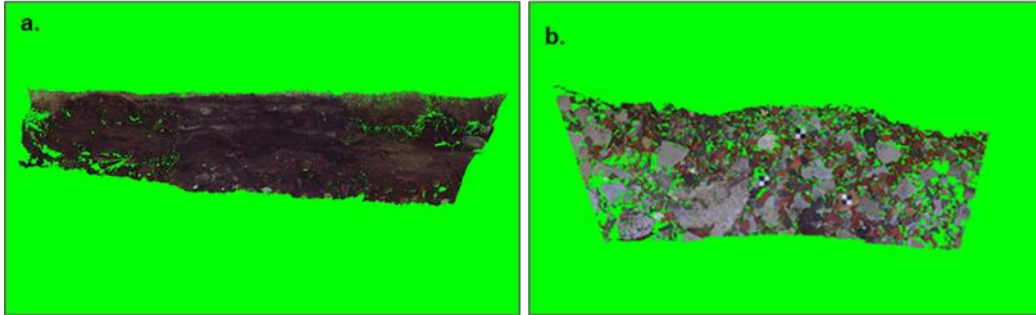


Figure 3.8: Segmented TLS point cloud for Completeness test. a) 2D cliff image with artificial background colouring used for filtering in Python OpenCV programming. b) 2D floor image with artificial background colour.

Each image was filtered using Python OpenCV image analysis functions. A python script was written to determine the number of green pixels present in the image (Appendix A). Using these numbers, the ratio of filtered pixels (i.e. holes) within an image was estimated:

$$(3) \quad R_s = (n_t - n_{fs})/n_t$$

$$(4) \quad R_t = (n_t - n_{ft})/n_t$$

where R_s and R_t are the ratio of filtered pixels, n_t is the total number of image pixels, and n_{fs} and n_{ft} are the number of filtered pixels in the SfM-MVS and TLS images respectively. The following was used to compare the ratio of filtered pixels in the SfM-MVS images to those within the TLS images:

$$(5) \quad M = \frac{R_s}{R_t}$$

The M value was calculated separately for floor (M_f) and cliff (M_c). The M_f and M_c values were each given a weighting of 50% to reflect their equal importance in the completeness metric:

$$(6) \quad C = 0.5(M_f) + 0.5(M_c)$$

GCP metric (G): This metric was used to compare the ability of TLS and SfM-MVS to reconstruct the GCPs in the scene. Equations (7) and (8) describe the test of accuracy for both TLS and SfM-MVS (P_s refers to the accuracy of SfM, P_t refers to the performance/precision of the TLS). Firstly, under- and over-measurement of the GCPs had to be treated equitably. The conditional statement ('if, then' denoted by the logical operator \rightarrow) occupying the numerator space between the parentheses in equations (7) and (8) describes this process.

Following this logical process, the result of the under- or over-representation from the method of reconstruction was then divided by the GCP known value (R) to obtain a ratio of each method of reconstruction's error relative to the known GCP dimensions. Subtracting this result from 1 provided a measure of how accurate the method of reconstruction had been at recreating the known dimensions of the GCP.

$$(7) \quad P_s = 1 - \left\{ \frac{[(S>R) \rightarrow (S-R)] \vee [(S<R) \rightarrow (R-S)]}{R} \right\}$$

$$(8) \quad P_t = 1 - \left\{ \frac{[(T>R) \rightarrow (T-R)] \vee [(T<R) \rightarrow (R-T)]}{R} \right\}$$

$$(9) \quad Q = \frac{P_s}{P_t}$$

$$(10) \quad G = 0.167(Q_1) + 0.167(Q_2) + 0.167(Q_3) + 0.167(Q_4) + 0.167(Q_5) + 0.167(Q_6)$$

Equation (9) assesses the capacity of SfM-MVS to accurately recreate the GCPs relative to the capacity of the TLS. If SfM-MVS proved more accurate than the TLS, a value for Q of >1 would be returned for each of the GCPs ($Q_1 - Q_6$). This test was applied to *the x* (alongshore direction) and *y* (cross-shore direction) axes of the three GCPs (six measurements in total). Each of these six measurements was then given an equal weighting of 0.167 in the overall test set out in Equation (10).

Aggregated Test of SfM-MVS Performance (A): Once the three comparative tests were completed (Deviation (B), Completeness (C) and GCP (G)) for each row on the camera grid, an aggregated weighted average (A) was calculated for each row:

$$(11) \quad A = 0.25(B) + 0.5(C) + 0.25(G)$$

3.3.5 Standalone Precision Assessment

The final point cloud from the comparative analysis was used for a precision assessment. The calculation of precision was used as a measure for the repeatability of the reconstruction. The spatial distribution of this precision was then mapped. Internal and external precision of the point cloud was generated to determine the most limiting factor on overall point cloud precision i.e. image network geometry or GCPs. The process of precision estimation and mapping was established in (James, Robson and Smith, 2017) which contains the underlying equations for analysis. The assessment uses a Monte-Carlo simulation in SfM-MVS software (Agisoft Photoscan) with python script to run repeat bundle adjustments. An overview of the fundamentals of the procedure is provided below.

The bundle adjustment procedure is originally used in the SfM-MVS workflow to minimise error on the image observations established in the image alignment stage. This reduction in error requires the adjustment of the estimated camera positions and the 3D tie points – these are the two parameters calculated during the image alignment stage. The adjustments made to these two parameters allow an estimate of precision to be established based on the variance of each parameter’s movement or adjustment.

As the bundle adjustment is repeated over a specified number of iterations (the greater the number of iterations, the higher probability of an accurate precision estimate) pseudo-random error offsets are added to an original error free version of the image network and GCP measurements. The scale of the random offsets is derived from the Root Mean Square (RMS) of the original error on the first point cloud. The subsequent precision estimations for each parameter (calculated 3D tie points and camera positions) are established by defining the variation in each parameter over a large series of bundle adjustments.

Following the repeated bundle adjustments the results of these are used in Sfm_georef software (v3.1) created for (James, Robson and Smith, 2017). The results are compiled in the software and precision estimates overlain onto the tie points. Two ASCII files were generated and exported to CloudCompare software. Each ASCII file contained a sparse point cloud – one containing the overall survey precision which includes GCP error (external precision) and the second contained the ‘shape only’ precision which excludes GCP error (internal precision). The values of the sparse point cloud were transferred to the dense point cloud using Nearest Neighbour analysis. The dense point cloud was then interpolated across a grid to create a DEM and transferred to and edited in ArcGIS (Version 10.4 – spatial analyst extension). The precision maps created represent the standard deviation of the distribution for all of the iterations for each tie point in the sparse point cloud. These values are separated into three raster maps that represent the precision in the x , y & z components of the point cloud.

The use of a standalone precision assessment is a way to independently examine SfM-MVS reconstruction results without a reference point cloud (e.g. TLS). This independent test can also help to confirm or refute the findings of the previous assessment during Stages One and Two which are dependent upon a reference (TLS) containing a degree of inherent error. The precision maps also enable the separation of some of the most influential factors that can impede SfM-MVS reconstruction (image network geometry and GCPs).

3.4 Methodology for Stage 2 of Research - Camera Rig

This section provides an initial overview for research design, development and deployment of a rig with multiple fixed cameras. Further details are provided in Chapter 5.

The use of a multi-camera rig for streamlining of image acquisition in the field requires multiple deployment locations to test the accuracy of the rig in different coastal settings. The optimal camera positions identified in Chapter Four (Godfrey et al., 2020) were used at three sites of coastal recession. Once again, the 3D reconstructions from each location were tested against industry standard TLS equipment to confirm the level of reconstructions possible. The camera rig was deployed at, Silverdale, Crosby and Thurstaston, North West England. These sites were chosen as they offered, variation in

height, alongshore distance and were vulnerable sites known to be actively receding. This section provides an overview of the methodology employed in Chapter 5.

3.4.1 Camera Rig Design

The camera rig was designed to accommodate the camera positions established in Chapter 4 (Godfrey et al., 2020). The rig was developed for use with multiple GoPro Hero 4 Black action cameras, all of which were of the same technical specification. As with the camera grid, the design of the rig ensured that all equipment was kept out of the camera's FOV. However, the variation in the scale of the sites meant that the rig had to be adaptable to accommodate these changes (Figure 3.9). Therefore, the height of the pole was variable and a calculation of the rigs movements along the cliff was necessary to ensure the continued overlap between images that was established in Chapter 4 (Godfrey et al., 2020). Consequently, the distance of each lateral rig stop along the front of the cliff was calculated using the equation 12.

$$(12) D = 2a + b$$

where D is the distance between successive camera stops, a is the distance from the central pole to the end camera's lens and b is the physical distance between cameras to ensure overlap. A Wi-Fi network was used between the cameras to synchronise image capture.

Exploring the use of a Multi-Camera Platform for 3D Reconstruction

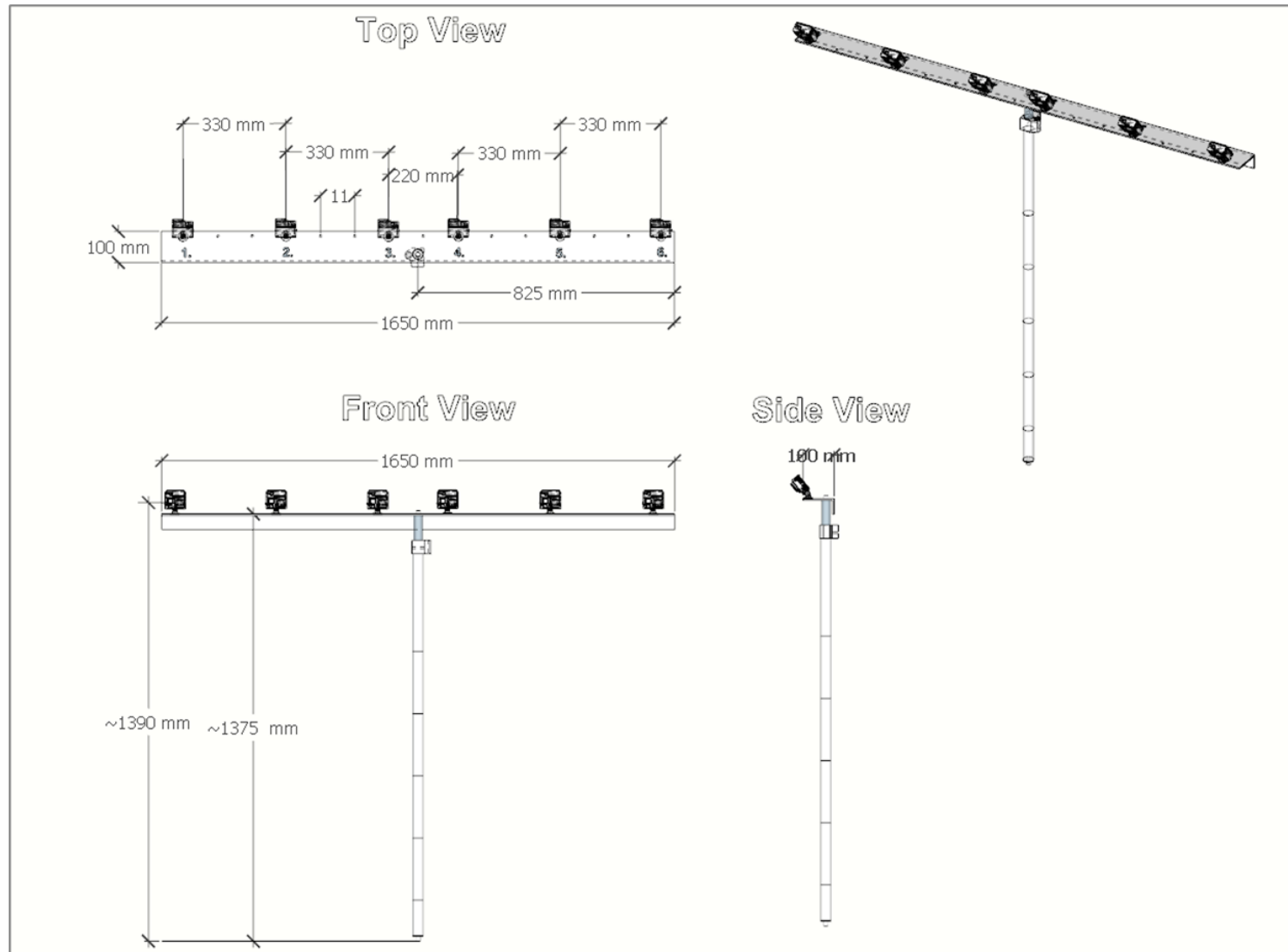


Figure 3.9: Technical drawing of Camera Rig. Height displayed is that used at Silverdale and Thurstaston with cliff heights of approximately 1 m.

3.4.2 Concurrent Data Acquisition

Consistent with Chapter 4 (Godfrey et al., 2020), the TLS was used as a benchmark for reconstruction quality. After images were acquired with the camera rig, a TLS survey was conducted. The TLS scans followed the same path as the camera rig, stopping at alternate positions to accommodate the TLS's wider scan radius. Scans were aligned using Faro SCENE 3D (v.7.1) software. GCPs were also used and measured following the procedure in section 3.3.3. Further detail on TLS and GCP data acquisition can be found in section 5.3.2 of Chapter 5.

3.4.3 Point Cloud Generation

Point cloud processing was reviewed at both stages – image alignment and densification. Therefore, a workflow was established to assess the impact of changing processing parameters at each stage. Figure 3.10 displays the procedure of point cloud generation and assessment. Stage One was used to identify image alignment parameters that reduced point cloud deformation. Stage Two built on the findings of the first stage to test the impact of densification parameters on overall point cloud quality. Stage Two results were compared to the TLS and the final output underwent a standalone precision assessment.

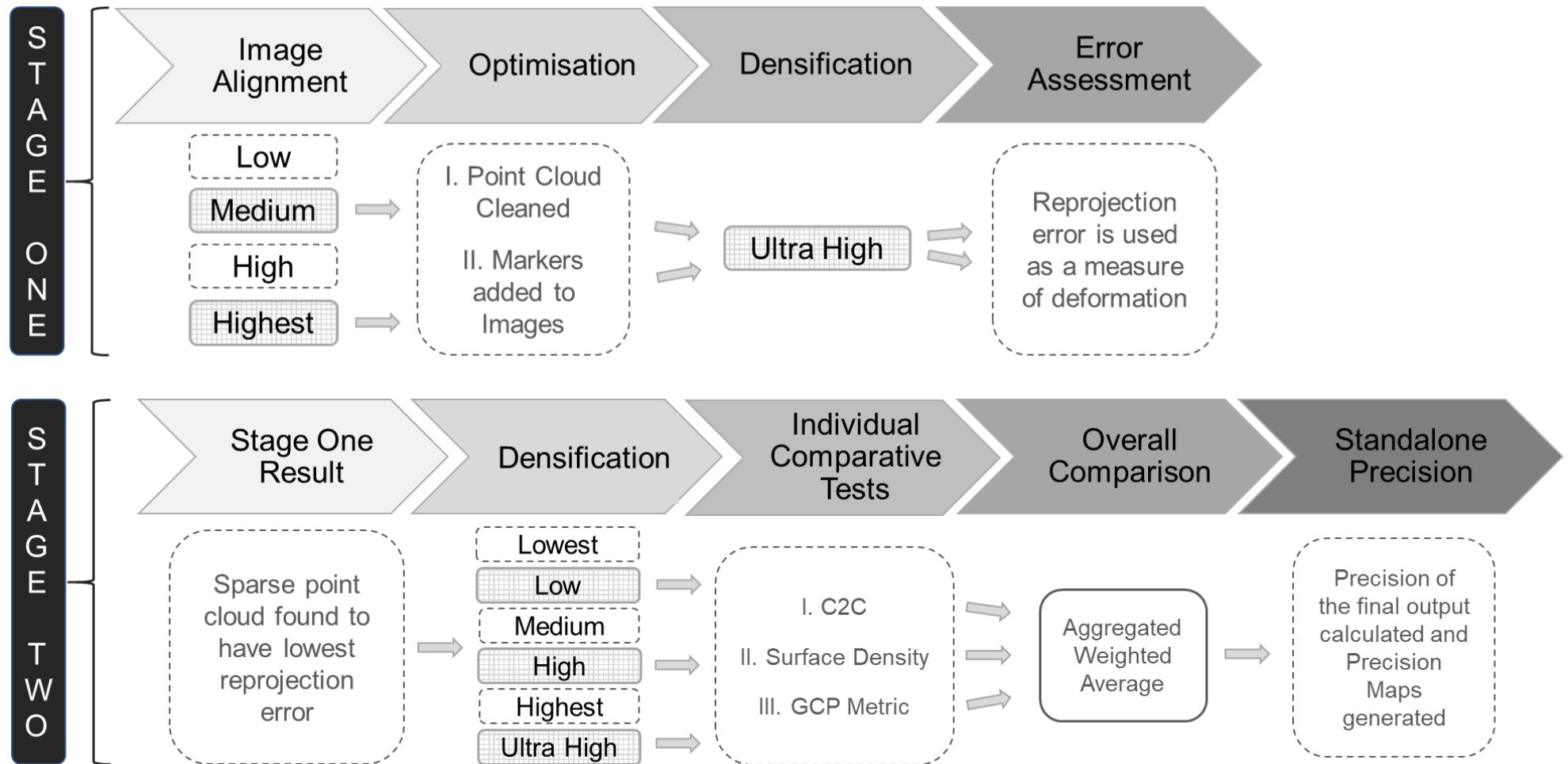


Figure 3.10: Workflow depicting the process of point cloud generation and assessment. Cross-hatching reflect the parameters used in processing.

3.4.4 Comparative Testing with TLS

Comparative testing with the TLS included two of the metrics described in section 3.3.4 of this chapter; Deviation metric (*B*) and GCP Metric (*A*). The Deviation Metric remained the same, however, an adaptation to the GCP metric was needed. Due to the complex nature of the sites, the Completeness Metric used previously, was not suitable. Therefore, a Surface Density Metric was used to provide a comparative test against the TLS.

- *Deviation Analysis (B)*: (Details provided in Section 3.3.4 of this Chapter)
- *Surface Density Metric (M)*: (Details provided in Section 5.3.4 of Chapter 5)
- *GCP Metric (G)*: (Details provided in Section 5.3.4 of Chapter 5)
- *Aggregated Weighted Average (A)*: An adapted version of Equation 11, from section 3.3.4 was used to assess the overall reconstruction performance under different densification parameters (Figure 3.10). Further details are provided in Section 5.3.4 of Chapter 5.

3.5 Methodology for Stage 3 of Research – Temporal Change using the Camera Rig

This section provides an overview of the methodology for the deployment of the camera rig through time and the analysis used to investigate the impact of wave hydrodynamics on erosion rates. Further details provided in Chapter 6.

The camera rig was used with the same systematic approach as described in Section 3.4 of this chapter at Silverdale saltmarsh margin, NW England, over a 4-month period. A series of standardised and novel approaches to erosion assessment were applied to evaluate changes at the site.

3.5.1 Data Acquisition

Overall, four surveys were undertaken between November 2018 and March 2019 to capture morphological changes over a winter season and record the impact of storms.

These surveys were undertaken on 16th November 2018, 14th December 2018, 15th January 2019, 18th March 2019. The choice of fieldwork dates was based on low-tide timings and weather conditions with sufficient cloud cover to provide suitable lighting conditions for SfM-MVS (James and Robson, 2012).

During each survey GCPs (0.15 m² checkerboards) were scattered across the scene approximately 1 m apart (details provided in section 6.3.1 of Chapter 6). First the camera rig was used to capture images of the scene, using the guidelines established throughout Chapter 5. As the camera rig had been tested against an industry standard on three previous occasions it was deemed unnecessary to conduct another TLS survey. The GCPs were georeferenced as described in section 3.3.3 of this chapter.

3.5.2 Point Cloud Generation

The processing of the Silverdale images followed the optimised steps established throughout Chapter 5. After each survey, images were uploaded in Agisoft Photoscan (V 1.3.2.4205) and point clouds generated for each date (see section 6.3.2, Chapter 6 for greater detail). The dense point clouds were then exported as LAZ files for assessment in CloudCompare V2.9 and ArcMap 10.4.1. The point clouds were aligned using ICP registration, cropped to equivalent sizes and vegetation removed, where possible, in the software CloudCompare (further detail is provided in section 6.3.3 of Chapter 6).

3.5.3 Geomorphological Change Assessment

Three assessments were undertaken in order to provide robust estimates of the changes at the saltmarsh margin. These tests were:

- Topographic Differencing for Volume
- Area Loss
- Area of Undercutting

The following three subsections describe these in more detail.

3.5.3.1 Topographic Differencing for Volume

The point clouds generated for each survey were uploaded into and converted in CloudCompare to DEMs from which DoDs were created in ArcMap (Version 10.4.1 – spatial analyst extension). The differencing of the DEMs allowed the depositional and

erosional changes to be analysed volumetrically, spatially, and temporally. Further details on this process are provided in section 6.3.3.1 of Chapter 6.

3.5.3.2 Profile Extraction & Area Loss

The extraction of the shoreline profile offers a way of viewing lateral recession of the saltmarsh margin through time. The furthest extent of the cliff is digitised in ArcMap 10.4.1 to create polylines that represent the cliff margin. The area between the intersected lines represented the area lost through erosion. The area of the established segments was calculated and represented the lateral area of the saltmarsh lost each month.

3.5.3.3 Area of Undercutting

An undercut area of cliff is generally associated with a greater likelihood of slumping and collapse. An innovative test was established to identify and estimate the area of undercutting. From the 3D point cloud, it is possible to generate two DEMs: one displaying the maximum elevation values for each grid square and the other displaying the minimum elevation value for the grid square. A comparison of these two DEMs made it possible to identify and quantify areas of undercutting present across the site. Further details on this procedure are provided in section 6.3.3.3 of Chapter 6.

4. Monitoring coastal morphology: The potential of low-cost fixed array action cameras for 3D reconstruction

EARTH SURFACE PROCESSES AND LANDFORMS

Earth Surf. Process. Landforms (2020)

© 2020 The Authors. Earth Surface Processes and Landforms published by John Wiley & Sons Ltd

Published online in Wiley Online Library

(wileyonlinelibrary.com) DOI: 10.1002/esp.4892

Samantha Godfrey,^{1*} Dr James Cooper,¹ Dr Frederic Bezombes² and Professor Andy Plater.¹

¹ School of Environmental Sciences, University of Liverpool, Liverpool, UK

² General Engineering Research Institute, Liverpool John Moores University, Liverpool UK

Received 14 July 2019; Revised 23 April 2020; Accepted 26 April 2020

*Correspondence to: Samantha Godfrey, School of Environmental Sciences, Roxby Building, University of Liverpool, Liverpool, L69 7ZT, UK. E-mail: s.godfrey@liverpool.ac.uk.

Data Availability Statement: The data that support the findings of this study are available from the corresponding author upon reasonable request.

Abstract

The combination of structure-from-motion with multi-view stereo (SfM-MVS) photogrammetry has become an increasingly popular method for the monitoring and three-dimensional (3D) reconstruction of coastal environments. Climate change is driving the potential for increased coastal landward retreat meaning geomorphological monitoring using methods such as SfM-MVS has become essential for detecting and tracking impacts. SfM-MVS has been well-researched with a variety of platforms and spatial and temporal resolutions using mainly rectilinear digital cameras in coastal settings. However, there has been no assessment of the potential of fixed multi-camera arrays to monitor landward retreat or on the significance of camera placement in relation to the scene. This study presents an innovative method of image acquisition using a purpose-built camera grid and GoPro® action camera to evaluate the combined effects of camera height, obliqueness and overlap at a site of known landward retreat. This approach examines the effect of camera placement on scene reconstruction to aid the design of a multi-camera array. SfM-MVS dense point clouds display millimetre accuracy when compared to equivalent terrestrial laser scans and strong image network geometry with internal precision estimates of <3 mm. Comparable point cloud reconstruction can be achieved with a small number of images stationed in appropriate positions. Initial results show as few as five images positioned at a cliff to camera ratio of 3:4.18 and camera obliqueness of 40° can provide reconstruction in the range of millimetres (mean error of 4.79 mm). These findings illustrate the importance of camera placement when using multiple cameras and aid the design of a low-cost, fixed multi-camera array for use at sites of small-scale landward retreat. © 2020 The Authors. Earth Surface Processes and Landforms published by John Wiley & Sons Ltd

KEYWORDS: action camera; coastal erosion; coastal monitoring; image optimization; structure-from-motion photogrammetry; 3D Reconstruction.

4.1 Introduction

Over the last decade advances in remote sensing and three-dimensional (3D) image reconstruction techniques have made it easier to monitor dynamic and rugged coastal environments (Maiti and Bhattacharya, 2009; Earlie et al., 2013; Mancini et al., 2013; Earlie et al., 2015; Conlin et al., 2018; Westoby et al., 2018). Technological

advancements have produced a range of surveying methods to monitor patterns of morphological change in various coastal settings. For example, large-scale spatial coverage can be achieved with airborne light detection and ranging (LiDAR) (Earlie et al., 2013; Dudzińska-Nowak and Węzyk, 2014), video monitoring with Argus systems (Holman and Stanley, 2007) and satellite imagery (Maiti and Bhattacharya, 2009). Smaller scale topographic coverage is achieved with a terrestrial laser scanner (TLS), capable of acquiring fine-resolution spatial data (in millimetres) at short stand-off distances (Anthony et al., 2006; Calligaro et al., 2014; Westoby et al., 2018) or roving Global Navigation Satellite System (GNSS) with high spatial accuracy (in centimetres) (Young, 2015). However, many of these surveying methods are expensive to acquire and operate meaning they are most commonly used in developed nations and, even in these settings, infrequently. The use of manual surveying methods such as Abney levels, the Emery Method or optical levels, provide a cost-effective option but offer very limited spatial resolution. There is, therefore, a case for alternative methods of monitoring coastal change that have high spatial resolution, are cost effective and can be used routinely. It would be essential that any such methods were of comparable accuracy to those that have become established as the 'industry standard' (Westoby et al., 2018).

Photogrammetric based methods of 3D reconstruction for topographic surveys have become increasingly popular due to their lower-cost and flexibility. Based on traditional photogrammetric principles, two-dimensional (2D) overlapping images are used to reconstruct 3D scene geometry. Advancements in computer vision (Bemis et al., 2014) have allowed the underlying mathematical calculations of this to be developed into structure-from-motion with multi-view stereo (SfM-MVS), the fundamentals of which have been described in Westoby et al. (2012) and James and Robson (2012). The incorporation of this process into automated commercial software packages and other open-source alternatives has made it accessible to both professional and 'non-expert' users.

The flexibility of SfM-MVS has provided opportunities for a wide range of geographic applications, including coastal monitoring. The majority of research has been undertaken with a single rectilinear (pin-hole) digital camera deployed from a variety of platforms including poles (Conlin et al., 2018), drones (Mancini et al., 2013), blimps (Fonstad et al., 2013) and kites (Duffy et al., 2018). Comparative studies between TLS

and SfM-MVS outputs have shown SfM-MVS compares well to TLS with centimetre accuracy (Wilkinson et al., 2016; Westoby et al., 2018). In addition, the impracticalities of TLS equipment such as reduced accuracy outside a specified temperature range and long surveying periods (James and Robson, 2012) during short tidal windows, lead some to favour SfM-MVS.

The quality of SfM-MVS output is often considered to be positively associated with the number of images used: the more images the better to optimize the number of keypoints present (Westoby et al., 2012). This has prompted recent studies (for example, Eltner et al., 2017) to experiment with multiple cameras. Although this work has produced many encouraging findings it has also identified the necessity for further research on the significance of camera position and setup. With this in mind, and the need for quick surveying during short tidal windows, the ability to simultaneously acquire images from a fixed array of multiple cameras would be advantageous – ideally with cameras set in positions to maximize efficacy. The potential approach of using a multiple fixed camera array contrasts with the previously cited studies where single cameras were used for image acquisition. However, to truly make this approach a possibility it is first necessary to understand the significance of camera placement in relation to the scene. Optimal camera placement would result in a simplification of image capture geometry and would entail fuller scrutiny of the combined effect of some positional parameters (beyond simply number of images) that effect image suitability: overlap, obliqueness and convergence (Eltner et al., 2016).

Another critically important consideration to multiple camera use is choice of camera. Action cameras offer an accessible, easily operable, manoeuvrable and rugged alternative to digital single lens reflex (DSLR) cameras. In addition, GoPro action cameras offer the option for wireless multi-camera synchronization – a significant advantage for a camera array. Previously, action cameras were considered inappropriate for accurate 3D reconstructions due to radial distortion created by the wide angle of view (AOV) or fisheye lens. AOV is a function of sensor size and lens type and describes the angular extent of a camera's view. The short focal length of action cameras allows a greater field of view (FOV) or measurable 'footprint' but creates image distortion – particularly on the extremities of the image frame (Thoeni et al., 2014; Phillips and Eliasson, 2018). The distortion previously rendered fisheye lenses

unsuitable for creating 3D models with accurate metric integrity (Perfetti et al., 2017). However, the advancement in commercial photogrammetric software has meant fisheye remapping functions are available to correct some of these previously unsuitable radial distortions. Research outside geomorphology has successfully used fisheye lenses with SfM-MVS (Ballarin et al., 2015; Hastedt et al., 2016). Increasing use of action cameras with SfM-MVS means that understanding potential 3D reconstruction quality is now essential.

The use of commercially popular and accessible action cameras, such as the GoPro Hero© range, and a simplification of image acquisition would allow regular close-range, high resolution surveys to be achieved with low-cost, rugged equipment. The question of how camera position affects fisheye image capture quality for SfM-MVS – and the degree to which attention to camera position may diminish the number of images required for a multi-camera setup – has received little academic attention. In this contribution the aim is to provide evidence on how the combined effect of camera height and obliqueness (the inclination of the optical camera axis towards the ground – see Figure 3.7, Chapter 3) impacts the overall reconstruction of the subsequent dense point cloud within a set of practical limitations for field deployment.

This article presents an innovative method of image acquisition using a purpose-built camera grid and GoPro© action camera to evaluate the combined effects of camera height, obliqueness and overlap. This evaluation was conducted to inform the design of a fixed multi-camera array which, once thoroughly tested, could be deployed at longer stretches of landward retreat. The grid was designed to allow controlled camera movement without changes to the optical axes (x , y & z) caused through human error or environmental conditions. A trial using the camera grid was conducted at a typical site of a small-scale landward retreat at Crosby, northwest England and compared against results obtained using an ‘industry standard’ TLS (assumed ground-truth).

4.2 Study Site

Crosby is located on the Sefton Coast in northwest England, UK (Figure 4.1a), situated north of the Mersey Estuary in Liverpool Bay. The Sefton coastline extends for ~36 km and is influenced by the processes occurring in the Irish Sea and the adjacent estuary (Dissanayake et al., 2014). The coastline is susceptible to some of the highest storm

surge conditions in the UK owing to the shallow nature of the north-eastern Irish Sea. The site is located in a macro-tidal environment with a mean spring tidal range of ~ 8 m (Gladstone Dock tide gauge). Local waves are generated by dominant west and north-westerly winds (Plater and Grenville, 2010).

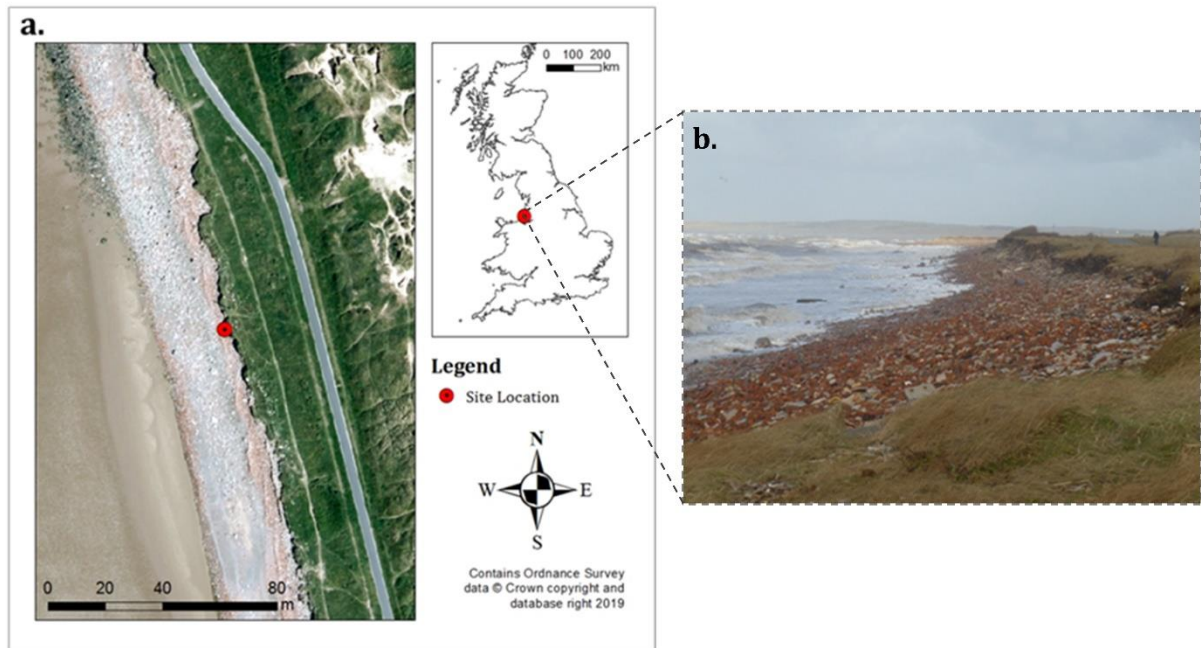


Figure 4.1: Study site location. a) Location map with marker indicating test location. b) General site photograph showing landward retreat with cliffs at a height of ~ 1.5 m taken January 2018.

The test location is a ~ 7 m long section of Crosby/Hightown coast (Figure 4.1b) surveyed in February 2018. The ~ 1.5 m high cliff is a combination of unconsolidated material and rubble which has become smoothed and sorted due to wave action. The rubble provides a level of protection but, deprived of sediment deposition, the wave and storm action can cause landward retreat during severe storms (Figure 4.1b). The underlying stratigraphy is glacial till variably overlain by peat and dune sand (Plater et al., 2010).

4.3 Methods

The research used systematically acquired images that were processed with SfM-MVS for comparison with TLS data. Point clouds were evaluated using a two-stage process of assessment. The first established optimal camera positions based on combined height and camera obliqueness within a camera grid. The second used that result to establish a minimal image capture network for a fixed multi-camera array and an estimate of

precision for the final output. This section provides an outline of camera grid design, initial site representation and fieldwork procedure which is followed by details on point cloud generation and the process of performance assessment.

4.3.1 Camera Grid Design

The camera grid was designed to test for ideal camera positions in a multi-camera setup using a GoPro Hero 4 Black action camera. This camera has a 1/2.3-inch (6.2 mm × 4.65 mm), 4:3 CMOS sensor with 1.55 µm pixels. The 'fisheye' lens has a fixed focal length (prime lens) of ~3 mm (17.2 mm equivalent). As with other GoPro cameras, the Hero4 Black has an ultra-wide AOV with differing image capture modes - 'Wide' was used. Still image resolution is 12 Megapixels (4000 × 3000 pixels). The GoPro has a small size, 80 mm × 80 mm × 38 mm with waterproof casing and stand, and a low weight, 152 g.

The camera grid was constructed from timber and wire to separate grid squares (Figure 4.2a). The specifications of the grid frame and mounting can be found in Chapter 3, section 3.3.1. The grid had 15 rows and 9 columns. The spacing of the grid squares created an image overlap of ~99% and a distance between adjacent cameras (baseline) of 0.11 m. The grid had a 2 m stand-off distance from the cliff which was held constant throughout image acquisition; distance to the scene has a known impact on image resolution and so it was important to maintain this parameter to ensure that any changes were the result of other tested variables (height, obliqueness and overlap). The distance of 2 m would be part of any systematic image acquisition procedure using the subsequent multi-camera setup. Though it is understood that convergent imagery may improve 3D reconstruction, for fixed multi-camera arrays this is not possible as neighbouring cameras may intrude into another camera's FOV. Convergent imagery, therefore, lies outside the scope of this research.

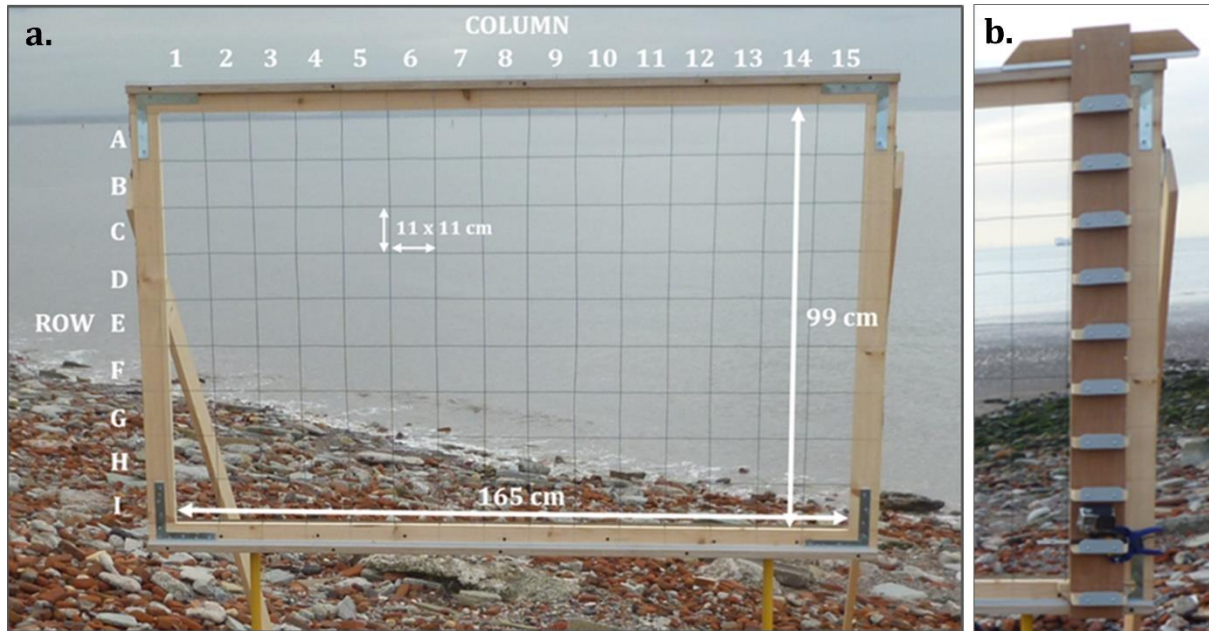


Figure 4.2: a) Camera Grid for image acquisition. Annotations display the labelled rows (A-I) and columns (1-15). The internal dimensions of the grid were set so each grid square was of equal size. b) Traveller used to move the camera seamlessly to each grid square.

The ‘traveller’ (Figure 4.2b) (see Figure 3.3 in Chapter 3 for technical specifications) on the front of the grid moved the camera into each grid square and maintained the x , y & z optical camera axes with no deviation in the camera orientation or angle (unless intentional). Further, the traveller allowed movement of the camera between columns and transfer of the camera to the next row. The overall camera grid and base platform was manually levelled using bricks as packers. A levelled platform was essential for the testing procedure to ensure all point clouds were the outcome of the tested inputs (changes to height, obliqueness and overlap) and not incorrect camera position. The grid was mounted on two tripods with props to maintain the z -axis (Chapter 3 – Figure 3.4). The practical design of the camera grid meant it had two heights: ‘Height 1’ in which the top of grid Row A was at a height of 1.64 m from the levelled base; ‘Height 2’ in which the top of grid Row A was at a height of 2.52 m. The result was that Row A of ‘Height 1’ and Row I of ‘Height 2’ were set at an equivalent height.

4.3.2 Initial Site Representation

A scaled 3D representation of the site and equipment was created to inform practical camera placement prior to fieldwork (Chapter 3 – Figures 3.5 and 3.6). The camera grid

equipment was reconstructed using SketchUp 2017 and the GoPro FOV estimated to provide prior knowledge on hypothetical scene capture before deployment. The 3D model depicted scene coverage at different positions on the camera grid. The aim was to ensure correct scene capture at different positions without the unintentional inclusion of equipment and to guarantee the scene was central in the image frame (see Chapter 3, section 3.3.2).

Visual analysis of the modelled setup revealed that varying camera angles would be required to maintain a viewshed of the target surface and prevent encroachment of equipment. This analysis revealed the potential change of camera obliqueness between Rows D and E at 'Height 2' where the angle moved from 40° declination from the z-axis to 30° (Chapter 3 – Figures 3.6 and 3.7). Another potential obliqueness change was needed at 'Height 1' Row A from 30° declination to 0° (Chapter 3 – Figures 3.6 and 3.7). Therefore, Heights 1 and 2 showed varied incidence angles to the scene.

4.3.3 Data Acquisition

Fieldwork was undertaken at spring low tide over a nine-hour period and covered a ~7 m section of coastal frontage. Meteorological conditions were suitably diffuse with overcast cloud (James and Robson, 2012).

First, camera grid 'Height 1' (Figure 4.3) was set-up with 0° camera angle as defined in the SketchUp Model. This camera angle captured images perpendicular to the cliff front. Image acquisition began from Row A, Column 1 and proceeded through the grid to Row I, maintaining camera angle. Second, the camera grid was increased to 'Height 2', reaching 2.52 m from the base to the top of Row A. Oblique imagery was acquired. The camera obliqueness was adjusted to 40° for Rows A to D. The obliqueness was then adjusted to 30° for Rows E to I to ensure appropriate viewshed for the target surface as interpreted from the SketchUp representation and confirmed in the field.



Figure 4.3: Camera grid at 'Height 1' on the levelled base - 2 m distance from frontage.

Images from Row A at 'Height 1' and Row I at 'Height 2' were at equivalent heights but different degrees of camera declination (0° for Row A and 30° for Row I). Therefore, they could be used to explore the impact of obliqueness on the dense point cloud.

Overall, 270 out of 288 images were used in processing; rejected images were those used for the purpose of identifying row change.

Three converging TLS scans were captured using a 'Faro 3D Focus 330' to provide thorough scene reconstruction. Overall scan time for the TLS was ~ 30 minutes (see section 3.3.3, Chapter 3 for further details). The three scans were processed in Faro SCENE 3D (version 7.1). The average point error was 3.2 mm.

Prior to image acquisition, ground control points (GCPs), in the form of three 0.15 m^2 checkerboards were placed in the scene approximately 1 m apart and georeferenced with Trimble RTK-GPS R6 (see section 3.3.3, Chapter 3).

4.3.4 SfM-MVS Point Cloud Generation

Point clouds were generated through a two-stage process of assessment. The first established optimal camera positions and the second used the first result to investigate the impact of decreased redundancy which is essential for establishing a fixed multi-camera array.

Initial SfM-MVS reconstruction for ideal camera positions was undertaken with eight alternate images from each row of the camera grid at both 'Height 1' and 'Height 2' (Figure 4.4). The eight images from each row were uploaded into the software Agisoft Photoscan Professional Edition (version 1.3.2.4205) and a dense point cloud was produced. Eight images from each row allowed a balance between computational speed and maintaining an equal baseline between images for initial assessment of dense point cloud reconstruction.

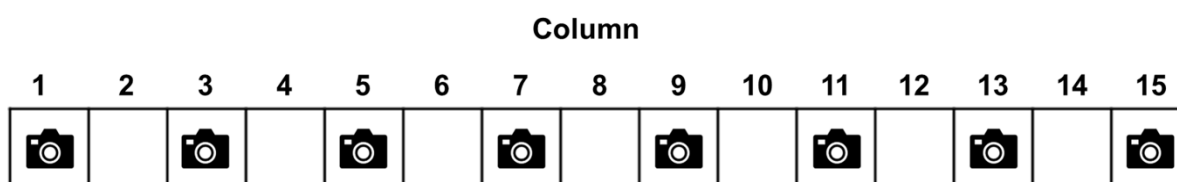


Figure 4.4: Representation of the position of images used along each row of the camera grid for Stage One Analysis. Camera symbol indicates the position of image that was used in the eight image set. Images taken from these positions had 98% overlap.

The software provides a workflow in which 3D reconstruction of the scene is established. As a fisheye lens was used for image capture, the camera model was changed to 'fisheye' to match the specifications of the GoPro Hero 4 Black. Initially, photographs are aligned (setting was 'Highest') through keypoints identified and tracked across the uploaded images. A bundle adjustment then solves external and internal camera parameters. This adjustment results in the creation of a sparse point cloud which is optimized with GCPs. The GCPs (British National Grid/OSNT02) were identified in the images and the Trimble data uploaded into the software to be referenced with the known GCP positions. The addition of coordinates meant the model had real-world reference, scale and orientation which would improve comparison with the TLS dense point cloud. A densification process (setting was 'Ultra High') builds the dense point cloud based on the image set and estimated camera positions. This was exported as LAZ files to maintain the coordinate system when uploaded for performance analysis. A more detailed description of the fundamentals of the SfM-MVS workflow can be found in Nouwakpo et al. (2016).

The procedure of generating dense point clouds was repeated for the second stage of assessment – establishing the impact of reduced redundancy. Images were systematically reduced from the image set established in the first stage of assessment.

4.3.5 Performance Assessment

To evaluate the impact of the different camera positions on point cloud reconstruction a systematic method of assessment was established. The goal at this stage was to identify the most suitably reconstructed dense point cloud by SfM-MVS compared to a TLS. This is a necessary first step to inform the design of a fixed multi-camera array.

The two-stage process of assessment first established the row with greatest overall performance. The second used the images from that row to investigate the impact of decreased redundancy and establish a minimal image capture network. The process of assessment followed three comparative tests using TLS as the benchmark; two of the tests evaluated positional point accuracy (deviation analysis and GCP analysis) and one, point cloud completeness (completeness analysis). After each stage an aggregated weighted average of the three tests was used to assess optimal camera position and image redundancy. The chosen point cloud was then assessed independently using precision estimates.

4.3.5.1 Stage One: Positional Camera Parameters

Earlier studies have discussed the need for greater scrutiny of the positional parameters that affect image suitability and interaction (Eltner et al., 2016). However, direct control over camera movement can be difficult due to environmental conditions and human error. Here, the reconstructed dense points clouds from a rigid camera grid with combined variations in camera height and obliqueness were evaluated with the aim to define an optimum set of positional parameters that could be used in a fixed multi-camera set-up.

A dense point cloud was created for each row of the camera grid based on eight alternate images (Figure 4.4). The comparative metrics are set out below:

- i. Deviation metric (*B*): Cloud-to-Cloud (C2C) closest point distance calculation is a direct method for 3D point cloud comparison (Lague et al., 2013). The C2C distance is calculated using 'Nearest Neighbour' analysis in CloudCompare V2.9 and is based on the point cloud generated by the TLS and those created from SfM-MVS. The method uses two aligned point clouds and defines each point's nearest neighbour in the reference point cloud with those in the compared point cloud (Ruggles et al., 2016). This test was used because the TLS and SfM-MVS point cloud were of a

similar point distribution and density, and C2C offered a direct comparison to the TLS point cloud. The distance (combined x, y & z) between the two points is calculated and the mean of these values is termed the mean C2C distance. The resulting mean C2C distance (j) was expressed relative to a 100 mm scale in the form of a deviation metric (B):

$$(2) \quad B = \lim_{j \rightarrow 100} 1 - \left(\frac{j}{100} \right)$$

A 100 mm scale was chosen as it offers a meaningful range of values against which C2C values could be understood (see Chapter 3, section 3.3.4 for further details).

- ii. Completeness metric (C): The estimation of 'holes' (areas of missing points) in point clouds is an important step to understanding a truly representative 3D reconstruction. Therefore, Python programming language (see section 3.3.4) was used to develop an estimation of 'holes' present within each point cloud based on 2D JPEGs with nadir views produced in CloudCompare (see section 3.3.4, Chapter 3 for details). This estimate was used to produce a completeness metric based on the ratio of filtered pixels in the SfM-MVS images to those within the TLS images.
- iii. GCP metric (G): The inclusion of GCPs of known dimensions in the scene allowed for a comparative test of the relative reconstruction accuracies of SfM-MVS and the TLS. The reconstructed GCPs were scaled by the inclusion of the GNSS data and x & y of each GCP measured using a 2-point measurement in CloudCompare. The degree to which SfM-MVS and TLS were able to accurately measure these 0.15 m² squares provided the basis for this test - set out in equations (7) – (10) in Chapter 3.
- iv. Aggregated Test of SfM-MVS Performance: Once three comparative tests were completed for each row on the camera grid an aggregated weighted average (A) was calculated for each row.

$$(11) \quad A = 0.25(B) + 0.5(C) + 0.25(G)$$

Deviation (B) and GCP (G) metrics evaluated positional point accuracy, and C analysed point cloud Completeness. Both positional metrics are essential for a truly representative reconstruction and so a 50% weighting was given to positional point accuracy (each of the two tests given a weighting of 25%) and 50% given to point cloud completeness – the calculation of which is shown in Equation (11). A score of 1 would imply that SfM-MVS had produced results that were (in aggregate across the three tests) of equivalent quality to those generated by the TLS. Similarly, a score of above 1 would imply that SfM-MVS had been more effective than its comparator in some regard. The row with the highest value from the aggregated test of SfM-MVS performance was deemed to be the optimal camera position and used in ‘Stage Two’ analysis.

4.3.5.2 Stage Two: Minimal Image Capture Parameters

The aim of Stage Two was to assess the impact of the number of images on dense point cloud reconstruction to create a minimal image network. The row with the most appropriate combined camera height and obliqueness, and therefore the best overall average, was established in Stage One. The images from this row were used to create dense point clouds from varying image combinations. Figure 4.5 displays these combinations and percentage overlap between neighbouring images. The maximum number of images used was 15 and the minimum was three.

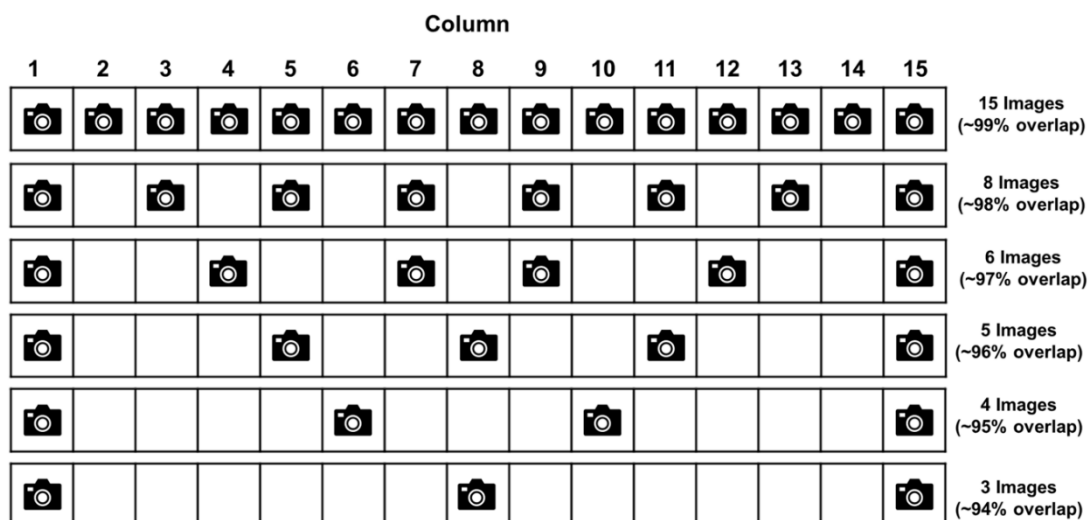


Figure 4.5: The position of images used in Stage Two analysis. Image combinations were taken from the successful row established in Stage One analysis. Camera symbol indicates the position of the image that was used in the creation of the point cloud. Image overlap moves from ~99% to ~94% as images are reduced.

The point clouds created from various image combinations (Figure 4.5) were assessed using the same three comparative tests (B, C, and G) described in section 4.3.5.1. For each combination the aggregated test of SfM-MVS performance (A) was calculated to establish suitable image redundancy in comparison to the TLS. Subsequently, the cloud with a suitable image redundancy was taken through a final precision assessment using precision maps (James et al., 2017). These maps were used to highlight the influence of image geometry on the overall point cloud quality, independent of the TLS. In order to have a practical system of image acquisition for a fixed multi-camera array, image combinations from different rows were not explored.

4.4 Results

4.4.1 Stage One: Positional Camera Parameters

Stage One analysis, which was to establish optimal camera position based on combined height and obliqueness, produced 18 point clouds. Nine from the camera grid positioned at 'Height 1' (maximum height = 1.64 m) and nine from 'Height 2' (maximum height = 2.52 m). The comparative tests provided TLS results with benchmark score of 1 from which the equivalent SfM-MVS result were compared.

4.4.1.1 Deviation Analysis

The mean C2C was in the range of millimetres for all rows from 'Height 1' and 'Height 2'. Camera grid 'Height 2' showed better replication and accuracy with lower mean differences overall in the order of 4 to 6 mm (Figure 4.6). Figure 4.6 also shows 'Height 2' provides better precision with generally lower standard deviation than 'Height 1'. Greater discrepancy in accuracy was present within 'Height 1' with a range of 4 to 10 mm.

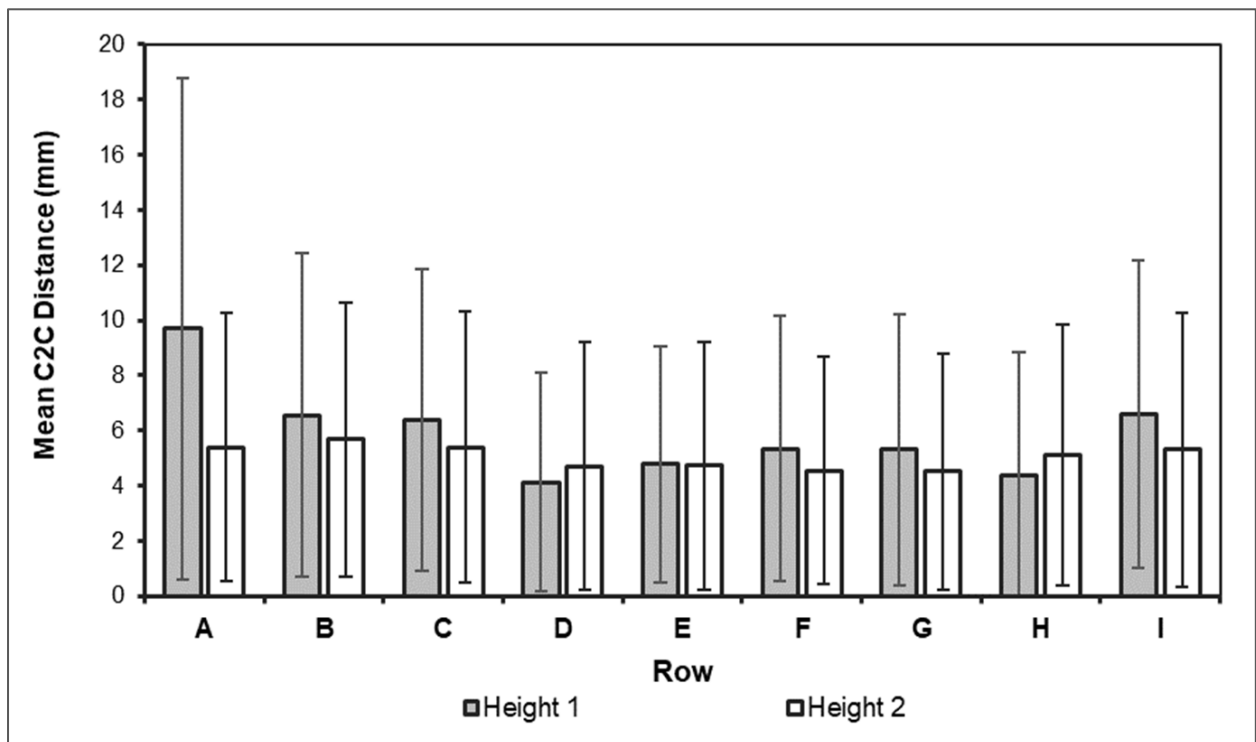


Figure 4.6: Mean C2C distance for point clouds created from each row of the camera grid when compared to the equivalent TLS point cloud.

The highest mean C2C value was Row A from 'Height 1' and the lowest, Row D from 'Height 1' (Figure 4.6). Differences between each SfM-MVS point cloud and the TLS were illustrated with a colour scale of difference. Greatest deviation is seen on the peripheries of the point clouds where there is less overlap of images, reflected in the long tail of the histograms of C2C (Figure 4.7).

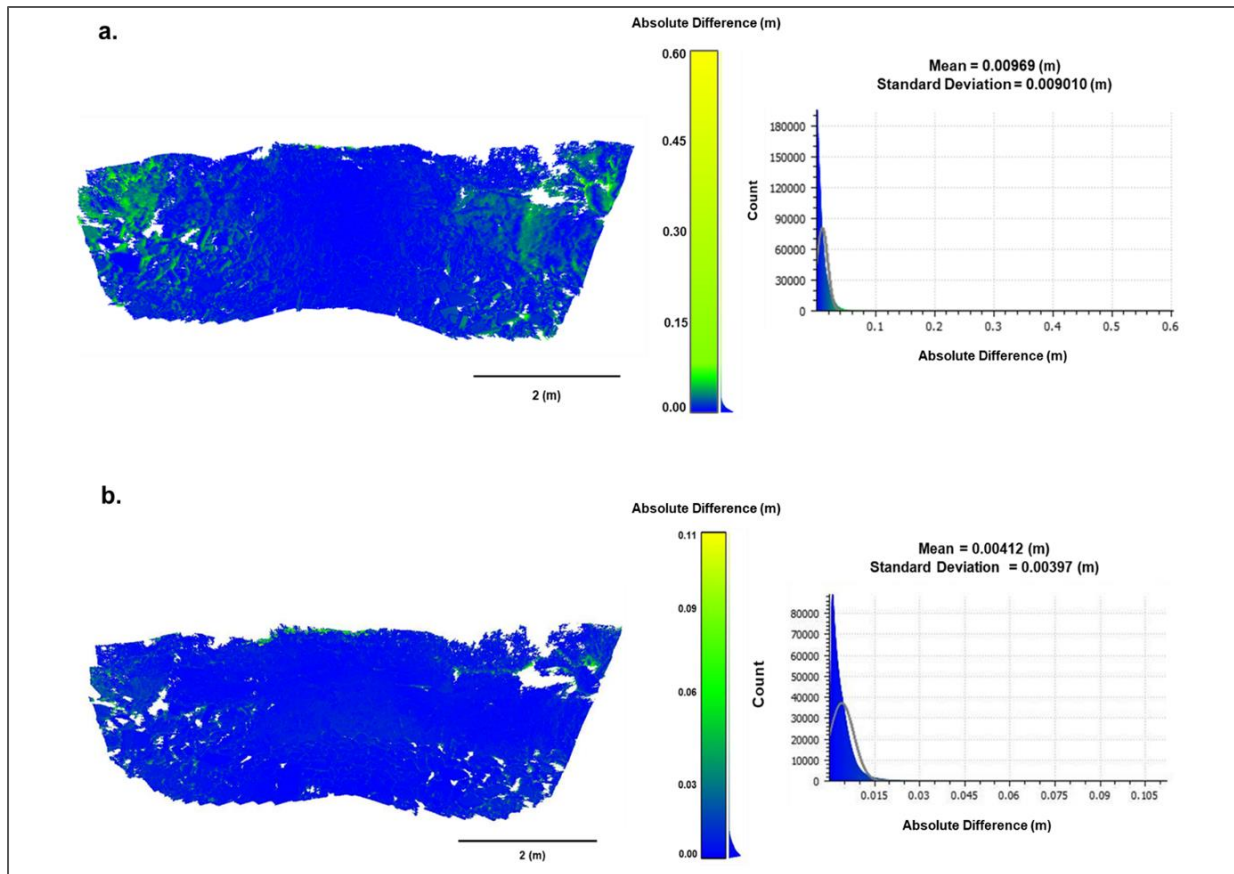


Figure 4.7: C2C scalar field for a) 'Height 1', Row A (highest mean C2C value – 9.69 mm) dense point cloud. b) 'Height 1', Row D (lowest mean C2C value – 4.12 mm) dense point cloud.

A change in camera obliqueness has an impact on the C2C result; Row I ('Height 2') and Row A ('Height 1'), at equivalent heights but different degrees of declination (Row I at 30° and Row A at 0°), show an increased C2C deviation from 5.30 to 9.69 mm (Figure 4.6). The increase occurs because of inadequate scene coverage in Row A, which subsequently impacts the ability of the SfM-MVS algorithms to locate and track keypoints within the image set, and therefore reconstruct scene geometry. This finding highlights the importance of correct camera positioning in the design of a fixed multi-camera array.

4.4.1.2 Completeness Analysis

Completeness results from each row were compared to the ground-truth set by the three TLS scans (given a representative value of 1). Completeness varied greatly by row and some rows offered better results than the TLS. Overall, rows from 'Height 2' displayed consistently higher completeness values than those from 'Height 1'. Figure 4.9(a, b) reveals Rows A–D on 'Height 2' offered 4% (Figure 4.8a) more coverage than

the reference TLS and the lowest coverage achieved was Row I from 'Height 1' (Figure 4.8b).

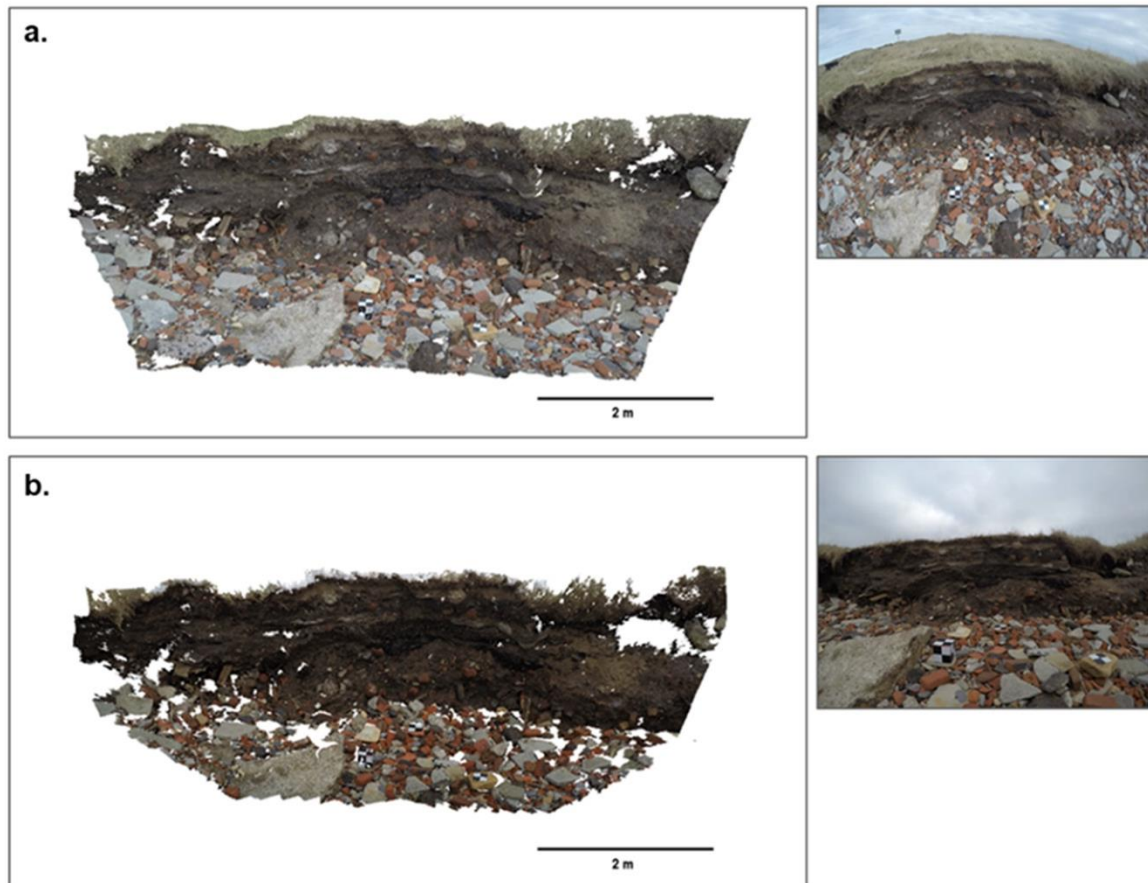


Figure 4.8: Perspective view of point clouds for the best and worst completeness results with a source image from the image set. a) Point cloud from Height 2 Row D had a value of 1.046 - above that of the TLS. b) Point cloud from Height 1 Row I which had the worst value for completeness at 0.795.

As with the previous C2C result, a change in camera obliqueness displayed an impact on the resultant dense point cloud. There was a coverage loss of 19.2% from 'Height 2' Row I to 'Height 1' Row A through which a 30° angle change was made. The increased obliqueness in 'Height 2', Rows A–D, improved overall completeness through reducing in the impact of shadowing from rock, debris and improving the overall camera FOV.

4.4.1.3 GCP Analysis

Figure 4.9(a, b) show the relative reconstruction accuracies of SfM-MVS and the TLS for each row of the camera grid at 'Height 1' and 'Height 2'. A result of 1 would imply that SfM-MVS and the TLS were equivalently accurate in surveying the GCPs.

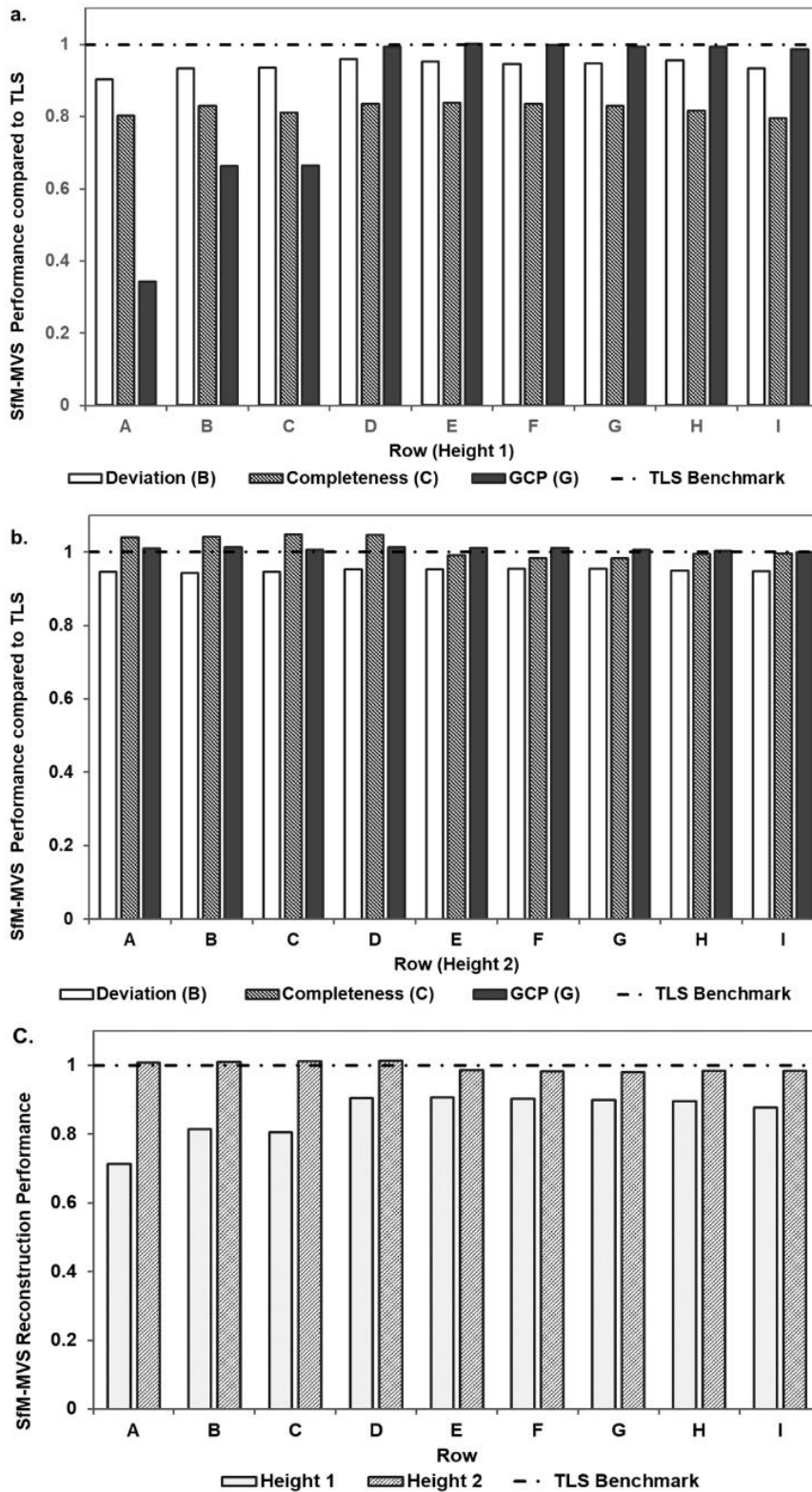


Figure 4.9: The results from the three comparative metrics (Deviation, Completeness, GCP) compared to the TLS reconstruction benchmark for a.) Height 1 b.) Height 2. c.) The overall SfM-MVS point cloud performance for each row of the camera grid at 'Height 1 and 'Height 2' compared to the equivalent TLS point cloud. Row D from Height 2 provided the best overall balance for camera positional parameters at a height of 2.13 m and an angle of declination of 40°.

Overall, rows in 'Height 2' provided higher GCP accuracy and reduced error than rows in 'Height 1', with all results above 0.99. Row D ('Height 2') provided the highest GCP reconstructions with an error range of 0.2 to 1.2 mm. The error range produced here is in line with a calculated theoretical error of 0.25 mm (James and Robson, 2012; Eltner et al., 2016). The calculation of the theoretical error is based on the use of parallel-axis imagery captured under ideal conditions. The oblique camera angles used in 'Height 2' is likely to have produced a reduction in occlusions and subsequent shadowing effect, improving detail in the images and the keypoint matching process.

4.4.1.4 Aggregated Test of SfM-MVS Performance

The calculation of an aggregate weighted average for the three tests provided each row with an overall score relative to the benchmark score of 1 for the TLS (Figure 4.9c). Overall, the rows from 'Height 2' represent the greatest level of performance; Rows A, B, C and D produced results higher than the TLS based on the three comparative tests. Row D at a height of 2.13 m from the base platform and an angle of 40° provided the highest score with 1.015; images taken from this row using SfM-MVS produced a point cloud with a 1.5% greater overall performance than that produced by the TLS, offering the best balance between point positional accuracy and point cloud completeness, both of which are vital for 3D reconstruction. The images from Row D ('Height 2') were used in the second stage of analysis to evaluate the impact of image redundancy.

4.4.2 Stage Two: Minimal Image Capture

Stage Two of the analysis examined six point clouds based on a combination of the 15 images captured along Row D at 'Height 2'. The maximum number of images used was 15 and the minimum was three.

4.4.2.1 Deviation Analysis

Mean C2C distance was in a range of 4.4 to 89.1 mm (Figure 4.10). The major difference in mean C2C and standard deviation was between three and four images resulting in an 84.7 mm decrease in accuracy. Above four images, there are only slight inconsistent changes in accuracy and precision with the number of images. Figure 4.11(b) displays the smallest value was the result of six images (4.43 mm) which had an image overlap of ~97 %; the greatest C2C value was the result of three images with an overlap ~94 %

(Figure 4.11a). This latter C2C value may also have resulted from the sensitivity of the C2C test to the larger gaps created by poorer image overlap in the three-image point cloud.

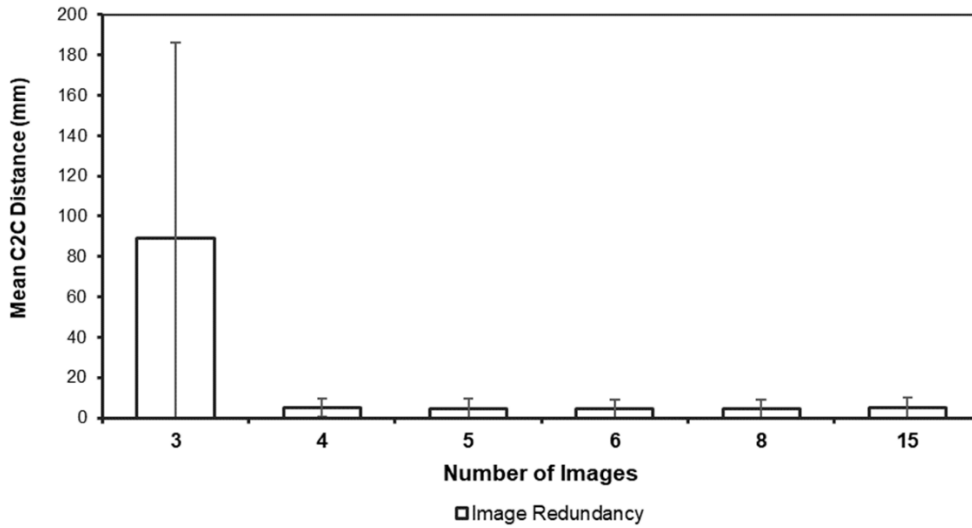


Figure 4.10: Mean C2C distance for point clouds created from image combination when compared to the equivalent TLS point cloud.

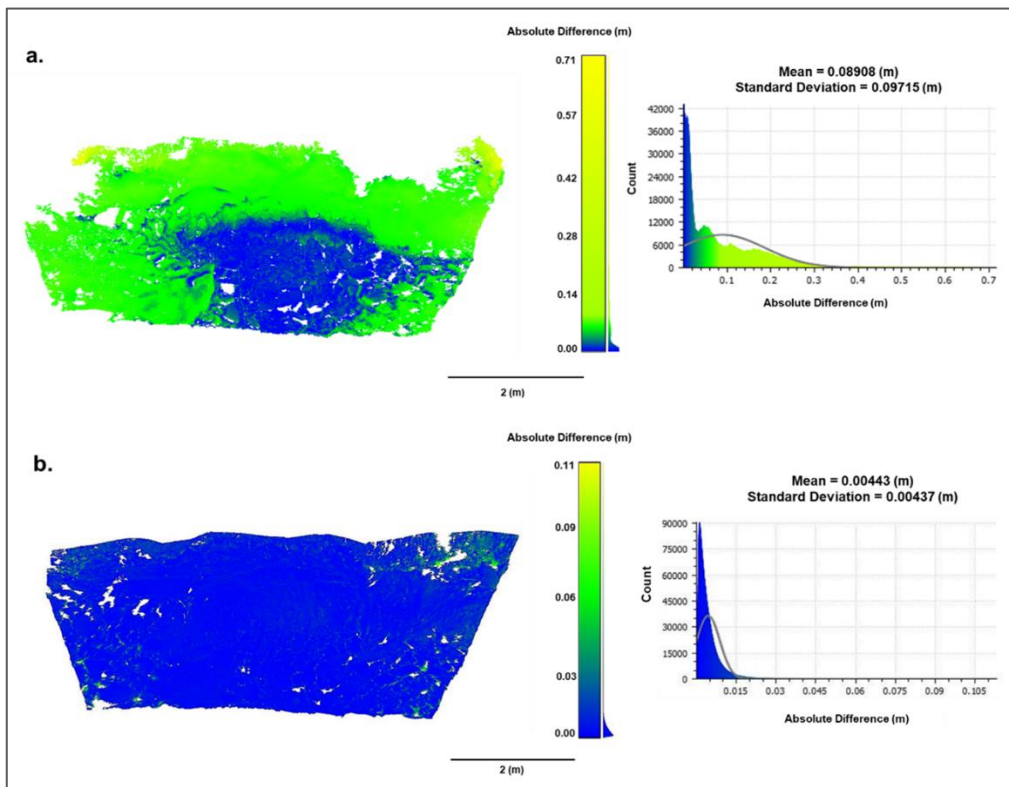


Figure 4.11: C2C scalar field for a) three images (highest deviation value – 89.08 mm) dense point cloud b) six images (lowest deviation value – 4.43 mm) dense point cloud.

The spatial error distribution of the three image point cloud (Figure 4.11a) appeared to show a severe deformation, similar in shape to that of a 'pincushion' lens distortion whereby the centre of the image bends inwardly – near opposite to that of a 'doming' effect (James and Robson, 2014). The distortion present within fisheye lenses means that the image has a high resolution near the centre or principal point where deformation is negligible. However, resolution decreases non-linearly towards the peripheries of the image and is at its most severe near the corners (Phillips and Eliasson, 2018) which could exacerbate errors. This feature is less prevalent in DSLR cameras but Agisoft Photoscan has proven effective at the modelling and removal of radial distortion for wide-angle lens cameras (Nouwakpo et al., 2014). However, during the self-calibration procedure within Agisoft Photoscan determination of key parameters, such as principal point coordinates, is vital for 3D reconstruction. Increasing the number of images used limits the negative impacts of potentially reduced accuracy of the self-calibrated parameters (Boufama and Habed, 2004; Nouwakpo et al., 2014). Bearing this in mind, the decrease in images to three displays a severe deformation of the point cloud, suggesting the limit of image redundancy has been reached, where the decrease in the image set has potentially impacted the self-calibration process and the accurate determination of key parameters such as the principal point. The reduction has also decreased the area of image overlap to areas of lower resolution and potentially more distorted portions of the image. This causes a reduction in image observations that can be tracked across the image set, and those that are tracked are present within the more highly distorted regions.

4.4.2.2 Completeness Analysis

Completeness results from each image combination were compared to the ground-truth set by the three TLS scans (given a representative value of 1). Figure 4.12(a) contains the completeness results; all image combinations above three provided a point cloud with completeness greater than or equivalent to the TLS. Similar to the deviation results earlier, there is a dramatic drop-off of 17.7% in completeness at the transition from three (Figure 4.12a) to four images. Fifteen images provided the highest completeness, 5.5% greater than the TLS. This result is likely owing to the increased number of images used during the densification process.

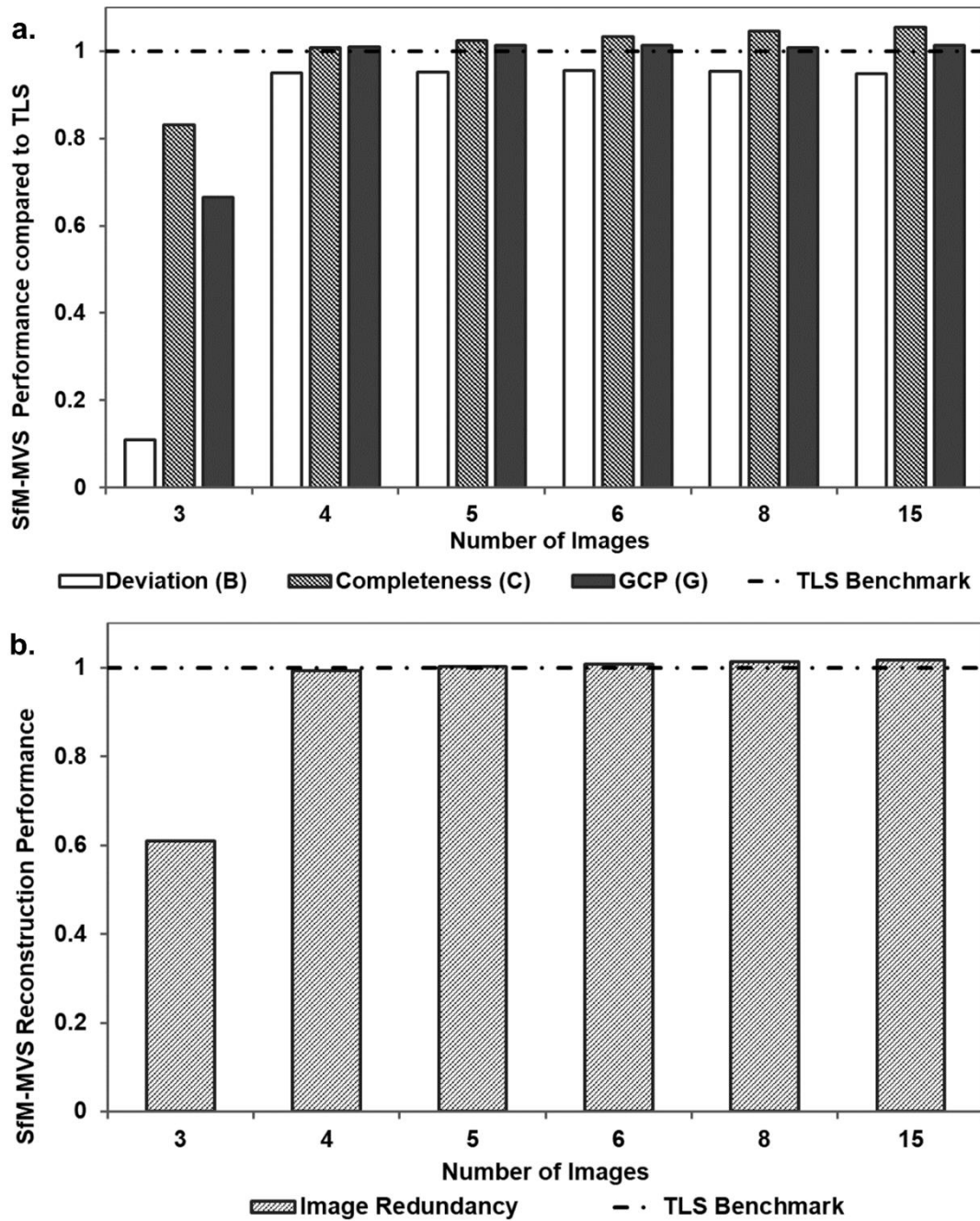


Figure 4.12: a.) The results of the three comparative metrics (Deviation, Completeness, GCP) compared to the TLS reconstruction benchmark for the impact of imagery redundancy b.) The overall SfM-MVS point cloud performance for different image combinations along Row D ('Height 2') compared to the equivalent TLS point cloud.

4.4.2.3 GCP Analysis

Greater than four images used in the SfM-MVS point cloud reconstruction was able to provide 0.82 to 1.4% higher reproduction accuracy than the TLS (Figure 4.12a). Fifteen

images produced the highest accuracy with an error range of 0.01 to 0.19 mm. The second highest accuracy was produced by six images with a range of 0.03 to 0.13 mm.

4.4.2.4 Aggregated Test of SfM-MVS Performance & Precision Maps

Figure 4.12(b) displays the results of the aggregate weighted average calculation for Stage Two analysis. All point clouds with greater than five images showed results equivalent or better than the TLS, whereas those created from three and four images showed poorer results. Three images, ~94% overlap, resulted in a 45% reduction in performance compared to the dense point cloud construction with four. The use of 15 images, the maximum number available, did not improve the reconstructed point cloud proportionately compared to the point cloud created with eight images. Indeed, just five or six images were required to produce a similar, if not better, performance score than the TLS and a smaller mean C2C value than the point cloud created with 15 images.

Therefore, the six-image point cloud was used for assessment of precision (Figure 4.13).

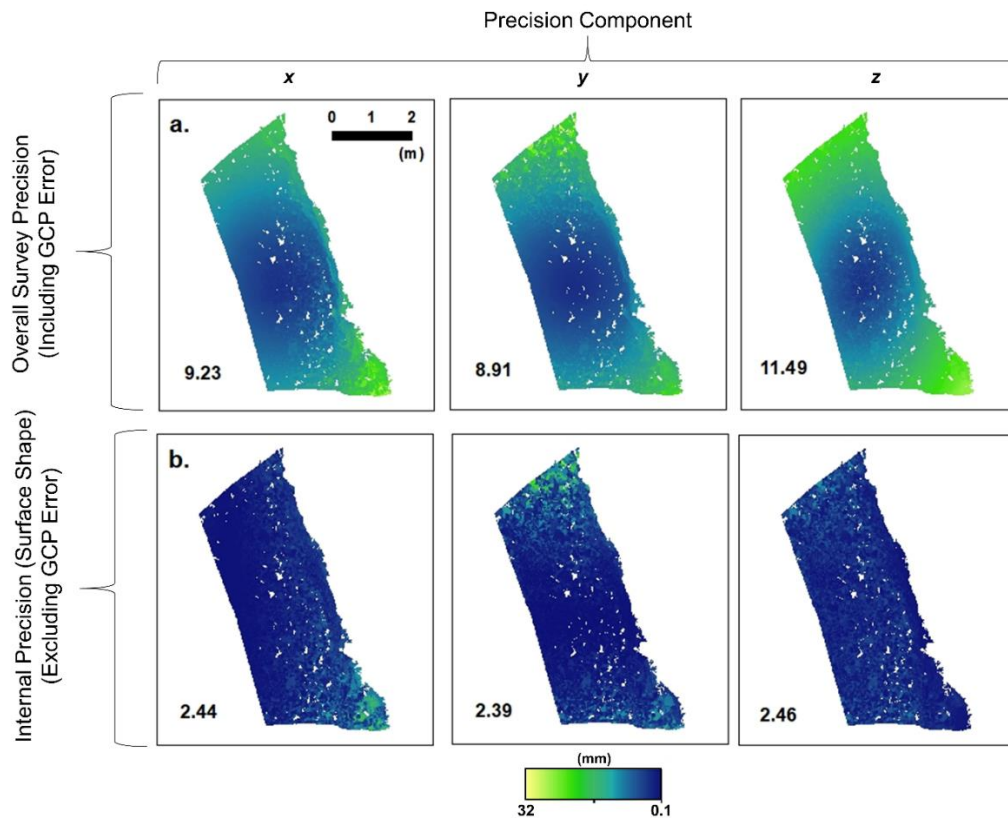


Figure 4.13: Precision error maps separated into x, y & z components for the six-image point cloud. a) displays overall survey precision including georeferencing error. b) displays internal precision (surface shape error) excluding any georeferencing error and reflects the relative precision of point cloud. Mean precision (mm) is displayed on the bottom left of each map.

The precision maps show results similar, both in scale and spatial distribution, to the C2C deviation results. All the precision estimates for the six-image point cloud produced from Row D (Height 2), are generally the same order of magnitude as C2C deviations from the TLS data. Point precision estimates have been separated into those associated with the external coordinate system and those associated with relative 'internal' precision (James et al., 2017). The mean values derived for overall survey precision (Figure 4.13a), which includes georeferencing error, display an offset from the internal precision of the point cloud (Figure 4.13b). The internal mean precision (i.e. relative measurable distances in the cloud) are < 3 mm for x , y and z components. The good internal precision suggests strong photogrammetry through high quality tie points and a strong network geometry created by the six images (James et al., 2017). The 'Surface Shape' error does not appear to show signs of systematic deformation but instead a reduced precision on the borders of the point cloud, equivalent to the C2C results. This lack of surface doming and good internal precision values (Figure 4.13b) would suggest impact from a reduction in image observations on the peripheries from reduced image overlap.

In comparison, overall survey precision appears to be limited by the distribution and, potentially, precision of GCPs. Overall survey georeferencing was calculated as < 3.7 mm in all three translational components (x , y and z) suggesting a good measurement precision. The strong internal precision (Figure 4.13b) means that relative measurable distances will be precise across the point cloud. When combined with a strong external precision the measurement of GCP dimensions (such as in the GCP metric) will potentially have sub-millimetre precision. However, despite good values for translational components the spatial distribution of overall survey precision (external) displays radial degradation (Figure 4.13a). The degradation shows georeferencing certainty reduces away from the GCPs, where the georeferencing datum is initially defined in the bundle adjustment stage (James et al., 2017), subsequently affecting overall external precision. Although translational precision is good, uncertainty may be the result of fewer GCPs distributed on the edges of the point cloud. This same uncertainty is not seen in the internal precision due to the strong image network and tie-points though oblique imagery and high image overlap.

4.5 Discussion

Overall, the results support the use of GoPro Hero 4 Black action cameras with Agisoft Photoscan to provide accurate photogrammetric results when acquiring topographic data at a small-scale site of landward retreat. SfM-MVS with GoPro is a low-cost alternative to TLS on the condition that images are captured from optimal camera positions. This result contrasts with those of Thoeni et al. (2014) who found that images from GoPro cameras provided poor 3D reconstruction capabilities. However, this contrast may be due to the use of optimal camera positions in this research, the updated versions of Agisoft allowing the calibration and rectification of fisheye lens distortion and the improvement in GoPro cameras to a 12 Megapixel sensor.

Camera height and obliqueness proved to be dominant factors in reconstruction performance. Overall, reconstructions from camera grid 'Height 2' evidenced superior replication than those in 'Height 1'. The keypoint matching algorithms used in SfM-MVS software rely on unobscured features to be visible in the scene. The presence of oblique imagery and improved viewshed of the camera created by the increased height reduced such surface occlusions and allowed previously shadowed areas from images in 'Height 1' to become visible in 'Height 2'. James and Robson (2014) and Nouwakpo et al. (2016) documented similar improvements in 3D reconstruction when an off-nadir or oblique image acquisition strategy was used.

All the comparative tests displayed a dependence on camera obliqueness. A change in angle from 0° to 30° (height remained consistent) produced a decrease in mean elevation difference between SfM-MVS and TLS of 4.39 mm. Point cloud completeness likewise responded with a 19.2% reduction following the same angle change. The change in angle from 0° to 30° resulted in oblique imagery which is likely to have strengthened image geometry and improved overall reconstruction.

Height, within the set parameters of the camera grid, displayed a more marginal impact on the results of the three comparative tests. The results displayed a general inverse trend; deviation results generally improved with a reduction in height (variation of approximately 1 mm) and point cloud completeness generally decreased with a reduction in height (approximately 1–2% variation). The increased deviation performance may be related to a somewhat improved resolution of images and ground

sampling distance (variation of ~ 0.01 mm per row) as the camera moved closer to the scene (Eltner et al., 2017).

For a fixed multi-camera system an optimum combination of both height and obliqueness parameters is essential. This combination (Row D, 'Height 2') was established through the use of an aggregate weighted average metric. With a camera obliqueness of 40° (declination) and a height of 2.13 m relative to the cliff, Row D, provided the best balance between the three comparative test results. The characteristics of Row D produced a height ratio of approximately 3:4.18 between cliff and camera height allowing the camera obliqueness to remain at 40° to benefit from more oblique imagery and improved viewshed. The use of this ratio would help to account for a degree of natural variability in cliff height at sites of small-scale landward retreat. There is always a compromise between operational practicalities and improving the image geometry for a fixed multi-camera array. However, optimal camera position and the inclusion of off-nadir or oblique imagery cannot only reduce the impacts of shadowing but may also aid the reduction of systematic error present within SfM-MVS processing (James and Robson, 2014).

The point clouds created from different combinations of image overlap were compared relative to the TLS. As few as five well positioned images provided a point cloud similar in accuracy and completeness to three TLS scans. In contrast, the use of three images produced a severe deformation of the point cloud and reduction in overall aggregated performance. Six images provided the least deviation in elevations between SfM-MVS and TLS. The internal precision estimates for the six-image point cloud were < 3 mm (x , y and z) on average suggesting a strong image network and high-quality tie point estimates. An increase in images from 6 to 15 produced a decrease in deviation accuracy by 0.73 mm. Though only a small change, capturing six images rather than 15 could reduce the cost of hardware and surveying and processing time for a fixed multi-camera array and potentially produce an improved performance. Micheletti et al. (2015b) discuss a similar result for non-fisheye lenses, where, when a strong image geometry is present within the image set, a large number of images is not always necessary for an accurate reconstruction. Consequently, these results question the idea that more images always result in a vastly improved dense point cloud (Westoby et al., 2012).

Previous work has shown that the position and overlap of cameras has a considerable impact on the subsequent point cloud (James and Robson, 2012; Smith and Vericat, 2015; Eltner et al., 2016). However, the positional parameters for a multi-camera system and cameras with fisheye lens is less well documented. This information may aid other research projects in the organization and implementation of ground-based image acquisition. This research has provided an adaptable and systematic method of image acquisition which will prove useful to other SfM-MVS projects. Additionally, the research has evidenced that small changes in camera parameters can improve the overall quality of dense point clouds.

The findings of this research point to the potential of SfM-MVS with an array of GoPros to play an important role in the future of low-cost coastal monitoring but also to the further development and uses of SfM-MVS applications. The importance of this article does not simply lie in its results but in the reported methodology and ideas around the use of controlled camera movement, where handheld cameras would have natural variability. Similarly, the work is innovative in exploring the possibilities for multiple camera systems (e.g. for time-lapse and rig setups) and also in its technical image acquisition that could be adapted and transferred to other research settings. However, there is further research that could build upon this study:

- a) The setup of cameras was designed for reconstructing the cliff and base of typical small-scale site of landward retreat which are common areas of environmental interest. However, exploring these optimal parameters in other landscapes is required to explore the potential of the fixed-array SfM-MVS further.
- b) The distance from sensor to the surface of reconstruction was set at 2 m and would be held constant for an image acquisition procedure using a multi-camera setup. However, distance is likely to impact the reconstruction as each pixel covers a larger area with increased distance from the surface (James and Robson, 2012; Fonstad et al., 2013; Smith and Vericat, 2015; Mosbrucker et al., 2017). Consequently, the impact of distance for other multi-camera scenarios remains an avenue for further research.
- c) Further scrutiny of other parameters that effect reconstruction such as lighting, complexity of object, the number and distribution of GCPs could be investigated in a laboratory setting.

- d) Reconstruction at a small-scale was essential for initial testing of camera capabilities and maintaining x , y & z optical axes. However, extending the size of the reconstruction along the cliff front and with small variations in cliff height would aid the development of the technique for larger scale coastal monitoring.
- e) The use of convergent imagery was not suitable for this investigation due to the nature of multi-camera setups. However, further scrutiny of the specific impacts of convergent imagery in a similar systematic format may advance SfM-MVS research.
- f) Further comparisons could also be made with other SfM-MVS image acquisition procedures (e.g. a single DSLR) to provide a further detailed analysis of the accuracy of fixed-camera arrays.

4.6 Conclusions

This article illustrates the viability of SfM-MVS with GoPros to inform the design of a fixed multi-camera array for correctly reconstructing sites of coastal landward retreat. The results of which provide a readily available alternative to TLS at a fraction of the financial investment. The performance tests undertaken illustrate that, when the crucially important positional variables are taken into account, a small number of well-sited GoPro images can produce a dense point cloud of equivalent and, on some measures, superior performance to three TLS scans. Moreover, the findings show that five images at a height ratio of 3:4.18 and obliqueness of 40° can produce a point cloud of sufficient reconstruction quality with an average error of 4.79 mm to the TLS. Generally, it is true that a larger number of images will achieve a higher quality output, but with a considered approach to image acquisition, this article shows that it is possible to reduce the number of images for a site of this scale which could potentially shorten survey and processing time. The implications of these findings point to the potential of creating an optimized fixed multi-camera array that minimizes the number of cameras needed for image acquisition through good camera placement. This optimization is particularly relevant to coastal zones at greatest risk in low- and middle-income countries where frequent monitoring is correspondingly most necessary and access to the repeated use of expensive equipment can be limited.

5. Monitoring Coastal Morphology: Using a Multi-Camera Array with Structure-from-Motion

This Chapter is written in the style of a journal manuscript and will be submitted in due course. Consequently, the chapter may contain some overlap with the thesis methodology chapter, Chapter 3.

Abstract

Regular monitoring is essential to the protection of vulnerable coastal locations such as areas of landward retreat. However, for many coastal managers and researchers, regular surveying can be limited by factors such as budget, availability of specialist personnel or equipment, and weather conditions. The use of Structure-from Motion combined with Multi-View Stereo (SfM-MVS), a 3D reconstruction technique using 2D overlapping images has helped to democratise the acquisition of topographic data. Terrestrial image acquisition with pole-mounted cameras is gaining traction due to fewer restrictions in comparison to aerial platforms. However, to guarantee effective site coverage and reconstruction quality, greater understanding is required on camera position and subsequent image network interaction. This study presents an alternative approach to image acquisition and processing (Agisoft Photoscan) using a multiple camera array to ensure accessible, efficient and rapid monitoring of coastal recession. The camera rig was deployed at three sites of active landward retreat and results were verified against a comparative TLS benchmark and independent precision estimates. The multi-camera approach provided a systematic and effective method of image acquisition that proved to be ~11 times faster than the TLS, on average, across the three test sites. Reconstruction quality was able to equal (>92 % similarity) or surpass the TLS benchmark, subject to selected processing parameters. Image alignment parameter demonstrated significant influence on point cloud deformation at all sites with a reduction in reprojection error of 94%, on average, through a change in processing parameter ('Medium' instead of 'Highest'). Processing times were heavily influenced by

densification parameter with 'Ultra High' increasing times by 87%, on average, compared to high. However, a marginally lower densification parameter ('High') offered results 4.39% dissimilar from the TLS on average and processing of approximately 1/8th of the time on average. Independent precision estimates across all three test locations were < 8.2 mm for *x*, *y* & *z* dimensions suggesting consistent levels of reconstruction across varying alongshore scales. These findings illustrate the potential of multiple camera systems and the importance of processing parameters on overall point cloud reconstruction quality and computation time.

KEYWORDS: camera array; camera rig; coastal monitoring; coastal recession; SfM-MVS processing parameters; structure-from-motion photogrammetry; 3D reconstruction

5.1 Introduction

Coastal monitoring is an essential part of coastal protection, and repeat surveying offers important insights into the impacts of hydrodynamics on local morphology. Frequent surveying enables understanding of erosion rates, storm response and longer-term trends (Harley et al., 2011), and is therefore important for the mitigation and prevention of flood and erosion hazards. Regular surveying can aid the identification of small-scale temporal trends, in addition to larger scale impacts from storms and changing wave climates (Nicholls et al., 2007; Harley et al., 2011).

Increasing the frequency of surveys for landward retreat can be complex and limited by factors such as budget, availability of specialist personnel or weather conditions. Recent decades have seen technological advances that have improved the availability of remotely sensed data. Methods such as, LiDAR, TLS, and Satellite Imagery have aided the monitoring of coastal settings considerably. These techniques provide different degrees of spatial coverage (m to km) over a variety of temporal scales (daily to yearly). TLS has been used frequently in recent years for monitoring coastal erosion (Dewez et al., 2013; Rosser et al., 2013; Letortu et al., 2018; Westoby et al., 2018) and is often considered as the 'industry standard' for high resolution monitoring of landward retreat due to the quality of the 3D reconstructions (Westoby et al., 2018). However, the deployment of a TLS survey can be extremely costly, skilled operators are required, and survey times can be long for high resolution reconstructions. These inherent obstacles for TLS surveying limit its use for frequent or repeat surveys.

The advent of SfM-MVS has allowed the geoscience community to create accurate topographic surveys at a fraction of the cost. Originally derived from photogrammetry and adapted by the computer science community, the technique allows 3D scene geometry to be reconstructed from 2D images. Greater access to low-cost, user-orientated techniques, such as SfM-MVS, along with the reduced cost and improved quality of consumer grade cameras, has opened up the possibility for coastal managers and researchers with little experience in reconstruction, to acquire data effectively. This advance improves the potential for more regular surveys to help understand morphological change.

SfM-MVS has been used with a variety of platforms when monitoring coastal environments; UAVs (e.g. Casella et al., 2020), poles (e.g. Pikelj et al., 2018) and other aerial platforms such as kites (e.g. Duffy et al., 2018) and hand-held cameras (e.g. James and Robson 2012). UAVs have become an increasingly popular platform for image acquisition. However, not all coastal researchers have the expertise or budget to use UAVs. In addition, the tightening of UAV regulations in many countries and the imposition of local byelaws for the protection of wildlife and practical safety precautions, has made the use of commercial flights problematic in some coastal areas (JNCC, 2019). Furthermore, high wind speeds experienced regularly at coastal sites can often mean that the use of UAVs is not practical; most UAVs are sensitive to wind speeds ≥ 10 m/s (Conlin, Cohn and Ruggiero, 2018). Terrestrial SfM-MVS with pole mounted-cameras, however, do not suffer as greatly in windy conditions and are not subject to the same restrictions.

The use of single cameras with telescopic poles, sometimes including photo cranes, has proved an effective image acquisition method for geomorphic change (Rossi, 2018; Visser et al., 2019). However, there are two main factors that must be considered when using a pole mounted camera. Firstly, it may be difficult to establish the camera's current FOV. Second, the overlap and interaction of images in the network is difficult to establish as both the FOV and the camera's position and orientation are harder to verify and maintain. These difficulties make it challenging to guarantee coverage of a site, making a significant degree of pre-planning for image acquisition necessary. To capture a complete and reliable 3D reconstruction it is necessary for images to be acquired in a systematic manner. Wessling, Maurer and Krenn-Lieb (2014) and Eltner et al. (2016)

emphasise the importance of experienced staff and a complex study design or set of guidelines to reduce the risk of inadequate results or predictable errors. However, for coastal managers with no experience of SfM-MVS this could be an intimidating prospect and would require learning and preparation for each field survey, increasing the time and cost of the survey.

These limitations highlight the need for an alternative approach to image acquisition and processing which could provide a more accessible, efficient and rapid method to frequently monitor landward retreat. The use of a pole mounted array of cameras or 'camera rig', along with systematic and predetermined guidelines for image acquisition, would define image interaction before deployment. Furthermore, an array of cameras has the potential to reduce surveying time in comparison to the TLS and provide a suitable degree of scene coverage and resolution for areas of coastal recession. Moreover, the identification of optimal processing parameters would not only reduce computational cost further but may aid the accurate reconstruction of the point cloud. Streamlining of image acquisition and processing parameters would provide a more rapidly achieved but still metrically sound 3D reconstruction, helping to increase the frequency of surveys.

To meet the above criteria, a multiple camera rig with fixed camera positions of known FOV interaction and prescribed image acquisition guidelines is necessary. To reduce costs and offer users accessible equipment, © GoPro action cameras provide an easily operable, rugged and low-cost option for image capture. Godfrey et al. (2020) have shown GoPro Hero 4 Black cameras, in optimal positions, can provide results similar to that of a TLS over a ~7 m stretch of coastal recession. Therefore, the aim of this paper is to build and use a bespoke fixed multi-camera rig that can achieve scene reconstruction similar to a TLS. The developed camera rig is deployed at three sites of known landward retreat. The objectives are three-fold: first, to test the degree to which acquiring images in this way can speed up data acquisition in comparison to a TLS, without over- or under-representing an area of the survey; secondly, to optimise SfM-MVS processing parameters to produce reconstructions similar to that of a TLS; and, thirdly, to assess the overall reconstruction quality compared to a TLS, a benchmark of reconstruction performance. In responding to these three objectives, the goal of the research is to provide a systematic and streamlined approach to using SfM-MVS for monitoring

landward retreat - from initial camera setup and image acquisition through to image processing and output.

5.2 Study Sites

In order to test the practicalities of the SfM-MVS camera rig, three sites of landward retreat were surveyed: Crosby, Thurstaston and Silverdale on the north-west coast of England, UK. Each site had different scale, sediment composition, vegetation cover and had been subject to different hydrodynamic conditions.

5.2.1 Crosby

Crosby is located on the Sefton Coast in North-West England, UK (Figure 5.1a), situated north of the Mersey Estuary in Liverpool Bay. The coastline is susceptible to some of the highest surge conditions in the UK owing to the shallow nature of the north-eastern Irish Sea. Crosby has a macro-tidal environment with a mean spring tidal range of ~ 8 m (Gladstone Dock tide gauge). The coastline has varied sea defences consisting of sea walls, rock armour and informal rubble groynes and revetments.

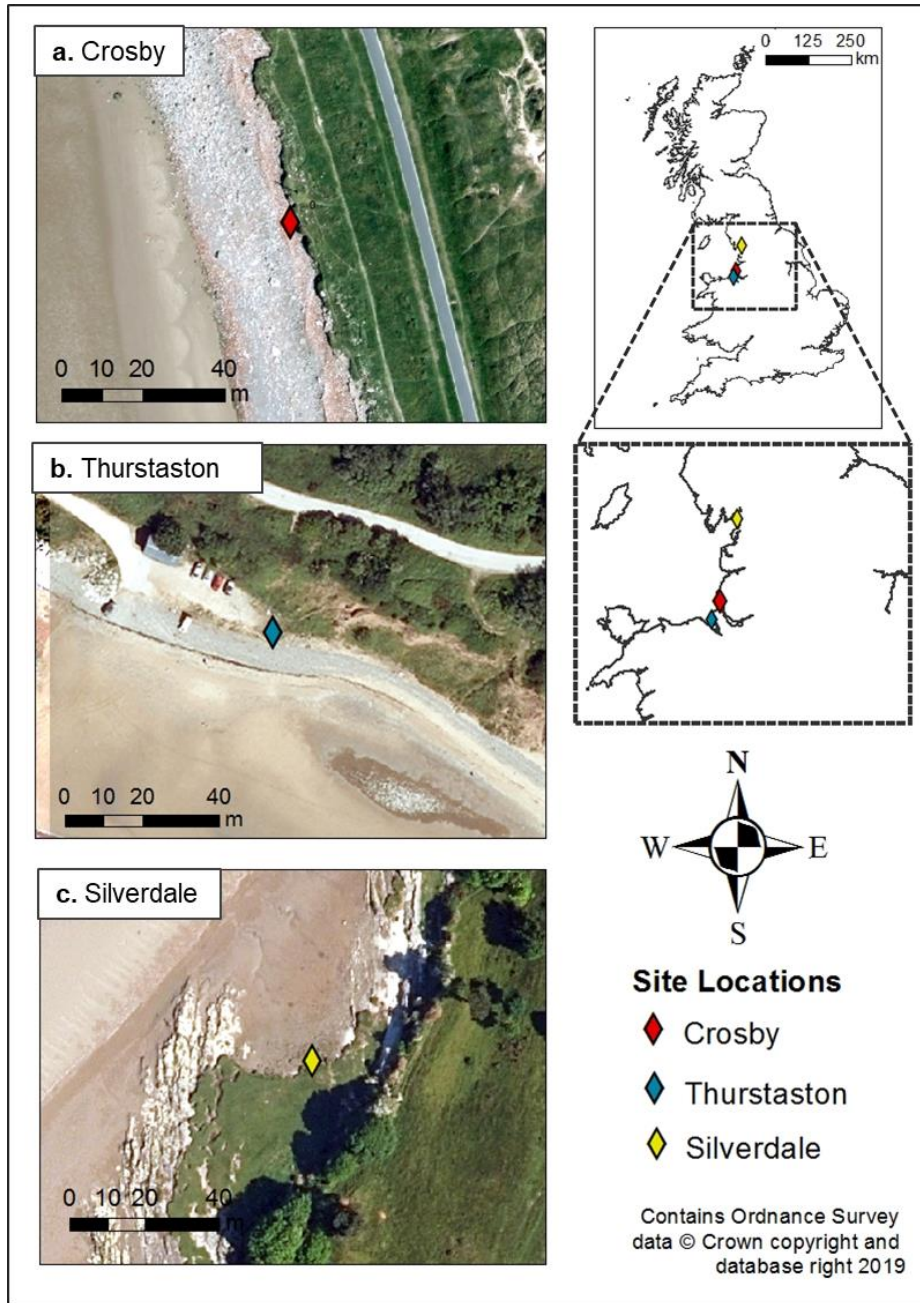


Figure 5.1: Locations and aerial images of Crosby (a), Thurstaston (b) and Silverdale (c) study sites.

The surveyed section of coast was selected because it is currently classified by the Environment Agency as ‘Erodible’ and the defence type ‘Natural’ (Environment Agency, 2019b) (Figure 5.1a). The average height of the cliff front is ~ 1.5 m with vegetation at the top of the cliff and rubble at the base. The rate of recession is estimated at 52 m at the 95th percentile over the medium term (20 years) (Environment Agency, 2019b). Here, the objective is to reconstruct ~ 27 m-long site of landward retreat to test the capabilities of the camera rig.

5.2.2 Thurstaston

Thurstaston is located on the west-side of the Wirral Peninsula, North West England (Figure 5.1b). The Dee estuary is hyper-tidal at its mouth with spring tidal range of 7-8 m (Moore et al., 2009). Over the medium term the retreat distance is estimated as ~10 m at the 95th percentile (Environment Agency, 2019b).

The cliffs are composed of glacial till and range from a height of ~30 m to areas of <1 m. The study site is a lower cliff platform (~1 m) with a less steep cliff front and alongshore distance of ~ 13 m. The top of the site has been heavily adapted and used for vehicle access to the beach. This section of the site has experienced progressive landward retreat over recent decades.

5.2.3 Silverdale

Silverdale is located near the border between the counties of Cumbria and Lancashire (Figure 5.1c). The Silverdale saltmarsh is situated on the north-east shore of the River Kent estuary. The Silverdale saltmarsh has suffered from cycles of sediment erosion and accretion that cut away at the saltmarsh edge. The coastline is considered 'Erodible' with 'Natural' defences. The natural defence is the saltmarsh and the retreat distance calculated by the Environment Agency (2019b) is ~1.7 m over the medium term.

The specific survey site is a section of saltmarsh edge at ~1 m in height and a length of ~28 m. The saltmarsh is mature and vegetated on the cliff.

5.3 Methods

A prototype camera rig, based on camera positions established in Godfrey et al. (2020), was used for systematic image acquisition. Images were processed with SfM-MVS software and the point clouds compared to TLS data through an overall 'performance' assessment. This section provides an outline of the camera rig design, data acquisition, point cloud processing and the procedure for assessing the overall performance of SfM-MVS reconstructions.

5.3.1 Camera Rig Design

Previous work using this camera rig at a small scale (length ~ 7 m) site of coastal retreat (Godfrey et al., 2020), revealed that the cameras should be positioned at a 'Cliff:

Camera' height ratio of 3:4.18 and a camera obliqueness angle of 40° declination from z-axis (i.e. elevation/vertical). In these optimal positions, ≥ five images were required along a rig length of 1.65 m with ~ 97 % overlap to produce a 3D reconstruction quality similar to a TLS. Therefore, six cameras were used on the camera rig, one above the threshold, to provide a balance between cost and the benefits of greater image redundancy. Since the camera rig was covering a larger distance along the cliff-front than previously tested, the distance between successive rig stops was calculated to ensure suitable image overlap. Based on the optimal overlap parameters established in Godfrey et al. (2020) (~97 %) the distance between successive rig stops (D) was calculated as follows:

$$(12) \quad D = 2a + b$$

where a represents the distance from the central pole to the end camera's lens (0.77 m) and b the distance specified for the correct overlap of images (0.33 m). This gave a D value of 1.87 m.

The camera rig was designed for a © 'GoPro Hero 4 Black' action camera. The rig design does not, however, preclude the use of other cameras so long as the optical specifications are equivalent to the GoPro or the optimal image capture positions have been established for the camera prior to deployment. The GoPro camera has a 1/2.3 inch (6.2 x 4.65 mm) CMOS sensor. The pixel dimensions are 1.55 μm with a 4:3 aspect ratio. As with many action cameras the GoPro has a fisheye lens, which is also a prime lens of ~3 mm. The AOV for the GoPro Hero Black is 120° horizontally and 94° vertically when used in 'Wide' image capture mode. The small dimensions of the GoPro (80 x 80 x 38 mm) and light weight (152 g) make it ideal for a multi-camera rig.

Exploring the use of a Multi-Camera Platform for 3D Reconstruction

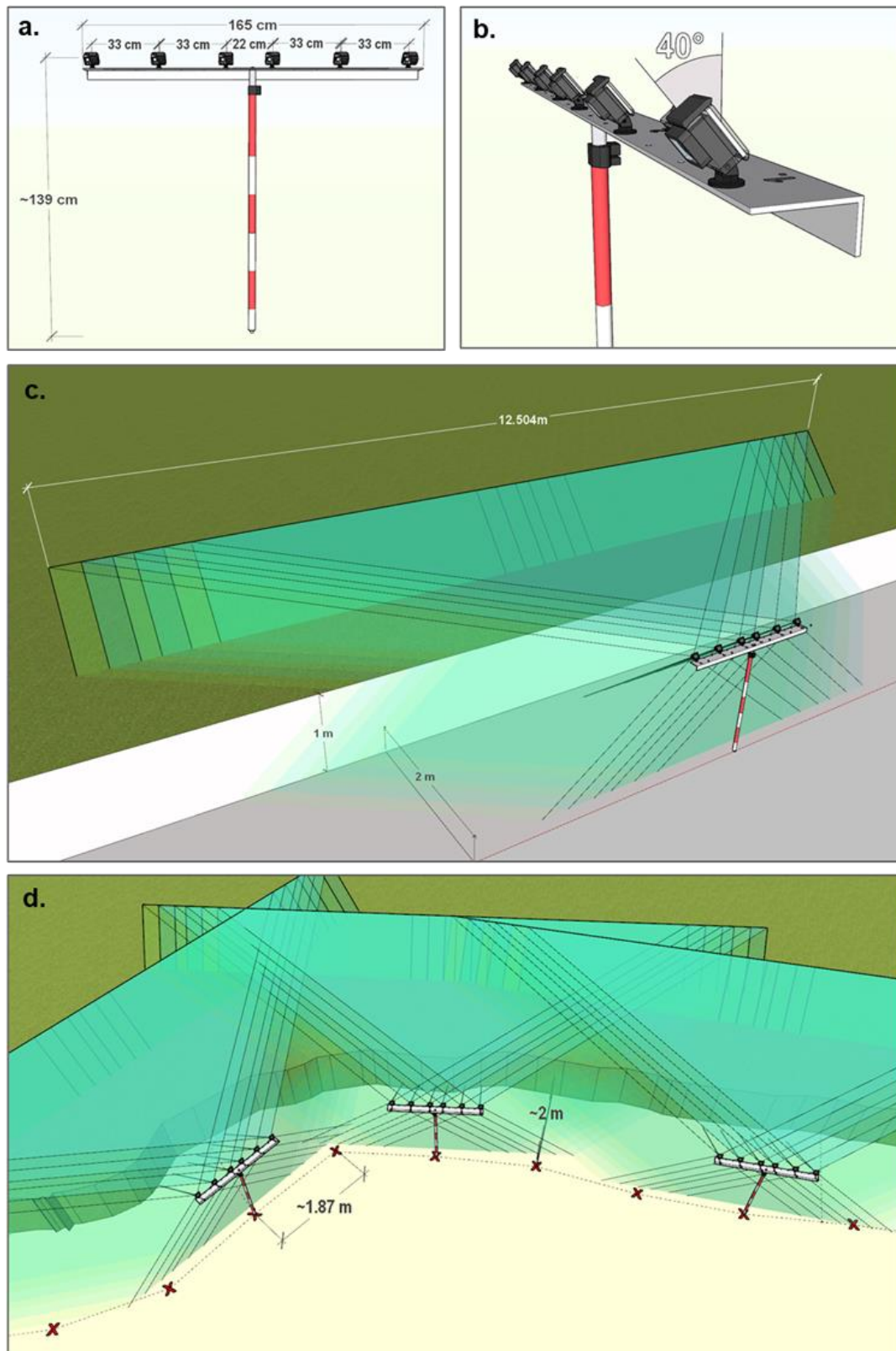


Figure 5.2: Camera Grid representation in SketchUp 2018. a) Camera grid dimensions showing height, width and spacing of camera. b) Camera declination from the z-axis. c) Estimated camera FOVs for the camera rig. d) Representation of camera rig movement in relation to the scene of reconstruction – the cross marks the location of the camera rig for image capture.

The rig was created based on the horizontal dimensions of the camera grid (Godfrey et al., 2020) which meant a horizontal length of 1.65 m and adjacent cameras positioned at ~0.33 m distance apart (baseline) (Figure 5.2). To achieve different height intervals for the Cliff: Camera height ratio, an extendable survey pole was used with a maximum extension of 2.5 m. The pole had a bubble level which was essential to ensure the images were level when captured. A GoPro remote was used to synchronise image capture via Wi-Fi.

5.3.2 Data Acquisition

Thurstaston and Silverdale were surveyed in November 2018 and Crosby in December 2018. These days were chosen based on low tide and suitable weather conditions with no rain, low to moderate wind and sufficient cloud cover to ensure a suitably diffuse illumination of the site (James and Robson, 2012). TLS surveys were acquired immediately after the SfM-MVS surveys.

At each site Ground Control Points (GCPs) (0.15 m² checkerboards) were scattered across the scene approximately 1 m apart. Checkerboards were chosen because they can be recognised in both Faro Scene and Agisoft Photoscan software. Post SfM-MVS and TLS surveys, the checkerboards were georeferenced using a Trimble RTK-GPS R6. The horizontal coordinates for the reference points were set to the British National Grid (OSTN02) while the vertical coordinates were referenced to mean sea level using the geoid model OSGM02.

The location of the camera rig stops were estimated based on Equation 12 (Section 5.3.1). The nature of areas of landward retreat and other cliff-like features means image acquisition was a linear process as images cannot be acquired in a circular motion. James and Robson (2012) discussed the increased potential of systematic distortion or ‘doming’ for reconstructions of this type. To reduce the potential impact of distortion, GCPs were distributed evenly across the site and continuous parallel imagery was avoided, where possible. Consequently, the camera rig had cameras positioned at 40° of obliqueness and the rig was moved in relation to the orientation of the cliff face, meaning that images captured sections of the site from more convergent perspectives (Figure 5.2d). Table 5.1 contains the number of camera rig and TLS stops for each of the three locations.

Table 5.1: Data acquisition information for TLS and camera rig SfM-MVS surveys at Thurstaston, Silverdale and Crosby.

Site	Date	Images Processed	Rig stops	TLS stops	TLS Data acquisition (mins)	TLS Mean error range (mm)	SfM-MVS Image acquisition (mins)	Cliff Height (~m)	Pole Height (m)
Thurstaston	04.11.18	80	8	4	35.52	3.8	9.03	1	1.39
Silverdale	16.11.18	102	17	10	88.8	3.7	4.93	1	1.39
Crosby	04.12.18	114	19	8	71.04	7.6	6.96	1.5	2.13

The TLS survey followed the same route as the camera rig but stopping at every alternate position to accommodate the TLS' greater scan coverage of ~30 m. The survey was undertaken using a Faro 330 which uses digital images captured at the scene to colour the dense point cloud. The scans from each site were processed in Faro SCENE 3D (v.7.1) and, as described in Godfrey et al. (2020), edited to remove noise, errors and crop the areas irrelevant to the survey. The scans for each site were registered together using GCPs as markers for correct orientation. Average TLS mean error (mm) for each site is in Table 5.1.

5.3.3 SfM-MVS Point Cloud Generation

SfM-MVS processing covers two main stages. First, a sparse point cloud is generated from the images. Secondly, this point cloud is intensified through a process of densification. The purpose of this research was to optimise these two stages by speeding up processing time whilst still producing a high-quality 3D reconstruction. The optimisation of software parameters, therefore, entails a two-stage process of assessment. The outcome of the first stage feeding into the second stage.

- Stage One or 'Initial Processing' tested for signs of deformation in the sparse point cloud which may have been exacerbated by the choice of image alignment parameter. At this stage in testing, deformation may be reduced or exacerbated by the selection of image alignment parameters in Agisoft Photoscan. The output from this stage is a sparse point cloud generated using image alignment parameters that provided the least deformation.
- Stage Two or 'Densification Processing' used the outputs from Stage One to investigate the impact of densification (the multiplication of points in the sparse point cloud) on reconstruction and compare the performance of SfM-MVS under differing densification parameters against the results of a TLS reconstruction.

Stage One or 'Initial Processing' began with the images being uploaded into Agisoft Photoscan (Version 1.3.2.42025). The Agisoft workflow allows for the selection of parameters depending upon the type of reconstruction required. As described in Godfrey et al. (2020), the camera model was changed to 'fisheye', which matched the calibration parameters of the GoPro Hero 4 Black. The choice of image alignment parameter at this stage effects whether the image is either downscaled or upscaled.

Software parameters run from 'Lowest' to 'Highest'. Image alignment identifies and tracks features across the uploaded image set; the external and internal camera parameters are solved through a bundle adjustment and a sparse point cloud is created.

The alignment parameters tested in Stage One or 'Initial Processing' were 'Highest', as previously used in Godfrey et al. (2020), which upscales the image by a factor of 4 and 'Medium' which downscales the image by a factor of 4 (2 times by height and width of the image) (Agisoft, 2018). 'Medium' was chosen to offer a potentially computationally faster option for larger sites but one that was not too low to impact the final output. This stage of testing examined the impact of image alignment parameters on point cloud deformation.

Each of the sparse point clouds were then cleaned to remove noise or erroneous points that could impact further reconstruction. Control points were identified in the images and Trimble data (British National Grid/ OSNT02) referenced to the GCP positions. The 'Optimise Cameras' option was then used to remove obvious deformation. This step re-runs the bundle adjustment using the GCPs which reduces image observation error, and in so doing adjusts the estimated camera positions and 3D tie points.

The software markers, which represent the locations of the GCPs on the image, were not placed on poorly observed GCPs (e.g. vegetated areas) and only on GCPs that were in focus on the image and appeared in the central portion of the images (Figure 5.3a-c). The placement of the markers in such a way aided the reduction in deformation brought on by the linear nature of the site or the use of a fisheye lens.



Figure 5.3: Example images used in the point cloud generation showing the estimated central placement of markers onto GCPs in Agisoft Photoscan a) Thurstaston b) Silverdale c) Crosby.

Once a sparse point cloud had been established (either on 'Medium' or 'Highest' alignment parameter) the point clouds were put through 'Ultra High' densification

(equivalent to Godfrey et al., 2020). The subsequent reprojection error, which provides an indication of deformation, was used to determine the image alignment parameters to be used for 'Stage Two' analysis.

Stage Two or 'Densification Testing' used the sparse point cloud with the lowest reprojection error to test the impact of Photoscan's densification parameters on point cloud reconstruction. The densification process produces a dense point cloud that is the fundamental structure or framework from which any model is based. The dense point cloud is an excellent way to test the performance of a reconstruction before a model is created. As with the image alignment step (Stage One), there are a range of parameters within Agisoft Photoscan for reconstruction quality, ranging from 'Lowest' to 'Ultra High'. Image downscaling underpins these parameters. However, the 'Ultra High' setting uses the images at their original scale and each lesser step is downsampled by a factor of 4 (Agisoft, 2018).

The densification parameters chosen for testing were 'Low', 'High' and 'Ultra High' to reflect a variety of quality and timescales for a SfM-MVS reconstruction. The dense point clouds produced using SfM-MVS under these three densification parameters were exported as LAZ files and their overall performance tested against a TLS benchmark for all three sites.

5.3.4 Performance Assessment

To evaluate the performance of the multi-camera rig for image acquisition and the optimal parameters within Agisoft Photoscan, a systematic method of performance assessment relative to the TLS was used in Stage Two. The performance assessment followed three comparative tests using a TLS as the benchmark. Two of the tests evaluated positional point accuracy (deviation analysis & GCP analysis) and one assessed point cloud density (surface density analysis). An aggregated weighted average of the three tests was used to assess the overall performance of the camera rig image acquisition under varying densification parameters. The comparative tests are set out below:

- I. Deviation analysis (*B*) (Godfrey et al., 2020): C2C closest point distance calculation is a direct method for 3D point cloud comparison. The C2C result

was calculated using ‘Nearest Neighbour’ analysis in CloudCompare V2.9 which compared the point clouds generated by SfM-MVS with those of the TLS. The method uses the two aligned point clouds and defines each point’s nearest neighbour in the reference point cloud with those in the compared point cloud (Ruggles at al., 2016). The C2C test calculated the mean distance (combined x, y & z) and standard deviation in distance across each point cloud. A scalar field was then generated which was coloured to represent areas of greater deviation. The resulting mean C2C distance (j) was expressed relative to a 100 mm scale in the form of a deviation metric (B) – Equation 2. The deviation metric (B) was then used in the overall performance assessment against the TLS (Equation 14).

$$(2) \quad B = \lim_{j \rightarrow 100} 1 - \left(\frac{j}{100} \right)$$

- II. Surface Density Analysis (C): The estimation of point cloud density is an important step to judge the coverage of the 3D reconstruction. The surface density was estimated using CloudCompare (V2.9) which calculates the number of points present within a sphere with a specified radius (5.5 mm). The sphere is aligned with each point in the point cloud and the number of surrounding points estimated. The result is the mean density, standard deviation in density and a scalar field which represents areas with higher or lower surface density. This process was also undertaken for the TLS point cloud as a benchmark for comparison and offers a method for comparing the level of coverage of the point cloud. Equation 5 was used to compare the surface density for SfM-MVS (R_s) relative to the TLS surface density (R_t). The surface density metric (M) was then used in the overall performance assessment (Equation 14)

$$(5) \quad M = \frac{R_s}{R_t}$$

III. *GCP metric (G)*: This metric was used to compare the ability of the TLS and SfM-MVS to reconstruct the GCPs in the scene (Godfrey et al., 2020). Expressions (7) and (8) describe the test of accuracy for both TLS and SfM-MVS (P_S refers to the accuracy of SfM, P_t refers to the performance of the TLS). Firstly, under- and over-measurement of the GCPs had to be treated equitably. The conditional statement ('if, then' denoted by the logical operator \rightarrow) occupying the numerator space in equations (7) and (8) describes this process (S represents SfM-MVS and T represents TLS measured values).

Following the logical process, the value was then divided by the GCP known value (R) to obtain a ratio of each method of reconstruction's error relative to reality. Subtracting this result from 1 provided a measure of how accurate the method of reconstruction had been at recreating the known dimensions of the GCP.

$$(7) \quad P_S = 1 - \left\{ \frac{[(S > R) \rightarrow (S - R)] \vee [(S < R) \rightarrow (R - S)]}{R} \right\}$$

$$(8) \quad P_t = 1 - \left\{ \frac{[(T > R) \rightarrow (T - R)] \vee [(T < R) \rightarrow (R - T)]}{R} \right\}$$

$$(9) \quad Q = \frac{P_S}{P_t}$$

Equation (9) describes the ratio of the results of equations 7 and 8 and compares the ability of SfM-MVS to accurately reconstruct the GCP compared to the TLS. If SfM-MVS proved more accurate than the TLS a value for Q of >1 would be returned for each of the GCPs. This test was applied to the x (alongshore) and y (cross-shore) axes of the GCPs at each site. There was a varying number of GCPs at each location, therefore, Equation 13 was used to accommodate the varying number of GCPs: i represented the varying number of GCPs and was equal to 18 at Thurstaston, 50 at Silverdale and 42 at Crosby:

$$(13) \quad G = \sum_{i=1}^n \frac{1}{i} (Q_i)$$

The Q value for each of the GCP measured in the point cloud was weighted by $1/i$ to reflect the number of GCP used in the metric. These calculations were only performed for GCPs at the base of the cliff where there was no impact from vegetation. If one of the techniques was able to reconstruct a GCP while the other was unable, the former was given a value of 2 in order to reflect the ability of one monitoring techniques ability to reconstruct a GCP over the other.

Aggregated Test of SfM-MVS Performance: Once the above three comparative tests were completed for the 'Low', 'High' and 'Ultra High' dense point clouds in Stage Two, an aggregated weighted average of SfM-MVS performance (A) was calculated for each point cloud. Point cloud deformation is a significant issue for sites with a linear image acquisition. Consequently, 50% weighting was given to the Deviation Metric (B) as it provides a clear indication of point cloud deformation and the remaining 50% was divided between GCP Analysis (25%) and Surface Density (25%) to reflect the accuracy and density of the point cloud (Equation 14).

$$(14) \quad A = 0.50(B) + 0.25(M) + 0.25(G)$$

A score of 1 implies that SfM-MVS produced results that were (in aggregate across the three tests) of equivalent quality to those generated by the TLS. Similarly, a score of above 1 indicates a better reconstruction of the scene.

The point clouds that provided scores most similar to the TLS for each site were then taken through an independent precision assessment to review the strength of the image network and influence of GCPs. The process of precision maps was developed by James, Robson and Smith (2017) and uses Monte Carlo simulations on the bundle adjustment procedure in Agisoft Photoscan to provide information for precision maps. Greater detail on this procedure can be found in James, Robson and Smith (2017).

5.4 Results

5.4.1 Stage One: Initial Processing Results

Stage One produced two dense point clouds for each of the three sites, one reconstructed using ‘Medium’ image alignment plus ‘Ultra High’ densification, and the second using ‘Highest’ image alignment plus ‘Ultra High’ densification. The purpose of this test was to identify the image alignment parameter that may exacerbate deformation.

All the point clouds created (Thurstaston, Silverdale and Crosby) initially contained visible signs of deformation or ‘doming’. As discussed in section 5.3.2, the nature of landward retreat sites requires images to be captured in a linear procedure and so reconstructions can be susceptible to the impacts of deformation, making GCPs essential. The inclusion of georeferenced data during optimisation helped to remove the majority of deformation by re-running the bundle adjustment with the inclusion of GCPs. This process reduces potential error on the estimated tie points and camera positions by adjusting their position to the reference coordinate system (James, Robson and Smith, 2017; Agisoft, 2018). The coordinates provided an external reference set and established an alternative method of point cloud correction without pre-processing of images.

Table 5.2: Reprojection Errors (m) for point clouds constructed under different Image Alignment parameters for Thurstaston, Silverdale and Crosby.

Site	Image Alignment Parameter	Densification Parameter	Reprojection Error (m)
Thurstaston	Medium	Ultra High	0.008
	Highest		0.255
Silverdale	Medium		0.012
	Highest		0.236
Crosby	Medium		0.012
	Highest		0.071

However, the choice of image alignment parameter revealed an impact on point cloud deformation. Table 5.2 displays higher reprojection errors for all three sites when using the 'Highest' image alignment parameter. For example, Crosby had a reprojection error of 0.071 m (Figure 5.4b). In comparison the use of 'Medium' photo alignment produced a reprojection error of 0.012 m (Figure 5.4a). The reprojection error is an indicator of poor accuracy at the image alignment which can result in false matches during feature tracking.



Figure 5.4: Crosby dense point cloud deformation under differing image alignment parameters. a) 'Medium' image alignment plus 'Ultra-High' densification. b) 'Highest' image alignment plus 'Ultra-High' densification.

Therefore, the 'Highest' image alignment parameter was excluded and processing for all future reconstructions in Stage Two used the 'Medium' parameter.

5.4.2 Stage Two: Densification Testing

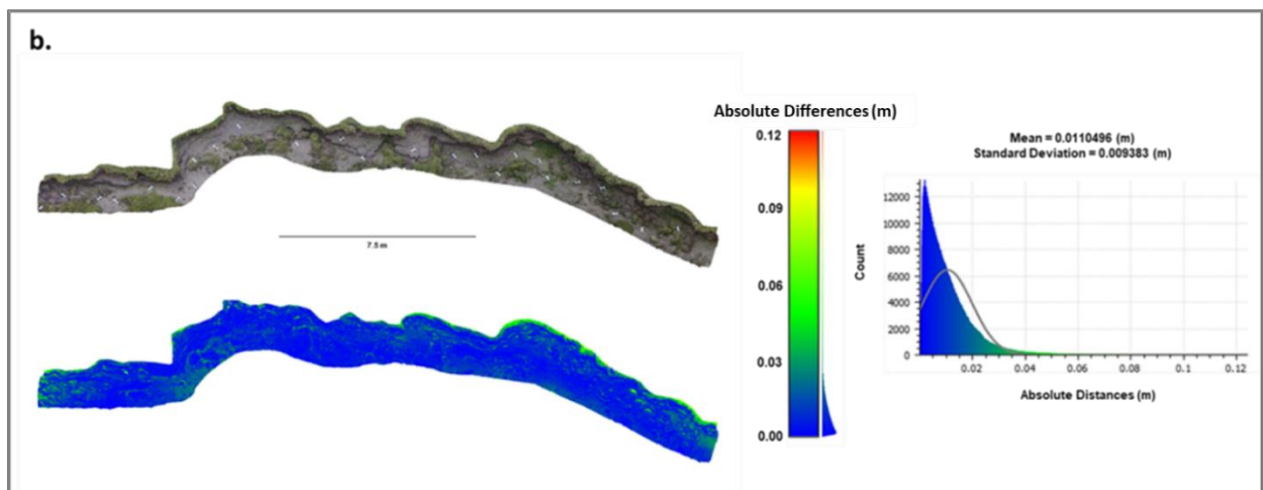
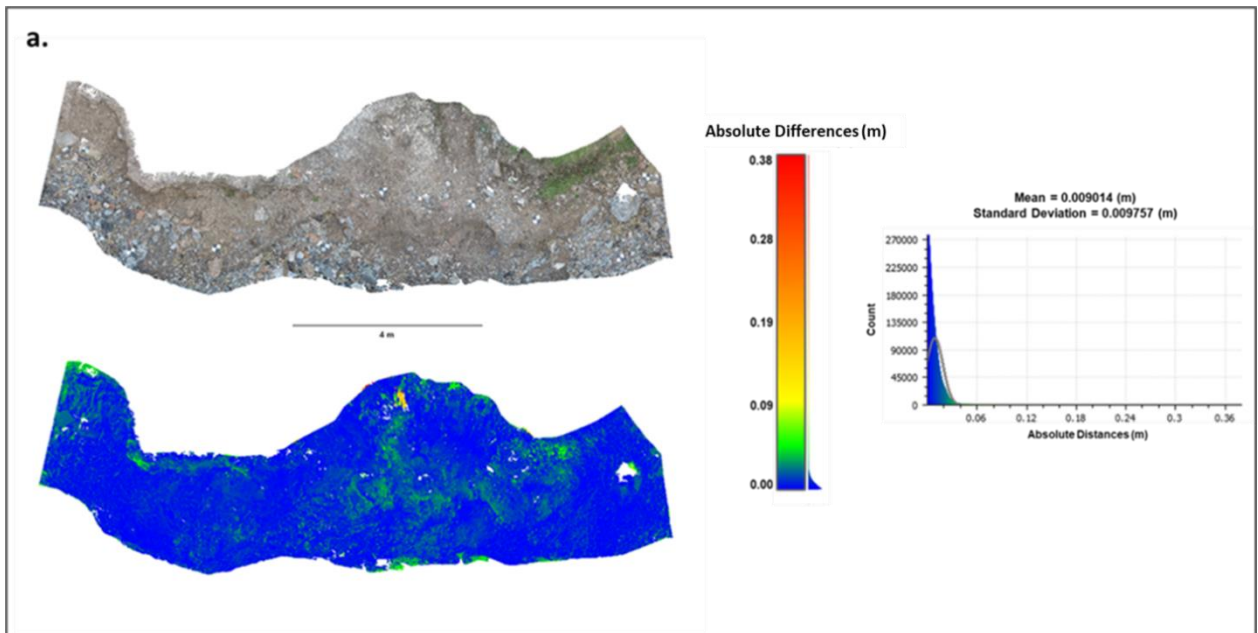
Stage Two analysis used point clouds created with a 'Medium' image alignment and a range of densification parameters: 'Low', 'High' and 'Ultra High' which were tested against a TLS benchmark.

5.4.2.1 Deviation Analysis

The mean C2C was in the range of 8-10.4 mm for all sites and densification parameters. Overall, images acquired by the camera rig displayed consistent levels of replication across all three sites in comparison to the TLS dense point cloud. The TLS point cloud mean errors were between 3.7 – 7.6 mm for the three sites (Table 5.1).

Higher deviation values are displayed by the 'Ultra High' and 'Low' densification processing parameter, with the exception of the 'Low' densification for the Thurstaston. Generally, improved C2C values were created by the densification parameter 'High'.

Deviation between the SfM-MVS point cloud and the TLS are illustrated by a colour scale of difference (Figure 5.5 a-c). The spatial distribution of error for all sites generally followed vegetation patterns. Deviation is highlighted along the cliff margin at Silverdale, Crosby and in a small section of Thurstaston where vegetation is present or overhanging. There is also a minor degree of difference on the peripheries of each point cloud, all below 0.1 m difference, which is consistent with reduced image overlap. The Thurstaston reconstruction also displays deviation in the centre of the point cloud where less features are present in the scene.



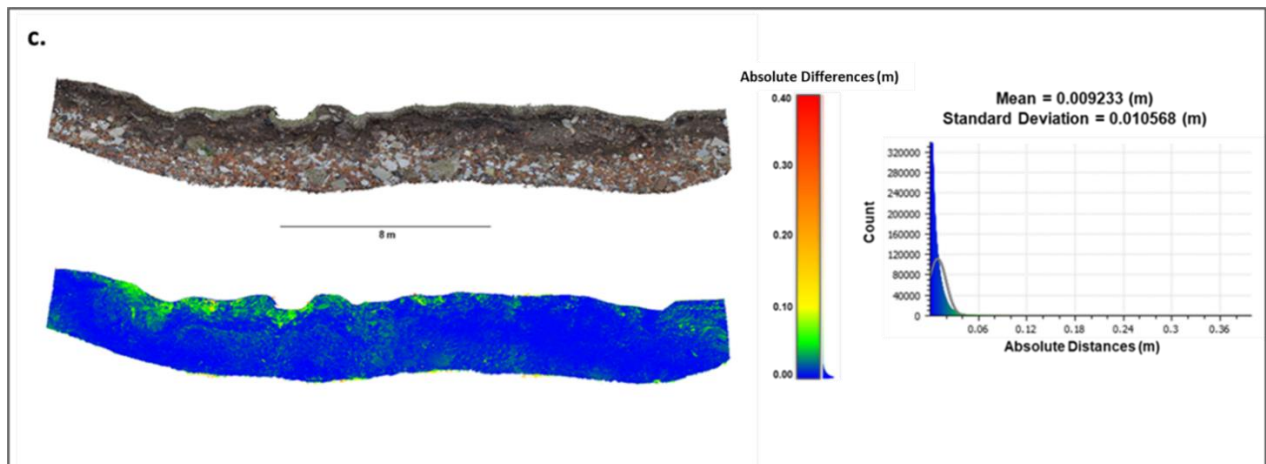


Figure 5.5: Scalar fields displaying the highest C2C values for each site a) Thurstaston, 'Ultra High' densification (highest mean C2C value – 9.01 mm) dense point cloud. b) Silverdale, 'Low' densification (highest mean C2C value – 10.4 mm) dense point cloud. c) Crosby, 'Ultra High' densification (highest mean C2C value 9.23 mm) dense point cloud.

5.4.2.2 Surface Density Analysis

The choice of densification parameter had a clear impact on surface density, with the 'Low' setting producing densities less than 10% of the TLS (Figure 5.6). The 'High' parameter offered similar densities to the TLS. The higher densification parameter, 'Ultra High', provided the highest levels of point cloud density. For example, this parameter produced point clouds for Thurstaston and Silverdale that were more than twice the density of those produced by TLS.

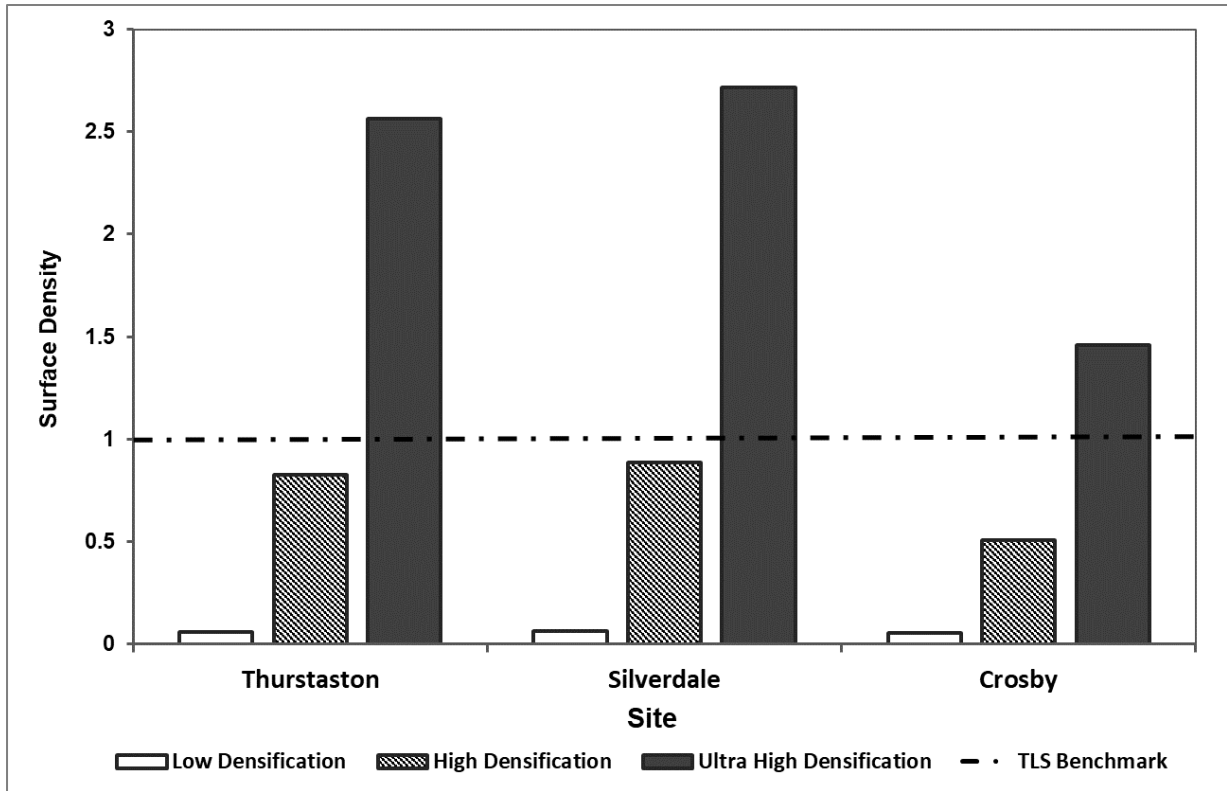


Figure 5.6: Surface density for each site and densification parameter compared to the equivalent TLS result.

As with the previous C2C result, vegetation had an impact on the resultant dense point cloud for both SfM-MVS and the TLS. Areas of low surface density for both techniques were those occluded by the shadowing vegetation from overhanging plants or tall plants in the foreground.

5.4.2.3 GCP Analysis

SfM-MVS provided consistently higher positional accuracy than TLS, with all G values above 1 across all sites and densification parameters (Figure 5.7 a-c). The 'High' densification parameter provided the highest positional accuracies with an error range of 0.03 – 14.7 mm and a mean measurement error of 1.5 mm for Thurstaston, 1.3 mm for Silverdale and 1.4 mm for Crosby. A probable cause for this is that the 'Ultra High' densification created a degree of 'noise' within the point cloud and the 'Low' parameter did not provide enough points to reconstruct the dimensions of the GCP accurately.

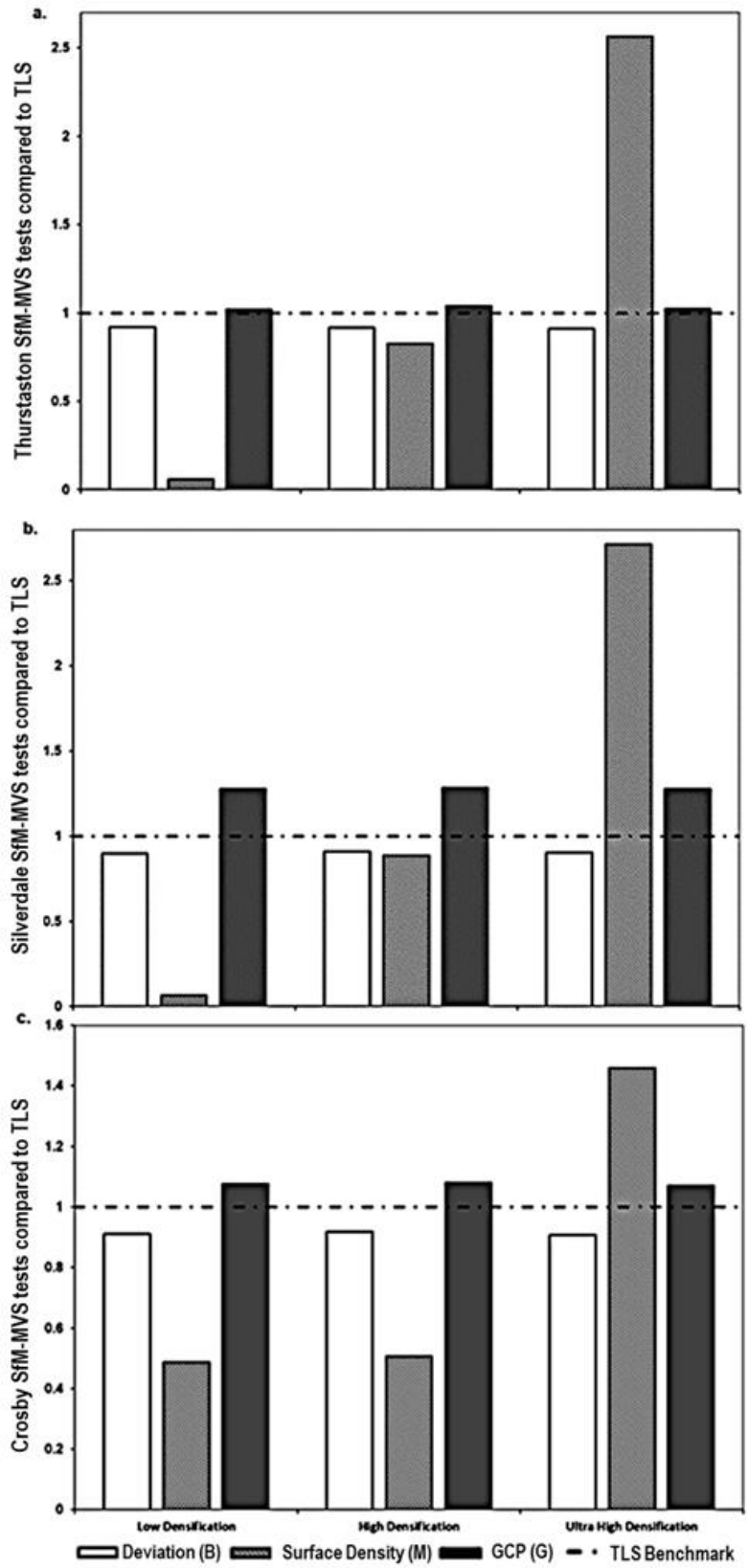


Figure 5.7: Results of the three comparative tests (Deviation, Surface Density, GCP) compared to the TLS reconstruction benchmark for a.) Thurstaston b.) Silverdale c.) Crosby. Reconstruction accuracies of SfM-MVS and the TLS for each site and densification parameter. A result of 1 would imply that SfM-MVS and the TLS were equivalently accurate in surveying the GCPs.

5.4.2.4 Aggregated Test of SfM-MVS Performance & Precision Maps

The calculation of an aggregate weighted average for the three tests provided each site and densification parameter with an overall score relative to the benchmark score of 1 for the TLS.

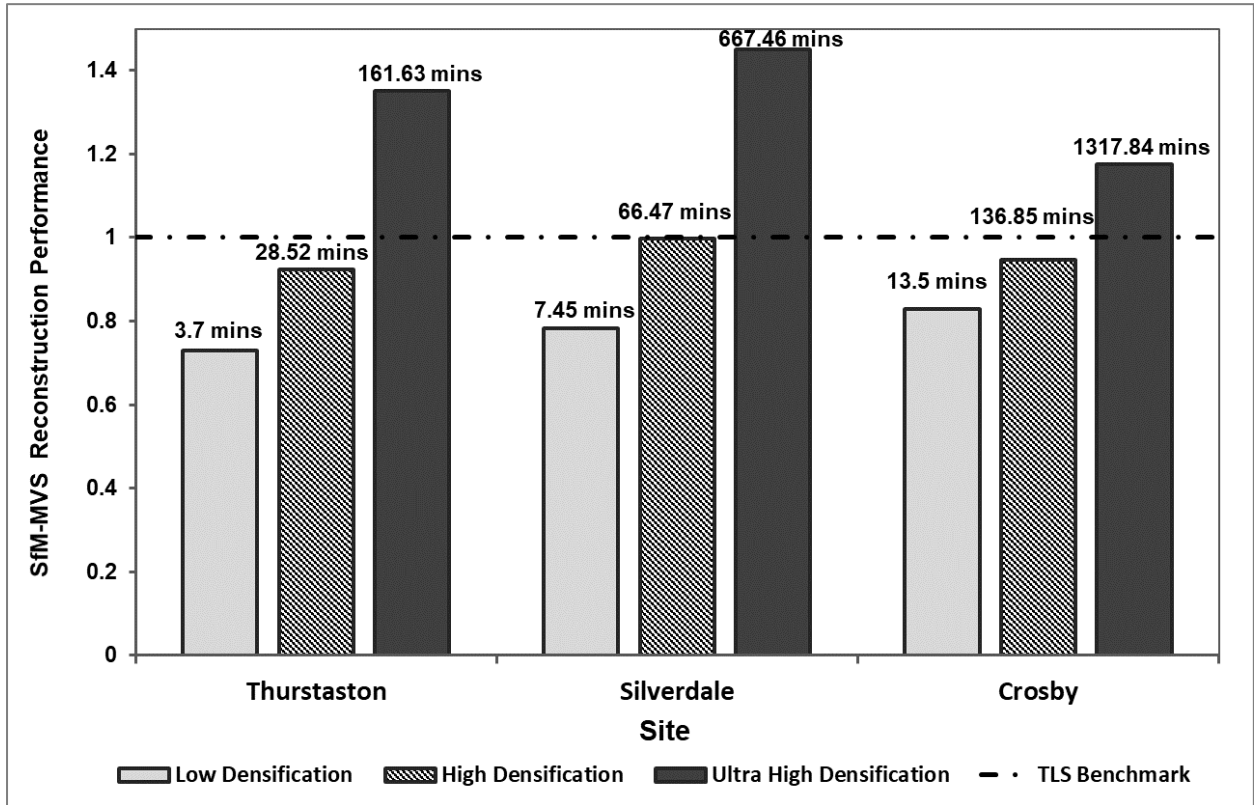


Figure 5.8: The overall SfM-MVS point cloud performance for each site and densification parameter compared to the TLS point cloud. The timescale for computer processing is included as a label on each column. 'Ultra High' provided the best overall score but poorest processing times.

Results show a consistent impact from the densification parameter on reconstruction performance across the three sites (Figure 5.8). 'Ultra Dense' produced the greatest level of performance. 'High' densification with a 'Medium' image alignment parameter provided very good replication with results reaching over 92% similarity to the TLS survey (Figure 5.8).

An increased densification parameter had the expected impact of increasing processing time significantly (Figure 5.8). For example, processing took in the region of a few minutes for lower settings but took over 21 hours for the Crosby 'Ultra High' setting (Laptop: MSI GL72 7QF Intel 7 with GEFORCE GTX 960M and 16 GB RAM). Although 'High' does not reach the levels of performance provided by 'Ultra High' densification, it

offers a result within >92 % similarity of the TLS with 87% less processing time on average. Consequently, the balance of lower processing times and SfM-MVS performance provided by ‘Medium’ image alignment and ‘High’ densification meant these point clouds were used to assess precision (Figures 5.9-5.11).

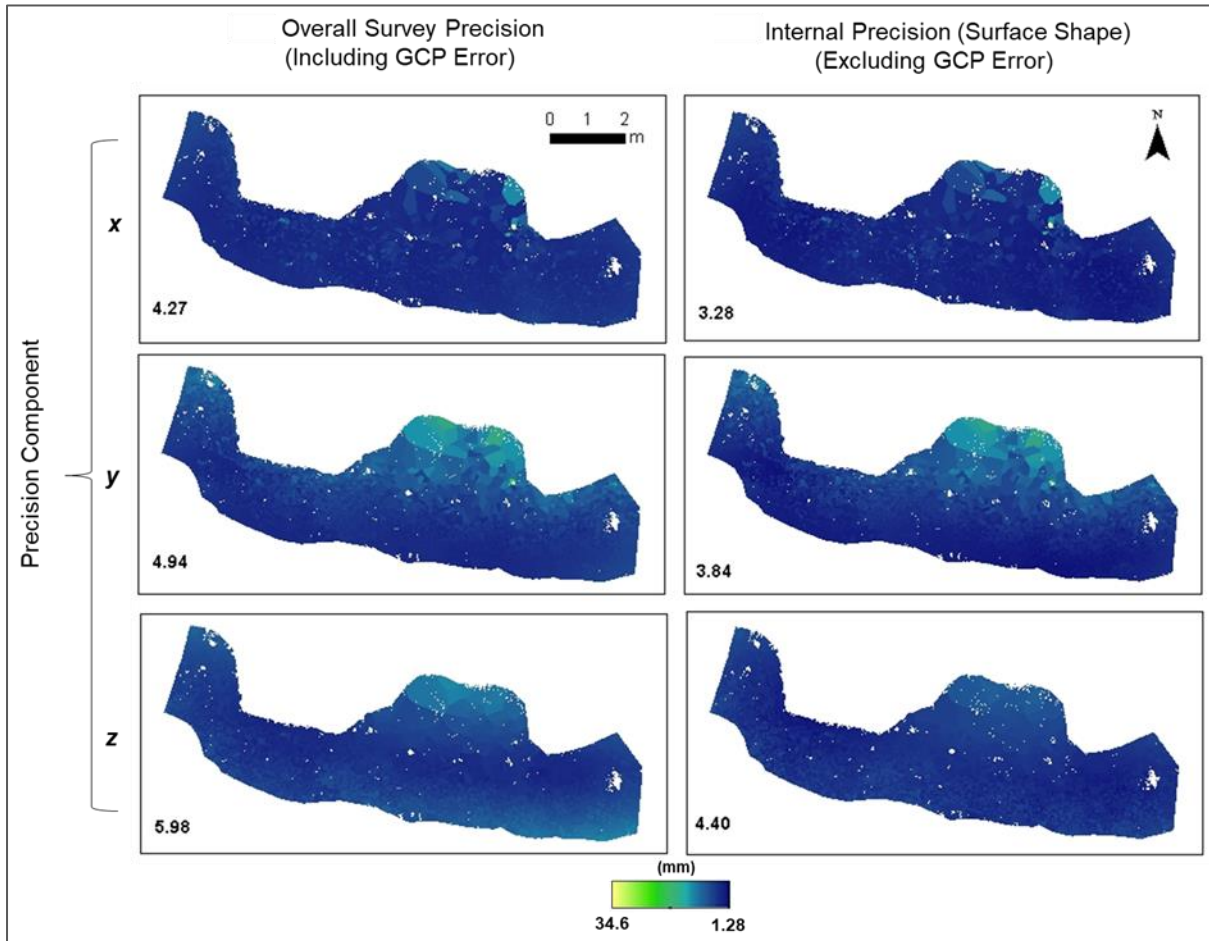


Figure 5.9: Precision error maps separated into x, y & z components for Thurstaston. Overall survey precision including georeferencing error and internal precision (surface shape error) excluding any georeferencing error are displayed in two columns. Mean precision (mm) is displayed on the bottom left of each map.

The Thurstaston reconstruction shows millimetre mean precision across all three dimensions, with all dimensions (x, y & z) providing values < 6 mm (Figure 5.9). Precision estimates for Thurstaston displayed a slight offset, approximately 1 mm, between internal (Shape) and external (Overall) precision. The lower internal precisions (Figure 5.9) suggest the image acquisition scheme provided a strong image network, producing robust feature tracking and tie points.

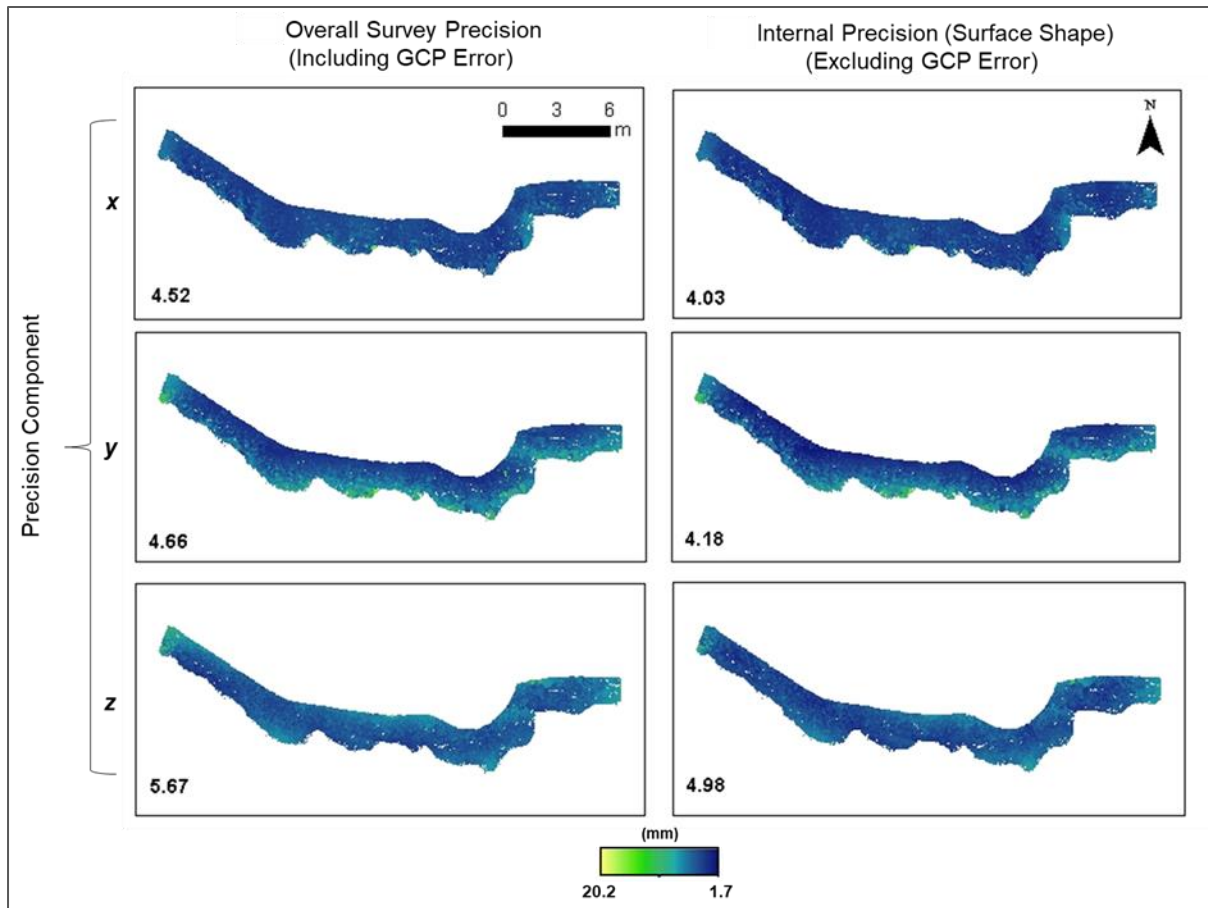


Figure 5.10: Precision error maps separated into x, y & z dimensions for Silverdale. Overall survey precision including georeferencing error and internal precision (surface shape error) excluding any georeferencing error are displayed in two columns. Mean precision (mm) is displayed on the bottom left of each map.

The precision maps for Silverdale also show millimetre mean precision for each dimension for both internal and external precision – all less than 6 mm (Figure 5.10). Overall, the Silverdale reconstruction has slightly higher precision values than Thurstaston but only a very minor offset between external and internal precision, suggesting strength in both the image and GCP network.

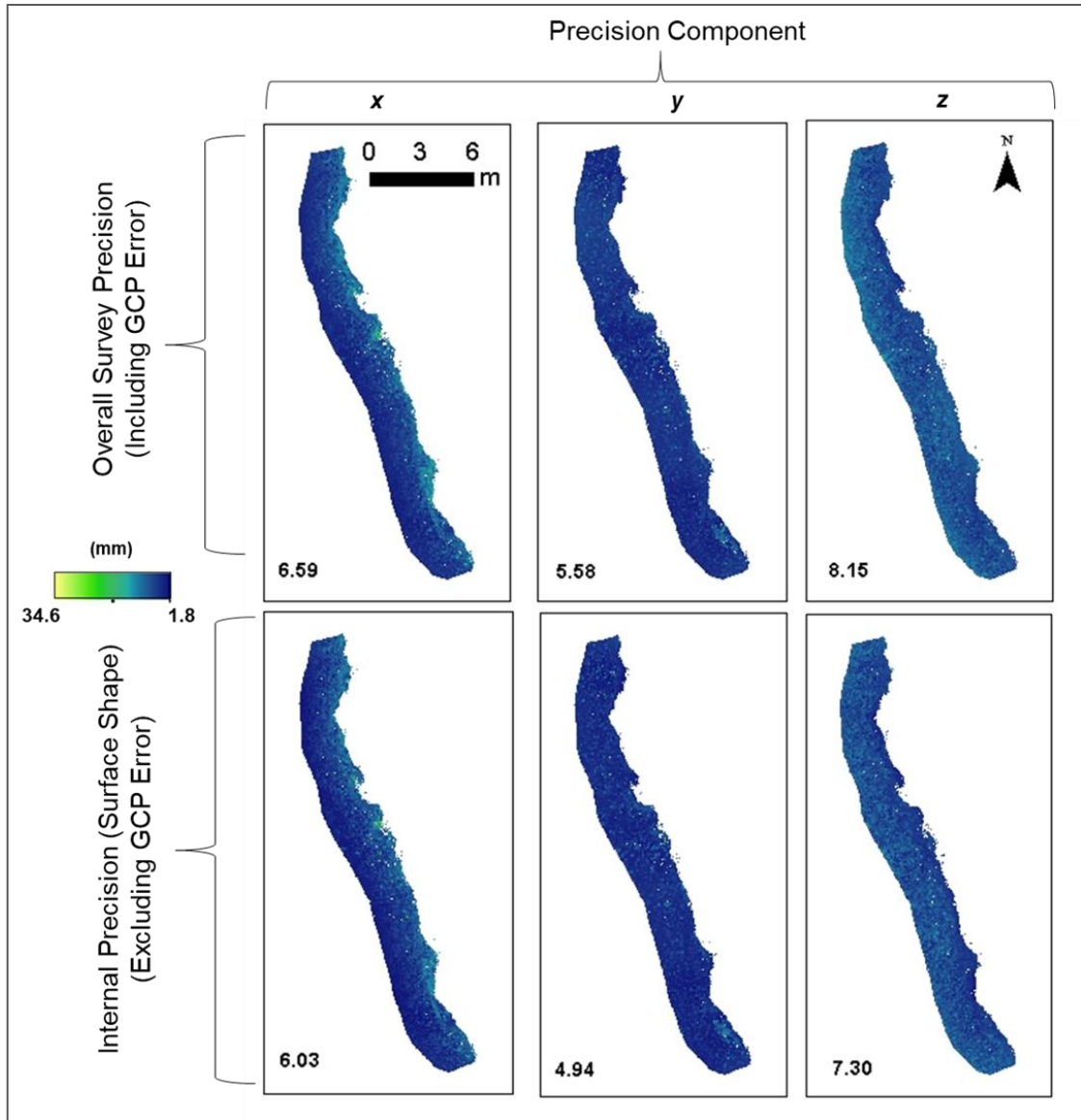


Figure 5.11: Precision error maps separated into x, y & z dimensions for Crosby. Overall survey precision including georeferencing error and internal precision (surface shape error) excluding any georeferencing error are displayed in two rows. Mean precision (mm) is displayed on the bottom left of each map.

The Crosby reconstruction assessment shows millimetre precision for each dimension (Figure 5.11). Precision estimates for both overall precision and shape values lie close together but with an offset of approximately 1 mm in each plane. However, the scale and similarity of magnitude in overall and shape precision suggest both good image network geometry and GCP distribution and measurement. The scale and spatial distribution of estimated precision both internally and externally corresponds with the C2C results (combined x, y & z) in section 5.4.2.1. Poorer precision estimates are present along the cliff where vegetation is present.

5.5 Discussion

5.5.1 Reconstruction Comparison

The research has provided an alternative, systematic and effective method of acquiring images for SfM-MVS using multiple cameras to monitor coastal recession. Images obtained using the camera rig produced point clouds with reconstruction quality similar to, and exceeding, a TLS. Furthermore, the systematic approach to image acquisition and processing with SfM-MVS was able to provide consistent reconstruction results across all three sites.

In regard to reconstruction quality, the use of the camera rig with SfM-MVS displayed an average error of 8.93 mm deviation from the TLS across all three sites and densification parameters. In this study, as with Castillo et al. (2012), Nouwakpo et al. (2016) and Westoby et al. (2018), the TLS is the assumed benchmark standard for comparison of image-based 3D reconstruction. However, error is inherent within all monitoring techniques including TLS and, therefore, during comparative analysis it is important to be aware of error levels present within the reference point cloud. The TLS surveys produced average errors in the range of 3.7 mm to 7.6 mm (Table 5.1). Consequently, when comparing the SfM-MVS point cloud to the TLS, the measured deviation may appear inflated when in reality it reflects some of the error present within the reference survey.

The standard deviation of distance between point clouds is used as an indicator of reconstruction quality. The average standard deviation across all three sites using 'medium' alignment and 'High' densification compared to the TLS was 7.8 mm. Nouwakpo et al. (2016) recorded standard deviation values of 5 mm over a 6 m plot when comparing a TLS and pole-mounted SfM-MVS image acquisition (DSLR). The standard deviation results display a similar order of magnitude, with an offset of 2.8 mm, on average. However, the scale of sites in this current paper is more than double that of Nouwakpo et al. (2016). A standard deviation measure relative to length of site offers the opportunity for improved context of these results (Table 5.3).

Table 5.3: Calculation of dimensionless indicator based on standard deviation.

	Mean Standard Deviation (mm)	Length of Site (m)	Dimensionless Indicator
Thurstaston	7.5	13	0.58
Silverdale	8	28	0.29
Crosby	7	30	0.23
Nouwakpo et al. (2016)	5	6	0.83

Based on the results in Table 5.3, Nouwakpo et al. (2016) displays reconstruction quality poorer than all three sites surveyed with the camera rig. The greatest difference from Nouwakpo et al. (2016) was at Crosby, where there was a 72 % improvement in the standard deviation relative to the length of site. Although there is a need for greater research into the impact of stand-off distance and site complexity, these results provide encouraging findings for systematic image acquisition using the camera rig.

Independent precision estimates for all sites showed millimetre-scale results. The inclusion of independent precision estimates helped to provide a holistic view of reconstruction quality. Precision estimates (both internal and external) for the three sites ranged from 3.28 mm – 8.15 mm (x, y & z). Internal precision displayed marginally lower values than external values suggesting a minor propagation of error produced from the measurement of the GCPs. James, Robson and Smith (2017) reported a much greater offset of 40 mm between internal and external precision for simulated UAV flights. The scale and distribution of precision across the three surveyed sites was consistent, and in line with the spatial distribution of error produced in the C2C analysis. The variation in precision between sites reached a maximum of 3 mm. All sites have shown ≤ 8.15 mm precision estimates in each dimension, suggesting a good image network through the use of oblique and well captured images that produced high quality tie points. Minor offsets between internal and external (includes GCP error) precision were present at all sites which suggests a good distribution of GCPs and good image network geometry. Crosby appears to show slightly poorer precision values than Thurstaston and Silverdale. This difference may be the consequence of increased linearity of the site, reducing the possibility of more convergent images and reducing

the quality of the reconstruction. Crosby and Thurstaston show a marginally higher but similar magnitude offset between internal (shape) and external precision (~ 1 mm) suggesting that the minor errors present in the GCP measurement propagated through the reconstruction to produce a slightly poorer external precision value. Therefore, a minor improvement could have been made to the GCP distribution either through increased number or improved placement.

In this research, as noted in Nouwakpo et al. (2016), the comparison of 3D reconstruction techniques and overall 3D reconstruction quality can be impacted by features present at the site. All the comparative tests displayed an impact from the presence of vegetation. For sites with heavier vegetation coverage, such as Crosby and Silverdale, this was more prevalent. Areas that showed greater deviation were present along the top of the point cloud where vegetation appears in the images. This is not an unexpected outcome of 3D reconstruction when vegetation is present. Castillo et al. (2012) and Mancini et al. (2013) also found that an increase in vegetation led to an increased deviation or disagreement between results of the TLS and those of SfM-MVS. Vegetation not only occludes the surface but its movement varies between images making it impossible for keypoint algorithms to track pixels successfully across the image set (Nouwakpo et al., 2016). Vegetation is also an issue for TLS scans and can lead to deviation of reconstructions in such areas.

5.5.2 Influence of Processing and GCPs

The comparative results provided above were made possible through the analysis of varying processing parameters in SfM-MVS software. The influence of processing proved to be a significant contributor to the overall reconstruction quality when using a systematic approach to SfM-MVS. First, the inclusion and correct placement of GCPs in software showed an impact on deformation. Secondly, the choice of processing parameters at each stage had a significant bearing on reconstruction quality, deformation and processing times.

5.5.2.1 GCP Influence

The inclusion of GCPs in the field is a necessary step for sites with a linear image acquisition procedure to reduce the impact of deformation (James and Robson, 2012). The three sites surveyed provided good texture for feature extraction but the thin linear

geometry of the site meant a potential for a 'drift' in the estimation of internal and external camera parameters (James and Robson, 2012). Drift can lead to systematic deformation and may be more prevalent in action cameras due to the increased lens distortion. The use of GCPs was essential to remove this type of larger scale systematic deformation. The distribution and number of GCPs in field surveying has been well-researched. Warrick et al. (2017) and Westoby et al. (2018) have shown that the increased use of GCPs in the scene during surveys can improve accuracy. Here, precision estimates across all sites showed good GCP networks with precision similar in scale to the image network estimates (all sites < 8.2 mm precision for x , y & z). The minor offset of internal and external (~ 1 mm) precision shows the GCP network has improved since Godfrey et al. (2020), in which the external precision estimate revealed a greater offset between internal and external precision (offset of ~ 7 mm on average across x , y & z). Here, the improvement in number and spatial distribution of GCPs in the field, relative to site scale, is likely to have aided this reduction. However, although precision estimates suggest a good image network geometry, it does not take into account the potential for systematic deformation. This form of deformation is more easily identified through the reprojection error and removed earlier in processing through the use of GCPs in the central portion of the images and additionally, as found in this research, the choice of processing parameters. Therefore, it is essential to include a strong GCP network and a strategic choice of processing parameters to reduce the impact of systematic deformation at locations of coastal recession.

5.5.2.2 Influence of Processing Parameters

The choice of processing parameter proved to be influential on overall point cloud reconstruction. The selection of the image alignment parameter, in Stage One, had a considerable impact on point cloud systematic deformation. The 'poorer' image alignment setting ('Medium') provided a reconstruction that had 18 times, on average, less reprojection error (an initial indicator for systematic deformation) than the 'Highest' image alignment setting. The 'Highest' image alignment parameter upscaled the image by a factor of four and, therefore, introduced an increased number of feature matches across distorted portions of the image. The quality of reconstructions from overlapping 2D images is significantly dependent on image content and subsequent feature matching (Gruen, 2012). Therefore, cameras with greater FOVs, such as action

cameras provide a high degree of feature tracking (Streckel & Koch, 2005). Furthermore, the linear nature of image acquisition for sites of landward retreat means that images generally run parallel to the scene (adjacent cameras moving along the cliff edge). The combination of a linear image capture and a wider FOV from the action camera encourages feature tracking across the distorted borders of the image, impairing the software's ability to adequately estimate camera pose, image network geometry and, therefore, reconstruction quality (Eltner et al., 2016). James and Robson (2012) discuss how poor camera model estimation is more likely at image borders where distortion is more prevalent. Therefore, the poorer reprojection error provided by the 'Highest' image alignment parameter may appear contradictory, but the upscaling of the image encourages matches with poor covariance and so a poor estimation of camera pose and orientation. Consequently, the downscaling of the image ('Medium' image alignment parameter) 'forces' the software to use larger, more stable features as keypoints and so there is less likelihood of systematic error through 'drift' in camera pose estimation. Prosdocimi et al. (2015) documented how decreasing image resolution (e.g. downscaling) led to reduced error potentially due to error smoothing. The choice of densification parameter (Stage Two) had a marked impact on SfM-MVS performance. Contrary to Stage One, which showed a lesser parameter providing an improved result, the densification process improved the reconstruction with each higher interval. This improvement is not an unexpected outcome, as densification multiplies the tie points established in the image alignment stage and does not optimise any aspects of the point cloud making it a less influential step (James, Robson and Smith, 2017). High quality feature matches in the initial image alignment stage (Stage One) is vital to the construction of a reliable sparse point cloud as all further processing relies on this initial estimation of camera orientation (Remondino et al., 2014) and errors, which, if present will propagate through the reconstruction (Eltner et al., 2016). The impact of densification choice on reconstruction quality is more easily assessed when compared to the TLS results. The choice of densification can provide users with a result that surpasses, equals or under-performs compared to the results of the TLS. Eltner & Schneider (2015) and Smith and Vericat (2015) also found SfM-MVS to outperform the TLS on small-scale sites with single cameras. When streamlining the processing of SfM-MVS the choice of parameter becomes significant, as the time and

computational cost associated with this parameter may outweigh the benefits the setting provides. In this research, the 'Ultra High' densification parameter required longer processing times than the 'High' setting (increase of 87% on average) and most of its benefit was accounted for by the sheer density of the point cloud. However, the 'High' densification parameter offers results only 4.39 % dissimilar to the TLS on average across all three sites and processing of approximately 1/8th of the time, on average. This is a significant gain in efficiency if processing power is limited or time constraints imposed.

5.5.3 Future Avenues for Research

Overall, the multi-camera rig has been shown to provide a rapid and systematic method of image acquisition for SfM-MVS. At all sites the 3D reconstructions from the rig have shown consistent results, both in comparison to the TLS, and through independent precision assessment. A combination of different processing parameters has proven optimal for accurate 3D reconstruction. The choice of a nominally lower image alignment parameter, 'Medium', provided decreased reprojection error and less deformation.

The combination of 'Medium' image alignment parameter with the 'High' densification setting provided results that were >92 % similar to TLS. The benefit of using a lower image alignment parameter in this research does not mean the choice of the 'Highest' parameter may not be advantageous for other reconstructions, as deformation may be less prevalent at sites where a 360° image capture is possible. However, this research does corroborate the suggestions of Brasington, Vericat and Rychkov (2012) and Eltner et al. (2016) that diligent selection of processing parameters post-image acquisition is an important step for reconstruction quality.

Data acquisition using the rig also proved to be considerably faster than using a TLS. The camera rig provided a data acquisition 10.71 times faster, on average, than the TLS across the three sites. The reduction in time is particularly important with respect to fieldwork in coastal settings. Tidal cycles and weather conditions can reduce the accessibility of sites and rapid acquisition of data can be vital to fully survey an area.

Based on this research, the camera rig has shown to be a potentially low cost (~£600) and efficient alternative to the TLS which cost in the region of £35,000 (Visser et al.,

2019). This work has also provided insight into the impact of processing parameter choice and how adjustments to these can produce results that are similar to, and in some cases even exceed, the TLS benchmark. The use of this form of data acquisition would provide systematic, easily followed guidelines to secure a level of coverage that may not be as achievable for less experienced users of SfM-MVS. The strong precision values established for all sites show the influence of good image network geometry and robust GCP networks, both of which are essential for a high-quality reconstruction. These values also point to the positive use of multiple cameras used systematically with SfM-MVS to acquire images effectively.

The research has provided a holistic approach to SfM-MVS for monitoring coastal recession. However, there is additional research that could build upon this study:

a) The setup of the multi-camera rig was specifically designed for sites of coastal recession of a particular height range and a specified stand-off distance. However, exploring the use of multi-camera setups in different environment settings and scales would expand the potential of the multiple cameras.

b) In this research, choice of processing parameters was a significant focus. However, software marker placement also displayed an influence on reconstruction.

Consequently, a focussed examination of the impact of software marker placement on 3D reconstruction quality would be an interesting avenue for research, particularly, the impact on different lens types e.g. DSLR compared to fish-eye.

c) The camera rig in this research was used for a roving image acquisition. However, further avenues of research could explore adaptations to the multi-camera rig such as in-situ monitoring with permanent camera positions.

d) Comparisons with other SfM-MVS image acquisition schemes such as single DSLRs or other platforms could provide further details on the accuracy and usability of multi-camera setups.

5.6 Conclusions

The purpose of this paper was to illustrate the viability of a multi-camera rig for image acquisition with SfM-MVS for three sites of landward retreat and to investigate optimal processing parameters within Agisoft Photoscan.

The rig provided a systematic and effective method of image acquisition that proved to be ~11 times faster than the TLS, on average across the three test sites. Comparative tests with a TLS showed overall reconstruction quality that could equal (> 92 % similarity) or surpass the TLS benchmark depending upon selected processing parameters. Image alignment parameter proved to significantly influence point cloud deformation at all three test locations with an average reduction of 94 % in reprojection error through a change in processing parameter ('Medium' instead of 'Highest'). The choice of densification parameter had a significant bearing on processing times with 'Ultra High' parameter increasing times by 87% on average. However, a marginally lower densification parameter ('High') offered results only 4.39 % dissimilar from the TLS and processing of approximately 1/8th of the time on average.

Independent precision estimates across all three test locations were < 8.2 mm for *x*, *y* & *z* dimensions suggesting consistent levels of reconstruction across varying alongshore scales. The research has revealed increased speed of data acquisition in comparison to a TLS, as well as the simplified nature of the image capture network allowing images to be acquired systematically for sites of coastal recession. The findings of this research provide users with guidelines on an alternative SfM-MVS image acquisition strategy and processing that can reduce survey and computational time without detriment to reconstruction quality.

6. Tracking Coastal Morphology using a Multi-Camera Array: A Novel Approach to Saltmarsh Monitoring

This Chapter is written in the style of a journal manuscript and will be submitted in due course. Consequently, the chapter may contain some overlap with the thesis's methodology chapter, Chapter 3.

Abstract

Saltmarsh environments offer numerous benefits such as natural forms of coastal protection. However, these environments are often subject to erosion which is accelerated by sea-level rise, restricted sediment supply, or human interventions. Erosion of the saltmarsh margin drives landward retreat; therefore, regular monitoring is essential to reveal saltmarsh response to wave hydrodynamics and to mitigate recession. This study presents an alternative approach to saltmarsh monitoring using a multi-camera array and 3D reconstruction to provide topographic surveys of a ~30 m stretch of saltmarsh margin over a 4-month period. Innovative spatial and temporal analysis of geomorphic change is related to wave hydrodynamics and meteorological forcing. The camera rig was deployed at Silverdale saltmarsh, NW England between November 2018 to March 2019. Erosion and undercutting were found to be prominent characteristics of the saltmarsh boundary. Erosional losses were calculated at 3.88 m^3 over a 4-month survey period with a monthly erosion rate of 0.97 m^3 . The saltmarsh cliff margin was progressively weakened over time by undercutting of the cliff profile leading to the reduction of undercut extent by 1.53 m^2 due to large areas of collapse. The deployment of the multi-camera rig revealed new understanding of changes to saltmarsh margins through high-resolution shoreline geometry and erosion estimates. In so doing, the technology provides a low cost, rapid technique that can detect seasonal and event-based variability in erosion rates that can be linked to undercutting progression and margin collapse.

KEYWORDS: camera array; camera rig; coastal monitoring; saltmarsh retreat; undercutting; structure-from-motion photogrammetry; 3D reconstruction

6.1 Introduction

Globally, 1.2 billion people reside within 100 km of the coast (Small & Nicholls, 2003) alongside highly valuable infrastructure and ecosystems. The coastal zone offers a natural barrier between land and the hydrodynamic power of tides, waves, and currents. The dissipation of energy causes morphological evolution, which can drive erosion and the landward retreat of the shoreline. For example, in the UK, 17.3 % of the coastline is eroding with 28 % of England and Wales experiencing erosion of 0.1 m yr⁻¹ or greater per year (Masselink and Russell, 2013). The rate of recession is often exacerbated during storm events when the water level is raised above ordinary tidal levels. Storm surges are a combination of strong winds, wave breaking height and low barometric pressure (Benavente et al., 2006). When combined with an astronomical high tide, storm surges can force the waves landwards producing significant destruction (Bryant, 2012). The elevated energy received at the coast during such events can be beyond dissipation capacity forcing sudden and large-scale coastal change. Damage resulting from flooding and erosion has an estimated cost of £260 million per year in the UK (Committee on Climate Change, 2018). The long-term threat of climate change is likely to intensify recession as the frequency of extreme weather increases, exposing vulnerable areas to wave propagation further onshore and encouraging coastal retreat (Mentaschi et al., 2018).

Coastal wetland environments, such as saltmarshes, can be particularly susceptible to erosion when exposed to moderate storm conditions (Leonardi, Ganju and Fagherazzi, 2016). Saltmarsh environments provide a significant number of ecosystem services including habitats for flora and fauna, carbon capture, nutrient cycling and recreational environments (Defra & Environment Agency, 2007). Furthermore, saltmarshes play a critical role in coastal zones across the UK and have, in recent years, been considered natural forms of coastal protection (e.g. Leonardi, Ganju and Fagherazzi, 2016). However, erosion and consistent inundation of saltmarshes has the potential to convert these environments into mud flats, tidal lagoons and eventually open water. The erosion of the saltmarsh edge can be accelerated by sea-level rise, human development or a restricted supply of sediments (Morton, Bernier and Kelso, 2009; Sapkota and White,

2019). Erosion of the saltmarsh edge drives shoreline retreat, with hydrodynamics, in particular wave action, causing the formation and evolution of saltmarsh cliff margins (Davidson-Arnott, 2010; Leonardi, Ganju and Fagherazzi, 2016). Moreover, the influence of sea-level rise is predicted to cause an 80 % retreat in saltmarshes globally by 2100 (Spencer et al., 2016; Horton et al., 2018) therefore reducing their previously associated benefits.

Consequently, monitoring is essential to reveal the response of saltmarshes to hydrodynamic action, such as storm surges and waves. However, surveys of these areas are often sporadic. For example, in the UK, monitoring gaps have been described by the National Ecosystem Assessment (Jones, 2011), revealing the need for thorough survey methodologies for each habitat to allow for accurate estimates of temporal change. The ability to rapidly, and routinely, gather a high-resolution time-series of topographic data would provide up-to-date information about the patterns and rates of saltmarsh retreat (Green et al., 2017).

LiDAR is a common remote sensing technique for monitoring saltmarsh environments and has a range of advantages for different environmental scenarios, such as large spatial coverage (e.g. Hladik, Schalles and Alber, 2013; Fernandez-Nunez, Burningham and Ojeda Zujar, 2017). However, the aerial nature of measurement makes this an expensive method and sensitive to adverse weather conditions. LiDAR also overlooks small-scale changes and the impacts of undercutting at the saltmarsh cliff margin (Eltner et al., 2016; Green et al., 2017). By contrast, the roving camera array, previously tested and described in Chapter 5, has the ability to provide an efficient, cost-effective, rugged, easy-to-use and regularly deployable sensing platform that could potentially address the current shortcomings in monitoring programmes.

In this paper, SfM-MVS and a roving camera array was used to monitor the morphological change of a saltmarsh cliff margin over a four-month period of the UK winter season. The main aims of the study are to: 1) monitor saltmarsh cliff retreat over a winter period of seasonal high wave energy and storms using a roving camera rig with SfM-MVS; 2) analyse spatial and temporal geomorphic change; and 3) calculate area loss rate and the extent of undercutting. The results provide measures of erosional and depositional change in response to hydrodynamic forcing, providing new insight into the future stability of saltmarshes.

6.2 Study Site

Silverdale is located on the North West coast of England, near the border between the counties of Cumbria and Lancashire (Figure 6.1). Situated in Morecambe Bay, Silverdale saltmarsh is influenced by sedimentary processes occurring in the Morecambe Bay estuary and those from the River Kent (north of the site) and River Keer (south) which drain into Morecambe Bay. The saltmarsh is situated on the north-east shore of the River Kent estuary.

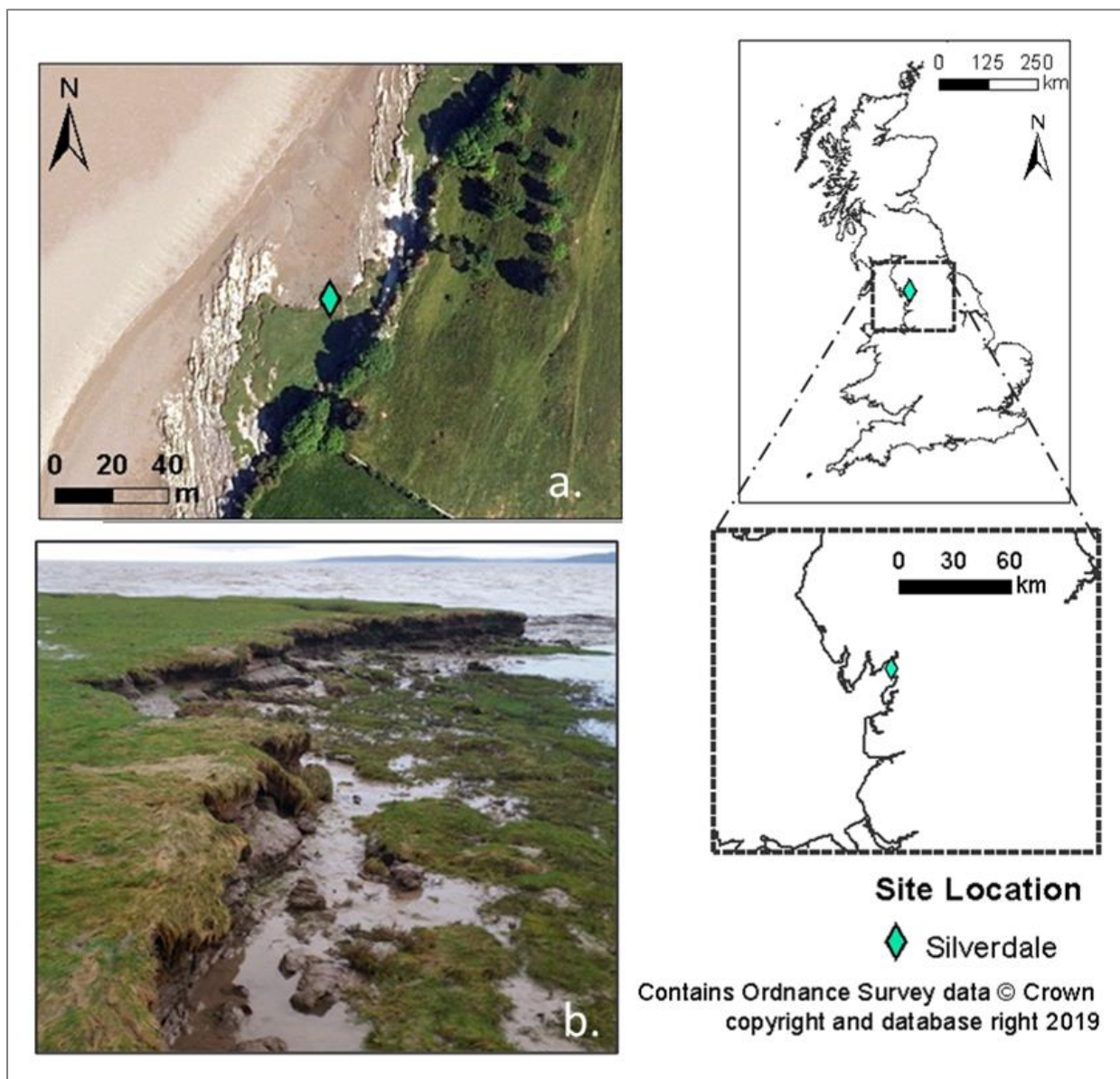


Figure 6.1: Study site location a) Aerial image showing location of Silverdale test site b) Photograph of Silverdale site with ebb tide (Photograph: Author's Own).

The surveyed site has suffered from cycles of sediment erosion and accretion, cutting away at the saltmarsh edge and causing ‘coastal narrowing’ (Pringle, 1995). These processes are caused by an intricate system of sediment circulation and deposition based upon the tidal regime of the Irish Sea interacting with estuarine sediment pathways (Arnside & Silverdale AONB Partnership, 2015). Erosion has been driven by the position of the River Kent main channel. The closer position of the Kent Channel to the Silverdale saltmarsh facilitated erosion as larger waves encroached on the land. Significant erosion was experienced at the saltmarsh historically but sediment deposition in Morecambe Bay has developed a sandbank protecting the saltmarsh from the worst waves. In 1967, the Silverdale saltmarsh covered an area of 244 ha but a phase of rapid erosion in the 1970s left only 40 ha by the 1990s (Table 6.1) (Pringle, 1995). Unless a drastic movement in the River Kent channel occurs, the saltmarsh will continue to be exposed to erosion (Arnside & Silverdale AONB Partnership, 2015).

Table 6.1: Silverdale Saltmarsh area (ha) after Gray, 1972; Pringle, 1995

Silverdale saltmarsh extent					
Year	1888	1910	1946	1967	1990
Area (ha)	128	40	109	244	40

The management plan for this area is conservation with the restoration of saltmarsh encouraged (Cumbria County Council, 2011). The current shoreline management plan for the area directly behind the saltmarsh is ‘No Active Intervention’ and the coastline is considered ‘Erodible’ with ‘Natural’ defences (Environment Agency, 2019b). The natural defence would be the saltmarsh but with the progressive erosion of the site it will make the current coastline (landward of the saltmarsh) increasingly susceptible to erosion. By tracking the changing morphology through time, this research will help to develop an understanding of current rates of saltmarsh erosion.

6.3 Methods

A roving camera rig was deployed in this study using the guidelines described in Chapter 5 which were based on camera positions established in Chapter 4 (Godfrey et al., 2020). The rig was used for the systematic acquisition of images at Silverdale

saltmarsh cliff margin. Images were processed with SfM-MVS software (Agisoft Photoscan) and the output DEMs sequentially analysed to track erosional impacts. This section provides an outline of the data acquisition, point cloud processing procedure and comparative analysis of point clouds to quantify erosion.

6.3.1 Data Acquisition

The surveys were conducted across ~30 m long section of saltmarsh cliff during a 4-month period between November 2018 and March 2019 (16th November 2018, 14th December 2018, 15th January 2019 and 18th March 2019). This period was chosen to monitor the overall trends of saltmarsh retreat experienced due to storms in winter conditions. Three surveys were undertaken, and fieldwork expeditions were selected based on low tide times and suitable cloud cover to provide diffuse lighting for images (James and Robson, 2012).

During each survey, GCPs (0.15 m² checkerboards) were scattered across the scene approximately 1 m apart. This distance was in accordance with guidance in Westoby et al. (2018), in which they advised GCPs should be separated by a distance equivalent to the height of the cliff being surveyed. Post SfM-MVS survey, GCPs were georeferenced using a Trimble RTK-GPS R6 GNSS system to provide scene scale and orientation, and reduce severe deformation (James, Robson and Smith, 2017). Horizontal coordinates for the reference points were set to the British National Grid (OSTN02), while vertical coordinates were referenced to mean sea level using the geoid model OSGM02.

The image acquisition procedure for each survey followed that described in Chapter 5, section 5.3.2, using a camera rig height of ~1.39 m relative to the 1 m cliff margin.

6.3.2 Point Cloud Processing

Point clouds were processed following the systematic approach established in Chapter 5, Section 5.3.3. After each survey images were uploaded into Agisoft Photoscan (Version 1.3.2.4205) software for processing. The systematic approach to image acquisition meant that each survey had an equal number of camera rig stops and images. The workflow present within Agisoft Photoscan allows users to specify processing parameters most suitable for their project, such as camera model, image alignment, GCP marker placement and densification. Software processing was based on

the optimal parameters established in Chapter 5 (sections 5.4 and 5.5). Consequently, the camera model 'fish-eye' was used with the image alignment parameters 'Medium'. Point clouds were then cleaned, GCPs markers placed in the central portion of the images and the point cloud optimised. The final setting of 'High' was used for the densification of the point cloud. The use of GCPs and the above processing parameters reduced systematic deformation in the point clouds caused by the linear nature of the surveyed site and a parallel image network (greater detail provided in sections 5.3-5.5 of Chapter 5). After processing, each dense point cloud was then exported as a LAZ file in order to maintain their coordinate system and used for the assessment of erosion in CloudCompare V2.9 software and ArcMap 10.4.1

6.3.3 Geomorphological Change Assessment

A series of assessments were conducted to establish morphological change estimates from the series of surveys. The generated point clouds were sequentially referenced to their preceding survey (i.e. January 2019 referenced to December 2018) with the November 2018 survey used as the initial point of reference. Stable reference points were visually identified in successive surveys and used to align the point clouds in CloudCompare (Version 2.9). Point clouds were then cropped to equivalent sizes and vegetation at the top of the cliff was segmented out of the point cloud. The removal of vegetation reduced the impact of local error caused by occlusion and wind-induced movement across the images. Remaining vegetation mostly comprised short grass along the very edge of the cliff, whose removal would impact the reconstruction of the cliff profile. Point clouds were further registered using an ICP registration that aligned the point clouds in the horizontal (x & y) and the elevation (z) (Dudzińska-Nowak & Wężyk, 2014).

Each morphological change assessment provides a different picture of erosion or deposition. Consequently, a series of three assessment were undertaken to provide a fuller picture of the changes at the saltmarsh margin. These tests were:

- Topographic Differencing for Volume
- Area Loss
- Area of Undercutting

6.3.3.1 Topographic Differencing for Volume

The point clouds generated for each survey were uploaded into and converted in CloudCompare to DEMs with 0.01 m grid resolution (Ground Sample Distance of 0.01 m) and the maximum elevation provided in each cell. The resolution was chosen at 0.01 m as it reflected the precision estimates established for the camera rig in Chapter 5. DoDs are a well-established method for qualitatively and quantitatively tracking geomorphological change in a range of environmental settings (Williams, 2012; Abellán et al., 2014; Westoby et al., 2018). The DEMs were saved as Geotiff. files and uploaded into ArcMap (Version 10.4.1) to evaluate surface change. DoDs were created using the following:

$$(15) \quad \text{DoD} = \text{DEM}_{i-1} - \text{DEM}_i$$

where i is the survey of interest (e.g. DEM_i is December 2018 and DEM_{i-1} is November 2018). The Cut/Fill command was used, which calculates erosional and depositional volumes between two surfaces (Dudzińska-Nowak and Wężyk, 2014). Misalignment of DEMs has shown to be a common issue for incorrect estimates of difference in DEMs or point clouds (Parente, Chandler and Dixon, 2019). Therefore, a change detection threshold was applied which removed the inclusion of change <0.01 m for either erosion or deposition. The threshold was selected at 0.01 m to remove false positives due to any misalignment of the point clouds or vegetation movement. The DoDs allowed the depositional and erosional changes to be analysed volumetrically, spatially, and temporally.

6.3.3.2 Profile Extraction & Area Loss

The extraction of a time-series of the shoreline profile was used as an estimate of lateral recession of the saltmarsh margin. The DEM included the maximum heights values in each of the grid squares, and therefore showed the full extent of the lateral cliff extent from an aerial perspective. The furthest extent of the cliff was then digitised in ArcMap 10.4.1 to create polylines that represent the cliff margin. This process was repeated for each month, and the polylines for each month then intersected. The area (m^2) between the intersected lines represented the area lost through erosion. The area between the polylines was calculated and represented the lateral area of the saltmarsh lost each month.

6.3.3.3 Area of Undercutting

Undercut areas of a cliff are generally associated with slumping and area loss. The extent of undercutting is often hard to identify from aerial monitoring. Lague, Brodu and Leroux (2013) speculated that DEMs were unsuitable for identifying areas of cliff undercutting due to their 2D nature. However, the use of oblique images captured by the camera rig has allowed a new method to be established. The method involved estimating the area of undercutting by generating two DEMs for comparison and using the varying height values present within the 3D point cloud.

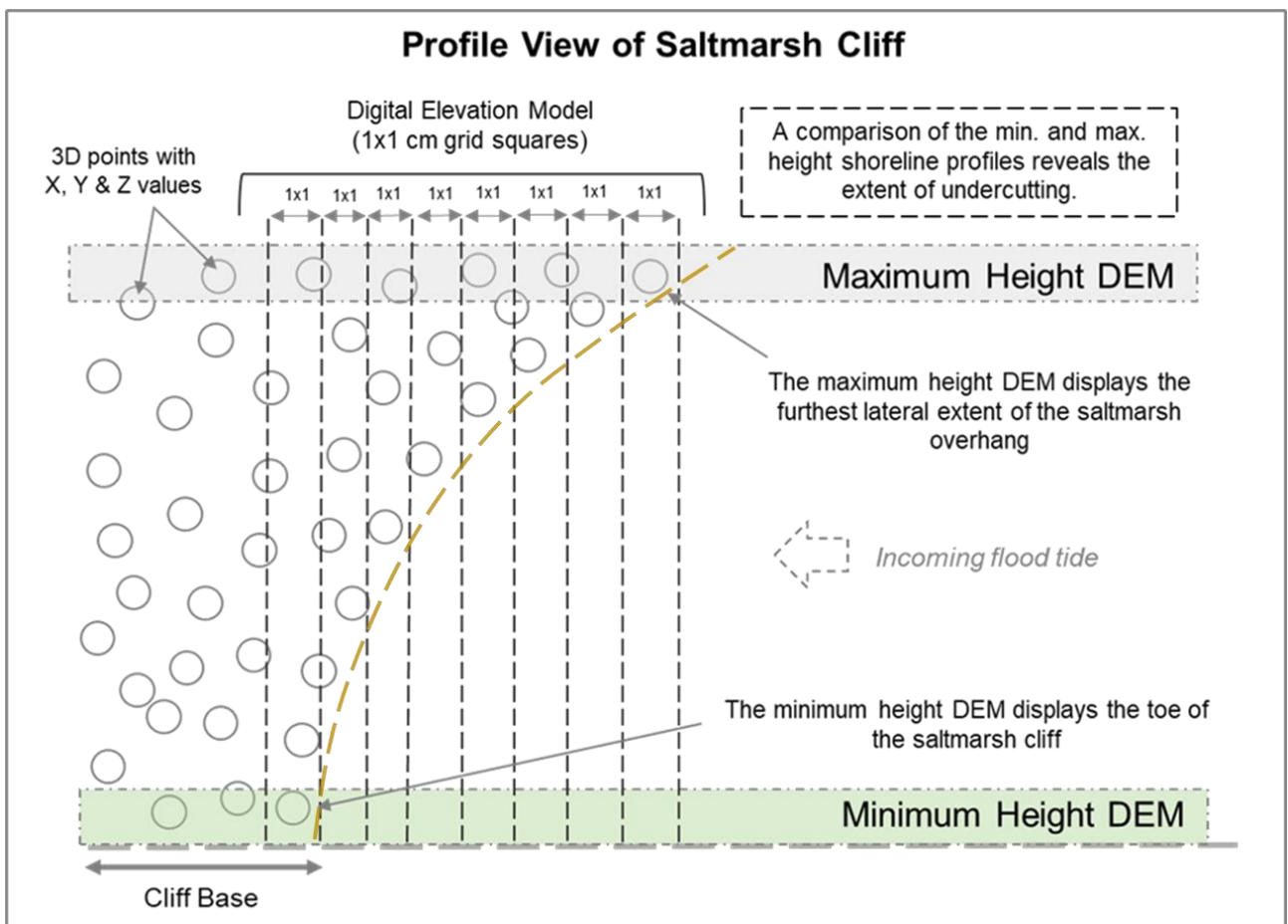


Figure 6.2: Depiction of how the choice of DEM enables undercutting to be identified.

During the transition from point cloud to DEM, data is transferred from a 3D state to a 2D state i.e., gridded elevation values of the DEM. As a point cloud is 3D, there are multiple elevation values that can be used to represent a height value for each grid square. The maximum height depicted the furthest lateral extent of the saltmarsh margin, and the minimum height values displayed the minimum lateral extent. In this

research, a novel method for measuring undercut extent was developed using an intersection of the two digitised shoreline profiles. A comparison of the profiles displayed the area of undercutting present at the site. Figure 6.2 provides a depiction of the process. The two shoreline profiles were compared in ArcMap 10.4.1 and the area (m^2) between the lines estimated for each month.

6.4 Results

6.4.1 Topographic Differencing for Volumetric Assessment

The calculation of volume change across the full extent of the domain allowed the identification of spatial changes in erosion and deposition. Volumetric change was used in comparison with the shoreline profiles to provide an understanding of whether the eroded material was kept within the vicinity of the site (common for slumped material) or transported away to other areas of the estuary.

The total volumetric loss across the ~ 30 m section during the 4-month period (November 2018-March 2019) was $3.88 m^3$, and total gain was $2.72 m^3$, indicating net erosion. Assuming a constant rate of volumetric change, the mean monthly rate of erosion for this 4-month period was $0.97 m^3$ equating to $\sim 11.64 m^3$ per annum. Monthly deposition rate was $0.68 m^3$ ($\sim 8.16 m^3$ per annum). Figure 6.3 displays the erosion and deposition volumes for each survey. The volume calculation was a spatially-averaged value for the whole survey site, and not simply for the eroded cliff profile. Consequently, a similarity in total volumetric values between erosion ($3.88 m^3$) and deposition ($2.72 m^3$) reflected the presence of eroded material from the saltmarsh cliff margin deposited across the sites.

Based on the estimated monthly erosion rate, $0.97 m^3$, the period between November and December 2018 displayed a higher than average erosion volume. Figure 6.4 displays the distribution of erosion both spatially and temporally from November to December 2018. The map insert displays a surface negative difference observed along the saltmarsh edge. This time-period experienced a monthly volume loss of $1.17 m^3$.

Depositional volumes were high between the period of December 2018 to January 2019 (Figure 6.5). However, on the spatial map for this period (Figure 6.5) no large-scale morphological change was recorded, suggesting a large number of small-scale changes.

Small-scale changes may reflect the addition of material deposited across the entire surface of the site by the flood tide.

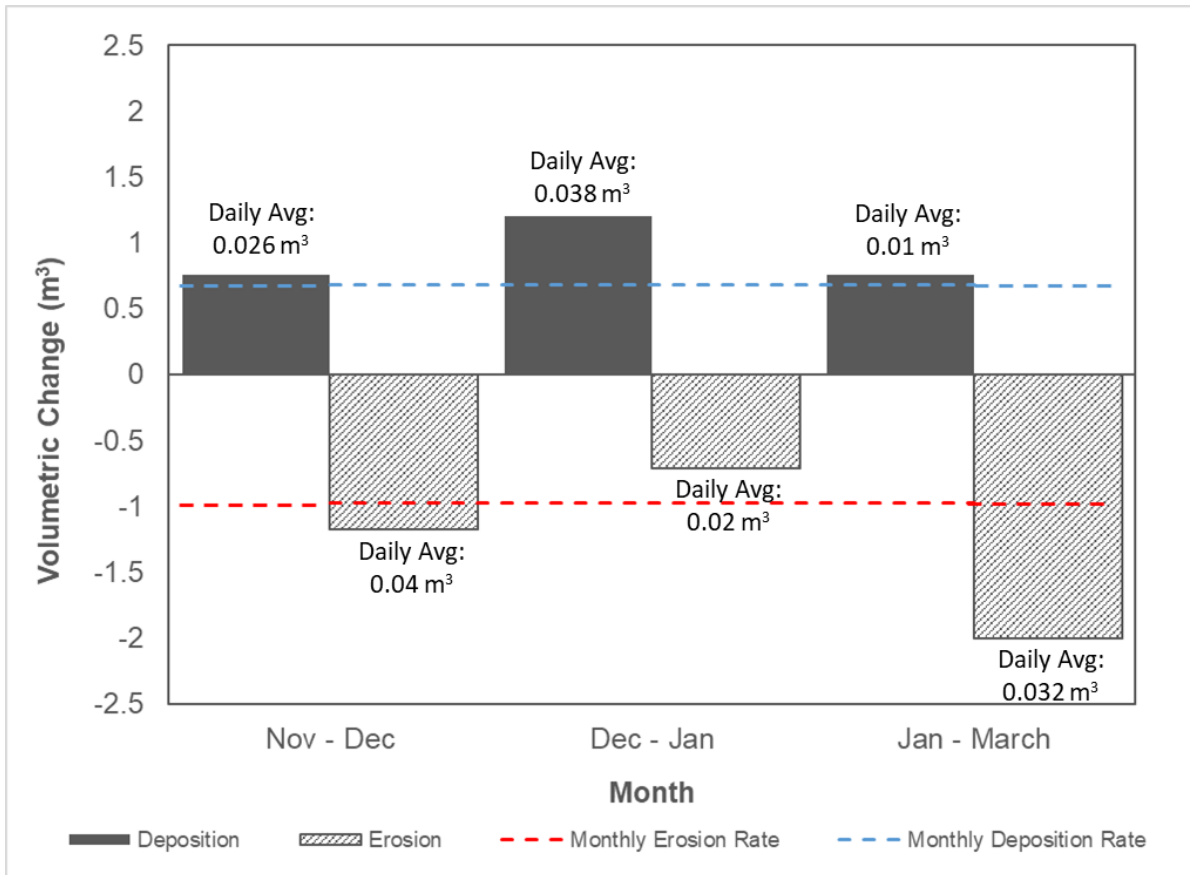


Figure 6.3: Negative (erosion) and positive (deposition) volume extracted from DoDs for the survey domain. Higher values for both erosion and deposition recorded between January and March represent 2-months of erosion and deposition. Numbers above bars represent the daily average volume change for that month.

The period between January and March 2019 represented a 2-month period of erosion and deposition and exhibited net erosion. The total erosion during this 2-month period was 2 m³ bringing the monthly average between January and March to 1 m³, near equivalent to the estimated monthly erosion rate of 0.97 m³. Figure 6.6 displays the spatial variability of erosion and deposition over the 2-month period between January and March, showing high levels of erosion along the saltmarsh margin.

Inspection of the spatial distribution of volumetric change provided in Figures 6.4, 6.5 & 6.6 plus photo evidence corroborates the volumetric estimations and indicated net erosion. Deposition estimates generally remained lower than for erosion over the 4-

month period and the spatial distribution of erosion followed the cliff profile. Figures 6.4 and 6.6 both show the location of slumped depositional material adjacent to erosion of the saltmarsh margin reflecting the increases in both depositional and erosional values.

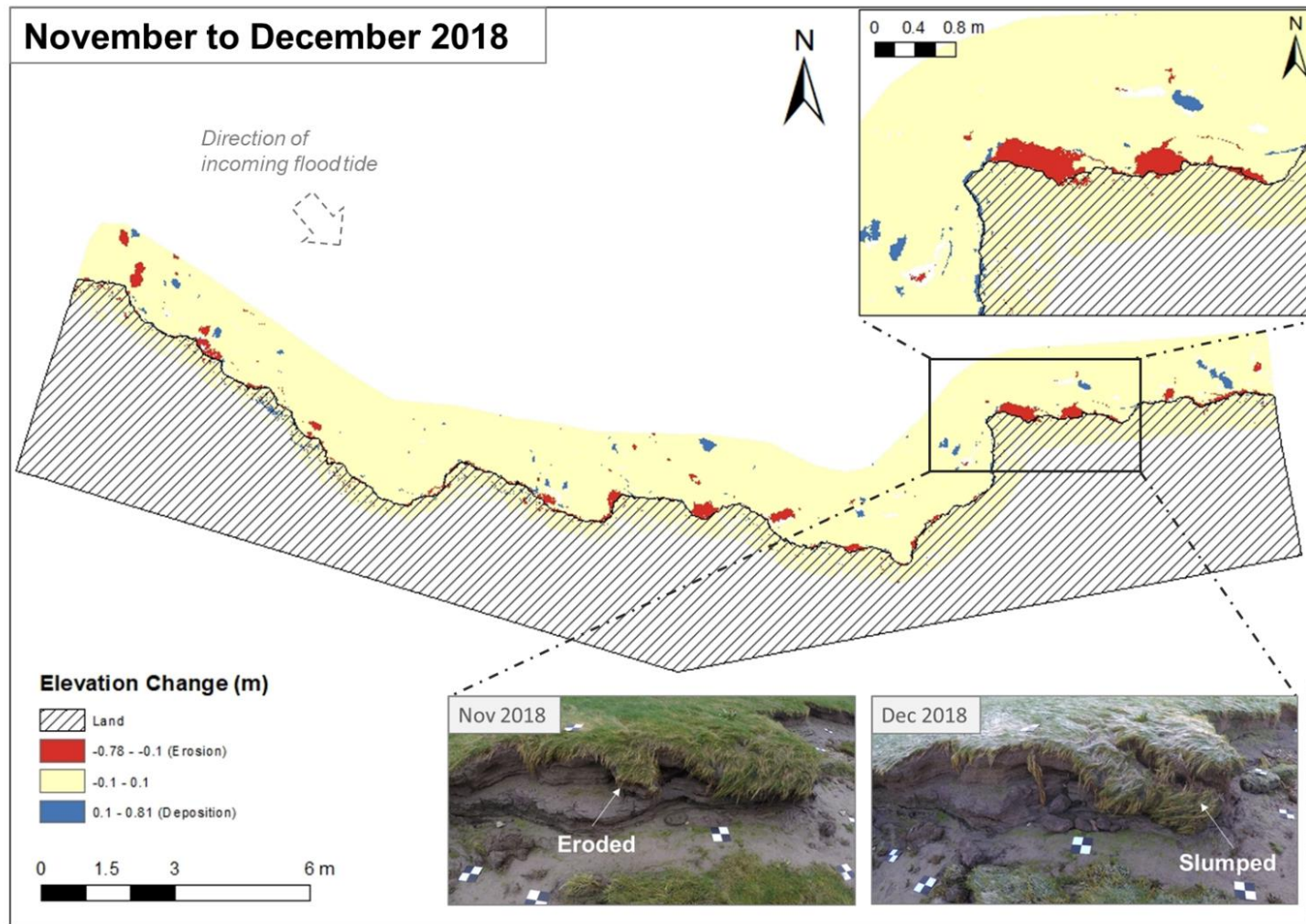


Figure 6.4: November to December 2018 elevation differencing map (DoD). Highlighted area shows notable erosion or deposition (>0.1 m) referenced to photographs from the site (aerial view).

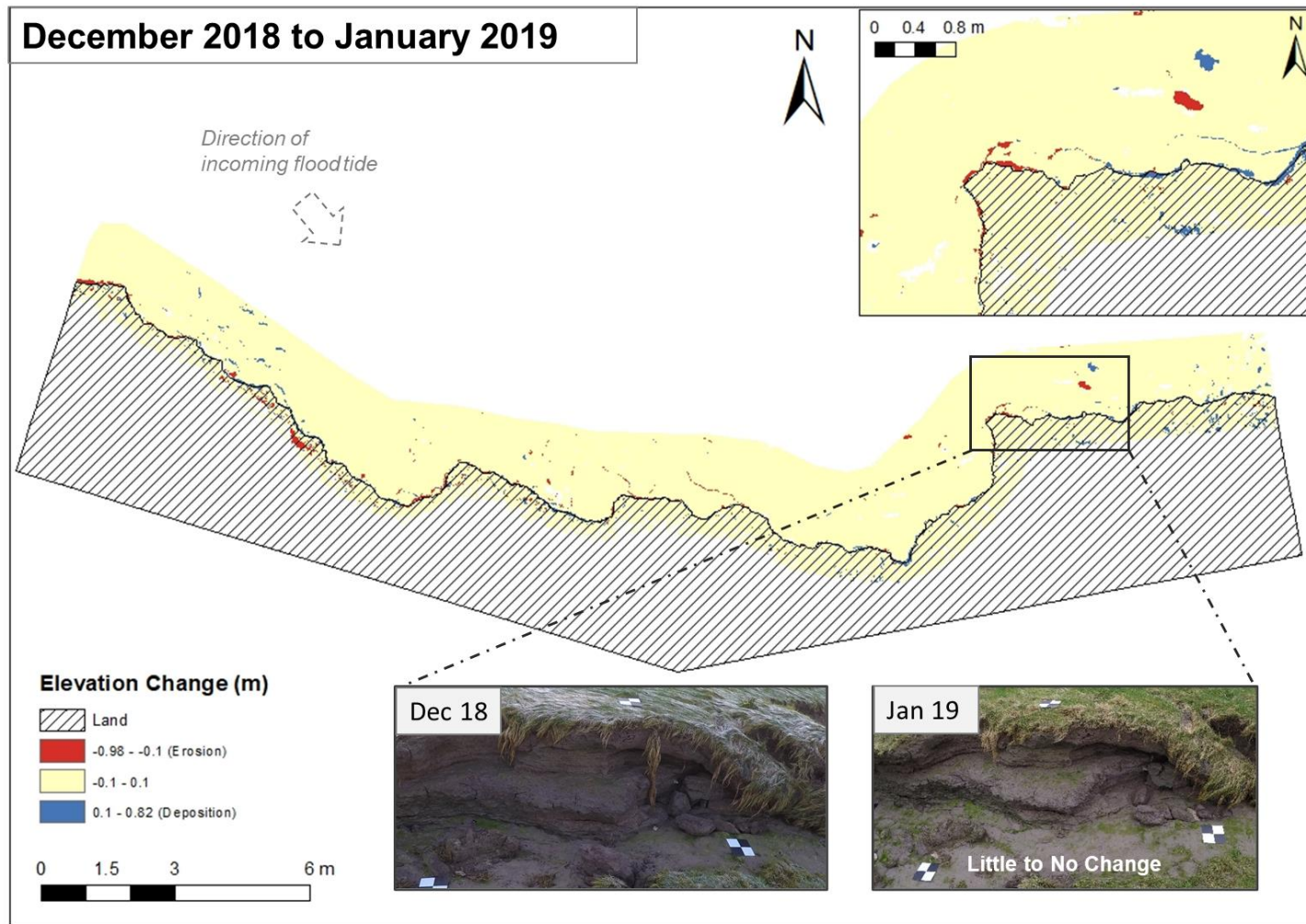


Figure 6.5: December 2018 to January 2019 elevation differencing map (DoD). Any notable erosion or deposition is highlighted (>0.1 m) referenced to photographs from the site (aerial view).

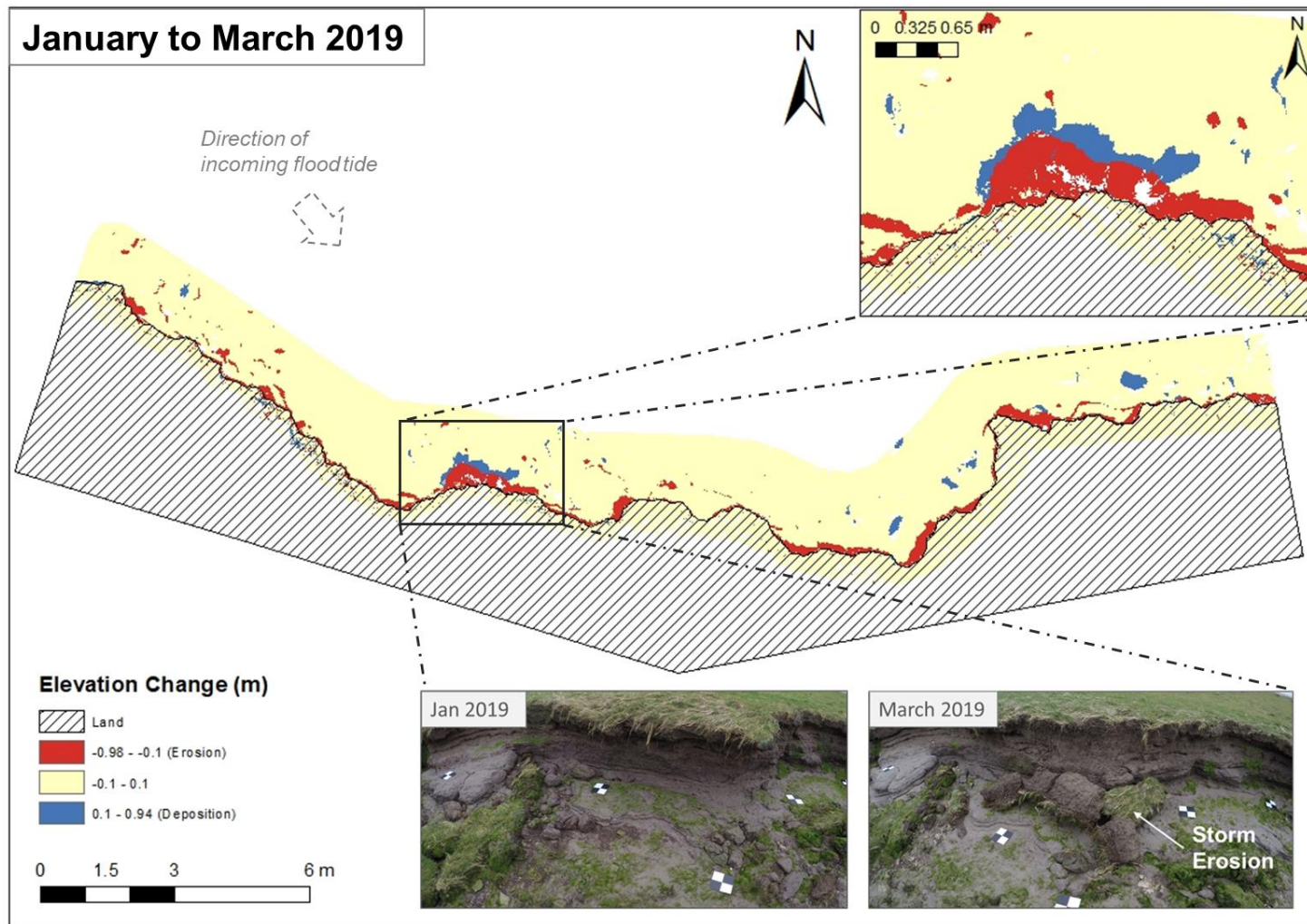


Figure 6.6: January to March 2019 elevation differencing map (DoD). Highlighted area shows notable (>0.1 m) erosion and deposition referenced to photographs from the site (aerial view). January to March represents two months' worth of change.

6.4.2 Alongshore Profile Extraction & Area Loss Analysis

Spatial analysis of the 4-month period showed progressive patterns of erosion at specific locations across the surveyed area, highlighted in Figures 6.7 and 6.8. The monthly rate of area lost was 0.8 m^2 (Figure 6.7) and the total area lost over the 4-month winter period was 3.27 m^2 . Although the volumetric and area loss estimates represent distinct ways of assessing morphological change, they both showed similar temporal trends. For example, the greatest loss of area was recorded during the period between January to March 2019 with 2.18 m^2 (Figure 6.7) which is also reflected in the high volumetric values calculated for this period. January to March represents a 2-month period resulting in a monthly area of loss of 1.09 m^2 , similar to the area loss experienced during November to December. The period between December 2018 and January 2019 displayed little to no area loss from the saltmarsh margin – corroborating the volumetric findings.

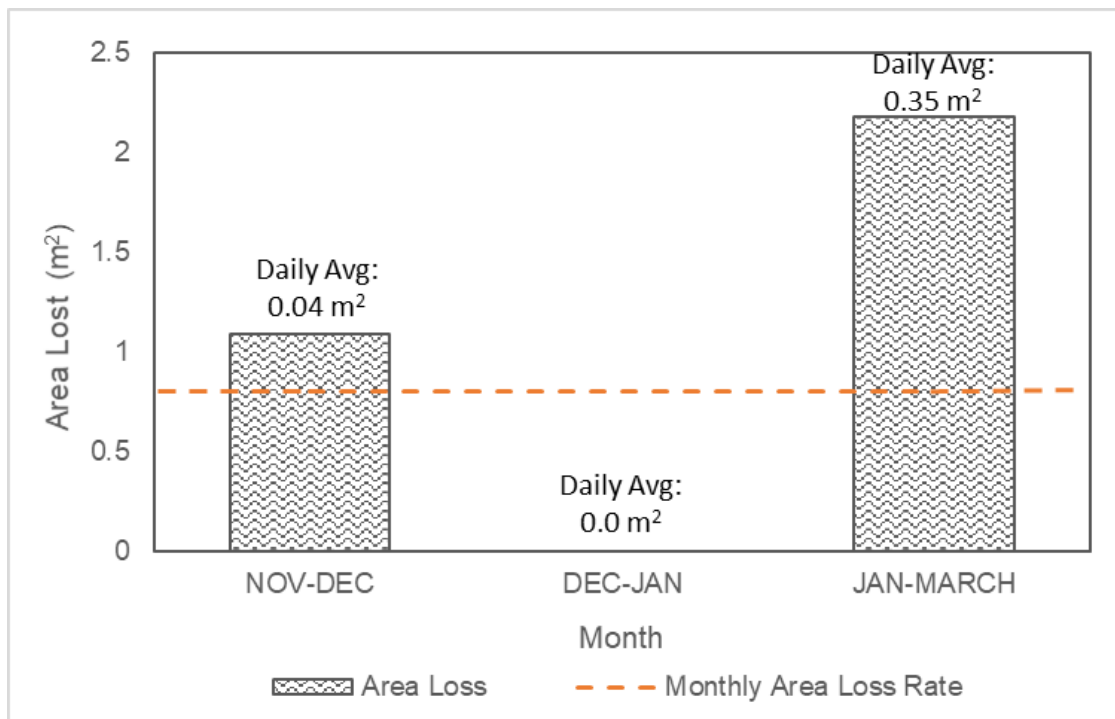


Figure 6.7: The area lost from the saltmarsh cliff between November 2018 and March 2019 plus the monthly area loss rate. Erosion rate based on the digitisation of shoreline profiles and polygonal area. January to March represents two months' worth of change. Numbers above bars represent the daily average area lost for that month.

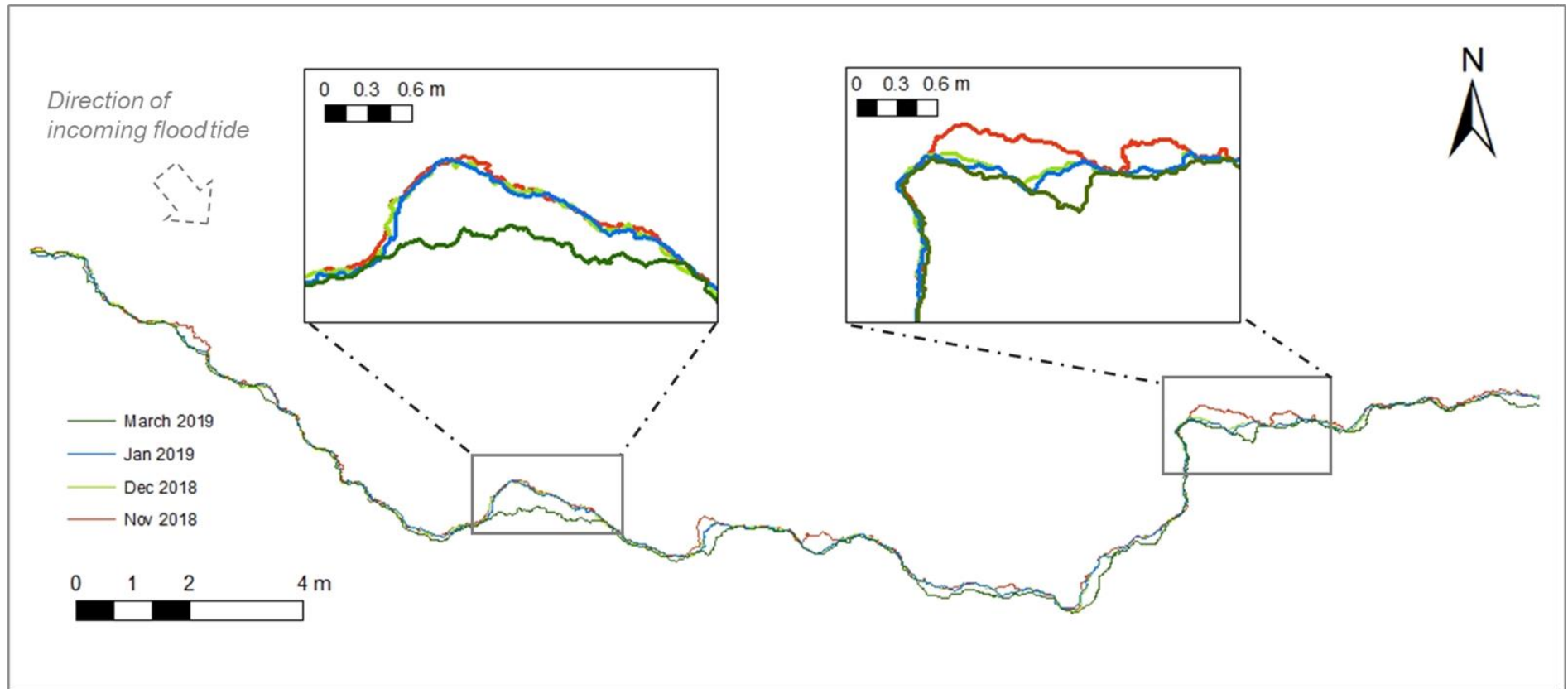


Figure 6.8: Spatial and temporal comparison of saltmarsh cliff profiles. Along shore profile of the cliff, digitised from the SfM-MVS generated DEMs (aerial view).

6.4.3 Identification of Undercutting Extent

Spatial assessment revealed persistent areas of undercutting across the ~30 m section during each month. The absolute measures of undercutting extent for each month are displayed in Figure 6.9, with relative change denoted between columns. Over the 4-month period the undercutting extent reduced by 1.53 m², a 23 % loss in undercut areas by March 2019 relative to November 2018. The undercut area lost per month is 0.38 m², equivalent to approximately a 6 % loss each month and 4.56 m² per annum. The total area of undercutting consistently reduced over the 4-month period but varied marginally from month to month.

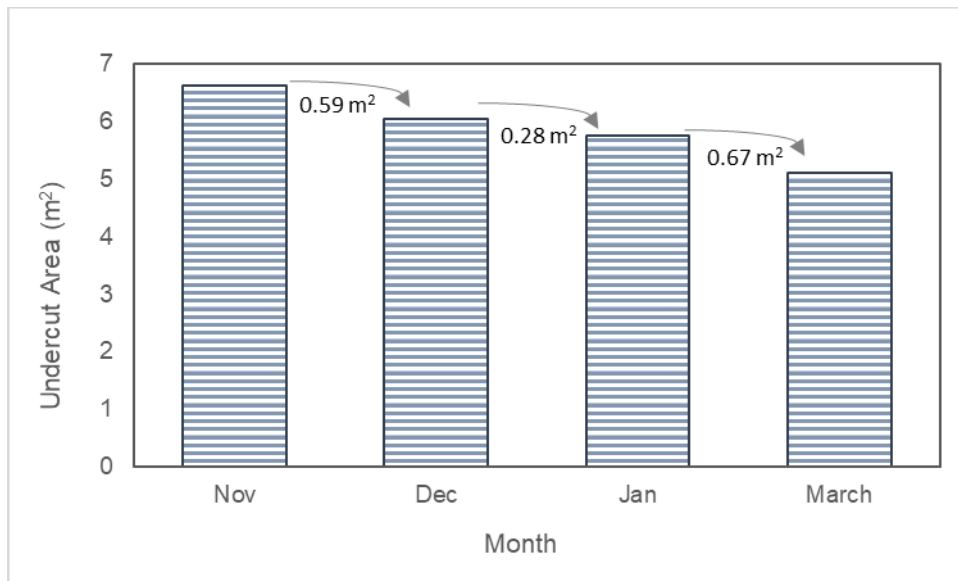


Figure 6.9: Total undercut area (m²) over the 4-month period (November 2018 – March 2019).

Undercutting extent varied spatially across the site with sudden decreases in extent a result of changes in cliff profile, such as from collapse. There is the potential that low-level undercutting may occur over the summer period and slumping and collapse take place during the winter months due to storms. Maps showing the monthly spatial variability of undercutting are included (Figures 6.10, 6.11, 6.12 & 6.13). These maps highlight two areas of significant morphological change (map inserts a and c) and one that showed a consistent extent of undercutting (map insert b).

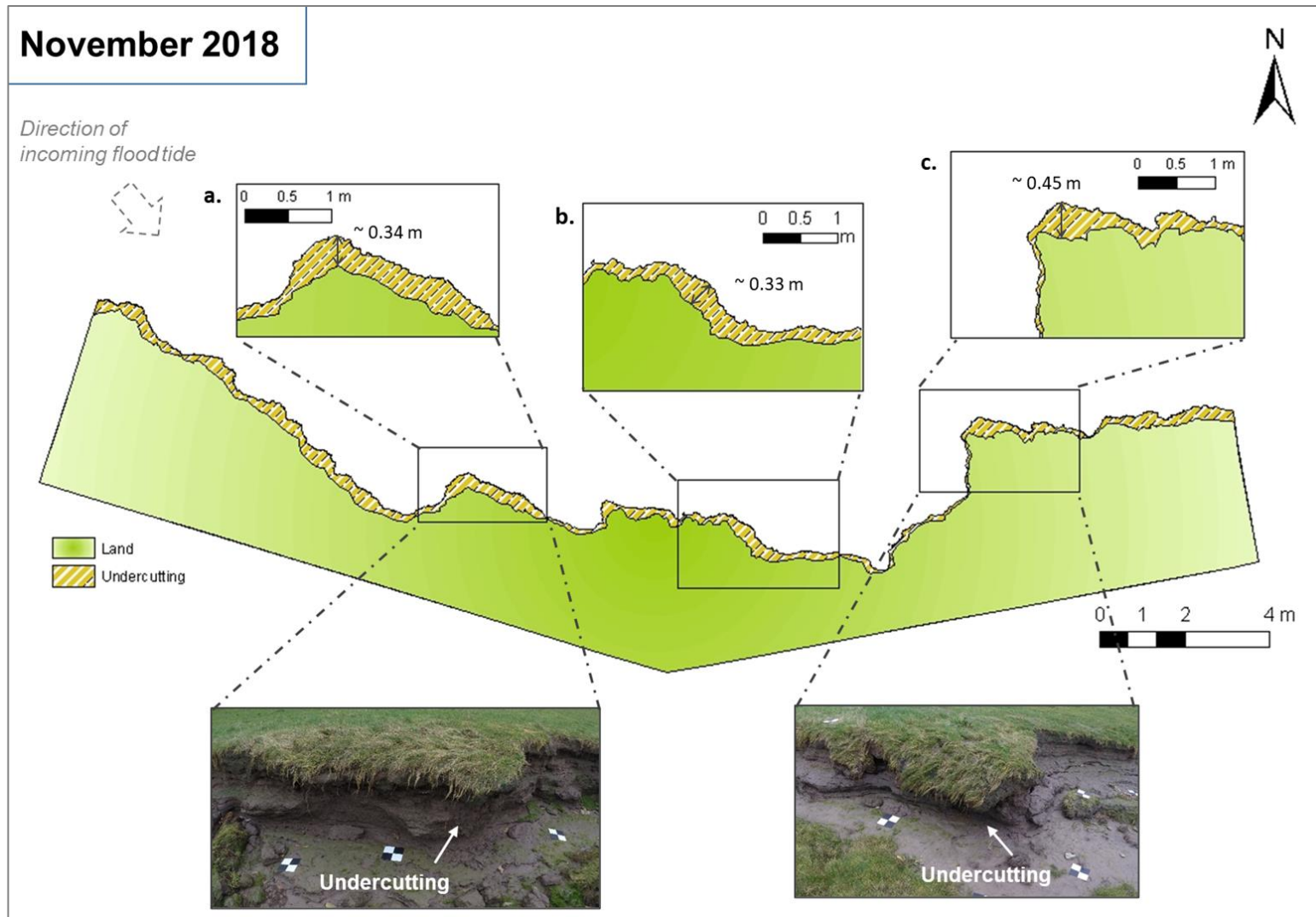


Figure 6.10: Undercutting extent in November 2018 based on the digitisation of maximum and minimum height DEM shoreline profiles. Notable undercutting is highlighted in maps inserts a, b and c (aerial view).

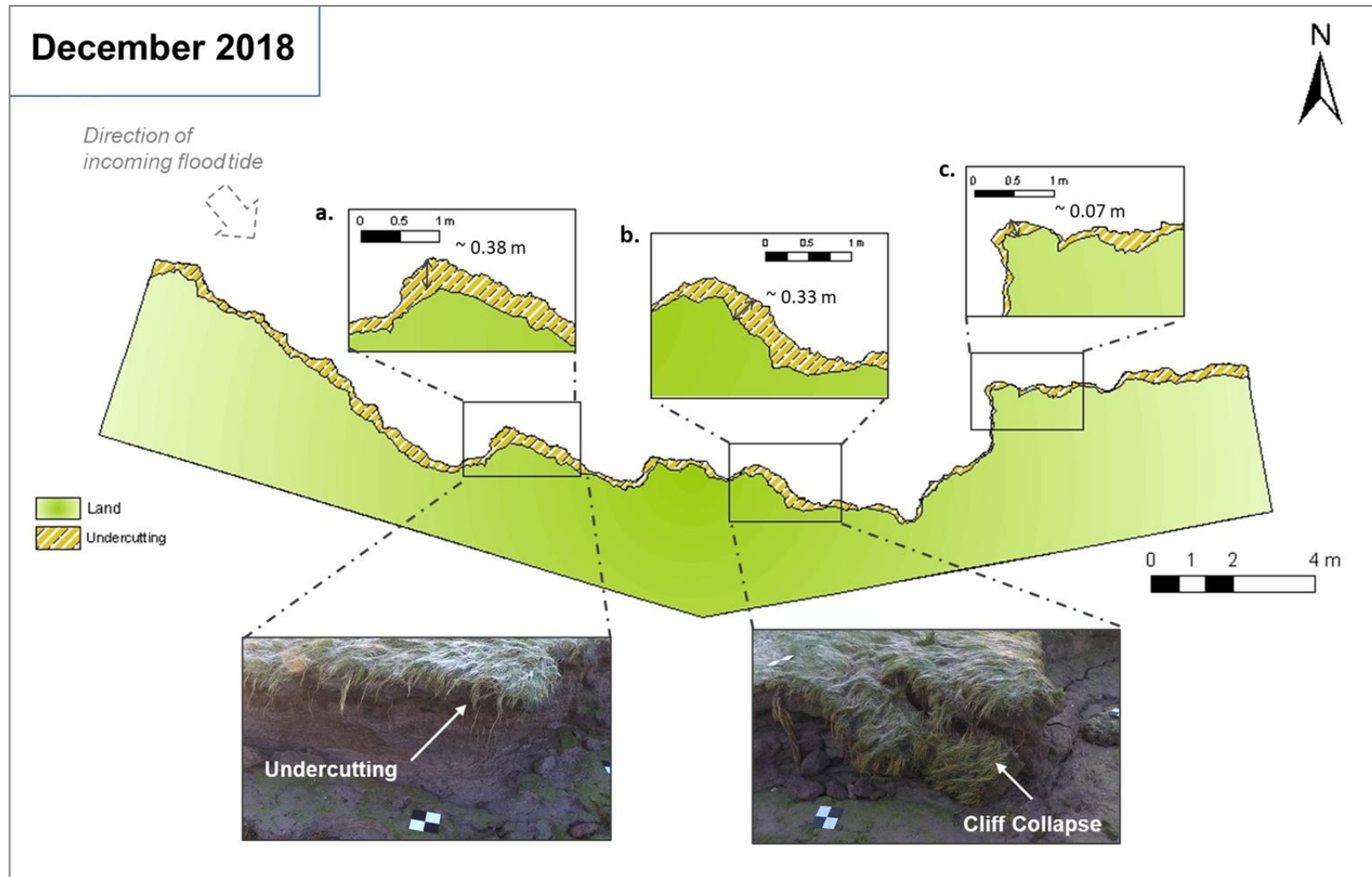


Figure 6.11: Undercutting extent in December 2018 based on the digitisation of maximum and minimum height DEM shoreline profiles. Notable undercutting is highlighted in maps inserts a, b and c (aerial view). Cliff collapse since November noted in insert map c.

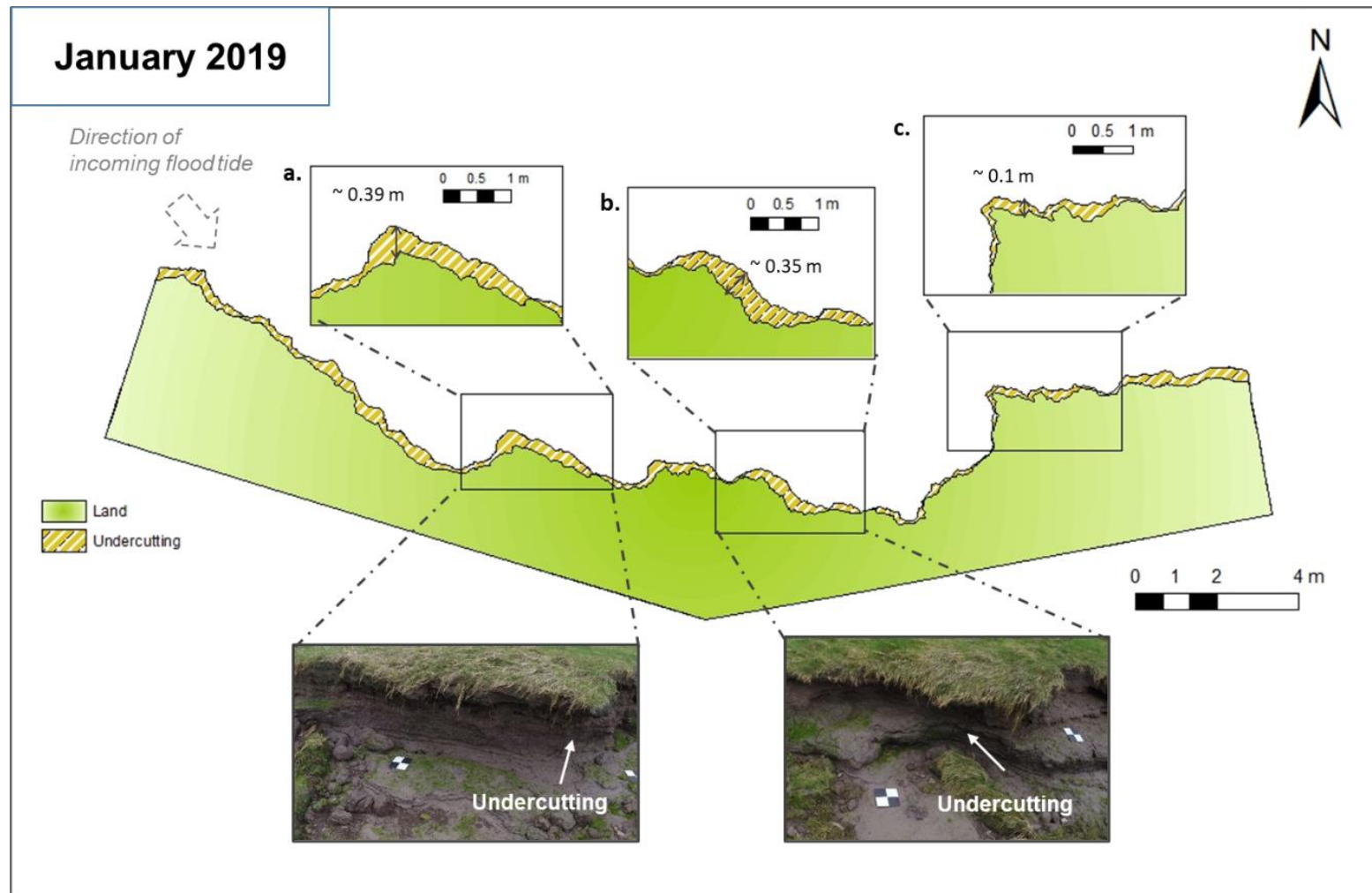


Figure 6.12: Undercutting extent in January 2019 based on the digitisation of maximum and minimum height DEM shoreline profiles. Notable undercutting is highlighted in maps inserts a, b and c (aerial view). Only minor changes to the area of undercutting were recorded from December 2018.

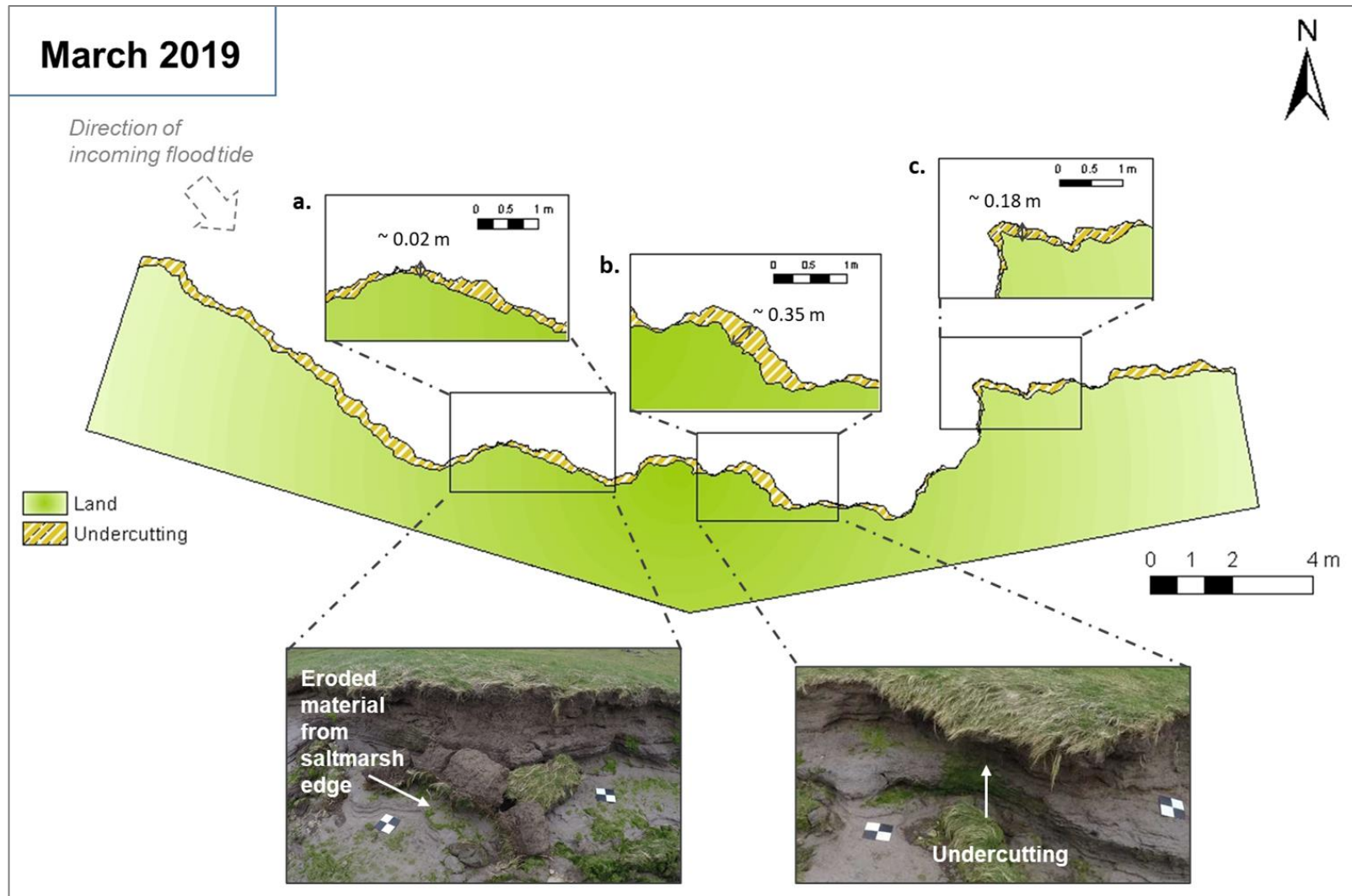


Figure 6.13: Undercutting extent in March 2019 based on the digitisation of maximum and minimum height DEM shoreline profiles. Notable undercutting is highlighted in maps inserts a, b and c (aerial view). Significant erosion since January 2019 (Insert a).

Figures 6.10 and 6.11 display the change in undercutting from November to December 2018 – this period displayed the largest monthly reduction in undercutting extent and exceeded the monthly average (0.38 m^2). A significant reduction in undercutting is highlighted in Figures 6.10 to 6.11 (insert c) which suggests a lateral loss of $\sim 0.38 \text{ m}$ in the extent of undercutting during November to December at that location.

The period between December 2018 to January 2019 displayed little change in undercutting extent with minor variations of approximately $0.01\text{-}0.02 \text{ m}$ across the three highlighted locations (Figure 6.12 a-c) suggesting slight increase of the undercut extent. The lack of erosion experienced between December to January is substantiated by the volumetric and area loss results which depict a similar lack of significant erosion during this period. Figure 6.12a displays an area of heightened undercutting ($\sim 0.39 \text{ m}$) that has slowly grown from November 2018 (previously $\sim 0.34 \text{ m}$ in November 2018). However, by March 2019 (Figure 6.13a) there was significant erosion and collapse of this section of saltmarsh margin reducing the undercut extent to $\sim 0.02 \text{ m}$. This erosion is confirmed by the images captured at the site and the equivalent DoD (Figure 6.6), displaying significant deposition and erosion at this location.

Overall, areas of significant undercutting have been shown to correspond with subsequent cliff collapse e.g. November to December (Figures 6.10c & 6.11c) and January to March (Figures 6.12a & 6.13a). These two examples suggest that the stability threshold of the saltmarsh margin has been breached, potentially through extreme hydrodynamic impacts (discussed in section 6.5), resulting in erosion and subsequent deposition of the material at the cliff base.

6.4.4 Meteorology & Hydrodynamics

The period of surveying covered the winter months (November 2018 – March 2019) and, according to UK Met Office data (2020), was subject to seasonal storm events and strong winds. This period was characterised by four classified, UK-wide storms (Figure 6.15 a-e) which brought high winds and heavy rain (Met Office, 2020). The severity of some of these storms is highlighted in the wave data which recorded wave heights (significant and maximum) above the storm threshold of 3.1 m (the significant wave height level that is exceeded four times a year, on average, as designated by the Channel Coastal Observatory, 2019) (Figure 6.15 a-c).

The overall temporal distribution of erosion fluctuated over the 4-month period. Higher volumetric and area loss values were recorded during the periods November to December 2018, which technically experienced no major UK-wide storm events, and January to March 2019 which experienced successive UK-wide storm events (Storm Erik, Storm Freya and Storm Gareth) (Met Office 2020). December 2018 to January 2019 experienced significantly less erosion, although the UK-wide ‘Storm Deirdre’ occurred during this survey period.

Therefore, there is a need to distinguish between the singular impact of UK-wide recorded storm events and the impact of local meteorological and hydrological conditions (waves and tides). Weather station records specific to Silverdale (Ehideaway, 2020) highlighted strong winds coinciding with spring tide levels during the 4-month period. Figures 6.14 a-d display wind direction and speeds specific to Silverdale marsh.

High local winds correspond to exceedance of significant and maximum wave heights above the storm threshold (Figures 6.14 a-d). A combination of increased wave heights and spring tides had a potentially greater impact on the saltmarsh than the occurrence of a classified UK-wide storm. For example, UK-wide Storm Deirdre (gusts of 69 mph) took place on the 15th and 16th December but coincided with lower tidal levels (Figure 6.15b). Consequently, the Silverdale marsh potentially experienced less impact from Storm Deirdre than the combination of high winds (~30 mph) and significant wave heights between the 7-8th December, which coincided with spring tides (Figure 6.15b).

The period between the 7th and 8th December was subject to an increased wave height maximum (~7.6 m) and significant (~3.6 m) wave height combined with augmented

high tide (~9.6 m OD). According to storm analysis by the Channel Coastal Observatory a storm surge of 0.58 m was recorded during the 7-8th December 2018. This storm surge combined with spring tides and strong westerly and north-westerly gusts of >20 mph (Figure 6.14a) would have driven increased wave heights towards the saltmarsh edge and was the likely cause of erosion along the margin before the subsequent survey on 14th December 2018.

December to January displayed less volumetric erosion (40% less than November to December), potentially an indicator of the reduced wave activity at the site. This lack of volumetric erosion corresponds with minor area loss along the margin for this month. Wind records show a period of significant calm with average wind speeds reaching a maximum of 5-8 mph. During this period there were no classified storm events and wind speeds were low causing wave heights to remain below the storm threshold (3.1 m) (Figure 6.15 b-c).

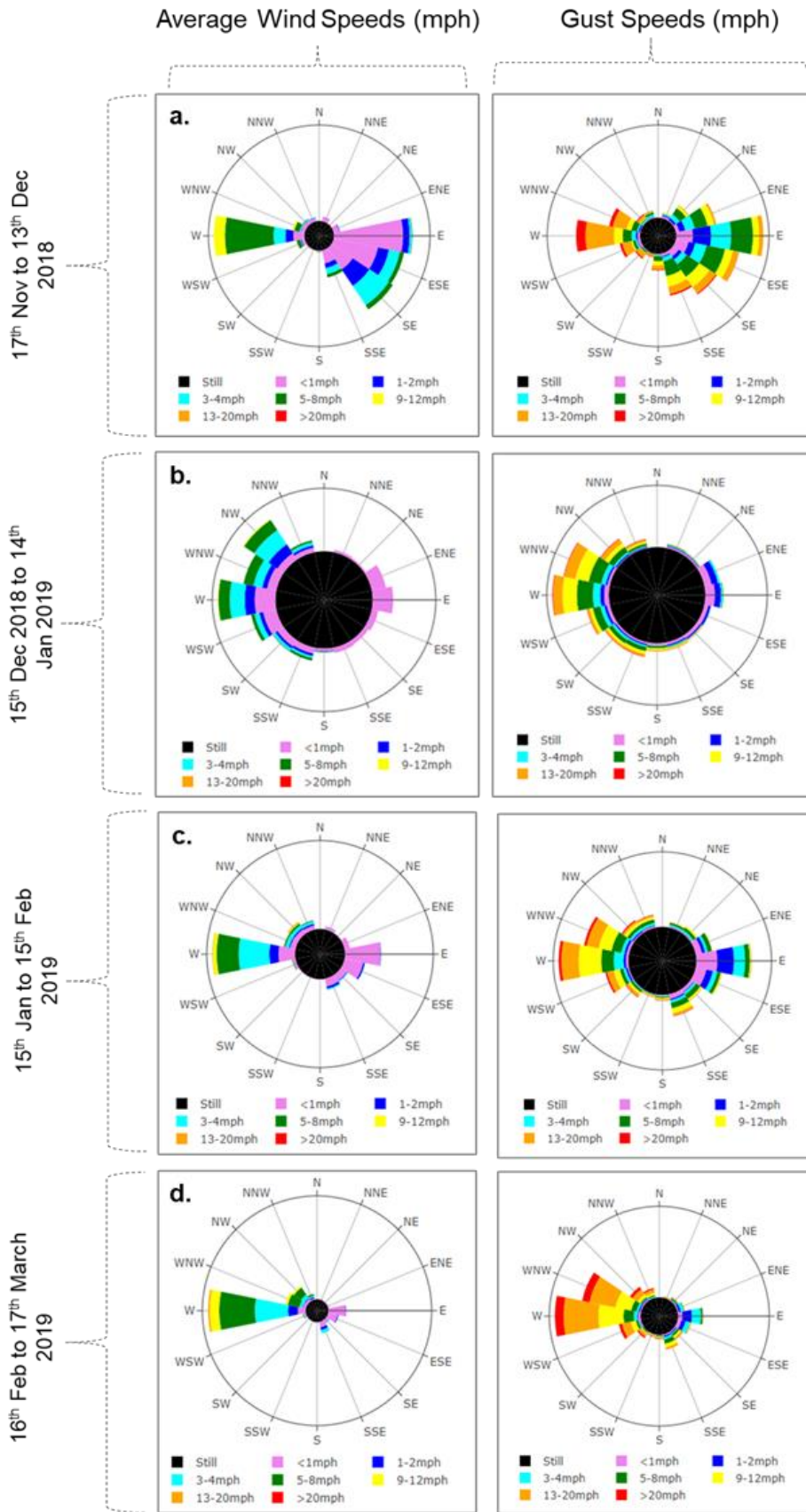
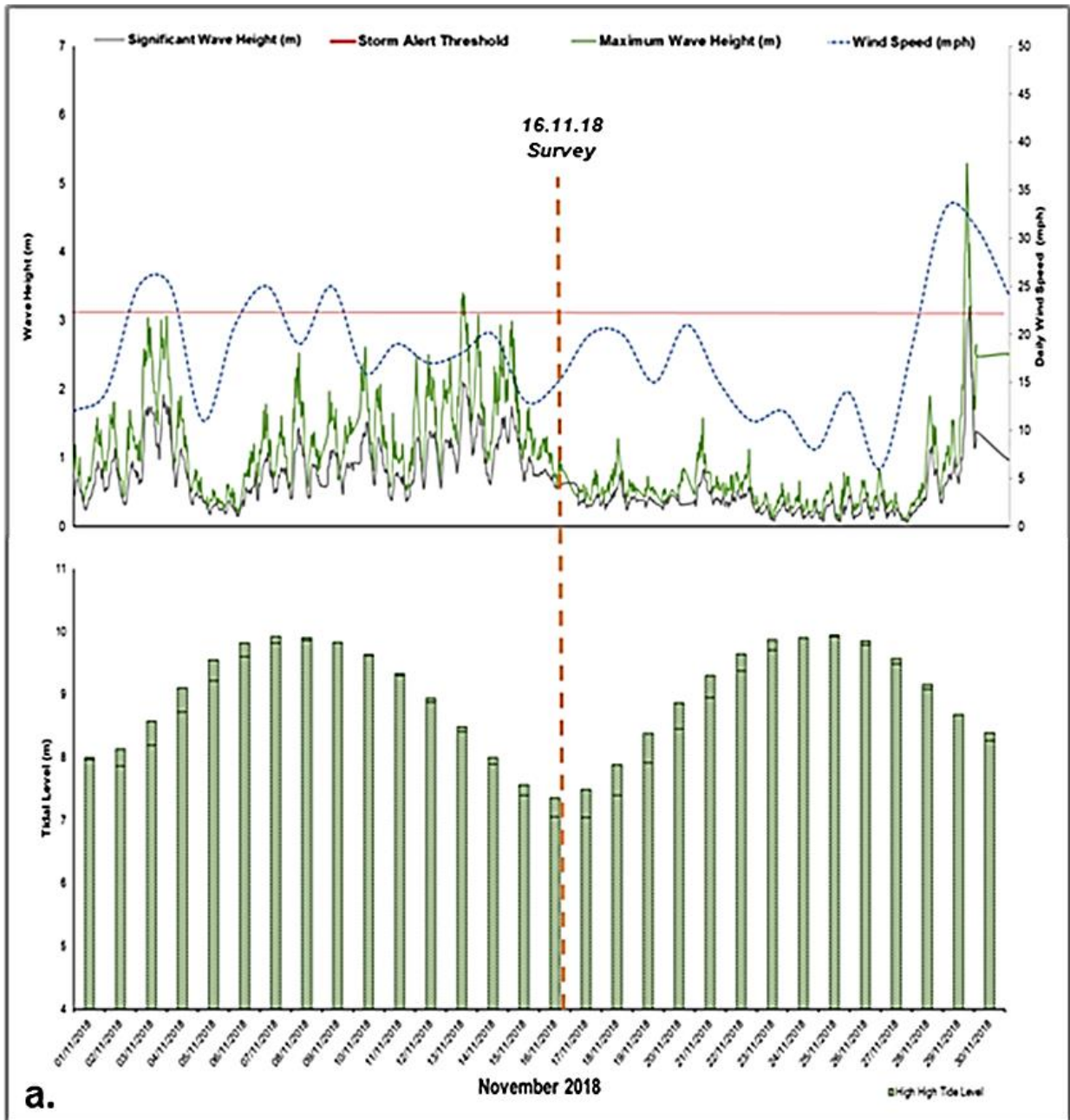
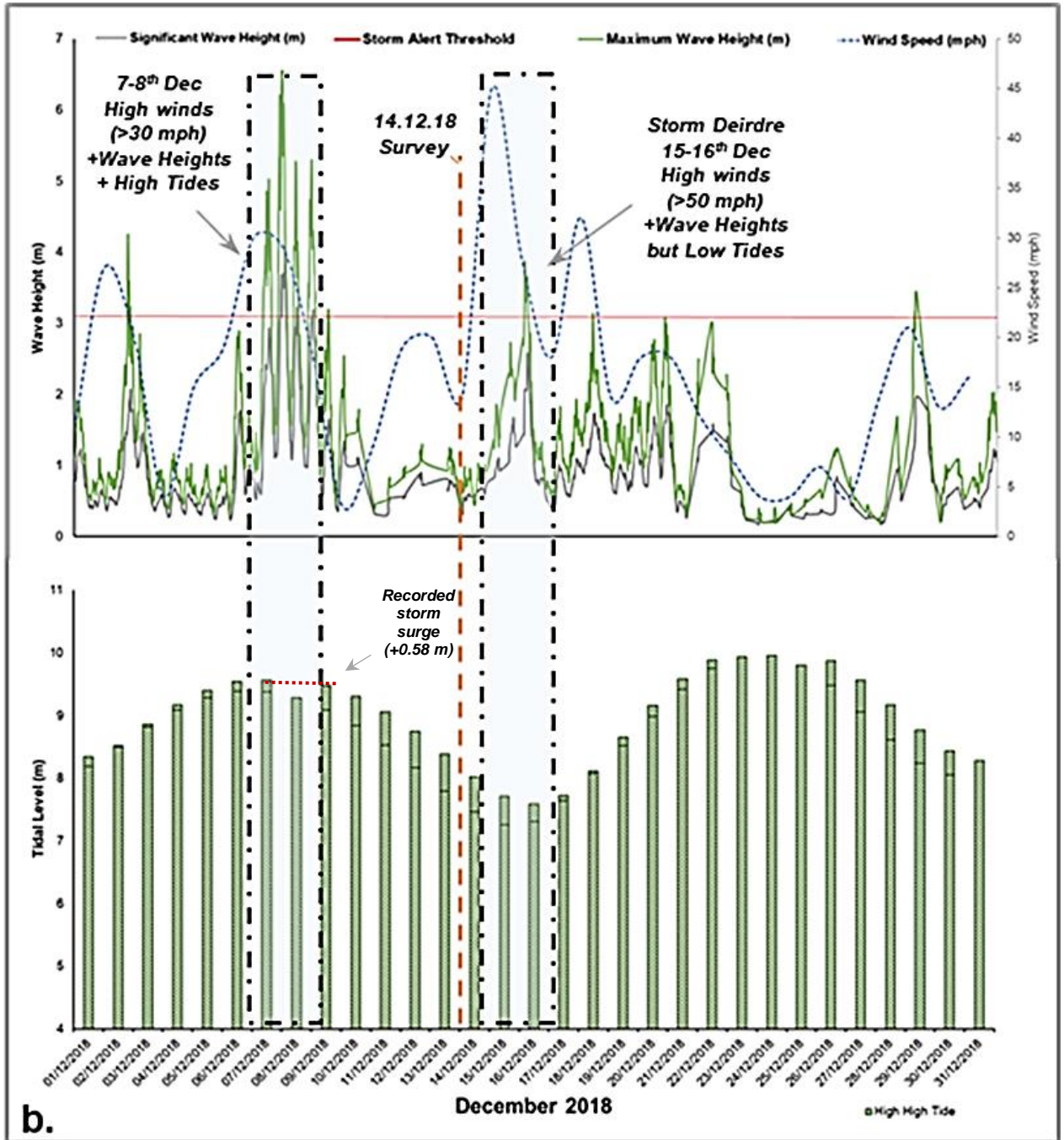
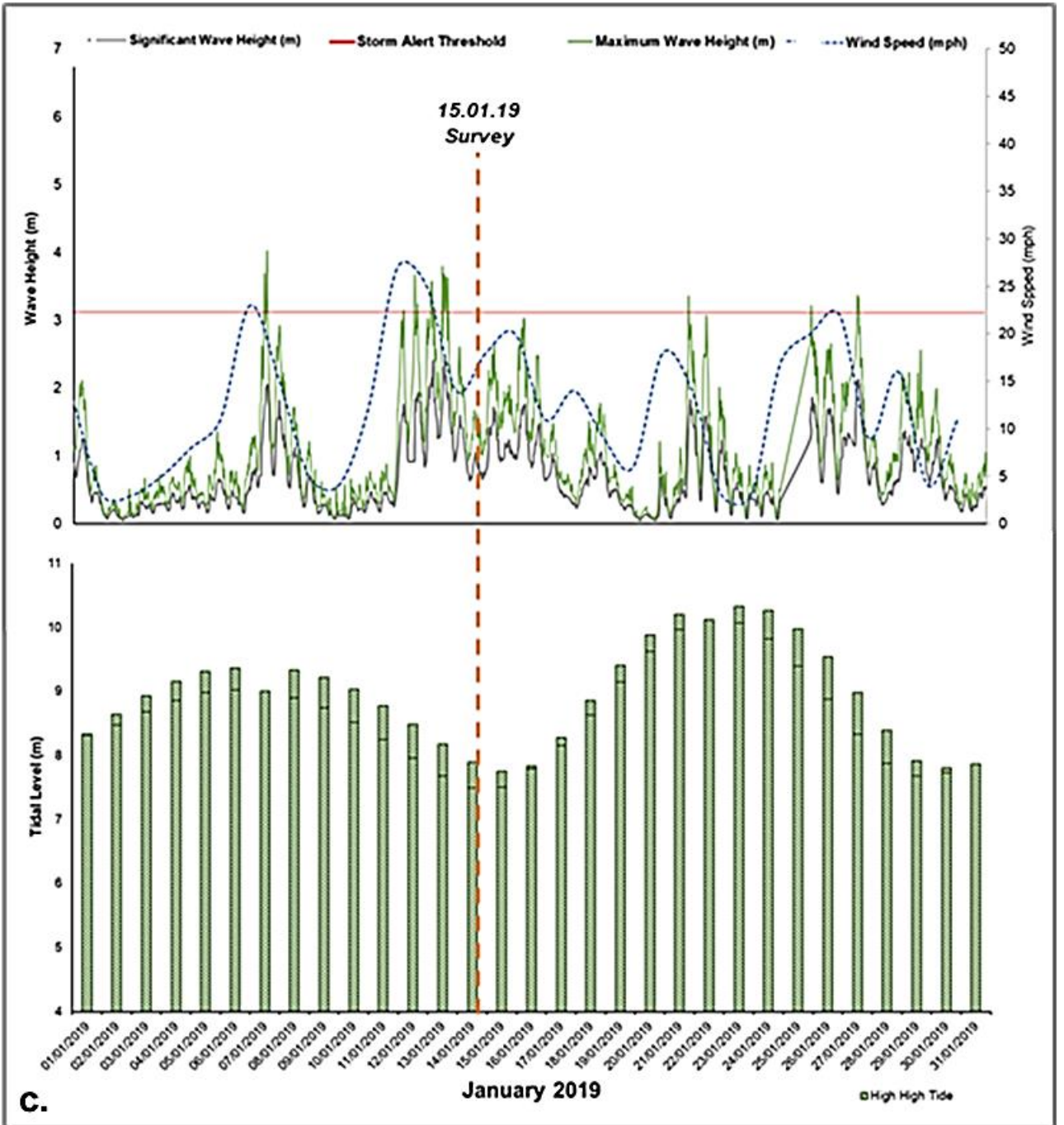


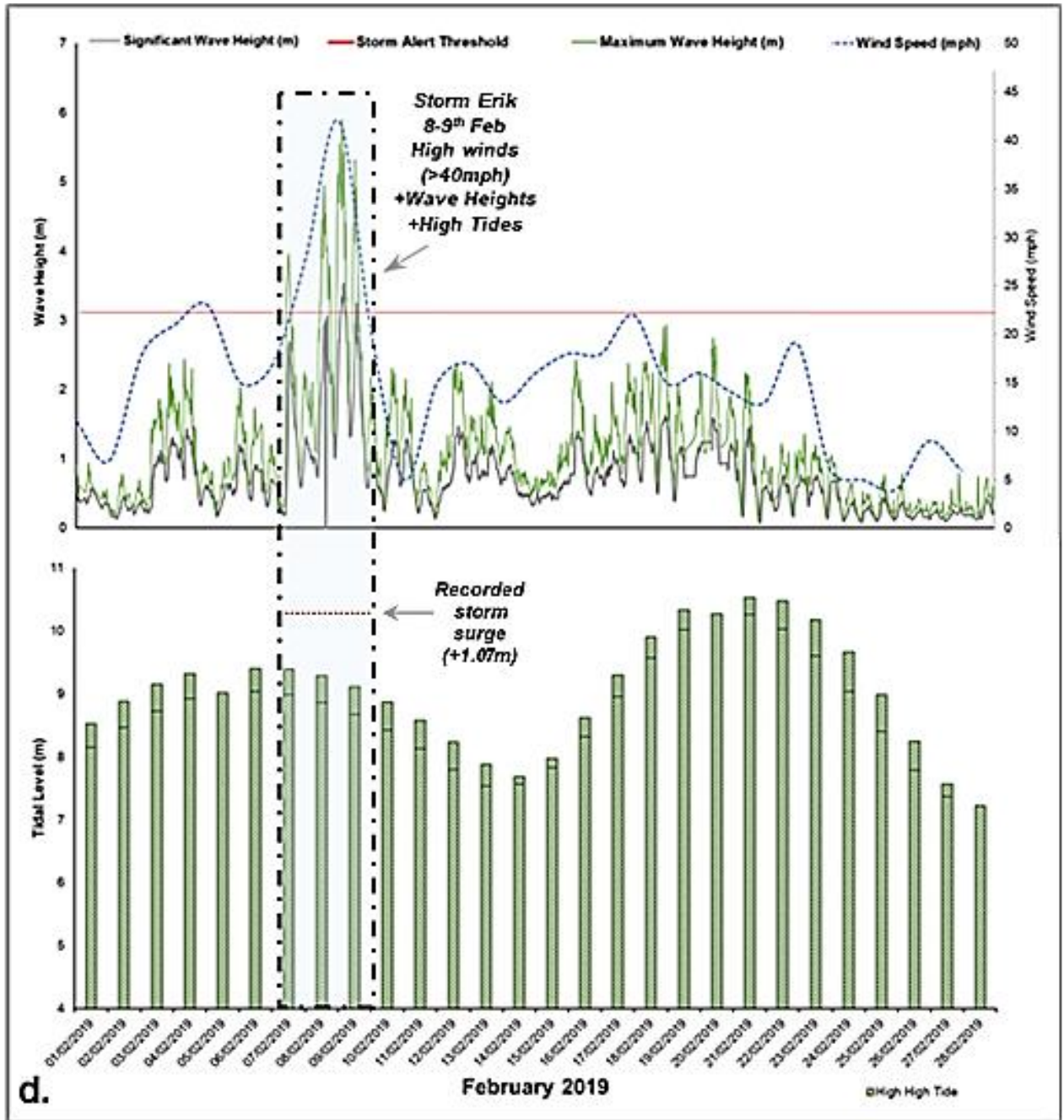
Figure 6.14: Average wind speed and gust speeds for Silverdale over the period from 17th November 2018 to 17th March 2019. Source: Ehideaway, 2020.

January to March 2019 recorded high area loss and deposition from shearing of the saltmarsh margin. This phase experienced the highest period of volumetric erosion along the cliff front (Figure 6.6) and significant deposition. January to March represents a 2-month survey period and, when halved, the area loss and volumetric values are similar to the calculated monthly average. Large sections of area loss released 0.66 m^2 into the coastal sediment budget and contributed 30 % of the total area loss over these two months. A series of UK-wide storm events coincided with spring tides – Storms Erik and Freya (Figure 6.15 c-e). The first was a low frequency, high magnitude event with increased wave heights coinciding with high tides (8th to 9th February – Storm Erik). Meteorological records showed a period of high westerly gust speeds of >20 mph (Figure 6.14c) and Morecambe Bay wave buoy data recorded a storm surge of 1.07 m occurring near to high water (Figure 6.15d). The second phase, incorporating Storm Freya (3-5th March), produced maximum wave heights of 6.7 m and was a period containing higher frequency but marginally smaller magnitude waves (Figure 6.15e). Average wind speeds were predominantly by a westerly for much of the month with lower average wind speeds but strong wind gusts of >20 mph suggesting short periods of higher wind. This increased gustiness is likely to have produced maximum wave heights frequently above the storm alert threshold and occurred prior to the March survey.









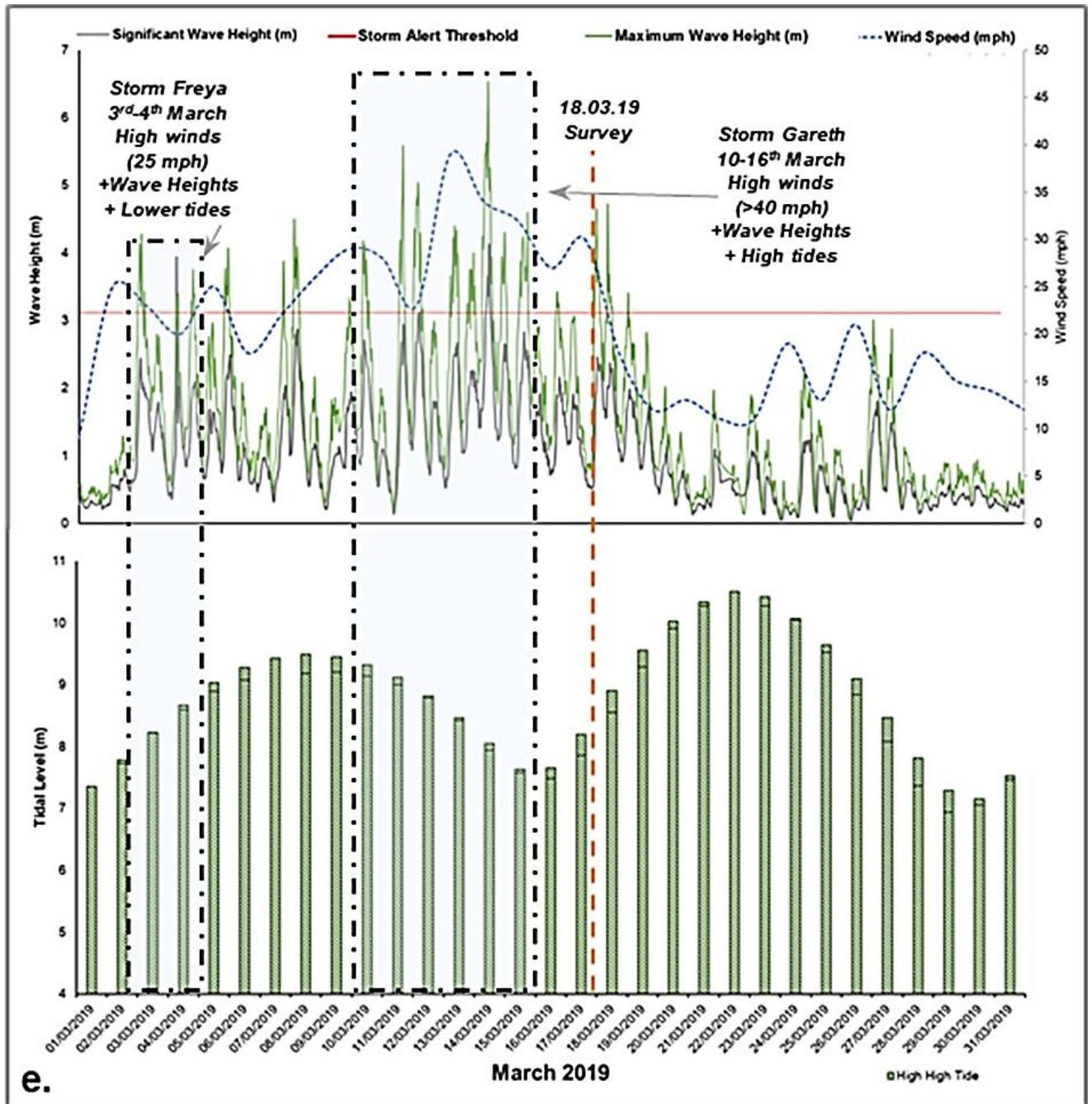


Figure 6.15: Wave buoy, tide gauge, wind and storm data for the Morecambe Bay Estuary from Nov 2018 to March 2019. Highlighted are survey dates and period of significantly higher wave heights. Source: Channel Coastal Observatory, Ehideaway (2020) & PolTips™ tidal prediction software (2020).

The correspondence with augmented high tides provided access for destructive waves to reach the saltmarsh margin – corroborated by the meteorological, wave and predicted tidal data. A third storm event also occurred during this period – Storm Gareth (10-16th March). However, Storm Gareth did not occur during spring tides and was therefore, less likely to produce a sudden erosional impact.

6.5 Discussion

This research used a new multi-camera approach to SfM-MVS image acquisition for the identification and tracking of morphological change across a saltmarsh margin over a 4-month winter period. A series of standardised and innovative morphological assessments were employed to develop a holistic view of changes at Silverdale saltmarsh margin.

Over the 4-month winter period there was systematic erosion of the saltmarsh margin. Most erosion was accounted for by larger scale slumping and collapse brought on by the presence of undercut areas. There were phases of heightened morphological change evidenced by area loss and subsequent fluctuations in volumetric deposition and erosion values. The consistent and significant feature of the survey site was the presence of saltmarsh margin undercutting. The spatially-averaged estimates of these areas showed an overall reduction in the extent of undercutting by 1.53 m² over the period November 2018 to March 2019. This spatially-averaged value would initially imply there has been less active erosion of the site during this period. However, when viewed spatially, using shoreline profile changes, the reduction in undercutting extent is more likely due to the sudden loss of undercut sections of cliff, made possible through exposure to the erosive power of waves.

Figure 6.16 illustrates the correlation between average monthly significant wave height and volumetric erosion (m³). The *r* value for Pearson's Correlation Coefficient suggests a strong positive correlation between significant wave height and volumetric erosion (0.92). The *p-value* for this calculation (0.25) is not sufficient to place a strong confidence rating on the correlation due to the small sample set. However, if the same relationship held for a further two observations a *p-value* of 0.02 would be returned which would support a strong positive correlation between erosion and significant wave height.

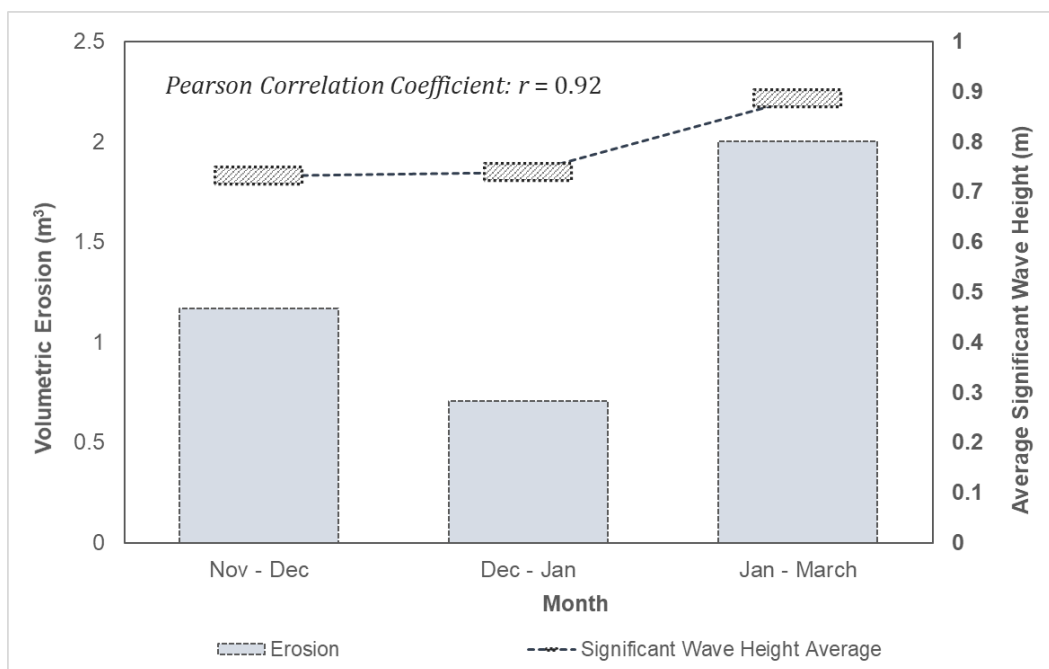


Figure 6.16: Relationship between monthly erosion and monthly significant wave height.

The correlation would suggest that waves are the predominant factor in determining the rate of erosion. Research undertaken at Silverdale saltmarsh by Pringle (1995) also suggests that greater magnitude changes, such as cliff margin collapse, are associated with strong onshore winds which generate high energy waves (Figures 6.16 d-e). The current correlation between monthly significant wave height and monthly erosion corroborates the idea that wind waves are the principal factors responsible for saltmarsh edge erosion, with the power of waves linearly related to the erosion of the saltmarsh edge (Leonardi, Ganju and Fagherazzi, 2016; Sapkota and White, 2019). Leonardi, Ganju and Fagherazzi (2016) suggest that the effect of wind waves on saltmarsh erosion is reduced during storms due to elevated tides flooding the saltmarsh surface, consequently reducing waves breaking on the saltmarsh margin. However, historical retreat of Silverdale saltmarsh was such that the Highest Astronomical Tide (HAT) currently only reaches the saltmarsh margin. Figure 6.17 displays the position of the current HAT (~10.3 m) at the survey site. The height of HAT (Figure 6.17) is similar to the highest surge conditions experienced during the 4-month survey period (Storm Erik – 8-9th Feb 2019) at ~10.4 m. Therefore, Figure 6.17 highlights the furthest location of breaking waves along the saltmarsh margin during the surveyed period. Consequently, the findings suggest that tidal access, and not simply the occurrence of storms, was a significant driver of saltmarsh retreat at Silverdale saltmarsh.



Figure 6.17: Location of Silverdale saltmarsh survey at HAT of ~10.3 m (Photograph: Author's own).

Therefore, these interpretations further confirm the influence of tidal cycles on saltmarsh erosion by aiding the propagation of waves to the saltmarsh margin (Leonardi, Ganju and Fagherazzi, 2016; Li, Leonardi and Plater, 2019). Depending upon location and orientation of the saltmarsh in relation to incoming hydrodynamics, edge erosion could be fundamentally driven by tidal cycles. For some saltmarshes, a lack of tidal access can reduce the impact of high magnitude storm events and consequently reduce the level of erosion.

Undercutting, due to consistent low-level erosion is a slower process than the destructive and intense nature of storms. The continued presence of slower rates of erosion such as undercutting throughout the period of surveying corresponds with the work of Leonardi, Ganju and Fagherazzi (2016) who describe the occurrence of this process even under light wind conditions. Persistent low-level undercutting was clearest in Figures 6.10-6.13 b, which documents a lateral increase (~ 0.02 m) in undercutting from November 2018 to March 2019. The presence of this undercutting is likely to persist in summer months as its occurrence is not solely dependent upon storm events. However, detachment of weakened areas, brought on by the continuous undercutting, does not happen immediately but during periods of more intense wave action (Castillo, 2000). These weakened areas, when subject to increased wave action during winter storms, finally begin to slump and collapse as increased wave energy is dissipated across the marsh edge. The formation of undercutting was aided by

vegetation presence in the upper extent of the saltmarsh cliff. The saltmarsh edge contained plant roots within the top 0.1 m of the cliff profile which helped to increase the resistance against erosion (Morton, Bernier and Kelso, 2009; Sapkota and White, 2019). The increased strength in the upper portions of the profile left the lower sediment layers vulnerable to hydrodynamic impacts. Sapkota and White (2019) found a similar mechanism of erosion across Louisiana saltmarsh environments, where erosion of the lower portions led to overhanging root mats that were eventually separated or toppled during wave attack (Davidson-Arnott, 2010). Furthermore, the current work identified significant cliff collapse and reduced undercut extent during months with increased wave heights combined with spring tides (Figure 6.16a-e).

6.5.1 Implications

6.5.1.1 Erosion management of Silverdale Saltmarsh

The Silverdale saltmarsh has shown to be particularly vulnerable to wave-generated erosion during high tide periods. Based on the findings of this research, the rate of margin erosion will further recede the saltmarsh, diminishing its total area (Allen, 1990; Davidson-Arnott, 2010). The saltmarsh will continue to erode unless there is a form of active intervention or the position of the river channel shifts as the tidal channels, at this site, are known to exert a significant degree of influence over the impact of wave energy to the shoreline (Halcrow, 2013). Halcrow (2013) described the estuary as “*in a current state of dynamic equilibrium*” in terms of saltmarsh area, suggesting erosion is permissible in certain areas of the estuary. However, the current Shoreline Management Policy of ‘No Active Intervention’ due to ‘Natural Defences’ suggests a dependence on the saltmarsh for protection, making it beneficial to maintain the saltmarsh extent. This study has found an ~30 m section of Silverdale saltmarsh edge to be actively eroding (erosion of 3.27 m² over a 4-month period) and is, therefore, reducing the natural level of protection offered to the surrounding area. The priority for the region is to conserve saltmarsh area (Cumbria County Council, 2011), however, these results imply that erosion is likely to continue.

6.5.1.2 Saltmarsh Monitoring and Assessment

The research has demonstrated the use of a new roving multi-camera rig with SfM-MVS for the reconstruction and monitoring of saltmarsh edge retreat. This method of

monitoring has previously shown to provide precision of < 8.2 mm (x, y & z) (detailed in Chapter 5). Unlike many aerial survey techniques, such as LiDAR, the SfM-MVS acquisition procedure used oblique images which allowed the vertical cliff face to be reconstructed. In so doing, this technique has allowed the development of an innovative assessment of undercutting extent (details in section 6.3.3.3). Analysis identified 1.53 m² of undercut area lost across an ~ 30 m section of saltmarsh edge during the surveyed period, such analysis could assist in pre-empting collapse and calculating retreat rates more effectively. This new information allowed a more direct analysis of the impact of wave hydrodynamics and meteorological conditions on retreat than possible with other aerial monitoring methods.

This form of monitoring lends itself to frequent and impromptu field surveys. Combined with the high-resolution capabilities of the technology, this method therefore provides a low cost, rapid technique that can detect seasonal and event-based variability in erosion rates that can be linked to undercutting progression and margin collapse.

6.6 Conclusions

The purpose of this paper was to demonstrate the capability of an innovative roving camera rig with SfM-MVS to provide understanding of the spatial and temporal variability of erosion at a ~ 30 m section of Silverdale saltmarsh margin, North West England. In particular, the findings have shown the potential of the technique to reveal changes to the saltmarsh margin through shoreline geometry profiles and erosion estimates. The high-resolution capabilities of the technique have enabled the distribution and severity of erosion to be established and linked to wave hydrodynamic and meteorological data.

Erosion and undercutting were found to be prominent characteristics of the saltmarsh boundary. Erosional losses were calculated at 3.88 m³ over a 4-month survey period with a monthly erosion rate of 0.97 m³. Undercut extent was able to be calculated through the development of an innovative assessment made possible through oblique images captured by the multi-camera rig. Assessment revealed undercut extent varied spatially and was reduced by 1.53 m² from November 2018 to March 2019 due to progressive weakening over time, leading to larger scale collapse. Monthly erosion rates strongly correlated with significant wave height but smaller scale, progressive

undercutting continued laterally across the site, at approximately 0.01-0.02 m per month as a result of high frequency, low intensity hydrodynamic activity.

The deployment of the multi-camera rig has shown to be an effective method of monitoring coastal change. The technology provides coastal managers and researchers with a rapid, low-cost and accurate survey option that can be used to regularly monitor sites of coastal recession.

7. Discussion

Coastal environments are becoming increasingly vulnerable to the effects of climate change. Increased storm severity and rising sea-levels have the potential to cause devastating flooding and erosion placing a significant financial burden on governments in response and recovery. This research was prompted by the need to protect these vulnerable areas of the coast from further erosion. Sites of coastal recession are a particular concern for coastal managers, but regular monitoring of these locations can help to prevent further land loss through pre-emptive management. However, acquisition of 3D data, essential for tracking and determining morphological change, is not always easily obtained.

In an increasingly digital world, the expectation for data with higher spatial and temporal resolution is growing. To address this expectation, the research has developed an innovative multi-camera system, from initial idea through to deployment. The development of this research, in combination with an industry partner, can be understood as part of the wider movement towards digital innovations aiming to reduce environmental risk.

This chapter begins with a comparison of the developed method with current remote sensing techniques. This is followed by a review of the wider implications of this research in relation to digital innovation development, flood and erosion risk management and SfM-MVS research. The chapter will conclude with an overview of future avenues for research.

7.1 Technique Comparison

Overall, the use of SfM-MVS with multiple cameras in comparison to larger scale monitoring techniques, such as satellite imagery, radar and video surveillance, offers a greater degree of flexibility. This flexibility is in terms of spatial and temporal resolution and the ability to adapt image acquisition according to the environment, e.g. adapting the camera rig movements in relation to the cliff profile. The autonomy and coverage of larger scale techniques is still a significant advantage as it requires little manual input. However, SfM-MVS offers autonomy from a fixed pattern of monitoring or specific scale

and allows monitoring to focus on particularly vulnerable areas rather than a 'blanket' approach to a site.

Airborne SfM-MVS platforms such as kites, and UAVs, can also be susceptible to adverse weather conditions and highly restrictive legislation mean that these types of platforms cannot be used frequently. Here, the camera rig has several advantages. As discussed in Chapter 5, the use of pole-mounted cameras is less restrictive than the use of airborne platforms, particularly UAVs. The use of UAVs in coastal settings can be highly restricted by air space regulators and local byelaws. Moreover, the camera rig also offers stability in comparison to airborne platforms e.g. UAVs and kites, which are highly susceptible to wind - a regular occurrence in coastal environments. Consequently, regular monitoring is not easily achieved even if all other weather conditions (e.g. diffuse lighting) and tide times are suitable.

In comparison to similar scale techniques, such as TLS, the option of a multi-camera rig is advantageous in terms of time. Chapter 5 showed how the multi-camera setup provided a data acquisition procedure 86 % faster, on average, than that of a TLS survey. In addition to time spent in the field, the cost of the camera rig is ~1.7 % that of a standard TLS setup. Based on this research, the camera rig has shown to be a potentially low cost (~£600) and efficient alternative to the TLS which costs in the region of £35,000 (Visser et al., 2019). There are also several logistical advantages to this form of data acquisition in comparison to the TLS. TLS equipment can be delicate and prone to temperature disturbance which affects data acquisition. Equipment can also be bulky and heavy, a disadvantage when trying to access remote areas. In comparison, the camera rig is a more rugged due to the waterproof and shockproof nature of the action cameras and the design of the camera rig.

In comparison to other SfM-MVS platforms and image acquisition procedures, the camera rig (Chapters 5 & 6) offers the ability to capture multiple images with a single control. The fixed camera positions on the rig means the cameras FOV is predetermined. Therefore, during fieldwork, interaction of the images is known. For example, with the current setup in Chapters 5 and 6 there is a guaranteed image overlap of ~97 %. In comparison, with a single handheld DSLR it is difficult to guarantee this overlap. This lack of awareness of FOV and image overlap can result in poor coverage and reduced feature tracking, ultimately leading to a poor 3D reconstruction. Pole-mounted image

acquisition with a single camera is particularly problematic due to the lack of information on image interaction (camera FOV). As a result, this requires a higher number of images to be captured to ensure coverage, and therefore, a much higher degree of processing and time spent in the field. The current work has presented a set of rigorously tested guidelines on all aspects of image acquisition for multi-camera setups at sites of coastal recession. These guidelines provide good overall coverage (surpassing the TLS) and reconstruction capabilities (precision of < 8.2 mm). The guidelines provide a holistic approach to image acquisition that predetermine image overlap, camera height and obliqueness and therefore improves upon the current more ambiguous image overlap requirements for both handheld and pole-mounted cameras.

7.2 Wider Implications

7.2.1 Fostering Innovation

This research has documented the development of a coastal monitoring technique using SfM-MVS. The thesis describes the process of construction and testing of the multi-camera system from first principles through to application. The research was the result of a university and industry collaboration which aimed to foster innovation – the Low Carbon Eco-Innovatory. This approach to innovation development sought to blend the results of academic research for use in practical, industry-based settings.

The production and subsequent use of the camera rig directly affects data acquisition for coastal researchers and practitioners through the removal of barriers to technological practices and the democratisation of previously specialist fields. This type of development not only has created an easy-to-use method for topographic data acquisition but the process by which the research has been conducted is part of a wider global trend towards research and innovation.

Over the last decade technological advances have changed the way we interact, work, and communicate. Increased accessibility and the emergence of new technologies such as artificial intelligence, automation and machine learning have the potential to revolutionise a multitude of disciplines, including topographic sensing. These advances were previously borne in research environments such as universities with little output into commercial or practical settings. The triple-helix model theorised by Etzkowitz & Leydesdorff (1995) suggested that improved interactions between academia, industry

and government would, through time, cause aspects of each sector to be implemented by the other. Consequently, this causes the adoption of innovations and ideas more rapidly into the market. As new digital technologies diffuse into economies, organisations are adapting to new products, services and business models (Goos et al., 2019). The increased local and global connectivity has also produced a shift in the approach to research and development. The creation and application of funding projects such as the Low Carbon Eco-Innovatory have established partnerships between research and businesses such as Marlan Maritime Technologies. These connections enable the identification of areas where research expertise and commercial demand are overlapping. The approach not only identifies the current needs within the market for specific innovations but also provides distribution of the innovation directly into the market - either for use or further development.

This model of increased connectivity and development continuously feeds a network of progressive ideas. The technological advances created during this 'Fourth Industrial Revolution' (DBEIS, 2019) are playing a progressively dominant role in national economic growth and as a result, governments are shifting their attention towards research and innovation (Branscomb, 2001). The UK government is, in particular, seeking to advance the UK's position in terms of technological innovation and wants to raise research and development investment to 2.4% of GDP by 2027 (DBEIS, 2019). This drive for innovation has extended into a multitude of disciplines including flood and erosion risk management.

7.2.2 Flood and Erosion Management

In the past 10 years, flood and erosion risk management has moved higher on local and global agendas due to an increase in the severity and frequency of extreme weather events brought on by climate change (Environment Agency, 2018). The increasingly integrated nature of academia, industry and government has led to new initiatives and policy adaptations that promote risk management through data-driven decision making (Towe et al., 2020). New technologies, such as those developed in this research, are driving increased data collection and analysis which are used to aid model prediction and decision making.

The presence of this technological revolution can be seen in the government's shift towards digital initiatives such as the creation of 'Defra Digital' which is used to find and fund innovative developments (Defra, 2021). Specific integration into flood and erosion risk management can be seen by the recently introduced funding of £200 million through the 'Flood and Coastal Risk Innovation' programme. The programme seeks to fund projects that demonstrate practical innovation actions which improve the resilience of communities to flooding and coastal erosion (Environment Agency and Defra, 2021). This active funding programme is an example of the growing need for innovative research and developments such as those provided in this project. Therefore, the research conducted here not only offers a low-cost product for coastal managers and researchers but also feeds the growing trend for increased data acquisition.

The camera rig provides a level of flexibility to data acquisition that was previously not as easily achieved. Consequently, the increased amount of data and subsequent analysis and interpretation available to decision makers is growing. As innovations feed and improve these networks users are provided with a greater evidence-base from which to draw substantive and informed decisions in terms of flood risk mitigation and management. Furthermore, the UK government recently announced a £5.2 billion investment in coastal defence schemes to prevent £32 billion in economic damage (Defra, 2020). The data obtained from coastal monitoring is important for helping to determine when, where and how these defences will be deployed. The increased frequency of data acquisition also means wave hydrodynamics can be more effectively linked to morphological changes and used to identify vulnerable areas before damaging erosion occurs.

7.2.3 SfM-MVS & Photogrammetry Research SfM-MVS

The research has developed a systematic and streamlined approach to 3D monitoring of coastal recession. Moreover, the research has highlighted and addressed previously overlooked aspects of SfM-MVS research. One of the overarching objectives of this work was to address gaps within SfM-MVS research, such as impact of camera type, position and processing parameters on the quality of 3D reconstructions. This information is a necessary step to advance the take-up and adaptation of the technique. The findings of this research point to the future possibilities of the technique, such as fixed camera in-

situ monitoring, action camera use, reduction of images through increased distances. However, there are broader possibilities such as crowd sourcing of images and citizen science endeavours.

Traditionally, large-scale data acquisition of widespread coastal erosion assessment would necessitate time-intensive research efforts by specialist surveyors. However, as techniques and information are democratised and become more accessible, through research such as this, it leaves the possibility for other routes for data acquisition. Crowd-sourcing and citizen science schemes offer the opportunity to outsource data acquisition and scientific processing to the general public whilst engaging with local communities (Pocock et al. 2014; See et al. 2016; See, 2019). The integration of digital technologies into our everyday lives has revolutionised the way in which data is gathered and analysed and means that crowd-sourcing initiatives can play a prominent role in risk reduction (McCallum et al., 2016). Crowd-sourcing offers the opportunity for SfM-MVS to be widely used to reconstruct coastal environments more regularly by outsourcing data collection to local communities. This step towards community engagement in assessing flood and erosion risk is precisely what is funded by the UK Government's Flood and Coastal Resilience Innovation Programme. The advances made in this research, in terms of SfM-MVS image interaction, makes the possibility of crowd-sourcing initiatives more feasible by democratising the technique.

7.3 Future Development and Research

This research not only informs the subject of coastal monitoring but also the general development of SfM-MVS research in the geosciences. The provision of monitoring options suitable for different settings, schemes or environments is always an important endeavour. However, several areas have been identified that could advance current research in SfM-MVS coastal monitoring. Specific recommendations for future work have been discussed within Chapters 4, 5 and 6. However, a general overview of further avenues for both research and practice are provided below:

- Camera stand-off distance was held constant throughout this research. SfM-MVS displays a scale-dependent practicality (Smith and Vericat, 2015; Eltner et al., 2016), whereby error tends to increase at greater distances. Maintenance of the stand-off distance was essential to ensure any changes to reconstruction quality

were the influence of the tested variables (height, obliqueness and overlap). However, increasing distance to the scene and overall scale of the surveyed site would be an important step forward. Increasing the distance from the scene is likely to reduce accuracy and precision. However, at what point does this become unsustainable for coastal recession monitoring and how do the results compare to an industrial benchmark? These are all considerations that could be investigated to build upon this research.

- GCP marker placement in software has shown to display an influence on model deformation. Further exploration and detailed examination of this impact would be an interesting point for further research. In particular, the influence of marker placement on images with less distortion and on sites with less of a linear image acquisition.
- A multi-camera roving rig was used for coastal monitoring. However, the results uncovered here, in terms of camera synchronisation and predetermined camera arrangements, reveals the potential for multi-camera time-lapse setups. An in-situ multi-camera setup for coastal monitoring could provide continuous or periodic data that would reduce manual input.
- The comparisons in this research are between SfM-MVS and an industrial standard TLS which was used as a benchmark for assessing accuracy and standalone precision. However, a comparison between action cameras and a DSLR image acquisition could be insightful. This comparison would allow the impact of lens distortion to be directly compared with a standard SfM-MVS image acquisition. In addition, the DSLR could be tested for speed of image acquisition and scene coverage compared to the camera rig.

8. Conclusions

The research was driven by the necessity to protect and monitor vulnerable coastlines and the potential of SfM-MVS to provide a low-cost multi-camera surveying platform. However, current gaps in SfM-MVS research, discussed in Chapter 2, indicated the need for experimental research into image interaction and processing before multi-camera setups were possible.

Therefore, the four principal objectives of the research were to:

1. Conduct an experimental SfM-MVS survey at a small-scale site of typical coastal recession using a novel method of image acquisition which controls the optical camera axes.
2. Explore the potential of a multi-camera array with SfM-MVS for image acquisition at different sites of coastal recession.
3. Identify the impact of software processing on point cloud reconstruction.
4. Investigate the capacity of techniques identified above for the monitoring of temporal changes in coastal morphology.

These objectives were addressed throughout Chapters 4, 5 and 6 and were established to provide a route to achieving the overall aim of producing a terrestrial multi-camera array for monitoring coastal retreat. Consequently, an efficient method of image acquisition using a multi-camera setup with SfM-MVS has been developed, constructed (Objective 2) and rigorously tested to ensure consistency of results across different test locations and comparative benchmarks (Objective 3). A comparison of results to an industrial benchmark (TLS) revealed an accuracy < 0.01 m (≤ 30 m alongshore) and standalone precision measurements of < 0.0082 m (x, y & z respectively) across all three research applications (Objectives 1, 2 & 3).

Furthermore, the research presented in this thesis highlights and addresses previously overlooked aspects of SfM-MVS research. One of the core objectives throughout this research was the impact camera pose and orientation has on reconstruction quality and how this could be adjusted to provide an optimal image acquisition network. The findings have helped to demystify the general outline of 'the more images the better'

(Micheletti, Chandler and Lane, 2015b) and provide a series of systematic guidelines for camera placement in relation to the scene. Chapter 4 revealed that as few as five images placed in appropriate positions (camera to cliff ratio of ~3:4 and 40° declination) provided results equivalent to three TLS scans (Objective 1). These findings are corroborated in Chapters 5 and 6 by using these designated parameters to produce accurate 3D reconstruction suitable for monitoring coastal retreat.

A further objective of the research was to identify processing parameters for the reduction of point cloud deformation and the streamlining of SfM-MVS (Objective 3). Previously under-researched, the choice of image alignment parameter had a significant impact on the systematic deformation of reconstructions. A 94 % reduction in reprojection error was recorded through a change in processing parameter ('Medium' instead of 'Highest') (Objective 3). Other previous research has been centred on the use of field GCPs (Westoby et al., 2018) and general camera orientation (James, Robson and Smith, 2017) as a correction for deformation. Field GCPs are an important aspect of point cloud correction. However, there has been little discussion about the choice of parameters or the specific placement of GCP markers in software and their impact on reconstruction. The findings of Chapter 5 demonstrate reduction in deformation through a change in software processing parameters (Objective 3) and marker placement. Subsequent surveys of Silverdale saltmarsh in Chapter 6 (Objective 4), supported the findings of Chapter 5 through the accurate and repeatable topographic 3D reconstruction of <0.01 m accuracy.

A dominant theme throughout this research is the use of GoPro action cameras for image acquisition. The research has been able to produce positive results with accurate metric integrity. Despite their wide popularity, action cameras were previously considered to be unsuitable for SfM-MVS as the inherent lens distortion meant that accurate reconstructions were less likely (Perfetti, Polari & Fassi, 2017). However, the research presented in this thesis provides evidence not only of their use for geomorphological reconstruction but their ability to be used in a multi-camera setup to produce millimetre level accuracy. Chapters 4 and 5 both document < 0.0082 m precision for all testing scenarios with action cameras. The use of these cameras is substantiated by the rigorous and comparative testing which showed the method to

equal and surpass the industrial benchmark (TLS) in terms of point cloud completeness and accuracy (Objectives 1 & 2).

The ultimate purpose of the camera rig was for regular monitoring at sites of coastal recession (Objective 4) and this was presented in Chapter 6 over a 4-month survey period at Silverdale saltmarsh. The surveys revealed persistent erosion and undercutting of the saltmarsh edge with erosion calculated at 3.88 m^3 over $\sim 30\text{m}$ section for 4 months. Innovative undercutting analysis, through the capture of oblique images by the multi-camera rig, revealed a reduction in undercut extent of 1.53 m^2 .

8.1 Concluding Remarks

The results reported in this thesis demonstrate the considerable potential for multi-camera setups to monitor coastal recession and potentially improve the temporal resolution of coastal monitoring. The rig offers a rugged, easily operable, cost effective, accurate and rapid piece of monitoring equipment. Furthermore, this research fundamentally develops the concepts and techniques in the field of SfM-MVS. The research has identified optimal camera positions, suitable processing parameters to aid the reduction of deformation and used a camera type previously less suitable for the creation of high accuracy 3D reconstructions. This research has sought to significantly develop current understanding of the SfM-MVS technique and provide usable guidelines to refine the previously broad approach to image acquisition.

Many coastal researchers and managers are faced with the problem of increasing coastal vulnerability due to climate change but with a finite budget for data acquisition and intervention. It is hoped that this research provides an alternative approach to coastal monitoring that is not dependent upon specialist, costly surveys and provides accurate data that can be used in the implementation of effective coastal management and protection.

9. References

- Abellán, A., Oppikofer, T., Jaboyedoff, M., Rosser, N. J., Lim, M. & Lato, M. J. (2014). Terrestrial laser scanning of rock slope instabilities. *Earth Surface Processes and Landforms*, 39(1), 80–97. <https://doi.org/10.1002/esp.3493>
- Abualhin, K. (2016). Mapping of underwater seabed morphology of the Gaza Strip coastal zone using remote sensing technique. *Turkish Journal of Engineering and Environmental Sciences*, 40(3), 19–29. <https://doi.org/10.15446/esrj.v20n2.50256>
- Agisoft. (2018). Agisoft PhotoScan User Manual Professional Edition, Version 1.4. Retrieved from <https://www.agisoft.com/downloads/user-manuals/>
- Allen, J. R. L. (1990). Salt-marsh growth and stratification: A numerical model with special reference to the Severn Estuary, southwest Britain. *Marine Geology*, 95(2), 77–96. [https://doi.org/10.1016/0025-3227\(90\)90042-I](https://doi.org/10.1016/0025-3227(90)90042-I)
- Anthony, E. J., Vanhee, S. & Ruz, M.H. (2006). Short-term beach–dune sand budgets on the north sea coast of France: Sand supply from shoreface to dunes, and the role of wind and fetch. *Geomorphology*, 81(3–4), 316–329. <https://doi.org/10.1016/j.geomorph.2006.04.022>
- Arkema, K. K., Guannel, G., Verutes, G., Wood, S. A., Guerry, A., Ruckelshaus, M. & Silver, J. M. (2013). Coastal habitats shield people and property from sea-level rise and storms. *Nature Climate Change*, 3(10), 913–918. <https://doi.org/10.1038/nclimate1944>
- Arnside & Silverdale AONB Partnership. (2015). Arnside & Silverdale Area of Outstanding Natural Beauty - Landscape and Seascape Character Assessment. Retrieved from https://www.arnsidesilverdaleaonb.org.uk/uploads/2016/05/lsc_a_introduction.pdf
- Askew, D. and Skelcher, G. (2014) Arnside & Silverdale Special Qualities Report. Available at: https://www.arnsidesilverdaleaonb.org.uk/uploads/2016/03/mp_specialqualitiesreport.pdf (Accessed: 6 January 2021).

Ballarin, M., Balletti, C. & Guerra, F. (2015, June 21). Action cameras and low-cost aerial vehicles in archaeology (F. Remondino & M. R. Shortis, eds.).

<https://doi.org/10.1117/12.2184692>

Baptista, P., Bastos, L., Bernardes, C., Cunha, T. & Dias, J. (2008). Monitoring Sandy Shores Morphologies by DGPS—A Practical Tool to Generate Digital Elevation Models. *Journal of Coastal Research*, 246, 1516–1528. <https://doi.org/10.2112/07-0861.1>

Barnard, P. L., Erikson, L. H., Foxgrover, A. C., Hart, J. A. F., Limber, P., O'Neill, A. C. & Jones, J. M. (2019). Dynamic flood modeling essential to assess the coastal impacts of climate change. *Scientific Reports*, 9(1), 1–13. <https://doi.org/10.1038/s41598-019-40742-z>

Bemis, S. P., Micklethwaite, S., Turner, D., James, M. R., Akciz, S., Thiele, S. T. & Bangash, H. A. (2014). Ground-based and UAV-Based photogrammetry: A multi-scale, high-resolution mapping tool for structural geology and paleoseismology. *Journal of Structural Geology*, 69, 163–178. <https://doi.org/10.1016/j.jsg.2014.10.007>

Benavente, J., Del Río, L., Gracia, F. J. & Martínez-del-Pozo, J. A. (2006). Coastal flooding hazard related to storms and coastal evolution in Valdelagrana spit (Cadiz Bay Natural Park, SW Spain). *Continental Shelf Research*, 26(9), 1061–1076.

<https://doi.org/10.1016/j.csr.2005.12.015>

(BGS), British Geological Society (2020) Geology of Britain. Available at: <https://mapapps.bgs.ac.uk/geologyofbritain/home.html> (Accessed: 6 January 2021).

Boufama, B. & Habed, A. (2004). Three-dimensional structure calculation: achieving accuracy without calibration. *Image and Vision Computing*, 22(12), 1039–1049.

<https://doi.org/10.1016/j.imavis.2004.03.015>

Branscomb, L. M. (2001) 'Technological Innovation', in *International Encyclopedia of the Social & Behavioral Sciences*. Elsevier, pp. 15498–15502. doi: 10.1016/b0-08-043076-7/03208-3

Brasington, J., Vericat, D. & Rychkov, I. (2012). Modeling river bed morphology, roughness, and surface sedimentology using high resolution terrestrial laser scanning. *Water Resources Research*, 48(11). <https://doi.org/10.1029/2012WR012223>

Brooks, S. M., Spencer, T. & Christie, E. K. (2017). Storm impacts and shoreline recovery: Mechanisms and controls in the southern North Sea. *Geomorphology*, 283, 48–60. <https://doi.org/10.1016/j.geomorph.2017.01.007>

Brunier, G., Fleury, J., Anthony, E. J., Pothin, V., Vella, C., Dussouillez, P. & Michaud, E. (2016). Structure-from-Motion photogrammetry for high-resolution coastal and fluvial geomorphic surveys. *Géomorphologie : Relief, Processus, Environnement*, 22(2), 147–161. <https://doi.org/10.4000/geomorphologie.11358>

Bryant, E. (2012). Oceanic Hazards. In *Natural Hazards* (pp. 155–176). <https://doi.org/10.1017/cbo9780511811845.009>

Calligaro, S., Sofia, G., Prosdocimi, M., Dalla Fontana, G. & Tarolli, P. (2014). Terrestrial Laser Scanner Data To Support Coastal Erosion Analysis: The Conero Case Study. *ISPRS - International Archives of the Photogrammetry, Remote Sensing and Spatial Information Sciences*, XL-5/W3, 125–129. <https://doi.org/10.5194/isprsarchives-XL-5-W3-125-2013>

Carbonneau, P. E. and Dietrich, J. T. (2017). ‘Cost-effective non-metric photogrammetry from consumer-grade sUAS: implications for direct georeferencing of structure from motion photogrammetry’, *Earth Surface Processes and Landforms*, 42(3), pp. 473–486. doi: 10.1002/esp.4012.

Casella, E., Drechsel, J., Winter, C., Benninghoff, M. & Rovere, A. (2020). Accuracy of sand beach topography surveying by drones and photogrammetry. *Geo-Marine Letters*, 255–268. <https://doi.org/10.1007/s00367-020-00638-8>

Castillo J. M. et al. (2000) ‘Causes and Consequences of Salt-Marsh Erosion in an Atlantic Estuary in SW Spain’, *Journal of Coastal Conservation*, 6(1), pp. 89–96. Available at: <https://search-ebscohost-com.liverpool.idm.oclc.org/login.aspx?direct=true&db=edsjsr&AN=edsjsr.25098325&site=eds-live&scope=site>.

Castillo, C., Pérez, R., James, M. R., Quinton, J. N., Taguas, E. V. & Gómez, J. A. (2012). Comparing the Accuracy of Several Field Methods for Measuring Gully Erosion. *Soil Science Society of America Journal*, 76(4), 1319–1332. <https://doi.org/10.2136/sssaj2011.0390>

Channel Coastal Observatory. (2019). Morecambe Bay 2018/2019. Retrieved July 13, 2020, from <http://www.channelcoast.org/reports/>

Chaumillon, E., Ozenne, F., Bertin, X., Long, N. & Ganthy, F. (2014). Control of wave climate and meander dynamics on spit breaching and inlet migration. *Journal of Coastal Research*, 70, 109–114. <https://doi.org/10.2112/si70-019.1>

CoastSnap (2020) Home - CoastSnap- Citizen Science App. Available at: <https://www.coastsnap.com/> (Accessed: 7 February 2021).

Committee on Climate Change. (2018). Managing the coast in a changing climate. Retrieved from www.theccc.org.uk/publications

Conlin, M., Cohn, N. & Ruggiero, P. (2018). A Quantitative Comparison of Low-Cost Structure from Motion (SfM) Data Collection Platforms on Beaches and Dunes. *Journal of Coastal Research*, 34(6), 1341. <https://doi.org/10.2112/JCOASTRES-D-17-00160.1>

Cumbria County Council. (2011). Cumbria Landscape Character Guidance and Toolkit Part 1. Retrieved from <https://www.cumbria.gov.uk/eLibrary/Content/Internet/538/755/2789/406869467>

Darnell, A. R., Tate, N. J. & Brunsdon, C. (2008). Improving user assessment of error implications in digital elevation models. *Computers, Environment and Urban Systems*, 32(4), 268–277. <https://doi.org/10.1016/j.compenvurbsys.2008.02.003>

Davidson-Arnott, R. (2010). R. Davidson-Arnott 2009. Introduction to Coastal Processes and Geomorphology. ISBN 978 0 521 69671 5. *Geological Magazine*, 147(6), 990–990. <https://doi.org/10.1017/s0016756810000658>

DBEIS (2019) Regulation for the Fourth Industrial Revolution - GOV.UK. Available at: <https://www.gov.uk/government/publications/regulation-for-the-fourth-industrial-revolution/regulation-for-the-fourth-industrial-revolution> (Accessed: 11 February 2021).

Defra. (2012). Climate Change Risk Assessment - Floods and Coastal Erosion: Summary. In Climate Change Risk Assessment. Retrieved from <http://randd.defra.gov.uk/Default.aspx?Module=More&Location=None&ProjectID=157>

Defra. (2020). Multi-billion pound investment as government unveils new long-term plan to tackle flooding. Retrieved July 14, 2020, from

<https://www.gov.uk/government/news/multi-billion-pound-investment-as-government-unveils-new-long-term-plan-to-tackle-flooding>

Defra (2021) Defra Digital: our story - Defra digital. Available at:

<https://defradigital.blog.gov.uk/about-defra-digital/> (Accessed: 11 February 2021).

Defra, & Environment Agency. (2007). Saltmarsh management manual R&D Technical Report SC030220. Retrieved from www.environment-agency.gov.uk

Dewez, T. J. B., Rohmer, J., Regard, V. & Cnudde, C. (2013). Probabilistic coastal cliff collapse hazard from repeated terrestrial laser surveys: case study from Mesnil Val (Normandy, northern France). *Journal of Coastal Research*, 65.

<https://doi.org/10.2112/SI65-119.1>

Dissanayake, P., Brown, J. & Karunarathna, H. (2014). Modelling storm-induced beach/dune evolution: Sefton coast, Liverpool Bay, UK. *Marine Geology*, 357, 225–242.

<https://doi.org/10.1016/j.margeo.2014.07.013>

Dudzińska-Nowak, J. & Wężyk, P. (2014). Volumetric changes of a soft cliff coast 2008–2012 based on DTM from airborne laser scanning (Wolin Island, southern Baltic Sea). *Journal of Coastal Research*, 70, 59–64. <https://doi.org/10.2112/si70-011.1>

<https://doi.org/10.2112/si70-011.1>

Duffy, J., Shutler, J., Witt, M., DeBell, L., Anderson, K., Duffy, J. P. & Anderson, K. (2018). Tracking Fine-Scale Structural Changes in Coastal Dune Morphology Using Kite Aerial Photography and Uncertainty-Assessed Structure-from-Motion Photogrammetry. *Remote Sensing*, 10(9), 1494. <https://doi.org/10.3390/rs10091494>

<https://doi.org/10.3390/rs10091494>

Dunford, R., Michel, K., Gagnage, M., Piégay, H. & Trémelo, M. L. (2009). Potential and constraints of Unmanned Aerial Vehicle technology for the characterization of Mediterranean riparian forest. *International Journal of Remote Sensing*, 30(19), 4915–4935. <https://doi.org/10.1080/01431160903023025>

<https://doi.org/10.1080/01431160903023025>

Earlie, C., Masselink, G., Russell, P. & Shail, R. (2013). Sensitivity analysis of the methodology for quantifying cliff erosion using airborne LiDAR – examples from Cornwall, UK. *Journal of Coastal Research*, 65, 470–475. <https://doi.org/10.2112/SI65-080.1>

Earlie, C. S., Young, A. P., Masselink, G. & Russell, P. E. (2015). Coastal cliff ground motions and response to extreme storm waves. *Geophysical Research Letters*, 42(3), 847–854. <https://doi.org/10.1002/2014GL062534>

Ehideaway. (2020). Silverdale Weather - Summary. Retrieved August 24, 2020, from <http://ehideaway.uk/silverdale/?dir=weather&pg=summary>

Eltner, A., Kaiser, A., Abellan, A. & Schindewolf, M. (2017). Time lapse structure-from-motion photogrammetry for continuous geomorphic monitoring. *Earth Surface Processes and Landforms*, 42(14), 2240–2253. <https://doi.org/10.1002/esp.4178>

Eltner, A., Kaiser, A., Castillo, C., Rock, G., Neugirg, F. & Abellán, A. (2016). Image-based surface reconstruction in geomorphometry – merits, limits and developments. *Earth Surface Dynamics*, 4(2), 359–389. <https://doi.org/10.5194/esurf-4-359-2016>

Eltner, A. & Schneider, D. (2015). Analysis of Different Methods for 3D Reconstruction of Natural Surfaces from Parallel-Axes UAV Images. *The Photogrammetric Record*, 30(151), 279–299. <https://doi.org/10.1111/phor.12115>

Environment Agency. (2009). UK Coastal Monitoring and Forecasting (UKCMF) Service - Strategy for 2009 to 2019. Retrieved from www.environment-agency.gov.uk

Environment Agency (2018) Climate change means more frequent flooding, warns Environment Agency - GOV.UK. Available at: <https://www.gov.uk/government/news/climate-change-means-more-frequent-flooding-warns-environment-agency>.

Environment Agency. (2019a). Long-term investment scenarios (LTIS) 2019. Retrieved from <https://www.gov.uk/government/publications/flood-and-coastal-risk-management-in-england-long-term-investment/long-term-investment-scenarios-ltis-2019#main-findings>

Environment Agency. (2019b). National Coastal Erosion Risk Mapping. Retrieved July 3, 2020, from <https://environment.maps.arcgis.com/apps/webappviewer/index.html?id=9cef4a084b4b4954b970cd35b099d94c>

Environment Agency and Defra (2021) Flood and coastal resilience innovation programme - GOV.UK. Available at: <https://www.gov.uk/guidance/flood-and-coastal-resilience-innovation-programme> (Accessed: 11 February 2021).

Etzkowitz, H. and Leydesdorff, L. (1995) 'The Triple Helix -- University-Industry-Government Relations: A Laboratory for Knowledge Based Economic Development by Henry Etzkowitz, Loet Leydesdorff :: SSRN', *EASST Review*, 14, pp. 14–19. Available at: https://papers.ssrn.com/sol3/papers.cfm?abstract_id=2480085.

Fernandez-Nunez, M., Burningham, H. & Ojeda Zujar, J. (2017). Improving accuracy of LiDAR-derived digital terrain models for saltmarsh management. *Journal of Coastal Conservation*, 21(1), 209–222. <https://doi.org/10.1007/s11852-016-0492-2>

Ferreira, E., Chandler, J., Wackrow, R. & Shiono, K. (2017). Automated extraction of free surface topography using SfM-MVS photogrammetry. *Flow Measurement and Instrumentation*, 54, 243–249. <https://doi.org/10.1016/j.flowmeasinst.2017.02.001>

Fisher, P. F. & Tate, N. J. (2006). Causes and consequences of error in digital elevation models. *Progress in Physical Geography: Earth and Environment*, 30(4), 467–489. <https://doi.org/10.1191/0309133306pp492ra>

Fonstad, M. A., Dietrich, J. T., Courville, B. C., Jensen, J. L. & Carbonneau, P. E. (2013). Topographic structure from motion: a new development in photogrammetric measurement. *Earth Surface Processes and Landforms*, 38(4), 421–430. <https://doi.org/10.1002/esp.3366>

Giménez, R., Marzoff, I., Campo, M. A., Seeger, M., Ries, J. B., Casali, J. & Álvarez-Mozos, J. (2009). Accuracy of high-resolution photogrammetric measurements of gullies with contrasting morphology. *Earth Surface Processes and Landforms*, 34(14), 1915–1926. <https://doi.org/10.1002/esp.1868>

Godfrey, S., Cooper, J., Bezombes, F. & Plater, A. (2020). Monitoring coastal morphology: the potential of low-cost fixed array action cameras for 3D reconstruction. *Earth Surface Processes and Landforms*, esp.4892. <https://doi.org/10.1002/esp.4892>

Goos, M. et al. (2019) The impact of Technological innovation on the Future of Work. Available at: <https://ec.europa.eu/jrc> (Accessed: 2 February 2021).

Green, D. R., Hagon, J., Mauquoy, D., Angus, S., Rennie, A., Gourlay, C. & Hansom, J. (2017). Monitoring, mapping and modelling saltmarsh. <https://doi.org/10.1201/9780429172410>

Gruen, A. (2012). Development and Status of Image Matching in Photogrammetry. *Photogrammetric Record*, 27(137), 36–57. <https://doi.org/10.1111/j.1477-9730.2011.00671.x>

Halcrow. (2013). North West Estuaries Processes Reports. Retrieved from <https://www.channelcoast.org/northwest>

Halcrow (2017) Wirral Coastal Processes Report. Available at: <https://www.coastalmonitoring.org> (Accessed: 6 January 2021).

Harley, M. D., Turner, I. L., Short, A. D. & Ranasinghe, R. (2011). A reevaluation of coastal embayment rotation: The dominance of cross-shore versus alongshore sediment transport processes, Collaroy-Narrabeen Beach, southeast Australia. *Journal of Geophysical Research: Earth Surface*, 116(4). <https://doi.org/10.1029/2011JF001989>

Harwin, S. & Lucieer, A. (2012). Assessing the Accuracy of Georeferenced Point Clouds Produced via Multi-View Stereopsis from Unmanned Aerial Vehicle (UAV) Imagery. *Remote Sensing*, 4(6), 1573–1599. <https://doi.org/10.3390/rs4061573>

Hastedt, H., Ekkel, T. & Luhmann, T. (2016). Evaluation Of The Quality Of Action Cameras With Wide-Angle Lenses In Uav Photogrammetry. *ISPRS - International Archives of the Photogrammetry, Remote Sensing and Spatial Information Sciences*, XLI-B1, 851–859. <https://doi.org/10.5194/isprs-archives-XLI-B1-851-2016>

Hattori, N., Sato, S. & Yamanaka, Y. (2019). Development of an imagery-based monitoring system for nearshore bathymetry by using wave breaking density. *Coastal Engineering Journal*, 61(3), 308–320. <https://doi.org/10.1080/21664250.2019.1588522>

Hladik, C., Schalles, J. & Alber, M. (2013). Salt marsh elevation and habitat mapping using hyperspectral and LIDAR data. *Remote Sensing of Environment*, 139, 318–330. <https://doi.org/10.1016/j.rse.2013.08.003>

- HM Government. (2016). National Flood Resilience Review. Retrieved from <https://www.gov.uk/government/publications/national-flood-resilience-review>
- Holman, R. A. & Stanley, J. (2007). The history and technical capabilities of Argus. *Coastal Engineering*, 54(6–7), 477–491. <https://doi.org/10.1016/j.coastaleng.2007.01.003>
- Horton, B. P., Shennan, I., Bradley, S. L., Cahill, N., Kirwan, M., Kopp, R. E. & Shaw, T. A. (2018). Predicting marsh vulnerability to sea-level rise using Holocene relative sea-level data. *Nature Communications*, 9(1), 1–7. <https://doi.org/10.1038/s41467-018-05080-0>
- Huang, W., Wang, K.-H. & Chen, Q. J. (2010). Coastal hazards. selected papers from EMI 2010. Retrieved June 29, 2020, from <https://www.semanticscholar.org/paper/Coastal-Hazards-%3A-selected-papers-from-EMI-2010-Los-Huang>
- International Panel on Climate Change. (2019). Technical Summary — Special Report on the Ocean and Cryosphere in a Changing Climate. Retrieved June 29, 2020, from <https://www.ipcc.ch/srocc/chapter/technical-summary/>
- James, M., Ilic, S. & Ružić, I. (2013). Measuring 3D coastal change with a digital camera. *Coastal Dynamics*. Retrieved from https://www.researchgate.net/publication/303062207_Measuring_3D_coastal_change_with_a_digital_camera
- James, M. R. & Robson, S. (2012). Straightforward reconstruction of 3D surfaces and topography with a camera: Accuracy and geoscience application. *Journal of Geophysical Research: Earth Surface*, 117(F3), n/a-n/a. <https://doi.org/10.1029/2011JF002289>
- James, M. R. & Robson, S. (2014). Sequential digital elevation models of active lava flows from ground-based stereo time-lapse imagery. *ISPRS Journal of Photogrammetry and Remote Sensing*, 97, 160–170. <https://doi.org/10.1016/j.isprsjprs.2014.08.011>
- James, M. R. & Robson, S. (2014). Mitigating systematic error in topographic models derived from UAV and ground-based image networks. *Earth Surface Processes and Landforms*, 39(10), 1413–1420. <https://doi.org/10.1002/esp.3609>
- James, M. R., Robson, S. & Smith, M. W. (2017). 3-D uncertainty-based topographic change detection with structure-from-motion photogrammetry: precision maps for

ground control and directly georeferenced surveys. *Earth Surface Processes and Landforms*, 42(12), 1769–1788. <https://doi.org/10.1002/esp.4125>

Jaud, M., Grasso, F., Le Dantec, N., Verney, R., Delacourt, C., Ammann, J. & Grandjean, P. (2016). Potential of UAVs for Monitoring Mudflat Morphodynamics (Application to the Seine Estuary, France). *ISPRS International Journal of Geo-Information*, 5(4), 50. <https://doi.org/10.3390/ijgi5040050>

Jaud, M., Letortu, P., Augereau, E., Le Dantec, N., Beauverger, M., Cuq, V. & Delacourt, C. (2017). Adequacy of pseudo-direct georeferencing of terrestrial laser scanning data for coastal landscape surveying against indirect georeferencing. *European Journal of Remote Sensing*, 50(1), 155–165. <https://doi.org/10.1080/22797254.2017.1300047>

Jebara, T., Azarbayejani, A. & Pentland, A. (1999). 3D structure from 2D motion. *IEEE Signal Processing Magazine*, 16(3), 66–84. <https://doi.org/10.1109/79.768574>

JNCC. (2019). Unmanned Aerial Vehicles for use in marine monitoring. *Marine Monitoring Platform Guidelines No. 3.*, 1–30. Retrieved from <http://data.jncc.gov.uk>

JNCC (2020) Morecambe Bay - Special Areas of Conservation. Available at: <https://sac.jncc.gov.uk/site/UK0013027> (Accessed: 6 January 2021).

Johnson, K., Nissen, E., Saripalli, S., Ramón Arrowsmith, J., MCGarey, P., Scharer, K. I. & Blisniuk, K. (2014). Rapid mapping of ultrafine fault zone topography with structure from motion. *Geosphere*, 10(5), 969–986. <https://doi.org/10.1130/GES01017.1>

Jones, L., Angus, S., Cooper, A., Doody, P., Everard, M., Garbutt, A., Gilchrist, P., Hansom, J., Nicholls, R. & Pye, K. (2011). UK National Ecosystem Assessment: Coastal Margins. 411–457. Retrieved from <http://nora.nerc.ac.uk/id/eprint/16134/>

Klemas, V. V. (2015). Coastal and Environmental Remote Sensing from Unmanned Aerial Vehicles: An Overview. *Journal of Coastal Research*, 315(5), 1260–1267. <https://doi.org/10.2112/jcoastres-d-15-00005.1>

Kolzenburg, S., Favalli, M., Fornaciai, A., Isola, I., Harris, A. J. L., Nannipieri, L. & Giordano, D. (2016). Rapid Updating and Improvement of Airborne LIDAR DEMs Through Ground-Based SfM 3-D Modeling of Volcanic Features. *IEEE Transactions on Geoscience and Remote Sensing*, 54(11), 6687–6699. <https://doi.org/10.1109/TGRS.2016.2587798>

Lague, D., Brodu, N. & Leroux, J. (2013). Accurate 3D comparison of complex topography with terrestrial laser scanner: Application to the Rangitikei canyon (N-Z). *ISPRS Journal of Photogrammetry and Remote Sensing*, 82, 10–26.

<https://doi.org/10.1016/j.isprsjprs.2013.04.009>

Leonardi, N., Ganju, N. K. & Fagherazzi, S. (2016). A linear relationship between wave power and erosion determines salt-marsh resilience to violent storms and hurricanes. *Proceedings of the National Academy of Sciences of the United States of America*, 113(1), 64–68. <https://doi.org/10.1073/pnas.1510095112>

Letortu, P., Jaud, M., Grandjean, P., Ammann, J., Costa, S., Maquaire, O. & Delacourt, C. (2018). Examining high-resolution survey methods for monitoring cliff erosion at an operational scale. *GIScience and Remote Sensing*, 55(4), 457–476.

<https://doi.org/10.1080/15481603.2017.1408931>

Li, X., Leonardi, N. & Plater, A. J. (2019). Wave-driven sediment resuspension and salt marsh frontal erosion alter the export of sediments from macro-tidal estuaries.

Geomorphology, 325, 17–28. <https://doi.org/10.1016/j.geomorph.2018.10.004>

Liu, J. G. & Mason, P. (2016). “Image Processing and GIS for Remote Sensing: Techniques and Applications.” Retrieved from <https://www.wiley.com/en-us>

Long, J., Napton, D., Giri, C. & Graesser, J. (2014). A Mapping and Monitoring Assessment of the Philippines’ Mangrove Forests from 1990 to 2010. *Journal of Coastal Research*, 294, 260–271. <https://doi.org/10.2112/jcoastres-d-13-00057.1>

Long, N., Millescamps, B., Guillot, B., Pouget, F. & Bertin, X. (2016). Monitoring the Topography of a Dynamic Tidal Inlet Using UAV Imagery. *Remote Sensing*, 8(5), 387.

<https://doi.org/10.3390/rs8050387>

Loos, E. A. & Niemann, K. O. (2002). Shoreline feature extraction from remotely-sensed imagery. *International Geoscience and Remote Sensing Symposium (IGARSS)*, 6, 3417–3419. <https://doi.org/10.1109/igarss.2002.1027201>

Lowe, J. A., Gregory, J. M. & Flather, R. A. (2001). Changes in the occurrence of storm surges around the United Kingdom under a future climate scenario using a dynamic storm surge model driven by Hadley Centre climate models. *Climate Dynamics*, 18(3–4), 179–188. <https://doi.org/10.1007/s003820100163>

- Maiti, S. & Bhattacharya, A. K. (2009). Shoreline change analysis and its application to prediction: A remote sensing and statistics based approach. *Marine Geology*, 257(1–4), 11–23. <https://doi.org/10.1016/j.margeo.2008.10.006>
- Mancini, F., Dubbini, M., Gattelli, M., Stecchi, F., Fabbri, S., Gabbianelli, G. & Gabbianelli, G. (2013). Using Unmanned Aerial Vehicles (UAV) for High-Resolution Reconstruction of Topography: The Structure from Motion Approach on Coastal Environments. *Remote Sensing*, 5(12), 6880–6898. <https://doi.org/10.3390/rs5126880>
- Marr, D. & Poggio, T. (1976). Cooperative Computation of Stereo Disparity. *Science*, 194(4262), 283–287. Retrieved from <https://science.sciencemag.org/content/194/4262/283>
- Masselink, G. & Russell, P. (2013). Impacts of climate change on coastal erosion. <https://doi.org/10.14465/2013.arc09.071-086>
- McCallum, I., Liu, W., See, L., Mechler, R., Keating, A., Hochrainer-Stigler, S., Mochizuki, J., Fritz, S., Dugar, S., Arestegui, M., Szoenyi, M., Bayas, J., Burek, P., French, A., Moorthy, I., (2016) ‘Technologies to Support Community Flood Disaster Risk Reduction’, *International Journal of Disaster Risk Science*. Beijing Normal University Press, 7(2), pp. 198–204. doi: 10.1007/s13753-016-0086-5.
- Mentaschi, L., Voudoukas, M. I., Pekel, J.-F., Voukouvalas, E. & Feyen, L. (2018). Global long-term observations of coastal erosion and accretion. *Scientific Reports*, 8(1), 12876. <https://doi.org/10.1038/s41598-018-30904-w>
- Merkens, J. L., Reimann, L., Hinkel, J. & Vafeidis, A. T. (2016). Gridded population projections for the coastal zone under the Shared Socioeconomic Pathways. *Global and Planetary Change*, 145, 57–66. <https://doi.org/10.1016/j.gloplacha.2016.08.009>
- Met Office. (2020). Past weather events - Met Office. Retrieved July 13, 2020, from <https://www.metoffice.gov.uk/weather/learn-about/past-uk-weather-events>
- Micheletti, N., Chandler, J. H. & Lane, S. N. (2015a). Investigating the geomorphological potential of freely available and accessible structure-from-motion photogrammetry using a smartphone. *Earth Surface Processes and Landforms*, 40(4), 473–486. <https://doi.org/10.1002/esp.3648>

- Micheletti, N., Chandler, J. H. & Lane, S. N. (2015b). Structure from Motion (SfM) Photogrammetry. In British Society for Geomorphology Geomorphological Techniques (Vol. 2). Retrieved from www.photosynth.net
- Mitasova, H., Overton, M. & Harmon, R. S. (2005). Geospatial analysis of a coastal sand dune field evolution: Jockey's Ridge, North Carolina. *Geomorphology*, 72(1–4), 204–221. <https://doi.org/10.1016/j.geomorph.2005.06.001>
- Moore, R. D., Wolf, J., Souza, A. J. & Flint, S. S. (2009). Morphological evolution of the Dee Estuary, Eastern Irish Sea, UK: A tidal asymmetry approach. *Geomorphology*, 103(4), 588–596. <https://doi.org/10.1016/j.geomorph.2008.08.003>
- Morang, A. & Gorman, L. T. (2005). Monitoring coastal geomorphology. In *Encyclopaedia of Earth Sciences Series* (Vol. 14, pp. 663–674). https://doi.org/10.1007/1-4020-3880-1_219
- Morton, R. A., Bernier, J. C. & Kelso, K. W. (2009). Recent subsidence and erosion at diverse wetland sites in the southeastern Mississippi Delta Plain. In *Open-File Report*. <https://doi.org/10.3133/OFR20091158>
- Mosbrucker, A. R., Major, J. J., Spicer, K. R. & Pitlick, J. (2017). Camera system considerations for geomorphic applications of SfM photogrammetry. *Earth Surface Processes and Landforms*, 42(6), 969–986. <https://doi.org/10.1002/esp.4066>
- Nagihara, S., Mulligan, K. R. & Xiong, W. (2004). Use of a three-dimensional laser scanner to digitally capture the topography of sand dunes in high spatial resolution. *Earth Surface Processes and Landforms*, 29(3), 391–398. <https://doi.org/10.1002/esp.1026>
- Natural England (2015) National Character Area Profile: Morecambe Limestone. Available at: www.gov.uk/natural-england (Accessed: 6 January 2021).
- Nicholls, R. J., Wong, P., Burkett, V., Codignotto, J., Hay, J. E., McLean, R. & Woodroffe, C. (2007). Coastal systems and low-lying areas. *Climate Change 2007: Impacts, Adaptation and Vulnerability. Contribution of Working Group II to the Fourth Assessment Report of the Intergovernmental Panel on Climate Change*, M, 315–356. Retrieved from <https://www.ipcc.ch/site/assets/uploads>

Nicholls, R. J., Marinova, N., Lowe, J. A., Brown, S., Vellinga, P., De Gusmão, D. & Tol, R. S. J. (2011). Sea-level rise and its possible impacts given a “beyond 4°C world” in the twenty-first century. *Philosophical Transactions of the Royal Society A: Mathematical, Physical and Engineering Sciences*, 369(1934), 161–181.

<https://doi.org/10.1098/rsta.2010.0291>

Nouwakpo, S. K., James, M. R., Weltz, M. A., Huang, C. H., Chagas, I. & Lima, L. (2014). Evaluation of structure from motion for soil microtopography measurement. *The Photogrammetric Record*, 29(147), 297–316. <https://doi.org/10.1111/phor.12072>

Nouwakpo, S. K., Weltz, M. A. & McGwire, K. (2016). Assessing the performance of structure-from-motion photogrammetry and terrestrial LiDAR for reconstructing soil surface microtopography of naturally vegetated plots. *Earth Surface Processes and Landforms*, 41(3), 308–322. <https://doi.org/10.1002/esp.3787>

Office for National Statistics. (2014). 2011 Census: Coastal Communities. Retrieved from <http://www.ons.gov.uk/ons/rel/census/2011-census/index.html>

Parente, L., Chandler, J. H. & Dixon, N. (2019). Optimising the quality of an SfM-MVS slope monitoring system using fixed cameras. *The Photogrammetric Record*, 34(168), 408–427. <https://doi.org/10.1111/phor.12288>

Perfetti, L., Polari, C. & Fassi, F. (2017). Fisheye Photogrammetry: Tests and Methodologies For The Survey Of Narrow Spaces. *ISPRS - International Archives of the Photogrammetry, Remote Sensing and Spatial Information Sciences*, XLII-2/W3, 573–580. <https://doi.org/10.5194/isprs-archives-XLII-2-W3-573-2017>

Phillips, J. B. & Eliasson, H. (2018). Camera Image Quality Benchmarking. <https://doi.org/10.1002/9781119054504>

Pierrot-Deseilligny, M. & Clery, I. (2012). Apero, An Open Source Bundle Adjustment Software for Automatic Calibration and Orientation Of Set Of Images. *International Archives of the Photogrammetry Remote Sensing and Spatial Information Sciences*. <https://doi.org/10.5194/isprsarchives-XXXVIII-5-W16-269-2011>

Pikelj, K., Ružić, I., Ilić, S., James, M. R. & Kordić, B. (2018). Implementing an efficient beach erosion monitoring system for coastal management in Croatia. *Ocean and Coastal Management*, 156, 223–238. <https://doi.org/10.1016/j.ocecoaman.2017.11.019>

Pittock, A. B., Walsh, K. & Mcinnes, K. (1996). Tropical cyclones and coastal inundation under enhanced greenhouse conditions. *Water, Air, and Soil Pollution*, 92(1–2), 159–169. <https://doi.org/10.1007/bf00175562>

Plater, A. J. & Grenville, J. (2010). Liverpool Bay: Linking the eastern Irish Sea to the Sefton Coast, in: *Sefton's Dynamic Coast*. [https://doi.org/ISBN 978-0-9566350-0-6](https://doi.org/ISBN%20978-0-9566350-0-6), 2010

Plater, A. J., Hodgson, D., Newton, M. & Lymbrey, G. (2010). Sefton South Shore: Understanding coastal evolution from past changes and present dynamics. *Sefton's Dynamic Coast, Proceeding of the Conference on Coastal and Geomorphology*. Retrieved from https://www.researchgate.net/publication/288623404_Sefton_South_Shore_Understanding_coastal_evolution_from_past_changes_and_present_dynamics

Pocock, M. J. O., Chapman, Daniel S., Sheppard, Lucy J., Roy, Helen E. (2014) A Strategic Framework to Support the Implementation of Citizen Science for Environmental Monitoring Final Report to SEPA by: A Strategic Framework to Support the Implementation of Citizen Science for Environmental Monitoring FINAL REPORT TO SEPA. Available at: <http://www.ceh.ac.uk/products/publications/understanding-citizen-science.html> (Accessed: 11 February 2021).

POLTIPS. (2020). Software. National Tidal and Sea Level Facility. Retrieved September 15, 2020, from <https://www.ntsfl.org/products/software>

Powell, E. J., Tyrrell, M. C., Milliken, A., Tirpak, J. M. & Staudinger, M. D. (2019). A review of coastal management approaches to support the integration of ecological and human community planning for climate change. <https://doi.org/10.1007/s11852-018-0632-y>

Prime, T., Brown, J. M. & Plater, A. J. (2015). Physical and Economic Impacts of Sea-Level Rise and Low Probability Flooding Events on Coastal Communities. *PLOS ONE*, 10(2), e0117030. <https://doi.org/10.1371/journal.pone.0117030>

Pringle, A. W. (1995). Erosion of a cyclic saltmarsh in Morecambe Bay, North-West England. *Earth Surface Processes and Landforms*, 20(5), 387–405. <https://doi.org/10.1002/esp.3290200502>

Prosdocimi, M., Calligaro, S., Sofia, G., Dalla Fontana, G. & Tarolli, P. (2015). Bank erosion in agricultural drainage networks: new challenges from structure-from-motion photogrammetry for post-event analysis. *Earth Surface Processes and Landforms*, 40(14), 1891–1906. <https://doi.org/10.1002/esp.3767>

Pye, K. & Blott, S. J. (2016). Assessment of beach and dune erosion and accretion using LiDAR: Impact of the stormy 2013-14 winter and longer term trends on the Sefton Coast, UK. *Geomorphology*, 266, 146–167. <https://doi.org/10.1016/j.geomorph.2016.05.011>

Remondino, F., Spera, M. G., Nocerino, E., Menna, F. & Nex, F. (2014). State of the art in high density image matching. *Photogrammetric Record*, 29(146), 144–166. <https://doi.org/10.1111/phor.12063>

Rosser, N. J., Brain, M. J., Petley, D. N., Lim, M. & Norman, E. C. (2013). Coastline retreat via progressive failure of rocky coastal cliffs. *Geology*, 41(8), 939–942. <https://doi.org/10.1130/G34371.1>

Rossi, R. (2018). Evaluation of 'Structure-from-Motion' from a Pole-Mounted Camera for Monitoring Geomorphic Change. All Graduate Theses and Dissertations. Retrieved from <https://digitalcommons.usu.edu/etd/6924>

Ruggles, S., Clark, J., Franke, K. W., Wolfe, D., Reimschiessel, B., Martin, R. A. & Hedengren, J. D. (2016). Comparison of SfM computer vision point clouds of a landslide derived from multiple small UAV platforms and sensors to a TLS-based model. *Journal of Unmanned Vehicle Systems*, 4(4), 246–265. <https://doi.org/10.1139/juvs-2015-0043>

Ružić, I., Marović, I., Benac, Č. & Ilić, S. (2014). Coastal cliff geometry derived from structure-from-motion photogrammetry at Stara Baška, Krk Island, Croatia. *Geo-Marine Letters*, 34(6). <https://doi.org/10.1007/s00367-014-0380-4>

Sapkota, Y. & White, J. R. (2019). Marsh edge erosion and associated carbon dynamics in coastal Louisiana: A proxy for future wetland-dominated coastlines world-wide. *Estuarine, Coastal and Shelf Science*, 226, 106289. <https://doi.org/10.1016/j.ecss.2019.106289>

See, L., Mooney, P., Foody, G., Bastin, L., Comber, A., Estima, J., Fritz, S., Kerle, N., Jiang, B., Laakso, M., Liu, Hai-Ying., Milčinski, G., Nikšič, M., Painho, M., Pődör, A., Olteanu-

- Raimond, A., Rutzinger, M. (2016) 'Crowdsourcing, Citizen Science or Volunteered Geographic Information? The Current State of Crowdsourced Geographic Information', *ISPRS International Journal of Geo-Information*. MDPI AG, 5(5), p. 55. doi: 10.3390/ijgi5050055.
- See, L. (2019) 'A Review of Citizen Science and Crowdsourcing in Applications of Pluvial Flooding', *Frontiers in Earth Science*. Frontiers Media S.A., 7, p. 44. doi: 10.3389/feart.2019.00044.
- Shortis, M. R., Bellman, C. J., Robson, S., Johnston, G. J. & Johnson, G. W. (2006). Stability of Zoom And Fixed Lenses Used With Digital SLR Cameras. *International Archives of Photogrammetry and Remote Sensing*. Retrieved from https://www.researchgate.net/publication/228858176_Stability_of_zoom_and_fixed_lenses_used_with_digital_SLR_cameras
- Small, C. & Nicholls, R. J. (2003). A global analysis of human settlement in coastal zones. *Journal of Coastal Research*, 19, 584–599. Retrieved from <https://www.jstor.org/stable/4299200>
- Smith, M. J. & Pain, C. F. (2009). Applications of remote sensing in geomorphology. *Progress in Physical Geography: Earth and Environment*, 33(4), 568–582. <https://doi.org/10.1177/0309133309346648>
- Smith, M.W., Carrivick, J. L. & Quincey, D. J. (2016). Structure from motion photogrammetry in physical geography. *Progress in Physical Geography: Earth and Environment*, 40(2), 247–275. <https://doi.org/10.1177/0309133315615805>
- Smith, M. W. & Vericat, D. (2015). From experimental plots to experimental landscapes: topography, erosion and deposition in sub-humid badlands from Structure-from-Motion photogrammetry. *Earth Surface Processes and Landforms*, 40(12), 1656–1671. <https://doi.org/10.1002/esp.3747>
- Snaveley, N., Seitz, S. M. & Szeliski, R. (2008). Modeling the world from Internet photo collections. *International Journal of Computer Vision*, 80(2), 189–210. <https://doi.org/10.1007/s11263-007-0107-3>
- Spencer, T., Schuerch, M., Nicholls, R. J., Hinkel, J., Lincke, D., Vafeidis, A. T. & Brown, S. (2016). Global coastal wetland change under sea-level rise and related stresses: The

DIVA Wetland Change Model. *Global and Planetary Change*, 139, 15–30.

<https://doi.org/10.1016/j.gloplacha.2015.12.018>

Streckel, B. & Koch, R. (2005). Lens model selection for visual tracking. *Lecture Notes in Computer Science*, 3663, 41–48. https://doi.org/10.1007/11550518_6

Stumpf, A., Malet, J. P., Allemand, P., Pierrot-Deseilligny, M. & Skupinski, G. (2015). Ground-based multi-view photogrammetry for the monitoring of landslide deformation and erosion. *Geomorphology*, 231, 130–145.

<https://doi.org/10.1016/J.GEOMORPH.2014.10.039>

Temmerman, S., Meire, P., Bouma, T. J., Herman, P. M. J., Ysebaert, T. & De Vriend, H. J. (2013, December 4). Ecosystem-based coastal defence in the face of global change. *Nature*, Vol. 504, pp. 79–83. <https://doi.org/10.1038/nature12859>

Thoeni, K., Giacomini, A., Murtagh, R. & Kniest, E. (2014). A comparison of multi-view 3D reconstruction of a rock wall using several cameras and a laser scanner. *ISPRS - International Archives of the Photogrammetry, Remote Sensing and Spatial Information Sciences*, XL-5, 573–580. <https://doi.org/10.5194/isprsarchives-XL-5-573-2014>

Towe, R. et al. (2020) 'Rethinking data-driven decision support in flood risk management for a big data age', *Journal of Flood Risk Management*. Blackwell Publishing Inc., 13(4), p. e12652. doi: 10.1111/jfr3.12652.

van Slobbe, E., de Vriend, H. J., Aarninkhof, S., Lulofs, K., de Vries, M. & Dircke, P. (2013). Building with Nature: In search of resilient storm surge protection strategies. *Natural Hazards*, 65(1), 947–966. <https://doi.org/10.1007/s11069-012-0342-y>

Vargo, L. J., Anderson, B. M., Horgan, H. J., Mackintosh, A. N., Lorrey, A. M. & Thornton, M. (2017). Using structure from motion photogrammetry to measure past glacier changes from historic aerial photographs. *Journal of Glaciology*, 63(242), 1105–1118.

<https://doi.org/10.1017/jog.2017.79>

Visser, F., Woodget, A., Skellern, A., Forsey, J., Warburton, J. & Johnson, R. (2019). An evaluation of a low-cost pole aerial photography (PAP) and structure from motion (SfM) approach for topographic surveying of small rivers. *International Journal of Remote Sensing*, 40(24), 9321–9351. <https://doi.org/10.1080/01431161.2019.1630782>

- Wamsley, T. V., Cialone, M. A., Smith, J. M., Atkinson, J. H. & Rosati, J. D. (2010). The potential of wetlands in reducing storm surge. *Ocean Engineering*, 37(1), 59–68. <https://doi.org/10.1016/j.oceaneng.2009.07.018>
- Warrick, J. A., Ritchie, A. C., Adelman, G., Adelman, K. & Limber, P. W. (2017). New Techniques to Measure Cliff Change from Historical Oblique Aerial Photographs and Structure-from-Motion Photogrammetry. *Journal of Coastal Research*, 33(1), 39. <https://doi.org/10.2112/jcoastres-d-16-00095.1>
- Wessling, R., Maurer, J. & Krenn-Leeb, A. (2014). Structure from Motion for Systematic Single Surface Documentation of Archaeological Excavations.
- Westoby, M. J., Brasington, J., Glasser, N. F., Hambrey, M. J. & Reynolds, J. M. (2012). 'Structure-from-Motion' photogrammetry: A low-cost, effective tool for geoscience applications. *Geomorphology*, 179, 300–314. <https://doi.org/10.1016/J.GEOMORPH.2012.08.021>
- Westoby, M. J., Lim, M., Hogg, M., Pound, M. J., Dunlop, L. & Woodward, J. (2018). Cost-effective erosion monitoring of coastal cliffs. *Coastal Engineering*, 138, 152–164. <https://doi.org/10.1016/J.COASTALENG.2018.04.008>
- White, K. & El Asmar, H. M. (1999). Monitoring changing position of coastlines using Thematic Mapper imagery, an example from the Nile Delta. *Geomorphology*, 29(1–2), 93–105. [https://doi.org/10.1016/S0169-555X\(99\)00008-2](https://doi.org/10.1016/S0169-555X(99)00008-2)
- Wilkinson, M. W., Jones, R. R., Woods, C. E., Gilment, S. R., McCaffrey, K. J. W., Kokkalas, S. & Long, J. J. (2016). A comparison of terrestrial laser scanning and structure-from-motion photogrammetry as methods for digital outcrop acquisition. *Geosphere*, 12(6), 1865–1880. <https://doi.org/10.1130/GES01342.1>
- Williams, D. (2012). DEMs of Difference. *British Society for Geomorphology Geomorphological Techniques*, 3(2). Retrieved from <https://www.geomorphology.org.uk>
- Willis, M., Koenig, C., Black, S. & Castaneda, A. (2016). Archaeological 3D mapping: the structure from motion revolution. *Journal of Texas Archeology and History*, 3(1). Retrieved from <https://doi.org/10.21112/ita.2016.1.110>

Wolf, P. & DeWitt, B. (2000). Elements of Photogrammetry (with Applications in GIS).

Retrieved from <https://dl.acm.org/doi/book/10.5555/556015>

Young, A. P. (2015). Recent deep-seated coastal landsliding at San Onofre State Beach, California. *Geomorphology*, 228, 200–212.

<https://doi.org/10.1016/j.geomorph.2014.08.005>

Zhang, F. & Li, M. (2019). Impacts of Ocean Warming, Sea Level Rise, and Coastline Management on Storm Surge in a Semienclosed Bay. *Journal of Geophysical Research: Oceans*, 124(9), 6498–6514. <https://doi.org/10.1029/2019JC015445>

Appendix A – Python Script

Python Script for Completeness Metric:

```
#Colour Filtering & Percentage
import numpy as np
import cv2
img = cv2.imread('Image File location')
#Resizing the Image (Not always necessary)
resized = cv2.resize(img, (1024, 768), interpolation=cv2.INTER_AREA)
#CONVERT FROM BGR TO HSV COLOUR
hsv = cv2.cvtColor(img, cv2.COLOR_BGR2HSV)
#Setting the colour range to search
lower_green = np.array([53,200,160])
upper_green = np.array([72,255,255])#the highest colour value in the range
#Creating a mask
mask = cv2.inRange(hsv,lower_green,upper_green)#mask uses the function range, on
the hsv image,using the upper
#Displaying colours based on mask
res = cv2.bitwise_and(img,img,mask=mask)
#Count the non-zeros
count = cv2.countNonZero(mask)
print('The number of green pixels:' + str(count))
#Displaying the results
cv2.imshow('img',img)
cv2.imshow('mask',mask)
cv2.imshow('res',res)
cv2.waitKey(0)
cv2.destroyAllWindows()
```

Appendix B – Risk Assessments

Crosby February 2018



UNIVERSITY OF
LIVERPOOL

SCHOOL OF
ENVIRONMENTAL
SCIENCES

FIELDWORK RISK ASSESSMENT

This form must be completed for:

- a) all residential fieldwork (except non-hazardous urban fieldwork in the UK)
- b) all day visits to rugged or remote areas
- c) Honours fieldwork projects
- d) Individual fieldwork by staff or research students which involves practical work, or hazards not likely to be encountered in everyday activities in non-remote areas
- e) Any travel outside the European Economic area, Switzerland, Canada, USA, Australia or NZ including placements and low hazard activities such as conferences.

Fieldwork must comply with the University of Liverpool Code of Practice for Safety in Fieldwork (2011) that is based on the UCEA Guidance on Safety in Fieldwork (2011). These should be consulted for more detailed guidance. **Complete shaded areas and provide additional information where appropriate.**

1. Department:	GEOGRAPHY AND PLANNING
Module code:	n/a

	Name	Status (Staff/PG/UG)	Minibus driver	1 st Aider
Leader / Supervisor:	Samantha Godfrey	PGR		
Additional staff:	John Godfrey	Other		

2. BRIEF DESCRIPTION OF PROJECT (include LOCATION and DATES):

Crosby Beach North – North of Hall Road. One full day between 20.02.18–22.02.18. All dependent on weather conditions and tide times.
Park at Sefton Council car park outside H.M Coastguard (53.497560, -3.058841).
Non-contact coastal survey (~7 m section at ~1.5 m height) with Terrestrial Laser Scanner (FARO 3000), Trimble and GoPro Hero 4.

3. For fully supervised courses state the number of students:
For small groups of (PhD / MSc / UG diss) students PRINT names of those carrying out fieldwork. They should also countersign at the end of the document.

Samantha Godfrey, John Godfrey.

4. FEASIBILITY OF PROJECT:

Have satisfactory arrangements been made in the following respects?

Give supporting information for responses, **DO NOT just tick boxes.**



Access	Yes + supporting information	N/A
Travel method	Yes – Car. Site has been visited previously so route is known.	
Passport, visas, tickets		X
Insurance - Uni/travel/other	Yes – covered by the University	
Accommodation		X
Permission to work obtained		X
Provision for disabled		X

Training	Yes + supporting information	N/A
1 st Aid		X
Languages		X
Specific skills – e.g. boats, corers, other	Yes – previous experience with survey equipment.	

5. EMERGENCY PLANNING FOR REMOTE LOCATIONS:

Remote is taken to mean where attendance of emergency services to a casualty is expected to take 20 minutes or more and includes all sites away from immediate roadside access.

Nearest Accident and Emergency Centre Postcode	Aintree University Hospital- Accident and Emergency Department, Aintree University Hospital, Longmoor Ln, Liverpool. L9 7LJ
Distance to nearest A+E	7.6 miles
Estimated arrival time for emergency services	~ 20 mins
Is there mobile phone coverage? If NO, what measure will be taken to manage situations described below? A) for communication with emergency services from remote location B) for communication between participants in emergency situation	Yes
Is area accessible by vehicles? If NO, what is max walk time to nearest access?	Yes
Potential for language problems – how manage?	No

6. HAZARD/RISK ANALYSIS:

Identify whether the following hazards exist. If 'YES,' please provide further details together with a strategy for mitigation. Hazards expected but not listed may be added into the box below:

Physical hazards	Yes + supporting information	N/A
Weather/climate (wet/cold/hot)	Yes – coast can be cold at this time of year. Ensure appropriate clothing and footwear is worn (waterproof, warm clothing)	
Mountains / moorland		X
Glaciers, crevasses, ice falls etc		X
Caves, mines and quarries		X
Forests (incl fire hazards)		X
Freshwater (rivers and lakes)		X
Sea / coast (tides, currents, cliffs etc)	Yes – Will only be doing fieldwork during low tide so not physically effected by tides or currents	
Marshes / quicksand		X
Excavations		X

Biological hazards (Coshh)	Yes + supporting information	N/A
Venomous/lively /aggressive animals		X
Toxic / irritant plants		X
Pathogenic organisms (eg tetanus/leptospirosis/rabies)		X
Vaccinations required		X

Chemical hazards (Coshh)	Yes + supporting information	N/A
Agrochemicals / pesticides		X
Dusts		X
Radioactivity		X
Chemicals taken to / found at site		X

Man-made hazards	Yes + supporting information	N/A
Machinery (incl noise/vibration)		X
Vehicles (other than group)		X
Power lines and pipelines		X
Electrical equipment	Yes – Survey equipment. Care will be taken during use to avoid unnecessary contact with water.	
Insecure buildings/confined spaces		X
Slurry and silage pits		X
Attack on the person or property		X
Civil / military unrest		X

Additional hazards not listed above;

NB - If the fieldwork does not involve any risks in excess of those in an average office, domestic kitchen or a visit to an average city park, and if the fieldwork is not remote, then no functional declarations are necessary and no occupational health assessments are needed.

7. ORGANISATION OF THE FIELDWORK:

Have satisfactory arrangements been made in the following respects?

Pre-planning	Yes + supporting information	N/A
Next of kin and GP noted		X
Functional Declaration completed by all staff and students		X
Home/Uni emergency numbers obtained	Yes - obtained	
Appropriate authorities (Police, Mt Rescue, Coast Guard etc) informed or contact details known		X
Written information to participants		X
Briefings for participants	Yes	
Night work required		X
Ethical considerations of project		X

Catering	Yes + supporting information	N/A
Food arrangements	Yes	
Drinks arrangements (+ hot climate)	Yes	
Dietary requirements considered		X
Hygiene (incl food prep and storage)		X
Stoves / Fuel		X

Group	Yes + supporting information	N/A
Leader experience/qualifications		X
Deputies/chain of command		X
Staff : student ratio		X
Working group size (min/max)	2 persons	

Individuals	Yes + supporting information	N/A
No lone working (helpers/buddies)	Yes – no lone working	
PPE requirements		X
Trained in techniques	Yes – previous/similar experience	
Physically capable	Yes	
Language problems		X

Equipment	Yes + supporting information	N/A
Appropriate for task	Yes – checked before use.	
Repairable (spares/duplicates)		X
Manual handling implications	Yes – some bulky/ heavy items of equipment – items will be carried as a team, rucksack for other equipment.	
Samples (handling/storage)		X

8. CONDUCT OF FIELDWORK:

Satisfactory arrangements will be made regarding the following:

Exploring the use of a Multi-Camera Platform for 3D Reconstruction

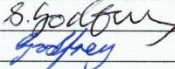
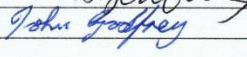
Local conditions	Yes + supporting information	N/A
Weather forecast	Yes – weather forecast will be checked the day before	
Local rules/knowledge	Yes – previous visits to the site	
Farming practices		X
Itinerary (distance/start/return)	Yes – Depends on tide times and weather conditions (cloudy is necessary)	
Daylight sufficient for task	Yes – setting off early to give us enough time. Will stop work before light disappears	

Transport	Yes + supporting information	N/A
Appropriately licensed drivers	Yes	
Co-drivers available if req		X
Vehicle (car/van/minibus/coach etc)	Personal Car	
Navigation	Yes – site has been previously visited, route is known.	

Group working practices	Yes + supporting information	N/A
Regular head counts / role calls		X
Communication with others in party		X
Communication with leaders		X
Call to Check-in / out of site		X
Buddy system / lookout		X
Appropriate footwear / clothing	Yes – appropriate clothing will be taken	
1 st aid kit / survival equip		X

Emergency planning	Yes + supporting information	N/A
Communication to summon help	Yes – mobile phone to contact emergency services	
Evacuation of party	Yes – return to car	
Availability of shelter	Yes – return to car	
Know how to report incidents	Yes	

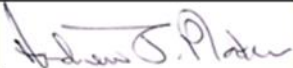
9. FIELDWORK PARTICIPANTS (small groups):

NAME (print)	SIGNATURE	STATUS	DATE
Samantha Godfrey		PGR	16.02.18
John Godfrey		Other	16.02.18

10. WORK MAY PROCEED SUBJECT TO THE CONDITIONS STATED IN THIS ASSESSMENT:

Countersigned: Head of School / Other nominated person

NAME (print)	SIGNATURE	STATUS	DATE

Professor Andrew Plater		Head of Department	16.02.18
-------------------------	---	-----------------------	----------

Thurstaston November 2018:



UNIVERSITY OF
LIVERPOOL

SCHOOL OF ENVIRONMENTAL SCIENCES

FIELDWORK RISK ASSESSMENT

This form must be completed for:

- a) all residential fieldwork (except non-hazardous urban fieldwork in the UK)
- b) all day visits to rugged or remote areas
- c) Honours fieldwork projects
- d) Individual fieldwork by staff or research students which involves practical work, or hazards not likely to be encountered in everyday activities in non-remote areas
- e) Any travel outside the European Economic area, Switzerland, Canada, USA, Australia or NZ including placements and low hazard activities such as conferences.

Fieldwork must comply with the University of Liverpool Code of Practice for Safety in Fieldwork (2011) that is based on the UCEA Guidance on Safety in Fieldwork (2011). These should be consulted for more detailed guidance.

Complete shaded areas and provide additional information where appropriate.

1. Department:	GEOGRAPHY AND PLANNING
Module code:	n/a

	Name	Status (Staff/PG/UG)	Minibus driver	1 st Aider
Leader / Supervisor:	Samantha Godfrey	PGR		
Additional staff:	John Godfrey	Other		

2. BRIEF DESCRIPTION OF PROJECT (include LOCATION and DATES):

Thurstaston Beach – near to Dee Sailing Club - Station Rd, Wirral CH61 0HN. One day between 02.11.18–04.11.18. All dependent on weather conditions and tide times. Park on Station Road car park near to Dee sailing Club (53.34708, -3.15789). Non-contact coastal survey (~13 m section at ~1 m height) with Terrestrial Laser Scanner (FARO 3000), Trimble and GoPro Hero 4 equipment.

3. For fully supervised courses state the number of students:
 For small groups of (PhD / MSc / UG diss) students PRINT names of those carrying out fieldwork. They should also countersign at the end of the document.

Samantha Godfrey, John Godfrey.

4. FEASIBILITY OF PROJECT:

Have satisfactory arrangements been made in the following respects?

Give supporting information for responses, **DO NOT just tick boxes.**

Access	Yes + supporting information	N/A
Travel method	Yes – Car. Site has been visited previously so route is known.	
Passport, visas, tickets		X
Insurance - Uni/travel/other	Yes – covered by the University	
Accommodation		X
Permission to work obtained		X
Provision for disabled		X

Training	Yes + supporting information	N/A
1 st Aid		X
Languages		X
Specific skills – e.g. boats, corers, other	Yes – previous experience with survey equipment.	

5. EMERGENCY PLANNING FOR REMOTE LOCATIONS:

Remote is taken to mean where attendance of emergency services to a casualty is expected to take 20 minutes or more and includes all sites away from immediate roadside access.

Nearest Accident and Emergency Centre Postcode	<u>Arrowe Park Hospital- Accident and Emergency Department, Arrowe Park Rd, Upton, Birkenhead, Wirral CH49 5PE</u>
Distance to nearest A+E	4.5 miles
Estimated arrival time for emergency services	~13 mins
Is there mobile phone coverage? If NO, what measure will be taken to manage situations described below? A) for communication with emergency services from remote location B) for communication between participants in emergency situation	Yes
Is area accessible by vehicles? If NO, what is max walk time to nearest access?	Yes
Potential for language problems – how manage?	No

6. HAZARD/RISK ANALYSIS:

Identify whether the following hazards exist. If 'YES,' please provide further details together with a strategy for mitigation. Hazards expected but not listed may be added into the box below:

Physical hazards	Yes + supporting information	N/A
Weather/climate (wet/cold/hot)	Yes – coast can be cold at this time of year. Ensure appropriate clothing and footwear is worn (waterproof, warm clothing)	
Mountains / moorland		X
Glaciers, crevasses, ice falls etc		X
Caves, mines and quarries		X
Forests (ign) fire hazards)		X
Freshwater (rivers and lakes)		X
Sea / coast (tides, currents, cliffs etc)	Yes – Will only be doing fieldwork during low tide so not physically effected by tides or currents. Coastal cliffs but we will not be near to the larger cliffs.	
Marshes / quicksand		X
Excavations		X

Biological hazards (Coshh)	Yes + supporting information	N/A
Venomous/lively /aggressive animals		X
Toxic / irritant plants		X
Pathogenic organisms (eg tetanus/leptospirosis/rabies)		X
Vaccinations required		X

Chemical hazards (Coshh)	Yes + supporting information	N/A
Agrochemicals / pesticides		X
Dusts		X
Radioactivity		X
Chemicals taken to / found at site		X

Man-made hazards	Yes + supporting information	N/A
Machinery (ign) noise/vibration)		X
Vehicles (other than group)		X
Power lines and pipelines		X
Electrical equipment	Yes – Survey equipment. Care will be taken during use to avoid unnecessary contact with water.	
Insecure buildings/confined spaces		X
Slurry and silage pits		X
Attack on the person or property		X
Civil / military unrest		X

Additional hazards not listed above;

NB - If the fieldwork does not involve any risks in excess of those in an average office, domestic kitchen or a visit to an average city park, and if the fieldwork is not remote, then no functional declarations are necessary and no occupational health assessments are needed.

7. ORGANISATION OF THE FIELDWORK:

Have satisfactory arrangements been made in the following respects?

Pre-planning	Yes + supporting information	N/A
Next of kin and GP noted		X
Functional Declaration completed by all staff and students		X
Home/Uni emergency numbers obtained	Yes - obtained	
Appropriate authorities (Police, Mt Rescue, Coast Guard etc) informed or contact details known		X
Written information to participants		X
Briefings for participants	Yes	
Night work required		X
Ethical considerations of project		X

Catering	Yes + supporting information	N/A
Food arrangements	Yes	
Drinks arrangements (+ hot climate)	Yes	
Dietary requirements considered		X
Hygiene (incl food prep and storage)		X
Stoves / Fuel		X

Group	Yes + supporting information	N/A
Leader experience/qualifications		X
Deputies/chain of command		X
Staff : student ratio		X
Working group size (min/max)	2 persons	

Individuals	Yes + supporting information	N/A
No lone working (helpers/buddies)	Yes – no lone working	
PPE requirements		X
Trained in techniques	Yes – previous/similar experience	
Physically capable	Yes	
Language problems		X

Equipment	Yes + supporting information	N/A
Appropriate for task	Yes – checked before use.	
Repairable (spares/duplicates)		X
Manual handling implications	Yes – some bulky/ heavy items of equipment – items will be carried as a team, rucksack for other equipment.	
Samples (handling/storage)		X

8. CONDUCT OF FIELDWORK:

Satisfactory arrangements will be made regarding the following:

Exploring the use of a Multi-Camera Platform for 3D Reconstruction

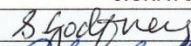
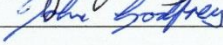
Local conditions	Yes + supporting information	N/A
Weather forecast	Yes – weather forecast will be checked the day before	
Local rules/knowledge	Yes – previous visits to the site	
Farming practices		X
Itinerary (distance/start/return)	Yes – Depends on tide times and weather conditions (cloudy is necessary)	
Daylight sufficient for task	Yes – setting off early to give us enough time.	

Transport	Yes + supporting information	N/A
Appropriately licensed drivers	Yes	
Co-drivers available if req		X
Vehicle (car/van/minibus/coach etc)	Personal Car	
Navigation	Yes – site has been previously visited, route is known.	

Group working practices	Yes + supporting information	N/A
Regular head counts / role calls		X
Communication with others in party		X
Communication with leaders		X
Call to Check-in / out of site		X
Buddy system / lookout		X
Appropriate footwear / clothing	Yes – appropriate clothing will be taken	
1 st aid kit / survival equip		X

Emergency planning	Yes + supporting information	N/A
Communication to summon help	Yes – mobile phone to contact emergency services	
Evacuation of party	Yes – return to car	
Availability of shelter	Yes – return to car	
Know how to report incidents	Yes	

9. FIELDWORK PARTICIPANTS (small groups):

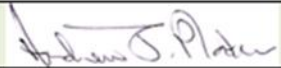
NAME (print)	SIGNATURE	STATUS	DATE
Samantha Godfrey		PGR	31.10.18
John Godfrey		Other	31.10.18

10. WORK MAY PROCEED SUBJECT TO THE CONDITIONS STATED IN THIS ASSESSMENT:

Countersigned: Head of School / Other nominated person

NAME (print)	SIGNATURE	STATUS	DATE

Exploring the use of a Multi-Camera Platform for 3D Reconstruction

Professor Andrew Plater		Head of Department	31.10.18
-------------------------	---	-----------------------	----------

Silverdale November 2018



UNIVERSITY OF
LIVERPOOL

SCHOOL OF
ENVIRONMENTAL
SCIENCES

FIELDWORK RISK ASSESSMENT

This form must be completed for:

- a) all residential fieldwork (except non-hazardous urban fieldwork in the UK)
- b) all day visits to rugged or remote areas
- c) Honours fieldwork projects
- d) Individual fieldwork by staff or research students which involves practical work, or hazards not likely to be encountered in everyday activities in non-remote areas
- e) Any travel outside the European Economic area, Switzerland, Canada, USA, Australia or NZ including placements and low hazard activities such as conferences.

Fieldwork must comply with the University of Liverpool Code of Practice for Safety in Fieldwork (2011) that is based on the UCEA Guidance on Safety in Fieldwork (2011). These should be consulted for more detailed guidance. **Complete shaded areas and provide additional information where appropriate.**

1. Department: GEOGRAPHY AND PLANNING
Module code: n/a

	Name	Status (Staff/PG/UG)	Minibus driver	1 st Aider
Leader / Supervisor:	Samantha Godfrey	PGR		
Additional staff:	John Godfrey	Other		

2. BRIEF DESCRIPTION OF PROJECT (include LOCATION and DATES):

Silverdale Saltmarsh – Shore Rd, Silverdale, Carnforth, LA5 0TS. One day between 14.11.18–16.11.18. All dependent on weather conditions and tide times.
 Park on Shore Road and walk 5 mins to saltmarsh (54.16456, -2.83387).
 Non-contact coastal survey (~30 m section at ~1 m height) with Terrestrial Laser Scanner (FARO 3000), Trimble and GoPro Hero 4 equipment.

3. For fully supervised courses state the number of students:
 For small groups of (PhD / MSc / UG diss) students PRINT names of those carrying out fieldwork. They should also countersign at the end of the document.

Samantha Godfrey, John Godfrey.

4. FEASIBILITY OF PROJECT:

Have satisfactory arrangements been made in the following respects?

Give supporting information for responses, **DO NOT just tick boxes.**

Access	Yes + supporting information	N/A
Travel method	Yes – Car. Site has been visited previously so route is known.	
Passport, visas, tickets		X
Insurance - Uni/travel/other	Yes – covered by the University	
Accommodation		X
Permission to work obtained		X
Provision for disabled		X

Training	Yes + supporting information	N/A
1 st Aid		X
Languages		X
Specific skills – e.g. boats, corers, other	Yes – previous experience with survey equipment.	

5. EMERGENCY PLANNING FOR REMOTE LOCATIONS:

Remote is taken to mean where attendance of emergency services to a casualty is expected to take 20 minutes or more and includes all sites away from immediate roadside access.

Nearest Accident and Emergency Centre Postcode	Queen Victoria Hospital - Thornton Rd, Morecambe LA4 5NN
Distance to nearest A+E	10.6 miles
Estimated arrival time for emergency services	~20 mins
Is there mobile phone coverage? If NO, what measure will be taken to manage situations described below? A) for communication with emergency services from remote location B) for communication between participants in emergency situation	Yes
Is area accessible by vehicles? If NO, what is max walk time to nearest access?	Yes
Potential for language problems – how manage?	No

6. HAZARD/RISK ANALYSIS:

Identify whether the following hazards exist. If 'YES,' please provide further details together with a strategy for mitigation. Hazards expected but not listed may be added into the box below:

Physical hazards	Yes + supporting information	N/A
Weather/climate (wet/cold/hot)	Yes – coast can be cold at this time of year. Ensure appropriate clothing and footwear is worn (waterproof, warm clothing)	
Mountains / moorland		X
Glaciers, crevasses, ice falls etc		X
Caves, mines and quarries		X
Forests (incl fire hazards)		X
Freshwater (rivers and lakes)		X
Sea / coast (tides, currents, cliffs etc)	Yes – Will only be doing fieldwork during low tide so not physically effected by tides or currents.	
Marshes / quicksand	Yes – saltmarsh. Mature marsh we easy access and no creeks.	
Excavations		X

Biological hazards (Coshh)	Yes + supporting information	N/A
Venomous/lively /aggressive animals		X
Toxic / irritant plants		X
Pathogenic organisms (eg tetanus/leptospirosis/rabies)		X
Vaccinations required		X

Chemical hazards (Coshh)	Yes + supporting information	N/A
Agrochemicals / pesticides		X
Dusts		X
Radioactivity		X
Chemicals taken to / found at site		X

Man-made hazards	Yes + supporting information	N/A
Machinery (incl noise/vibration)		X
Vehicles (other than group)		X
Power lines and pipelines		X
Electrical equipment	Yes – Survey equipment. Care will be taken during use to avoid unnecessary contact with water.	
Insecure buildings/confined spaces		X
Slurry and silage pits		X
Attack on the person or property		X
Civil / military unrest		X

Additional hazards not listed above;

NB - If the fieldwork does not involve any risks in excess of those in an average office, domestic kitchen or a visit to an average city park, and if the fieldwork is not remote, then no functional declarations are necessary and no occupational health assessments are needed.

7. ORGANISATION OF THE FIELDWORK:

Have satisfactory arrangements been made in the following respects?

Pre-planning	Yes + supporting information	N/A
Next of kin and GP noted		X
Functional Declaration completed by all staff and students		X
Home/Uni emergency numbers obtained	Yes - obtained	
Appropriate authorities (Police, Mt Rescue, Coast Guard etc) informed or contact details known		X
Written information to participants		X
Briefings for participants	Yes	
Night work required		X
Ethical considerations of project		X

Catering	Yes + supporting information	N/A
Food arrangements	Yes	
Drinks arrangements (+ hot climate)	Yes	
Dietary requirements considered		X
Hygiene (incl food prep and storage)		X
Stoves / Fuel		X

Group	Yes + supporting information	N/A
Leader experience/qualifications		X
Deputies/chain of command		X
Staff : student ratio		X
Working group size (min/max)	2 persons	

Individuals	Yes + supporting information	N/A
No lone working (helpers/buddies)	Yes – no lone working	
PPE requirements		X
Trained in techniques	Yes – previous/similar experience	
Physically capable	Yes	
Language problems		X

Equipment	Yes + supporting information	N/A
Appropriate for task	Yes – checked before use.	
Repairable (spares/duplicates)		X
Manual handling implications	Yes – some bulky/ heavy items of equipment – items will be carried as a team, rucksack for other equipment.	
Samples (handling/storage)		X

8. CONDUCT OF FIELDWORK:

Satisfactory arrangements will be made regarding the following:

Exploring the use of a Multi-Camera Platform for 3D Reconstruction

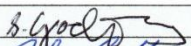
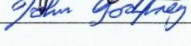
Local conditions	Yes + supporting information	N/A
Weather forecast	Yes – weather forecast will be checked the day before	
Local rules/knowledge	Yes – previous visits to the site	
Farming practices		X
Itinerary (distance/start/return)	Yes – Depends on tide times and weather conditions (cloudy is necessary)	
Daylight sufficient for task	Yes – setting off early to give us enough time. Will stop work before light disappears	

Transport	Yes + supporting information	N/A
Appropriately licensed drivers	Yes	
Co-drivers available if req		X
Vehicle (car/van/minibus/coach etc)	Personal Car	
Navigation	Yes – site has been previously visited, route is known.	

Group working practices	Yes + supporting information	N/A
Regular head counts / role calls		X
Communication with others in party		X
Communication with leaders		X
Call to Check-in / out of site		X
Buddy system / lookout		X
Appropriate footwear / clothing	Yes – appropriate clothing will be taken	
1 st aid kit / survival equip		X

Emergency planning	Yes + supporting information	N/A
Communication to summon help	Yes – mobile phone to contact emergency services	
Evacuation of party	Yes – return to car	
Availability of shelter	Yes – return to car	
Know how to report incidents	Yes	

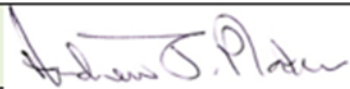
9. FIELDWORK PARTICIPANTS (small groups):

NAME (print)	SIGNATURE	STATUS	DATE
Samantha Godfrey		PGR	12.11.18
John Godfrey		Other	12.11.18

10. WORK MAY PROCEED SUBJECT TO THE CONDITIONS STATED IN THIS ASSESSMENT:

Countersigned: Head of School / Other nominated person

NAME (print)	SIGNATURE	STATUS	DATE

Professor Andrew Plater		Head of Department	12.11.18
-------------------------	--	-----------------------	----------



Crosby December 2018



UNIVERSITY OF
LIVERPOOL

SCHOOL OF
ENVIRONMENTAL
SCIENCES

FIELDWORK RISK ASSESSMENT

This form must be completed for:

- a) all residential fieldwork (except non-hazardous urban fieldwork in the UK)
- b) all day visits to rugged or remote areas
- c) Honours fieldwork projects
- d) Individual fieldwork by staff or research students which involves practical work, or hazards not likely to be encountered in everyday activities in non-remote areas
- e) Any travel outside the European Economic area, Switzerland, Canada, USA, Australia or NZ including placements and low hazard activities such as conferences.

Fieldwork must comply with the University of Liverpool Code of Practice for Safety in Fieldwork (2011) that is based on the UCEA Guidance on Safety in Fieldwork (2011). These should be consulted for more detailed guidance. **Complete shaded areas and provide additional information where appropriate.**

1. Department: GEOGRAPHY AND PLANNING
Module code: n/a

	Name	Status (Staff/PG/UG)	Minibus driver	1 st Aider
Leader / Supervisor:	Samantha Godfrey	PGR		
Additional staff:	John Godfrey	Other		

2. BRIEF DESCRIPTION OF PROJECT (include LOCATION and DATES):

Crosby Beach North – North of Hall Road. One full day between 03.12.18–06.12.18. All dependent on weather conditions and tide times.
Park at Sefton Council car park outside H.M Coastguard (53.497560, -3.058841).
Non-contact coastal survey (~30 m section at ~1.5 m height) with Terrestrial Laser Scanner (FARO 3000), Trimble and GoPro Hero 4 equipment.

3. For fully supervised courses state the number of students:
For small groups of (PhD / MSc / UG diss) students PRINT names of those carrying out fieldwork. They should also countersign at the end of the document.

Samantha Godfrey, John Godfrey.

4. FEASIBILITY OF PROJECT:

Have satisfactory arrangements been made in the following respects?

Give supporting information for responses, **DO NOT just tick boxes.**

Access	Yes + supporting information	N/A
Travel method	Yes – Car. Site has been visited previously so route is known.	
Passport, visas, tickets		X
Insurance - Uni/travel/other	Yes – covered by the University	
Accommodation		X
Permission to work obtained		X
Provision for disabled		X

Training	Yes + supporting information	N/A
1 st Aid		X
Languages		X
Specific skills – e.g. boats, corers, other	Yes – previous experience with survey equipment.	

5. EMERGENCY PLANNING FOR REMOTE LOCATIONS:

Remote is taken to mean where attendance of emergency services to a casualty is expected to take 20 minutes or more and includes all sites away from immediate roadside access.

Nearest Accident and Emergency Centre Postcode	Aintree University Hospital- Accident and Emergency Department, Aintree University Hospital, Longmoor Ln, Liverpool. L9 7LJ
Distance to nearest A+E	7.6 miles
Estimated arrival time for emergency services	~20 mins
Is there mobile phone coverage? If NO, what measure will be taken to manage situations described below? A) for communication with emergency services from remote location B) for communication between participants in emergency situation	Yes
Is area accessible by vehicles? If NO, what is max walk time to nearest access?	Yes
Potential for language problems – how manage?	No

6. HAZARD/RISK ANALYSIS:

Identify whether the following hazards exist. If 'YES,' please provide further details together with a strategy for mitigation. Hazards expected but not listed may be added into the box below:

Physical hazards	Yes + supporting information	N/A
Weather/climate (wet/cold/hot)	Yes – coast can be cold at this time of year. Ensure appropriate clothing and footwear is worn (waterproof, warm clothing)	
Mountains / moorland		X
Glaciers, crevasses, ice falls etc		X
Caves, mines and quarries		X
Forests (incl fire hazards)		X
Freshwater (rivers and lakes)		X
Sea / coast (tides, currents, cliffs etc)	Yes – Will only be doing fieldwork during low tide so not physically effected by tides or currents	
Marshes / quicksand		X
Excavations		X

Biological hazards (Coshh)	Yes + supporting information	N/A
Venomous/lively /aggressive animals		X
Toxic / irritant plants		X
Pathogenic organisms (eg tetanus/leptospirosis/rabies)		X
Vaccinations required		X

Chemical hazards (Coshh)	Yes + supporting information	N/A
Agrochemicals / pesticides		X
Dusts		X
Radioactivity		X
Chemicals taken to / found at site		X

Man-made hazards	Yes + supporting information	N/A
Machinery (incl noise/vibration)		X
Vehicles (other than group)		X
Power lines and pipelines		X
Electrical equipment	Yes – Survey equipment. Care will be taken during use to avoid unnecessary contact with water.	
Insecure buildings/confined spaces		X
Slurry and silage pits		X
Attack on the person or property		X
Civil / military unrest		X

Additional hazards not listed above;

NB - If the fieldwork does not involve any risks in excess of those in an average office, domestic kitchen or a visit to an average city park, and if the fieldwork is not remote, then no functional declarations are necessary and no occupational health assessments are needed.

7. ORGANISATION OF THE FIELDWORK:

Have satisfactory arrangements been made in the following respects?

Pre-planning	Yes + supporting information	N/A
Next of kin and GP noted		X
Functional Declaration completed by all staff and students		X
Home/Uni emergency numbers obtained	Yes - obtained	
Appropriate authorities (Police, Mt Rescue, Coast Guard etc) informed or contact details known		X
Written information to participants		X
Briefings for participants	Yes	
Night work required		X
Ethical considerations of project		X

Catering	Yes + supporting information	N/A
Food arrangements	Yes	
Drinks arrangements (+ hot climate)	Yes	
Dietary requirements considered		X
Hygiene (incl food prep and storage)		X
Stoves / Fuel		X

Group	Yes + supporting information	N/A
Leader experience/qualifications		X
Deputies/chain of command		X
Staff : student ratio		X
Working group size (min/max)	2 persons	

Individuals	Yes + supporting information	N/A
No lone working (helpers/buddies)	Yes – no lone working	
PPE requirements		X
Trained in techniques	Yes – previous/similar experience	
Physically capable	Yes	
Language problems		X

Equipment	Yes + supporting information	N/A
Appropriate for task	Yes – checked before use.	
Repairable (spares/duplicates)		X
Manual handling implications	Yes – some bulky/ heavy items of equipment – items will be carried as a team, rucksack for other equipment.	
Samples (handling/storage)		X

8. CONDUCT OF FIELDWORK:

Satisfactory arrangements will be made regarding the following:

Exploring the use of a Multi-Camera Platform for 3D Reconstruction

Local conditions	Yes + supporting information	N/A
Weather forecast	Yes – weather forecast will be checked the day before	
Local rules/knowledge	Yes – previous visits to the site	
Farming practices		X
Itinerary (distance/start/return)	Yes – Depends on tide times and weather conditions (cloudy is necessary)	
Daylight sufficient for task	Yes – setting off early to give us enough time. Will stop work before light disappears	

Transport	Yes + supporting information	N/A
Appropriately licensed drivers	Yes	
Co-drivers available if req		X
Vehicle (car/van/minibus/coach etc)	Personal Car	
Navigation	Yes – site has been previously visited, route is known.	

Group working practices	Yes + supporting information	N/A
Regular head counts / role calls		X
Communication with others in party		X
Communication with leaders		X
Call to Check-in / out of site		X
Buddy system / lookout		X
Appropriate footwear / clothing	Yes – appropriate clothing will be taken	
1 st aid kit / survival equip		X

Emergency planning	Yes + supporting information	N/A
Communication to summon help	Yes – mobile phone to contact emergency services	
Evacuation of party	Yes – return to car	
Availability of shelter	Yes – return to car	
Know how to report incidents	Yes	

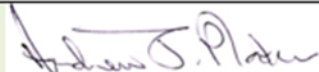
9. FIELDWORK PARTICIPANTS (small groups):

NAME (print)	SIGNATURE	STATUS	DATE
Samantha Godfrey	<i>S. Godfrey</i>	PGR	30.11.18
John Godfrey	<i>John Godfrey</i>	Other	30.11.18

10. WORK MAY PROCEED SUBJECT TO THE CONDITIONS STATED IN THIS ASSESSMENT:

Countersigned: Head of School / Other nominated person

NAME (print)	SIGNATURE	STATUS	DATE

Professor Andrew Plater		Head of Department	30.11.18
-------------------------	---	-----------------------	----------

Silverdale December 2018



UNIVERSITY OF
LIVERPOOL

SCHOOL OF ENVIRONMENTAL SCIENCES

FIELDWORK RISK ASSESSMENT

This form must be completed for:

- a) all residential fieldwork (except non-hazardous urban fieldwork in the UK)
- b) all day visits to rugged or remote areas
- c) Honours fieldwork projects
- d) Individual fieldwork by staff or research students which involves practical work, or hazards not likely to be encountered in everyday activities in non-remote areas
- e) Any travel outside the European Economic area, Switzerland, Canada, USA, Australia or NZ including placements and low hazard activities such as conferences.

Fieldwork must comply with the University of Liverpool Code of Practice for Safety in Fieldwork (2011) that is based on the UCEA Guidance on Safety in Fieldwork (2011). These should be consulted for more detailed guidance. **Complete shaded areas and provide additional information where appropriate.**

1. Department:	GEOGRAPHY AND PLANNING
Module code:	n/a

	Name	Status (Staff/PG/UG)	Minibus driver	1 st Aider
Leader / Supervisor:	Samantha Godfrey	PGR		
Additional staff:	John Godfrey	Other		

2. BRIEF DESCRIPTION OF PROJECT (include LOCATION and DATES):

Silverdale Saltmarsh – Shore Rd, Silverdale, Carnforth, LA5 0TS. One day between 12.12.18–14.12.18. All dependent on weather conditions and tide times.
 Park on Shore Road and walk 5 mins to saltmarsh (54.16456, -2.83387).
 Non-contact coastal survey (~30 m section at ~1 m height) with Terrestrial Laser Scanner (FARO 3000), Trimble and GoPro Hero 4 equipment.

3. For fully supervised courses state the number of students:
 For small groups of (PhD / MSc / UG diss) students PRINT names of those carrying out fieldwork. They should also countersign at the end of the document.

Samantha Godfrey, John Godfrey.

4. FEASIBILITY OF PROJECT:

Have satisfactory arrangements been made in the following respects?

Give supporting information for responses, **DO NOT just tick boxes.**

Access	Yes + supporting information	N/A
Travel method	Yes – Car. Site has been visited previously so route is known.	
Passport, visas, tickets		X
Insurance - Uni/travel/other	Yes – covered by the University	
Accommodation		X
Permission to work obtained		X
Provision for disabled		X

Training	Yes + supporting information	N/A
1 st Aid		X
Languages		X
Specific skills – e.g. boats, corers, other	Yes – previous experience with survey equipment.	

5. EMERGENCY PLANNING FOR REMOTE LOCATIONS:

Remote is taken to mean where attendance of emergency services to a casualty is expected to take 20 minutes or more and includes all sites away from immediate roadside access.

Nearest Accident and Emergency Centre Postcode	Queen Victoria Hospital - Thornton Rd, Morecambe LA4 5NN
Distance to nearest A+E	10.6 miles
Estimated arrival time for emergency services	~20 mins
Is there mobile phone coverage? If NO, what measure will be taken to manage situations described below? A) for communication with emergency services from remote location B) for communication between participants in emergency situation	Yes
Is area accessible by vehicles? If NO, what is max walk time to nearest access?	Yes
Potential for language problems – how manage?	No

6. HAZARD/RISK ANALYSIS:

Identify whether the following hazards exist. If 'YES,' please provide further details together with a strategy for mitigation. Hazards expected but not listed may be added into the box below:

Physical hazards	Yes + supporting information	N/A
Weather/climate (wet/cold/hot)	Yes – coast can be cold at this time of year. Ensure appropriate clothing and footwear is worn (waterproof, warm clothing)	
Mountains / moorland		X
Glaciers, crevasses, ice falls etc		X
Caves, mines and quarries		X
Forests (inc fire hazards)		X
Freshwater (rivers and lakes)		X
Sea / coast (tides, currents, cliffs etc)	Yes – Will only be doing fieldwork during low tide so not physically effected by tides or currents.	
Marshes / quicksand	Yes – saltmarsh. Mature marsh we easy access and no creeks.	
Excavations		X

Biological hazards (Coshh)	Yes + supporting information	N/A
Venomous/lively /aggressive animals		X
Toxic / irritant plants		X
Pathogenic organisms (eg tetanus/leptospirosis/rabies)		X
Vaccinations required		X

Chemical hazards (Coshh)	Yes + supporting information	N/A
Agrochemicals / pesticides		X
Dusts		X
Radioactivity		X
Chemicals taken to / found at site		X

Man-made hazards	Yes + supporting information	N/A
Machinery (inc noise/vibration)		X
Vehicles (other than group)		X
Power lines and pipelines		X
Electrical equipment	Yes – Survey equipment. Care will be taken during use to avoid unnecessary contact with water.	
Insecure buildings/confined spaces		X
Slurry and silage pits		X
Attack on the person or property		X
Civil / military unrest		X

Additional hazards not listed above;

NB - If the fieldwork does not involve any risks in excess of those in an average office, domestic kitchen or a visit to an average city park, and if the fieldwork is not remote, then no functional declarations are necessary and no occupational health assessments are needed.

7. ORGANISATION OF THE FIELDWORK:

Have satisfactory arrangements been made in the following respects?

Pre-planning	Yes + supporting information	N/A
Next of kin and GP noted		X
Functional Declaration completed by all staff and students		X
Home/Uni emergency numbers obtained	Yes - obtained	
Appropriate authorities (Police, Mt Rescue, Coast Guard etc) informed or contact details known		X
Written information to participants		X
Briefings for participants	Yes	
Night work required		X
Ethical considerations of project		X

Catering	Yes + supporting information	N/A
Food arrangements	Yes	
Drinks arrangements (+ hot climate)	Yes	
Dietary requirements considered		X
Hygiene (incl food prep and storage)		X
Stoves / Fuel		X

Group	Yes + supporting information	N/A
Leader experience/qualifications		X
Deputies/chain of command		X
Staff : student ratio		X
Working group size (min/max)	2 persons	

Individuals	Yes + supporting information	N/A
No lone working (helpers/buddies)	Yes – no lone working	
PPE requirements		X
Trained in techniques	Yes – previous/similar experience	
Physically capable	Yes	
Language problems		X

Equipment	Yes + supporting information	N/A
Appropriate for task	Yes – checked before use.	
Repairable (spares/duplicates)		X
Manual handling implications	Yes – some bulky/ heavy items of equipment – items will be carried as a team, rucksack for other equipment.	
Samples (handling/storage)		X

8. CONDUCT OF FIELDWORK:

Satisfactory arrangements will be made regarding the following:

Exploring the use of a Multi-Camera Platform for 3D Reconstruction

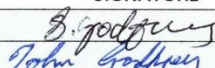
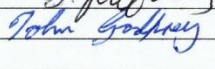
Local conditions	Yes + supporting information	N/A
Weather forecast	Yes – weather forecast will be checked the day before	
Local rules/knowledge	Yes – previous visits to the site	
Farming practices		X
Itinerary (distance/start/return)	Yes – Depends on tide times and weather conditions (cloudy is necessary)	
Daylight sufficient for task	Yes – setting off early to give us enough time. Will stop work before light disappears	

Transport	Yes + supporting information	N/A
Appropriately licensed drivers	Yes	
Co-drivers available if req		X
Vehicle (car/van/minibus/coach etc)	Personal Car	
Navigation	Yes – site has been previously visited, route is known.	

Group working practices	Yes + supporting information	N/A
Regular head counts / role calls		X
Communication with others in party		X
Communication with leaders		X
Call to Check-in / out of site		X
Buddy system / lookout		X
Appropriate footwear / clothing	Yes – appropriate clothing will be taken	
1 st aid kit / survival equip		X

Emergency planning	Yes + supporting information	N/A
Communication to summon help	Yes – mobile phone to contact emergency services	
Evacuation of party	Yes – return to car	
Availability of shelter	Yes – return to car	
Know how to report incidents	Yes	

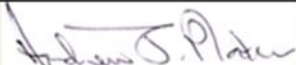
9. FIELDWORK PARTICIPANTS (small groups):

NAME (print)	SIGNATURE	STATUS	DATE
Samantha Godfrey		PGR	07.12.18
John Godfrey		Other	07.12.18

10. WORK MAY PROCEED SUBJECT TO THE CONDITIONS STATED IN THIS ASSESSMENT:

Countersigned: Head of School / Other nominated person

NAME (print)	SIGNATURE	STATUS	DATE

Professor Andrew Plater		Head of Department	07.12.18
-------------------------	---	-----------------------	----------

Silverdale January 2019



UNIVERSITY OF
LIVERPOOL

SCHOOL OF
ENVIRONMENTAL
SCIENCES

FIELDWORK RISK ASSESSMENT

This form must be completed for:

- a) all residential fieldwork (except non-hazardous urban fieldwork in the UK)
- b) all day visits to rugged or remote areas
- c) Honours fieldwork projects
- d) Individual fieldwork by staff or research students which involves practical work, or hazards not likely to be encountered in everyday activities in non-remote areas
- e) Any travel outside the European Economic area, Switzerland, Canada, USA, Australia or NZ including placements and low hazard activities such as conferences.

Fieldwork must comply with the University of Liverpool Code of Practice for Safety in Fieldwork (2011) that is based on the UCEA Guidance on Safety in Fieldwork (2011). These should be consulted for more detailed guidance. **Complete shaded areas and provide additional information where appropriate.**

1. Department: GEOGRAPHY AND PLANNING
Module code: n/a

	Name	Status (Staff/PG/UG)	Minibus driver	1 st Aider
Leader / Supervisor:	Samantha Godfrey	PGR		
Additional staff:	John Godfrey	Other		

2. BRIEF DESCRIPTION OF PROJECT (include LOCATION and DATES):

Silverdale Saltmarsh – Shore Rd, Silverdale, Carnforth, LA5 0TS. One day between 14.01.19–15.01.19. All dependent on weather conditions and tide times.
 Park on Shore Road and walk 5 mins to saltmarsh (54.16456, -2.83387).
 Non-contact coastal survey (~30 m section at ~1 m height) with Terrestrial Laser Scanner (FARO 3000), Trimble and GoPro Hero 4 equipment.

3. For fully supervised courses state the number of students:
 For small groups of (PhD / MSc / UG diss) students PRINT names of those carrying out fieldwork. They should also countersign at the end of the document.

Samantha Godfrey, John Godfrey.

4. FEASIBILITY OF PROJECT:

Have satisfactory arrangements been made in the following respects?

Give supporting information for responses, **DO NOT just tick boxes.**

Access	Yes + supporting information	N/A
Travel method	Yes – Car. Site has been visited previously so route is known.	
Passport, visas, tickets		X
Insurance - Uni/travel/other	Yes – covered by the University	
Accommodation		X
Permission to work obtained		X
Provision for disabled		X

Training	Yes + supporting information	N/A
1 st Aid		X
Languages		X
Specific skills – e.g. boats, corers, other	Yes – previous experience with survey equipment.	

5. EMERGENCY PLANNING FOR REMOTE LOCATIONS:

Remote is taken to mean where attendance of emergency services to a casualty is expected to take 20 minutes or more and includes all sites away from immediate roadside access.

Nearest Accident and Emergency Centre Postcode	Queen Victoria Hospital - Thornton Rd, Morecambe LA4 5NN
Distance to nearest A+E	10.6 miles
Estimated arrival time for emergency services	~20 mins
Is there mobile phone coverage? If NO, what measure will be taken to manage situations described below? A) for communication with emergency services from remote location B) for communication between participants in emergency situation	Yes
Is area accessible by vehicles? If NO, what is max walk time to nearest access?	Yes
Potential for language problems – how manage?	No

6. HAZARD/RISK ANALYSIS:

Identify whether the following hazards exist. If 'YES,' please provide further details together with a strategy for mitigation. Hazards expected but not listed may be added into the box below:

Physical hazards	Yes + supporting information	N/A
Weather/climate (wet/cold/hot)	Yes – coast can be cold at this time of year. Ensure appropriate clothing and footwear is worn (waterproof, warm clothing)	
Mountains / moorland		X
Glaciers, crevasses, ice falls etc		X
Caves, mines and quarries		X
Forests (incl fire hazards)		X
Freshwater (rivers and lakes)		X
Sea / coast (tides, currents, cliffs etc)	Yes – Will only be doing fieldwork during low tide so not physically effected by tides or currents.	
Marshes / quicksand	Yes – saltmarsh. Mature marsh we easy access and no creeks.	
Excavations		X

Biological hazards (Coshh)	Yes + supporting information	N/A
Venomous/lively /aggressive animals		X
Toxic / irritant plants		X
Pathogenic organisms (eg tetanus/leptospirosis/rabies)		X
Vaccinations required		X

Chemical hazards (Coshh)	Yes + supporting information	N/A
Agrochemicals / pesticides		X
Dusts		X
Radioactivity		X
Chemicals taken to / found at site		X

Man-made hazards	Yes + supporting information	N/A
Machinery (incl noise/vibration)		X
Vehicles (other than group)		X
Power lines and pipelines		X
Electrical equipment	Yes – Survey equipment. Care will be taken during use to avoid unnecessary contact with water.	
Insecure buildings/confined spaces		X
Slurry and silage pits		X
Attack on the person or property		X
Civil / military unrest		X

Additional hazards not listed above;

NB - If the fieldwork does not involve any risks in excess of those in an average office, domestic kitchen or a visit to an average city park, and if the fieldwork is not remote, then no functional declarations are necessary and no occupational health assessments are needed.

7. ORGANISATION OF THE FIELDWORK:

Have satisfactory arrangements been made in the following respects?

Pre-planning	Yes + supporting information	N/A
Next of kin and GP noted		X
Functional Declaration completed by all staff and students		X
Home/Uni emergency numbers obtained	Yes - obtained	
Appropriate authorities (Police, Mt Rescue, Coast Guard etc) informed or contact details known		X
Written information to participants		X
Briefings for participants	Yes	
Night work required		X
Ethical considerations of project		X

Catering	Yes + supporting information	N/A
Food arrangements	Yes	
Drinks arrangements (+ hot climate)	Yes	
Dietary requirements considered		X
Hygiene (incl food prep and storage)		X
Stoves / Fuel		X

Group	Yes + supporting information	N/A
Leader experience/qualifications		X
Deputies/chain of command		X
Staff : student ratio		X
Working group size (min/max)	2 persons	

Individuals	Yes + supporting information	N/A
No lone working (helpers/buddies)	Yes – no lone working	
PPE requirements		X
Trained in techniques	Yes – previous/similar experience	
Physically capable	Yes	
Language problems		X

Equipment	Yes + supporting information	N/A
Appropriate for task	Yes – checked before use.	
Repairable (spares/duplicates)		X
Manual handling implications	Yes – some bulky/ heavy items of equipment – items will be carried as a team, rucksack for other equipment.	
Samples (handling/storage)		X

8. CONDUCT OF FIELDWORK:

Satisfactory arrangements will be made regarding the following:

Exploring the use of a Multi-Camera Platform for 3D Reconstruction

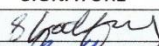
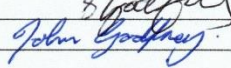
Local conditions	Yes + supporting information	N/A
Weather forecast	Yes – weather forecast will be checked the day before	
Local rules/knowledge	Yes – previous visits to the site	
Farming practices		X
Itinerary (distance/start/return)	Yes – Depends on tide times and weather conditions (cloudy is necessary)	
Daylight sufficient for task	Yes – setting off early to give us enough time. Will stop work before light disappears	

Transport	Yes + supporting information	N/A
Appropriately licensed drivers	Yes	
Co-drivers available if req		X
Vehicle (car/van/minibus/coach etc)	Personal Car	
Navigation	Yes – site has been previously visited, route is known.	

Group working practices	Yes + supporting information	N/A
Regular head counts / role calls		X
Communication with others in party		X
Communication with leaders		X
Call to Check-in / out of site		X
Buddy system / lookout		X
Appropriate footwear / clothing	Yes – appropriate clothing will be taken	
1 st aid kit / survival equip		X

Emergency planning	Yes + supporting information	N/A
Communication to summon help	Yes – mobile phone to contact emergency services	
Evacuation of party	Yes – return to car	
Availability of shelter	Yes – return to car	
Know how to report incidents	Yes	

9. FIELDWORK PARTICIPANTS (small groups):


NAME (print)	SIGNATURE	STATUS	DATE
Samantha Godfrey		PGR	10.01.19
John Godfrey		Other	10.01.19

10. WORK MAY PROCEED SUBJECT TO THE CONDITIONS STATED IN THIS ASSESSMENT:

Countersigned: Head of School / Other nominated person

NAME (print)	SIGNATURE	STATUS	DATE

Exploring the use of a Multi-Camera Platform for 3D Reconstruction

Professor Andrew Plater		Head of Department	10.01.19
-------------------------	---	--------------------	----------

Silverdale March 2019



UNIVERSITY OF
LIVERPOOL

SCHOOL OF
ENVIRONMENTAL
SCIENCES

FIELDWORK RISK ASSESSMENT

This form must be completed for:

- a) all residential fieldwork (except non-hazardous urban fieldwork in the UK)
- b) all day visits to rugged or remote areas
- c) Honours fieldwork projects
- d) Individual fieldwork by staff or research students which involves practical work, or hazards not likely to be encountered in everyday activities in non-remote areas
- e) Any travel outside the European Economic area, Switzerland, Canada, USA, Australia or NZ including placements and low hazard activities such as conferences.

Fieldwork must comply with the University of Liverpool Code of Practice for Safety in Fieldwork (2011) that is based on the UCEA Guidance on Safety in Fieldwork (2011). These should be consulted for more detailed guidance. **Complete shaded areas and provide additional information where appropriate.**

1. Department:

GEOGRAPHY AND PLANNING

Module code:

n/a

	Name	Status (Staff/PG/UG)	Minibus driver	1 st Aider
Leader / Supervisor:	Samantha Godfrey	PGR		
Additional staff:	John Godfrey	Other		

2. BRIEF DESCRIPTION OF PROJECT (include LOCATION and DATES):

Silverdale Saltmarsh – Shore Rd, Silverdale, Carnforth, LA5 0TS. One day between 18.03.19-22.03.19. All dependent on weather conditions and tide times.
Park on Shore Road and walk 5 mins to saltmarsh (54.16456, -2.83387).
Non-contact coastal survey (~30 m section at ~1 m height) with Terrestrial Laser Scanner (FARO 3000), Trimble and GoPro Hero 4 equipment.

3. For fully supervised courses state the number of students:

For small groups of (PhD / MSc / UG diss) students PRINT names of those carrying out fieldwork. They should also countersign at the end of the document.

Samantha Godfrey, John Godfrey.

4. FEASIBILITY OF PROJECT:

Have satisfactory arrangements been made in the following respects?

Give supporting information for responses, **DO NOT just tick boxes.**

Access	Yes + supporting information	N/A
Travel method	Yes – Car. Site has been visited previously so route is known.	
Passport, visas, tickets		X
Insurance - Uni/travel/other	Yes – covered by the University	
Accommodation		X
Permission to work obtained		X
Provision for disabled		X

Training	Yes + supporting information	N/A
1 st Aid		X
Languages		X
Specific skills – e.g. boats, corers, other	Yes – previous experience with survey equipment.	

5. EMERGENCY PLANNING FOR REMOTE LOCATIONS:

Remote is taken to mean where attendance of emergency services to a casualty is expected to take 20 minutes or more and includes all sites away from immediate roadside access.

Nearest Accident and Emergency Centre Postcode	Queen Victoria Hospital - Thornton Rd, Morecambe LA4 5NN
Distance to nearest A+E	10.6 miles
Estimated arrival time for emergency services	~20 mins
Is there mobile phone coverage? If NO, what measure will be taken to manage situations described below? A) for communication with emergency services from remote location B) for communication between participants in emergency situation	Yes
Is area accessible by vehicles? If NO, what is max walk time to nearest access?	Yes
Potential for language problems – how manage?	No

6. HAZARD/RISK ANALYSIS:

Identify whether the following hazards exist. If 'YES,' please provide further details together with a strategy for mitigation. Hazards expected but not listed may be added into the box below:

Physical hazards	Yes + supporting information	N/A
Weather/climate (wet/cold/hot)	Yes – coast can be cold at this time of year. Ensure appropriate clothing and footwear is worn (waterproof, warm clothing)	
Mountains / moorland		X
Glaciers, crevasses, ice falls etc		X
Caves, mines and quarries		X
Forests (incl fire hazards)		X
Freshwater (rivers and lakes)		X
Sea / coast (tides, currents, cliffs etc)	Yes – Will only be doing fieldwork during low tide so not physically effected by tides or currents.	
Marshes / quicksand	Yes – saltmarsh. Mature marsh we easy access and no creeks.	
Excavations		X

Biological hazards (Coshh)	Yes + supporting information	N/A
Venomous/lively /aggressive animals		X
Toxic / irritant plants		X
Pathogenic organisms (eg tetanus/leptospirosis/rabies)		X
Vaccinations required		X

Chemical hazards (Coshh)	Yes + supporting information	N/A
Agrochemicals / pesticides		X
Dusts		X
Radioactivity		X
Chemicals taken to / found at site		X

Man-made hazards	Yes + supporting information	N/A
Machinery (incl noise/vibration)		X
Vehicles (other than group)		X
Power lines and pipelines		X
Electrical equipment	Yes – Survey equipment. Care will be taken during use to avoid unnecessary contact with water.	
Insecure buildings/confined spaces		X
Slurry and silage pits		X
Attack on the person or property		X
Civil / military unrest		X

Additional hazards not listed above;

NB - If the fieldwork does not involve any risks in excess of those in an average office, domestic kitchen or a visit to an average city park, and if the fieldwork is not remote, then no functional declarations are necessary and no occupational health assessments are needed.

7. ORGANISATION OF THE FIELDWORK:

Have satisfactory arrangements been made in the following respects?

Pre-planning	Yes + supporting information	N/A
Next of kin and GP noted		X
Functional Declaration completed by all staff and students		X
Home/Uni emergency numbers obtained	Yes - obtained	
Appropriate authorities (Police, Mt Rescue, Coast Guard etc) informed or contact details known		X
Written information to participants		X
Briefings for participants	Yes	
Night work required		X
Ethical considerations of project		X

Catering	Yes + supporting information	N/A
Food arrangements	Yes	
Drinks arrangements (+ hot climate)	Yes	
Dietary requirements considered		X
Hygiene (inc) food prep and storage)		X
Stoves / Fuel		X

Group	Yes + supporting information	N/A
Leader experience/qualifications		X
Deputies/chain of command		X
Staff : student ratio		X
Working group size (min/max)	2 persons	

Individuals	Yes + supporting information	N/A
No lone working (helpers/buddies)	Yes – no lone working	
PPE requirements		X
Trained in techniques	Yes – previous/similar experience	
Physically capable	Yes	
Language problems		X

Equipment	Yes + supporting information	N/A
Appropriate for task	Yes – checked before use.	
Repairable (spares/duplicates)		X
Manual handling implications	Yes – some bulky/ heavy items of equipment – items will be carried as a team, rucksack for other equipment.	
Samples (handling/storage)		X

8. CONDUCT OF FIELDWORK:

Satisfactory arrangements will be made regarding the following:

Exploring the use of a Multi-Camera Platform for 3D Reconstruction

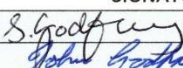
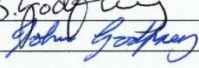
Local conditions	Yes + supporting information	N/A
Weather forecast	Yes – weather forecast will be checked the day before	
Local rules/knowledge	Yes – previous visits to the site	
Farming practices		X
Itinerary (distance/start/return)	Yes – Depends on tide times and weather conditions (cloudy is necessary)	
Daylight sufficient for task	Yes – setting off early to give us enough time. Will stop work before light disappears	

Transport	Yes + supporting information	N/A
Appropriately licensed drivers	Yes	
Co-drivers available if req		X
Vehicle (car/van/minibus/coach etc)	Personal Car	
Navigation	Yes – site has been previously visited, route is known.	

Group working practices	Yes + supporting information	N/A
Regular head counts / role calls		X
Communication with others in party		X
Communication with leaders		X
Call to Check-in / out of site		X
Buddy system / lookout		X
Appropriate footwear / clothing	Yes – appropriate clothing will be taken	
1 st aid kit / survival equip		X

Emergency planning	Yes + supporting information	N/A
Communication to summon help	Yes – mobile phone to contact emergency services	
Evacuation of party	Yes – return to car	
Availability of shelter	Yes – return to car	
Know how to report incidents	Yes	

9. FIELDWORK PARTICIPANTS (small groups):

NAME (print)	SIGNATURE	STATUS	DATE
Samantha Godfrey		PGR	15.03.19
John Godfrey		Other	15.03.19

10. WORK MAY PROCEED SUBJECT TO THE CONDITIONS STATED IN THIS ASSESSMENT:

Countersigned: Head of School / Other nominated person

NAME (print)	SIGNATURE	STATUS	DATE

Exploring the use of a Multi-Camera Platform for 3D Reconstruction

Professor Andrew Plater		Head of Department	15.03.19
-------------------------	---	-----------------------	----------